Edited by Songjun Li, Jagdish Singh, He Li, and Ipsita A. Banerjee

WILEY-VCH

# Biosensor Nanomaterials

*Edited by*
*Songjun Li, Jagdish Singh,*
*He Li, and Ipsita A. Banerjee*

**Biosensor Nanomaterials**

## *Related Titles*

Kumar, C. S. S. R. (ed.)

**Nanomaterials for the Life Sciences**

**10 Volume Set**

2011
ISBN: 978-3-527-32261-9

Guo, J. (ed.)

**X-Rays in Nanoscience**

**Spectroscopy, Spectromicroscopy, and Scattering Techniques**

2011
978-3-527-32288-6

Mirsky, V. M., Yatsimirsky, A. (eds.)

**Artificial Receptors for Chemical Sensors**

2011
ISBN: 978-3-527-32357-9

Ohtsu, M. (ed.)

**Nanophotonics and Nanofabrication**

2009
ISBN: 978-3-527-32121-6

Hierold, C. (ed.)

**Carbon Nanotube Devices**

**Properties, Modeling, Integration and Applications**

2008
ISBN: 978-3-527-31720-2

Ruiz-Hitzky, E., Ariga, K., Lvov, Y. M. (eds.)

**Bio-inorganic Hybrid Nanomaterials**

**Strategies, Syntheses, Characterization and Applications**

2008
ISBN: 978-3-527-31718-9

Köhler, M., Fritzsche, W.

**Nanotechnology**

**An Introduction to Nanostructuring Techniques**

2007
ISBN: 978-3-527-31871-1

Kumar, C. S. S. R. (ed.)

**Nanotechnologies for the Life Sciences**

**10 Volume Set**

2007
ISBN: 978-3-527-31301-3

*Edited by Songjun Li, Jagdish Singh, He Li, and Ipsita A. Banerjee*

# Biosensor Nanomaterials


WILEY-VCH Verlag GmbH & Co. KGaA

**The Editors**

***Prof. Songjun Li***
Key Lab. Pesticide & Chem. Bio
Ministry of Education
Ctrl. China Normal University
Wuhan 430079
China

***Prof. Dr. Jagdish Singh***
North Dakota State University
Dept. Pharmac. Sciences
Fargo, ND 58108-6050
USA

***Prof. Dr. He Li***
University of Jinan
School of Medical and Life Sciences
No 106 Jiwei Road
Jinan, Shandong 250022
China

***Prof. Dr. Ipsita A. Banerjee***
Fordham University
Dept. of Chemistry
Bronx, NY 10458
USA



**Library of Congress Card No.:** applied for

**British Library Cataloguing-in-Publication Data**
A catalogue record for this book is available from the British Library.

**Bibliographic information published by the Deutsche Nationalbibliothek**
The Deutsche Nationalbibliothek lists this publication in the Deutsche Nationalbibliografie; detailed bibliographic data are available on the Internet at <http://dnb.d-nb.de>.



**Composition** Toppan Best-set Premedia Ltd., Hong Kong
**Printing and Binding** betz-druck GmbH, Darmstadt
**Cover Design** Adam Design, Weinheim

Printed in the Federal Republic of Germany
Printed on acid-free paper

**ISBN:** 978-3-527-32841-3

# Contents



*Biosensor Nanomaterials*. Edited by Songjun Li, Jagdish Singh, and Ipsita A. Banerjee

ISBN: 978-3-527-32841-3

# Preface

There is a tremendous interest in reliable sensors and detection systems. Growing concerns about public exposure to harmful agents have fueled the essential requirement of developing and designing new sensing and detection systems. An immense knowledge base on biosensor materials is already assessable, but most of the available biosensor materials are limited to detecting both biological and chemical reagents under a relatively simple and undisturbed background. These available sensors have only limited ability for rapid sensing and discrimination of small amounts of harmful agents embedded in large amounts of a chemically inert but complex background. Scientists in this field are working under pressure to meet these challenges. Nanomaterials, because of the excellent electronic, magnetic, acoustic, and light properties, as well as their unique nanosize effects, have provided a key solution to these impending challenges.

Impressive progress has been made over the past few years because of the timely use of nanomaterials in the field of biosensors. Nanomaterials with the most promising outlook enable us to alter the texture in sensing and controlled modes by their unique electronic, magnetic, acoustic, and light properties or through external stress, electric and magnetic fields, temperature, moisture and pH, and so on. Nanotechnology, coupled with the recent advances in molecular device materials, biomimetic polymers, hybridized composites, supramolecular systems, information- and energy-transfer materials, environmentally friendly materials, and so on, has led to a profound revolution in the field of biosensors. This book summarizes the main applications of nanotechnology in the field of biosensors. The emphasis is to highlight the latest and most significant progress made in this field. Other aspects such as the biosensing principle, mechanism, design, and methods are also described. When providing a relatively comprehensive description on the current knowledge and technologies, we hope to provide an insight into some new directions in this field. As such, this book can be used not only as a textbook for advanced undergraduate and graduate students, but also as a reference book for researchers in biotechnology, nanotechnology, biomaterials, medicine, bioengineering, and other related disciplines.

Several books, each composed of many chapters, are probably not enough to cover all details in the field of biosensor nanomaterials. Thus, it is difficult to live up to the ideal of an absolute and comprehensive summary. Fortunately, because

*Biosensor Nanomaterials*. Edited by Songjun Li, Jagdish Singh, and Ipsita A. Banerjee

ISBN: 978-3-527-32841-3

of their expert backgrounds, all of the contributors have done their best when describing their chapters. Owing to the multidisciplinary nature of this subject, a large number of experts with different backgrounds have been invited to contribute their research. Without doubt, if it was not for the participation of such a diverse group of experts, we would not have been able to accomplish our goal of developing a systematic book in the field of biosensor nanomaterials.

*Songjun Li, PhD (Email: Lsjchem@gmail.com)*
*Jagdish Singh, PhD (Email: Jagdish.Singh@ndsu.edu)*
*He Li, PhD (Email: lihecd@gmail.com)*
*Ipsita A. Banerjee, PhD (Email: banerjee@fordham.edu)*
*Editors*

## About the Editors

**Dr. Songjun Li**, the leading editor of *Biosensors Nanomaterials*, is a Professor of Chemistry. He received his PhD degree in 2005 from the Chinese Academy of Sciences. Subsequently, he was appointed by Central China Normal University (CCNU) as an Associate Professor with a research interest in molecular recognition. He doubles also as an Invited Professor at the University of Jinan (China) and an Adjunct Professor at Jiangsu University (China). From 2005 to 2008, he worked as Deputy Director of the Chemical Experimental Center of CCNU. He was a postdoctoral fellow in the University of Wisconsin-Milwaukee (USA) during the period from August 2008 to August 2009. Currently, he is working in Cranfield Health (one of the most successful biosensor R & D centers around the world) of Cranfield University (UK) as the Marie Curie Fellow of Europe. During the past 10 years, Dr. Li, as the principal investigator and first author (excluding non-principal investigator and coauthor), has published about 40 papers in international peer-reviewed journals. He was also the leading editor for three other books: *Smart Polymer Materials for Biomedical Application* (Nova Science, USA, 2010), *Smart Nanomaterials for Sensor Applications* (Bentham Science, USA, 2010), and *Current Focus on Colloids and Surfaces* (Transworld Research Network, India, 2009). In March 2010, he cofounded the international principal journal *Advanced Materials Letters* and has been the Editor-in-Chief since then. He also serves as an editorial member or on the editorial boards of *American Journal of Environmental Sciences*, *Journal of Public Health and Epidemiology*, *Open Electrochemistry Journal*, and *Journal of Computational Biology and Bioinformatics Research*. He has been invited over 100 times to be a reviewer for various grants and international journals. His recent interest is focused on designing and developing novel, highly substrate-selective molecular recognition systems with molecular imprinting.

**Dr. Jagdish Singh** is Professor and Chair of the Department of Pharmaceutical Sciences at North Dakota State University (NDSU) College of Pharmacy, North Dakota, and a Fellow of the American Association of Pharmaceutical Scientists and a Fellow of Pharmacy and Biotechnology. Dr. Singh's research efforts focus

on mechanistic studies for developing and testing novel delivery technologies to deliver biotechnologically derived molecules (e.g., peptides, proteins, and genes). His research has been funded by the US Department of Defense, National Institutes of Health, PhRMA Foundation, and American Foundation for Pharmaceutical Education. Recently, he has been successful in establishing an Economic Development Center of Excellence in Vaccinology, called the Center of Biopharmaceutical Research and Production. He has published over 138 peer-reviewed papers and 250 abstracts. Dr. Singh has twice received the NDSU College of Pharmacy Researcher of the Year award, and was recognized with the Fred Waldron Research Award in 2002 in recognition of his outstanding contribution in research and creative activities at NDSU. Dr. Singh has supervised 30 graduate students and postdoctoral fellows, and over two dozen undergraduate and professional (PharmD) research students. He is a member and actively participates in several national and international professional and scientific societies (e.g., American Association of Advancement of Science, American Association of Pharmaceutical Scientists, American Association of Colleges of Pharmacy, and Controlled Release Society, Inc.). He is also a member of the US Pharmacopeia (1995–current), and serves as reviewer of grants and manuscripts for numerous pharmaceutical and biomedical journals.

**Dr. He Li** is a Professor of Chemistry. He is currently the Associate Editor for the international principal journal *Advanced Materials Letters*. He received his PhD degree in 2004 from the Chinese Academy of Sciences. Subsequently, he joined the University of Jinan (China), and became an Associate Professor with research interests in nanomaterials and their biomedical applications. He doubled also as Chair of the Pharmaceutical Engineering Department during the period from 2007 to 2009. At present, he is working in the University of Wisconsin (USA) as a Senior Visiting Scientist. In his personal database, he has published over 30 papers in international peer-reviewed journals. He has also been an invited reviewer for various grants and journals (over 40 times). His recent works are focused on designing and developing advanced functional materials for nanomedicine and biosensor applications. Specifically, he is designing and synthesizing multifunctional nanocarriers for cancer therapy and diagnosis, and fabricating biosensors (especially electrochemical biosensors) made of nanomaterials to detect various biomolecules in the field of clinical diagnosis, bioaffinity assays, and environmental monitoring.

**Dr. Ipsita Banerjee** received her PhD Degree in Chemistry from the University of Connecticut (USA) in 2001, following which she worked as a Postdoctoral Research Associate at the University of Notre Dame, Indiana (2001–2002), at the Chemical and Biomolecular Engineering Department and at Hunter College, New York (2002–2004), Department of Chemistry and Biochemistry in the field of Bionanotechnology. She then joined the Chemistry Department at Fordham University, New York in fall 2004 as a Faculty Member. Her current research focuses on the area of molecular self-assembly and supramolecular nanostructures in order to understand the important fundamental aspects of the surface chemistry associated with the growth and development of functional nanobiomaterials. She also

works on the development of nanomaterials with tailored properties wherein the shape, size, and porosity can be controlled via new bioengineering routes. Specifically, her research interests are geared toward the design and synthesis of nanomaterials for potential biomedical applications and molecular therapeutics for tissue regeneration, drug delivery, examining the mechanisms of peptide folding (both natural and artificial), catalysis and green synthetic methods for the preparation of nanoparticles for preparation of new improved materials for catalysis and applications as antibacterials, and device fabrication for optoelectronics and biosensors. Over the past 9 years, Dr. Banerjee has authored/coauthored over 45 articles in journals and various proceedings, and has presented at many conferences leading to over 70 presentations. She serves as a reviewer for multiple international journals and is also an Editorial Board Member of the journal *Advanced Materials Letters*.

## List of Contributors

***Francesca Berti***
Cranfield University
Cranfield Health
Vincent Building
College Road
Cranfield MK43 0AL
UK
Università degli Studi di Firenze
Dipartimento di Chimica "Ugo Schiff"
Via della Lastruccia 3
50019 Sesto Fiorentino, Firenze
Italy

***Shunsheng Cao***
Jiangsu University
School of Materials Science and Engineering
Xuefu Road 301
Zhenjiang 212013
China

***Juanrong Chen***
Jiansu University
School of Environment
Xuefu Road 301
Zhenjiang 212013
China

***William Cheung***
Rutgers University
Chemistry Department
73 Warren Street
Newark, NJ 07102
USA

***Christian Cimorra***
Cranfield University
Cranfield Health
Vincent Building
College Road
Cranfield MK43 0AL
UK

***Bin Du***
University of Jinan
School of Chemistry and Chemical Engineering
No 106 Jiwei Road
Jinan 250022
China

***Dan Fei***
De Montfort University
School of Pharmacy
Gateway Street
Leicester LE1 9BH
UK

*Biosensor Nanomaterials*. Edited by Songjun Li, Jagdish Singh, and Ipsita A. Banerjee

ISBN: 978-3-527-32841-3

***Yi Ge***
Cranfield University
Cranfield Health
Vincent Building
College Road
Cranfield MK43 0AL
UK

***Huixin He***
Rutgers University
Chemistry Department
73 Warren Street
Newark, NJ 07102
USA

***Ryne C. Hendrickson***
North Dakota State University
Department of Pharmaceutical Sciences
1401 Albrecht Boulevard
Fargo, ND 58102
USA

***Xin Jin***
Jiangsu University
School of Materials Science and Engineering
Xuefu Road 301
Zhenjiang 212013
China

***Bernard Knudsen***
University of Wisconsin-Milwaukee
Department of Mechanical Engineering
3400 North Maryland Avenue
Milwaukee, WI 53211
USA

***Premlata Kumari***
Sardar Vallabhbhai National Institute of Technology
Applied Chemistry Department
Ichchhanath
Surat, Gujarat 395007
India

***Benedict Law***
North Dakota State University
Department of Pharmaceutical Sciences
1401 Albrecht Boulevard
Fargo, ND 58105-6050
USA

***Buddhadev Layek***
North Dakota State University
Department of Pharmaceutical Sciences
1401 Albrecht Boulevard
Fargo, ND 58102
USA

***He Li***
University of Jinan
School of Medical and Life Sciences
No 106 Jiwei Road
Jinan 250022
China

***Songjun Li***
Central China Normal University
College of Chemistry
Key Laboratory of Pesticide & Chemical Biology of Ministry of Education
152 Luoyu Road
Wuhan, 430 079
China

***Ruchi Malik***
North Dakota State University
Department of Pharmaceutical Sciences
1401 Albrecht Boulevard
Fargo, ND 58105-6050
USA

***Sanku Mallik***
North Dakota State University
Department of Pharmaceutical Sciences
1401 Albrecht Boulevard
Fargo, ND 58102
USA

***Rhishikesh Mandke***
North Dakota State University
Department of Pharmaceutical Sciences
1401 Albrecht Boulevard
Fargo, ND 58102
USA

***Ajay K. Mishra***
University of Johannesburg
Department of Chemical Technology
PO Box 17011
Doornfontien, 2028 Johannesburg
Republic of South Africa

***Rajeev Mishra***
Nihon University
School of Medicine
Department of Cancer Genetics
Tokyo 1738 610
Japan

***Shivani B. Mishra***
University of Johannesburg
Department of Chemical Technology
PO Box 17011
Doornfontien, 2028 Johannesburg
Republic of South Africa

***Erin K. Nyren-Erickson***
North Dakota State University
Department of Pharmaceutical Sciences
1401 Albrecht Boulevard
Fargo, ND 58102
USA

***Zhiyong Qian***
Sichuan University
West China Medical School
West China Hospital
State Key Lab of Biotherapy
No 1 Branch Park Four of Gaopeng Road
Chengdu 610041
China

***Radheshyam Rai***
Universidade de Aveiro
Departmento de Engenharia Cerâmica e do Vidro and CICECO
Campus Universitário de Santiago
3810-193 Aveiro
Portugal

***Gitanjali Sharma***
North Dakota State University
Department of Pharmaceutical Sciences
1401 Albrecht Boulevard
Fargo, ND 58102
USA

***Jagdish Singh***
North Dakota State University
Department of Pharmaceutical Sciences
1401 Albrecht Boulevard
Fargo, ND 58102
USA

***Ashutosh Tiwari***
Jiangsu University
Science and Engineering
Zhenjiang 212013
China
National Institute for Materials Science
Sengen 1-2-1
Tsukuba 305 0047
Japan

***Anthony P. F. Turner***
Cranfield University
Cranfield Health
Vincent Building
College Road
Cranfield MK43 0AL
UK

***Anil V. Wagh***
North Dakota State University
Department of Pharmaceutical Sciences
1401 Albrecht Boulevard
Fargo, ND 58105-6050
USA

***Chunyan Wang***
University of Wisconsin-Milwaukee
Department of Mechanical Engineering
12901 Bruce B. Downs Blvd.
Tampa, FL, 33613
USA

***Qin Wei***
University of Jinan
School of Chemistry and Chemical Engineering
Street No 106 Jiwei Road
Jinan 250022
China

***Weiwei Wu***
Jiangsu University
School of Materials Science and Engineering
Street Xuefu Road 301
Zhenjiang 212013
China

***Minghui Yang***
University of Jinan
School of Chemistry and Chemical Engineering
No 106 Jiwei Road
Jinan 250022
China

***Xueji Zhang***
University of South Florida
Department of Chemistry
4202 East Fowler Avenue
Tampa, FL 33620-5250
USA
University of Science & Technology
Institute of Biomedicine and Bioengineering
No. 30 Xueyuan Rd.
Beijing 100083
China

***Zhiyuan Zhao***
Jiangsu University
School of Materials Science and Engineering
Xuefu Road 301
Zhenjiang 212013
China

# 1
# New Micro- and Nanotechnologies for Electrochemical Biosensor Development

*Francesca Berti and Anthony P. F. Turner*

## 1.1
## Introduction

Over the last decade, great attention has been paid to the inclusion of newly developed nanomaterials such as nanowires, nanotubes, and nanocrystals in sensor devices. This can be attributed to the ability to tailor the size and structure, and hence the properties of nanomaterials, thus opening up excellent prospects for designing novel sensing systems and enhancing the performance of bioanalytical assays [1]. Considering that most biological systems, including viruses, membranes, and protein complexes, are naturally nanostructured materials and that molecular interactions take place on a nanometer scale, nanomaterials are intuitive candidates for integration into biomedical and bioanalytical devices [2, 3]. Moreover, they can pave the way for the miniaturization of sensors and devices with nanometer dimensions (nanosensors and nanobiosensors) in order to obtain better sensitivity, specificity, and faster rates of recognition compared to current solutions.

The chemical, electronic, and optical properties of nanomaterials generally depend on both their dimensions and their morphology [4]. A wide variety of nanostructures have been reported in the literature for interesting analytical applications. Among these, organic and inorganic nanotubes, nanoparticles, and metal oxide nanowires have provided promising building blocks for the realization of nanoscale electrochemical biosensors due to their biocompatibility and technologically important combination of properties, such as high surface area, good electrical properties, and chemical stability. Moreover, the integration of nanomaterials in electrochemical devices offers the possibility of realizing portable, easy-to-use, and inexpensive sensors, due to the ease of miniaturization of both the material and the transduction system. Over the last decade, this field has been extensively investigated and a huge number of papers have been published. This chapter principally summarizes progress made in the last few years (2005 to date) in the integration of nanomaterials such as carbon nanotubes (CNTs), nanoparticles, and polymer nanostructures in electrochemical biosensing systems.

*Biosensor Nanomaterials*. Edited by Songjun Li, Jagdish Singh, and Ipsita A. Banerjee

ISBN: 978-3-527-32841-3

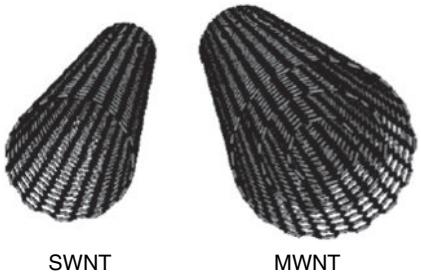


**Figure 1.1** Schematic representations of a SWNT and a MWNT (http://www-ibmc.u-strasbg.fr/ict/vectorisation/nanotubes_eng.shtml).

Since their discovery in 1991 [5], CNTs have generated great interest for possible applications in electrochemical devices [6–8]. CNTs are fullerene-like structures (Figure 1.1) that can be single-walled (SWNTs) or multiwalled (MWNTs) [9]. SWNTs are cylindrical graphite sheets of 0.5–1 nm diameter capped by hemispherical ends, while MWNTs comprise several concentric cylinders of these graphitic shells with a layer spacing of 0.3–0.4 nm. MWNTs tend to have diameters in the range 2–100 nm. CNTs can be produced by arc-discharge methods [10], laser ablation [11], or chemical vapor deposition (CVD) [12], which has the advantage of allowing the control of the location and alignment of synthesized nanostructures.

In a SWNT every atom is on the surface and exposed to the environment. Moreover, charge transfer or small changes in the charge environment of a nanotube can cause drastic changes to its electrical properties. The electrocatalytic activity of CNTs has been related to the "topological defects" characteristic of their particular structure; the presence of pentagonal domains in the hemispherical ends or in defects along the graphite cylinder produces regions with charge density higher than in the regular hexagonal network, thus increasing the electroactivity of CNTs [8, 13, 14]. For these reasons they have found wide application as electrode materials and a huge number of electrochemical biosensors have been described employing CNTs as a platform for biomolecule immobilization as well as for electrochemical transduction. The only limitation can be their highly stable and closed structure, which does not allow a high degree of functionalization [15]. Adsorption or covalent immobilization can only be achieved at the open end of functionalized nanotubes, after a proper oxidative pretreatment [16].

Another class of organic nanomaterials that, compared to CNTs, allows easier chemical modification is conductive polymer nanostructures. Conducting polymers are multifunctional materials that can be employed as receptors as well as transducers or immobilization matrices in electrochemical biosensing. They are characterized by an extended $\pi$-conjugation along the polymer backbone, which promotes an intrinsic conductivity, ranging between $10^{-14}$ and $10^{2}$ S cm$^{-1}$ [17]. Their electrical conductivity results from the formation of charge carriers ("doping") upon oxidizing (p-doping) or reducing (n-doping) their conjugated backbone [18]. In this way they assume the electrical properties of metals, while having the characteristics

of organic polymers, such as light weight, resistance to corrosion, flexibility, and ease of fabrication [19]. When formed as nanostructures, conductive polymers assume further appealing properties: ease of preparation by chemical or electrochemical methods, sensitivity towards a wide range of analytes, considerable signal amplification due to their electrical conductivity, and fast electron transfer rate. Moreover, they allow easy chemical functionalization of their structure in order to obtain high specificity towards different compounds, and are amenable to fabrication procedures that greatly facilitate miniaturization and array production [20].

Nanostructured conductive polymers can be obtained by "template" or "template-free" methods of synthesis, as widely reviewed [21–25]. "Template" synthesis involves the employment of physical templates, such as fibers or membranes (hard templates), or chemical template processes (soft templates), such as emulsion with surfactants, interfacial polymerization, radiolytic synthesis, sonochemical and rapid mixing reaction methods, liquid crystals, and biomolecules [25].One of the most versatile classes of nanomaterials is the nanoparticle. Depending on their composition (metal, semiconductor, magnetic), nanosize particles (or beads) exemplify different functions in electroanayltical applications. Metal nanoparticles provide three main functions: enhancement of electrical contact between biomolecules and electrode surface, catalytic effects, and, together with semiconductor ones, labeling and signal amplification [26]. They are typically obtained by chemical reduction of corresponding transition metal salts in the presence of a stabilizer (self-assembled monolayers, microemulsions, polymers matrixes), which give the surface stability and proper functionalization, in order to modulate charge and solubility properties [27]. Among them, the most widely used have been gold nanoparticles (Au-NPs) because of their unique biocompatibility, structural, electronic, and catalytic properties.

Magnetic particles act mainly as functional components for immobilization of biomolecules, separation, and delivery of reactants. The magnetic core–shell is commonly constituted by iron oxides, obtained by coprecipitation of Fe(II) and Fe(III) aqueous salts by addition of a base. Upon modulating synthetic parameters, it is possible to obtain the required characteristics for biomedical and bioengineering applications, such as uniform size (smaller than 100 nm), specific physical and chemical properties, and high magnetization [28]. Moreover, with proper surface coating, biomodification and biocompatibility can be achieved.

The next three sections are dedicated to illustrating the most interesting applications of each class of these materials for the realization of catalytic as well as affinity electrochemical biosensors.

## 1.2 Carbon Nanotubes

Different types of devices have been reported depending on the CNT electrode constitution, bioreceptor employed (enzymes, antibodies, DNA), and immobilization strategy (covalent, noncovalent). The majority of them have been obtained by

modifying carbon electrode surfaces (mainly glassy carbon (GC) or carbon paste) with a dispersion of CNTs in polymers or solvents, thus increasing the sensitivity of the analysis by orders of magnitude with respect to the bare electrode surface. Solvents like dimethylformamide (DMF), ethanol, or polymeric compounds like chitosan and Nafion are the most used dispersion matrices for this kind of process. Moreover, further advantages have been demonstrated to derive from the employment of electrode surfaces based on highly ordered and vertically aligned CNTs.

### 1.2.1 Carbon Nanotubes Used in Catalytic Biosensors

Many CNT-based enzymatic biosensors have been reported for the determination of various biochemicals (e.g., glucose, cholesterol, etc.) and environmental pollutants (e.g., organophosphate pesticides). A simple solution was achieved by Carpani *et al*. [29] by dispersing SWNTs in DMF with the aid of ultrasonication and dropping the suspension directly onto the electrochemically activated surface of GC electrodes. Glucose oxidase (GOx) was immobilized by treatment with glutaraldehyde as a cross-linker, both on bare GC- and SWNT-modified electrodes, and the response of the two types of sensor to glucose was evaluated. The SWNT/GC/GOx electrodes exhibited a more sensitive response, due to the enhanced electron transfer rate in the presence of CNTs. However, GC/GOx electrodes exhibited a lower background current, giving rise to a better signal to noise ratio.

Radoi *et al*. [30] modified carbon screen-printed electrodes (SPEs) with a suspension of SWNTs in ethanol. The nanotubes had been previously oxidized in a strong acid environment to generate carboxyl groups and covalently functionalized with Variamine blue, a redox mediator, by the carbodiimide conjugation method. The sensor was tested for the detection of nicotinamide adenine dinucleotide (NADH) by flow-injection analysis and the resulting catalytic activity was higher than that obtained using an unmodified SPE. Thus, nanostructured sensors were subsequently employed in $NAD^+$-dependent biosensors (i.e., for lactate detection). Upon detecting similar analytes, Gorton's group [31] reported an interesting study of the sensitivity-enhancing effect of SWNTs in amperometric biosensing, which depended on their average length distribution. They modified carbon electrodes with the enzyme diaphorase (which catalyzes the oxidation of NADH to $NAD^+$) and SWNTs using an osmium redox polymer hydrogel, then tested the sensor response towards NADH by varying the length of the nanotubes. Surprisingly, the best performance was achieved using SWNTs of medium length. The proposed explanation was a sensitivity-increasing effect caused mainly by the structural and electrical properties of the SWNTs, which have an optimum length (mainly depending on the type of redox enzymes) that allows both efficient blending and charge transport over large distances.

Jeykumari and Narayanan [32] developed a glucose biosensor based on the combination of the biocatalytic activity of GOx with the electrocatalytic properties of CNTs and the redox mediator Neutral red for the determination of glucose. MWNTs were functionalized with the mediator through the carbodiimide reac-

tion, and mixed with GOx and Nafion as a binder. The suspension was finally deposited on paraffin-impregnated graphite electrodes. The MWNT/Neutral red/GOx/Nafion nanobiocomposite film combined the advantages of the electrocatalytic activity of MWNTs with the capability of the composite material to decrease the electrochemical potential required. In this way the response to interfering substrates such as urea, glycine, ascorbic acid, and paracetamol became insignificant. In 2009, the same group [33] proposed an interesting approach to low-level glucose detection by creating a bienzyme-based biosensor. MWNTs were oxidized, functionalized with the redox mediator Toluidine blue, and grafted with GOx and horseradish peroxidase (HRP). These functionalized MWNTs were dissolved in a Nafion matrix and deposited on GC electrodes. In this way glucose reacts with GOx, in the presence of the natural cosubstrate $O_2$, to produce $H_2O_2$. $H_2O_2$, then, serves as substrate for HRP, which is converted to oxidized form by the redox mediator immobilized on MWNTs. The proximity of a mediator that transfers electrons between the enzyme and the electrode reduced the problem of interferences by other electroactive species. Moreover, the use of multiple enzymes enhanced sensor selectivity and chemically amplified the sensor response.

Another amperometric CNT/Nafion composite was developed by Tsai and Chiu [34] for the determination of phenolic compounds. MWNTs were dispersed within the Nafion matrix together with the enzyme tyrosinase and deposited on GC electrodes. In this way, MWNTs act as efficient conduits for electrons transfer, Nafion is an electrochemical promoting polymeric binder and tyrosinase is the biological catalyst that facilitates the translation of phenols into *o*-quinones, which can be electrochemically reduced to catechol without any mediator on an electrode surface. The MWNT/Nafion/tyrosinase nanobiocomposite-modified GC electrode exhibited a 3-fold higher sensitive response with respect to the Nafion/tyrosinase biocomposite-modified electrode, due to the inclusion of MWNTs within Nafion/tyrosinase matrices and the amperometric response was proportional to the concentration of several phenolic compounds in the analytically important micromolar range. A similar format had been previously developed by Deo *et al.* [35] in 2005, by casting with Nafion organophosphorus hydrolase on a CNT-modified transducer. Since the electrochemical reactivity of CNTs is strongly dependent upon their structure and preparation process, an interesting comparison between arc-produced MWNT and CVD-synthesized MWNT- and SWNT-modified electrodes was shown. By comparing their response towards *p*-nitrophenol, both the SW- and MW-CVD-CNT-coated surfaces exhibited a dramatic enhancement of the sensitivity compared to the arc-produced CNT and bare electrodes. The higher sensitivity of the CVD-CNT-modified electrode reflects a higher density of edge-plane-like defects that lead to higher electrochemical reactivity than previously found [8, 13, 14].

A better way to control the thickness of CNT/polymer films was described by Luo *et al.* [36], who reported a simple and controllable method for the modification of gold electrodes with a chitosan/CNT nanocomposite through electrodeposition. Compared to other solvents, chitosan can prevent biological molecules from denaturing and its primary amines facilitate enzymes attachment. Upon applying

current at the cathode, $H^+$ ions in the solution were reduced to $H_2$, thus increasing the pH near the electrode surface. As the solubility of chitosan is pH-dependent, when the pH exceeded the p$K_a$ of chitosan (about 6.3), chitosan became insoluble and entrapped CNTs onto the cathode surface. In this way, the thickness of the deposited nanocomposite film could be controlled by changing the concentration of the chitosan solution, deposition time and applied voltage. The nanocomposite exhibited excellent electrocatalytic ability for the reduction and oxidation of $H_2O_2$ and, by simply adding GOx to the CNT/chitosan solution before the electrodeposition, a glucose biosensor was developed. Chitosan was also employed by Qian and Yang [37] for the development of an amperometric biosensor for $H_2O_2$ detection, based on cross-linking HRP by glutaraldehyde with MWNT/chitosan composite film coated on a GC electrode. The enzyme-modified electrode exhibited excellent electrocatalytic activity and rapid response for $H_2O_2$ in the absence of a mediator, good repeatability, and absence of interferences by ascorbic acid, glucose, citrate acid, and lactic acid.

In 2007, Rubianes and Rivas [38] demonstrated a highly efficient way to immobilize CNTs on GC electrodes by dispersing them in polyethylenimine. The resulting electrodes showed a dramatic increase in sensitivity for $H_2O_2$ detection compared to bare GC electrodes and analogous dispersion in Nafion. This was explained by presupposing an irreversible adsorption of polyethylenimine onto the side walls of SWNTs, which causes an n-doping of the nanotubes due to the electron-donating ability of amine groups in the polymer. This approach was subsequently exploited by Mascini's group [39] for the modification of carbon SPEs for the realization of a disposable glucose biosensor with a wide linear range (0.5–3.0 mM). MWNTs were also coupled with screen-printing technology by Sanchez *et al.* [40], who described a CNT/polysulfone composite thick-film SPE for amperometric HRP-based biosensing. In this case, MWNTs were mixed with polysulfone and DMF, and used as ink for serigraphic deposition on previously printed working electrodes. The result was an interconnected CNT/polymer network, which was highly flexible, porous, and biocompatible with immobilized enzyme. The amperometric signal response was increased in comparison with analog graphite/polysulfone electrodes, thus demonstrating that the electrocatalytic properties of MWNTs are not diminished by incorporating them in polysulfone matrix. An interesting application of CNT-modified SPEs has been recently reported by Bareket *et al.* [41] to monitor the efficiency of prodrugs for the treatment of the human glioblastoma cell line U251 based on the release of formaldehyde. The biosensor, based on the coupling of formaldehyde dehydrogenase and CNT-modified SPEs, was placed in a chamber in the presence of cancer cells and different prodrugs were tested. The current response was 3-fold higher on the SPE-CNT than on an unmodified SPE biosensor. Moreover, it was higher for prodrugs that release two molecules of formaldehyde than for prodrugs that release only one molecule and no signal was obtained using homologous prodrugs that release acetaldehyde. Mineral oil [42], polyvinylchloride [43], and Teflon [44] were also employed as dispersing matrices by the groups of Rivas, Merkoci, and Pingarron, respectively, for NADH and glucose detection.

Pingarron's group [45] also synthesized a hybrid composite of MWNTs and the conductive polymer poly(3-methylthiophene) by electrodeposition on GC electrodes, and employed them as platform for lactate dehydrogenase immobilization and lactate detection. The biosensor showed an improved electrochemical oxidation of NADH, used as a cofactor for lactate dehydrogenase, compared to a GC electrode modified either with CNTs or with the conducting polymer separately. The synergistic effect observed with the hybrid material was attributed to the fact that the conducting polymer can immobilize and connect MWNTs, while the presence of MWNTs can interact with the polymer forming aggregates that facilitate charge transfer and increase the conductivity of the polymeric film.

Another conductive polymer, polypyrrole (PPy), was employed also by Ammam and Fransaer [46] for the realization of a highly sensitive MWNT-based glutamate oxidase amperometric sensor. The sensor was assembled by firstly electropolymerizing PPy onto a platinum electrode to serve as inner membrane to block interferences. Then a layer of MWNTs was deposited by AC electrophoresis in order to obtain a support for enzyme (glutamate oxidase) deposition and to increase the effective surface area of the sensor. A high sensitivity towards glutamate, a detection limit lower than 0.3 μM, low interference from endogenous interferences, fast response time (less than 8 s), and reasonable stability (30 days) was obtained. PPy was also employed by Ozoner *et al.* [47] to prepare a highly sensitive nanostructured surface obtained by electropolymerizing pyrrole monomers in the presence of MWNTs and tyrosinase on GC electrodes. The biosensor was tested for catechol detection and also in this case, in comparison with non-nanostructured films, the presence of CNTs enhanced the electron transfer between electrode and enzyme, allowing a detection limit of 0.671 μM, a linear range between 3 and 50 μM, a short response time (10 s), and long-term stability.

Zeng *et al.* [48] showed that DNA is an excellent dispersing matrix for SWNTs due the π–π interactions between the nanotube side walls and the nucleic acid bases, and applied this strategy to the realization of an HRP biosensor. The resulting HRP/DNA/SWNT composite was deposited on GC electrodes and the sensor showed excellent electrochemical activity to the reduction of $H_2O_2$ without using redox mediators, thus achieving a wide linear range ($6.0 \times 10^{-7}$ to $1.8 \times 10^{-3}$ M) and low detection limit ($3 \times 10^{-7}$ M).

Another highly promising CNT deposition approach is layer-by-layer self-assembly, which is based on electrostatic interactions. The alternate adsorption of negatively and positively charged individual components has become a simple and powerful method for the construction of a suitable microenvironment to retain enzyme activity [49]. Recently, this technique has been used to fabricate a CNT–enzyme multilayer composites for $H_2O_2$, glucose, and pesticides biosensing [50–52].

Zhang *et al.* [50] have reported a simple method to obtain a multilayer HRP biosensor. Firstly they dispersed carboxylated (negative) MWNTs and positively charged Methylene blue in barbital–HCl buffer, then, through electrostatic interactions, the nanocomposite was assembled in multiple layers with HRP on the gold electrode modified with precursor polyelectrolyte films. The enzyme

maintained its catalytic activity and a fast response towards $H_2O_2$ was achieved, producing a linear response range from 4.0 μM to 3.78 mM and a detection limit of 1.0 μM.

Another strategy for self-assembling a MWNT/GOx multilayer was elaborated by Yan *et al.* [51] on a flexible, transparent polyethylene terephthalate substrate. MWNTs were treated with sodium dodecyl sulfate (SDS) in order to facilitate CNT solubilization and, at the same time, to create a distribution of negative charges on the tube surfaces. After depositing a thin titanium and gold layer on the polymer substrate, an organic monolayer was formed on it via alternative electrostatic adsorption of the positively charged polyelectrolyte poly(dimethyldiallylammonium chloride) (PDDA) with negatively charged SDS/MWNTs and GOx. In this way the amperometric response could be controlled by varying the quantity of MWNTs and GOx by adding or reducing the layers. The glucose sensor obtained showed a linear response to glucose in the concentration range of 0.02–2.2 mM, with a very low detection limit of 10 μM. This particular format allowed great flexibility, light weight, portability, and low cost, and is well suited to commercial applications such as *in vivo* implantation, monitoring of changes in disease states and the effects of therapeutic agents. A layer-by-layer approach was also developed by Liu and Lin [52] for monitoring organophosphate pesticides by self-assembling acetylcholinesterase (AChE) on a GC electrode. CNTs were oxidized and kept at pH 8 in order to achieve negatively charged carboxylate anions, dispersed in DMF, and deposited on a GC electrode surface. The enzyme AChE was immobilized on the negatively charged CNT surface by alternatively assembling a cationic PDDA and AChE, thus obtaining a nanometer composite layer (thickness approximately 9 nm) that provided a favorable microenvironment to maintain the bioactivity of AChE. The developed biosensor integrated with an amperometric flow-injection system was used to detect paraoxon and a limit of detection (0.4 pM), 2.5 times better than that achieved with a nanoporous carbon matrix was obtained.

Despite progress made with layer-by-layer techniques, the main drawback of CNT-modified macroelectrodes is the low reproducibility of the nanostructured layer. Moreover, charge–charge attraction or hydrophobic interactions, which are the basis of enzyme entrapment, often lead to conformational changes of the protein that diminish its electrocatalytic function. A great improvement in this respect has been obtained by creating vertically aligned CNT arrays, which on the one hand work as electrode surface by themselves, while on the other hand provide a suitable platform for highly ordered immobilization of biosensing elements.

A possible approach has been demonstrated by Viswanathan *et al.* [53], who realized self-assembled monolayers of SWNTs on gold electrode surfaces by wrapping them with thiol-terminated single-strand oligonucleotide. A polyaniline (PANI) matrix was then electropolymerized on them for AChE immobilization and subsequent organophosphorus insecticide detection. The presence of SWNTs not only provided the conductive pathways to promote the electron transfer, but also increased the surface area and the flexibility of the enzyme supporting layer.

One limitation of such an assembly is that the highly conductive CNTs were not in direct contact with the electrode surface and thus electron transfer could be hindered.

A really powerful solution to this problem is directly aligned CNT fabrication, normally achieved by CVD technology. Up to now only a few papers have reported this kind of approach for the creation of enzyme biosensors. Lin *et al.* [54] reported a glucose biosensor based on CNT nanoelectrode ensembles made of low-site density aligned CNTs grown on a chromium-coated silicon substrate by plasma-enhanced CVD, using nickel nanoparticles as a catalyst. An epoxy-based polymer was then spin-coated on the substrate and covered half of the CNTs. Finally, the protruding parts of the CNTs were removed by polishing. In this way, each nanotube worked as an individual nanoelectrode and signal-to-noise ratio as well as detection limits could be improved. Moreover, good electrical conductivity was ensured by directly growing CNTs on the conductive substrate. GOx was immobilized directly on the broken tips of CNTs via carbodiimide chemistry for glucose detection, thus eliminating the need for permselective membrane barriers and mediators for delivering electrons from the enzyme center to the electrode. A different CNT array was realized by Withey *et al.* [55] using anodized aluminum oxide as template. MWNTs grown by CVD from hexagonally patterned template features were virtually identical in length, diameter, and spacing. Within the array, each individual tube was physically separated and electrically insulated by the insulating aluminum oxide template, and a direct electrical contact for each tube was made by sputtering the backside of the array with a layer of gold. Sensor response to glucose detection was evaluated by covalently linking GOx to the nanotube tips or noncovalently adsorbing the enzyme to the side walls. The first format exhibited a higher level of bioelectrocatalytic activity due to the highly ordered array configuration. A similar approach was also developed by Maghsoodi *et al.* [56] to obtain a highly porous CNT layer for GOx immobilization and highly sensitive glucose detection without a need for electron mediators. In this case a Fe/MgO catalyst layer was spin-coated on the insulating alumina, substrate and a mixture of SWNTs and MWNTs was obtained by CVD of methane at 950 °C.

One really innovative strategy in this field has recently been reported by Boo *et al.* [57] who fabricated a nanoneedle consisting of a MWNTs attached to the end of an etched tungsten tip, which is the smallest needle-type biosensor reported to date (diameter = 30 nm, length = 2–3 μm). A tungsten tip was electrochemically etched to form a sharp, long-tip geometry, to which a MWNT was coupled using a field-emission scanning electron microscope equipped with two piezoelectric nanomanipulators. The nanoneedle tungsten portion was sealed with a UV-hardening polymer to insulate it from the solution under study (only the MWNT was exposed) and to provide mechanical support. Glutamate oxidase was electropolymerized on the nanoelectrode and the amperometric biosensor was able to respond to the neurotransmitter glutamate in the 100–500 μM range. Due the sensitivity and the nanoscale, such a tool could offer considerable opportunities to investigate cell signaling and the dynamics of living cells.

### 1.2.2 Carbon Nanotubes Used in Affinity Biosensors

Despite the huge amount of papers published over the past few years regarding enzymatic biosensors, there has been little research done on CNT-based electrochemical immunosensors. In this case antibody orientation is crucial for molecular recognition. For this reason, despite some interesting work reporting casting of antibodies on SPEs [58–62], most of the work has been realized by preparing highly ordered vertical aligned CNTs arrays [62–68] with well-defined properties and uniform length and diameter, which also provide unique controllability of nanotube spatial density and conductivity compared to powder-type CNT electrodes.

In 2007, Sanchez *et al.* [58] reported the fabrication of a carbon nanotube–polysulfone/rabbit IgG "immunocomposite" on carbon SPEs. The construction procedure was similar to the one described by the same group for HRP biosensor development [40], in which serigraphy was employed to print the MWNT/polysulfone/rabbit IgG immunocomposite onto the reaction region of carbon SPE working electrodes. The biosensor was based on a competitive assay between free and labeled anti-IgG for the available binding sites of immobilized rabbit IgG. The electrochemical transduction was performed by labeling with HRP enzyme and using hydroquinone as mediator. Upon comparing the electrochemical response obtained using MWNTs with different length and diameter, 200-μm long nanotubes exhibited a sensitivity 5-fold higher then bare graphite, thus demonstrating that carbon nanostructures maintained their highly conducting properties even though they were immersed in a polysulfone matrix modified with rabbit-IgG antibody. The immunosensor was able to discriminate anti-rabbit IgG concentrations ranging from 2 to 5 μg/ml, showing lower nonspecific adsorption of anti-rabbit IgG/HRP.

Buch and Rishpon [59] employed Protein A to improve anti-C-reactive protein antibody orientation on SPEs modified with MWNTs. After modifying carbon surfaces with CNTs, polyethylenimine and glutaraldehyde cross-linker, Protein A was covalently immobilized on the electrodes in order to facilitate the orientation of the bound immunoglobulin. The electrodes were then immersed in human serum solutions containing different concentrations of protein and finally labeled with goat anti-C-reactive protein antibody conjugated with HRP. This format allowed the determination of C-reactive protein down to a concentration of $0.5\,ng\,ml^{-1}$, 20-fold lower than that obtained using unmodified electrodes ($10\,ng\,ml^{-1}$), due to the improved electron transfer kinetics and increased surface available for immobilization. In this way, higher dilution of the samples could be achieved thus reducing interferences given by serum matrix. A similar modification strategy was developed by Viswanathan *et al.* [60] for the design of a disposable electrochemical immunosensor for the detection of carcinoembryonic antigen (CEA)–a cancer marker glycoprotein. Polyethylenimine chains were ionically wrapped on the surface of carboxylic acid-functionalized MWNTs and dropped on carbon SPEs. The amine groups present in the polymer chains were further used

for anti-carcinoembryonic antibodies immobilization, and a sandwich immunoassay was performed with antigens and antibodies tagged ferrocene carboxylic acid encapsulated liposomes. The release of ferrocene carboxylic acid from the immunoconjugated liposomes on the electrode surface was detected by square wave voltammetry (SWV). This process was highly facilitated by the intimate connection with MWNTs, which provides a highly precise and sensitive determination of CEA in human blood serum and saliva samples. Another tumor marker, prostate-specific antigen (PSA), was detected by Panini *et al.* [61], by using an immunosensing microfluidic system formed by a GC electrode modified with MWNTs dispersed in a mixture of methanol, water, and Nafion. GC electrodes were also modified by He *et al.* [62] with MWNTs covalently linked to clenbuterol, a poisonous animal feed additive, for quantitative determination of the molecule using a competitive mechanism.

In addition to these interesting results, recent advances in nanotechnology and in semiconductor processing have made it possible to fabricate CNT arrays with extremely high density and compatibility for improved nanoimmunosensors. Such an innovative platform for bioelectroanalytical applications was reported by Okuno *et al.*, in 2007 [63]. They developed a CNT-based compact sensor by growing SWNTs directly on platinum electrodes, by thermal CVD. Platinum and titanium were patterned on a $SiO_2$ substrate, and covered with a second $SiO_2$ passivation film (100 nm). The film was partially etched using photolithography, thus creating an array of microelectrodes onto which SWNTs were synthesized by a thermal CVD method using an iron-containing catalyst. In this way, an array of 30 microelectrodes, with SWNT modification, was built on a single substrate. Electrochemical measurements of $K_3[Fe(CN)_6]$ and amino acids revealed that the electrochemical signals achieved using SWNT-arrayed microelectrodes were about 100-fold higher than those obtained using bare platinum microelectrodes. After this encouraging result, the chip was further employed by the same group [64] for the label-free detection of the cancer marker, total PSA, using differential pulse voltammetry (DPV). Total prostate-specific monoclonal antibodies were covalently immobilized on SWNTs and the amount of antigen detected by monitoring the increase of current signals, derived from the oxidation of tyrosine and tryptophan residues. High peak current signals were clearly observed using the SWNT-modified microelectrodes, whereas no signal was obtained with the bare platinum ones, thus indicating total PSA and the corresponding antibody were not nonspecifically adsorbed on the bare platinum microelectrodes. The detection limit for total PSA was determined as 0.25 ng $ml^{-1}$, 16-fold lower than the cut-off limit between prostate hyperplasia and cancer, thus proving promising for clinical applications.

CVD was also employed by Yun *et al.* [65] for the construction of CNT arrays cast in epoxy. Highly aligned MWNTs were grown on a $Fe/Al_2O_3/SiO_2/Si$ substrate. The substrate was subsequently patterned in blocks of 100 $\mu m^2$ and CNT towers up to 2 mm in height were grown within the blocks. Nanotubes were then peeled off the silicon substrate and cast in epoxy. Both ends were polished: one end for electrical connection, and the other end for chemical activation and covalent modification with anti-mouse IgG for an immunosensing application.

Electrochemical impedance spectroscopy (EIS) was used for label-free detection of the binding of mouse IgG to its specific antibody immobilized on the nanotube electrode surface, by monitoring the enhancement of electron transfer resistance with increase of analyte concentration (Detection Limit 200 ng $l^{-1}$). This procedure also facilitated scaling down the size of electrodes, thus improving the sensitivity and possibility of biomedical applications. A further step forward was achieved by same group in 2008 [66], by using a similar method to fabricate 8-mm long aligned MWNT array electrodes and electrochemically depositing Au-NPs onto the nanotube tips at the top of the array. This new approach could be the foundation for further nanobiosensor development using self-assembled monolayers and bioconjugation of antibodies on gold.

Other ways to obtain a so-called "SWNTs nanoforest" were based on SWNTs vertically assembled from DMF dispersions onto thin iron hydroxide-decorated Nafion conductive films [67–69]. Yu *et al.* [67] developed an alternative biosensor design based on orthogonally oriented SWNTs on conductive substrates, with higher packing density and thus superior mechanical properties than vertical SWNTs grown by CVD. These "forests" were assembled on pyrolytic graphite by forming a thin layer of Nafion on the surfaces onto which aqueous acidic (pH 1.7–1.9) $FeCl_3$ was adsorbed to precipitate $Fe(OH)_x$ on the surface. After the immersion of the substrates into DMF dispersions of shortened and oxidized SWNTs, vertical assemblies of nanotubes are formed (SWNT forests). The initial driving force for the formation of SWNT forests originated from acid–base neutralization between one of the two SWNT ends with basic $Fe(OH)_x$ domains formed by slow precipitation on Nafion-adsorbed $Fe^{3+}$ ions, involving trace amounts of water during the DMF washing step. The lateral bundled growth of the vertical SWNT domains was driven by the tendency of the assembly to reduce the overall hydrophobic surface area that originates from SWNT side walls. Protein immunosensors were obtained by covalently attaching antibodies to the carboxylated ends of nanotube forests and applied to the detection human serum albumin [68] and cancer biomarkers [69], with detection limits in the picomolar range.

Another really appealing aspect in the field of CNT-based electrodes is their employment for DNA sensing (nano-genosensors). Nanoscale geno-electronics represents the ideal molecular interfacing approach that, by exploiting DNA recognition event, could allow the realization of arrays able to measure the expression patterns of thousands of genes in parallel, helping to identify appropriate targets for therapeutic intervention and to monitor changes in gene expression in response to drug treatments [70]. Over the last 5 years, several genosensors have been realized employing CNTs as a platform for DNA immobilization and electrochemical transduction. While several platforms have been created by dispersing CNTs in polymers and solvents, only a few papers have reported genosensors based on self-standing CNT films.

Erdem *et al.* [71] reported a comparison between GC and graphite pencil electrodes modified with a suspension of DMF, by monitoring changes in the oxidation signal of guanine in a label-free assay based on the immobilization of a guanine-free DNA probe. MWNTs were oxidized, dispersed in DMF, and depos-

ited on the carbon surfaces. Both kinds of CNT-modified electrodes displayed higher voltammetric responses over their bare counterparts and especially over modified graphite pencil electrodes. The improved behavior was explained as originating from the highly porous composite structure of the graphite pencil electrode that allowed a higher inclusion of CNTs and consequently a higher surface area. A signal enhancement of 89% in comparison to bare unmodified electrodes was achieved. This aspect was further exploited by the same authors [72] for the study of the interaction between DNA and anticancer drugs, using SWNT-modified graphite pencil electrodes and covalently coupling amine group in the guanine bases of DNA to the carboxylated ends of nanotubes.

As already reported for other biosensors, several polymeric matrixes have been employed to fix CNTs on electrode surfaces. A dispersion of MWNTs in chitosan was combined with $ZrO_2$ nanoparticles by Yang *et al.* [73], in order obtain a composite layer on GC electrodes that, with its large surface area and good charge transport characteristics, provided a synergistic increase of DNA loading, current response towards the redox indicator employed (daunomycin) and improved detection sensitivity for DNA hybridization compared to MWNT/chitosan- or $ZrO_2$/chitosan-modified GC electrodes. Chitosan was also employed by Yang *et al.* [74] for the modification of GC electrodes with a highly performing nanocomposite based on MWNT and PANI nanofibers. Electrochemical characterization showed a considerable enhancement in conductivity and electrochemical activity of the sensors due to the synergistic effect of the two nanostructured components. Moreover, the very large surface area of the composites greatly increased the loading of the DNA probe, thus allowing a highly sensitive detection specific for DNA sequences related to transgenic genes in genetically modified crops, such as the phosphinothricin acetyltransferase gene and the terminator of nopaline synthase gene. Other composite coatings were obtained on carbon paste electrode surfaces by casting CNTs, Nafion, and tris(2,2′-(bipyridyl)ruthenium(II) ($Ru(bpy)_3^{2+}$) layers [75]. The genosensing format involved physical sorption of DNA onto an electrode surface, and guanine and adenine oxidation, catalyzed by $Ru(bpy)_3^{2+}$ present in the film.

Due to its negatively charged backbone, DNA can also be easily immobilized by electrostatic interaction. For this reason, cationic polymers also proved particularly appealing for CNT dispersion. Jiang *et al.* [76] electropolymerized poly-L-lysine with well-dispersed SWNTs (in DMF) on GC electrodes to prepare poly-L-lysine/SWNT/GC films for EIS detection of polymerase chain reaction (PCR) fragments. Carboxylic functionalized SWNTs were firstly dispersed in DMF, deposited on GC electrodes and then poly-L-lysine films were electropolymerized on them by cyclic voltammetry. DNA probes were easily immobilized on the poly-L-lysine films via electrostatic adsorption, since the amino groups of poly-L-lysine can bind the phosphate skeleton of DNA via electrostatic forces. The hybridization event was detected by monitoring the increasing of electron transfer resistance using electrochemical impedance spectroscopy, in the presence of an anionic redox couple as indicator, $[Fe(CN)_6]^{3-/4-}$. Electropolymerization was also used by Xu *et al.* [77], who reported an analog electrochemical impedance-based DNA biosensor by

using a composite material of PPy and MWNTs to modify a GC electrode. As a result of the PPy–MWNTs modification, the electrode showed properties characteristic of both constituent components, such as large surface area, as well as mechanical stability and efficient thermal/electrical conduction. A detection limit of $5.0 \times 10^{-12}$ mol $l^{-1}$ was achieved as well as good selectivity towards one-base mismatched sequence (the signal was 35.5% of the one obtained with the complementary sequence).

A really interesting application of nanostructured genosensors was shown by Huska *et al*. [78] who coupled gel electrophoresis, a standard and reliable separation technique, with CNT-based SPEs for quantification of PCR-amplified sequences ("off-line coupling"). Carbon SPEs and carbon-modified analogs were placed in the wells of the agarose electrophoretic gel, and the amount of migrated amplicons detected by SWV. By using this approach, amplicons obtained after two cycles were detected in the presence on CNTs (and after 10 cycles without CNTs).

Even greater advantage may be derived from the employment of highly ordered and vertically aligned CNT surfaces. Vertical orientation of the nanostructures could in turn greatly facilitate vertical orientation of the immobilized probe, making it more accessible for the complementary sequence. Moreover, technologies required for the construction of such surfaces are compatible with device miniaturization, thus allowing the realization of nanoscale genomic arrays. He *et al*. [79] proposed a genosensor obtained by covalently grafting DNA on the tip and wall of gold-supported aligned CNTs, generated from pyrolysis of Fe(II) phtalocyanine in acetic acid atmosphere. Upon using ferrocene carboxaldehyde as a redox indicator, the hybridization event was achieved with high sensitivity and selectivity. More recently, Berti *et al*. [80] reported the design and testing of different vertically aligned MWNTs thin films for DNA immobilization and genosensor development. The sensors were realized by thermal CVD onto insulators ($SiO_2$, $Si_3N_4$) as well as metallic substrates using acetylene and ammonia as precursor gases, and the best performance was obtained with nanotubes grown on an aluminum layer able to serve as growing substrate as well as electrical contact. Combining such an electrode platform with covalent DNA immobilization on the open ends of the tubes and enzyme labeling of the hybrid, a detection limit in the nanomolar range of oligonucleotide target was achieved.

Another very interesting platform was realized by Meyyappan *et al*. [81], consisting of nanoelectrode arrays obtained by embedding vertically aligned CNTs in a $SiO_2$ matrix, thus providing structural support to the nanostructures and improving their chemical coupling to nucleic acid. MWNTs were grown using a plasma-enhanced CVD process and oxidized for further covalent DNA immobilization using a plasma treatment. In order to assure the mechanical stability of the nanotubes, a film of spin-on glass was used to fill the gaps between the individual CNTs in the array, thus providing structural support to nanostructures, enabling them to retain their vertical configuration during the subsequent purification and tip opening process. Moreover, it served as a dielectric material, able to insulate the individual nanotubes from their neighbors. This format, in combination with $Ru(bpy)_3^{2+}$-mediated guanine oxidation was employed for the determination of a few attomoles of oligonucleotide DNA [82] as well as PCR amplicons with a sen-

sitivity comparable with florescence-based DNA microarray techniques (hundreds of hybridized targets per spot) [83]. Recently, this method has been further developed [84] by coupling optical and electron beam lithography with CVD in order to obtain a chip formed of nine individually addressable arrays of vertically aligned carbon nanofibers. Thanks to the combination of the three techniques, nanofibers were precisely grown on 100-nm nickel dots deposited with 1-μm spacing on each of the nine micro pads that formed the array. The sensor was tested for the electrochemical detection of DNA targets from *Escherichia coli* by exploiting the array format for simultaneously testing a positive control (mismatch probe), a negative control (no probe), and specific hybridization. The proposed method has the potential to be scaled up to $N \times N$ arrays (with $N$ up to 10), which could be ideal for detecting hundreds of different organisms.

## 1.3 Conductive Polymer Nanostructures

As stated above, conductive polymers are very easy to functionalize, thus proving particularly promising for biosensing applications. However, an important aspect to be considered, when using them in the design of electrochemical sensors, is the integration between the electron transfer mechanism at the electrode surface and the subsequent charge transport through the polymer backbone [25]. Both covalent and noncovalent strategies have been developed and reviewed for this purpose [85–87].

Covalent approaches may comprise grafting of polymer nanostructures with functional groups. This strategy ensures that the nanomorphology is unaffected [88]. Alternatively, properly functionalized monomers can be used that, after polymerization, confer specific binding sites for different bioreceptors (such as antibodies, enzymes, nucleic acids, aptamers, or cells). Moreover, covalent binding processes often require aqueous buffer solutions that preserve the catalytic activity or the recognition properties of the biomolecule [86]. Noncovalent methods are mainly based on physical entrapment or electrostatic interactions between the polycationic matrix (consisting of the oxidized polymer) and negative biomolecules such as DNA or proteins (enzymes, antibodies), provided that the pH is higher than the isoelectric point (p*I*) [85]. The drawback in this case is worse control of the orientation of the bioreceptor, which can lead to a less accessibility for the substrate.

The following sections provide an overview of the progress made in the application of conductive polymers in the biosensor field. The main classes of conductive polymers are illustrated in Figure 1.2.

### 1.3.1 Conductive Polymer Nanostructures Used in Catalytic Biosensors

Among conductive polymers, PPy is arguably the most widely employed in biosensing, especially as an immobilization substrate for biomolecules. Compared to

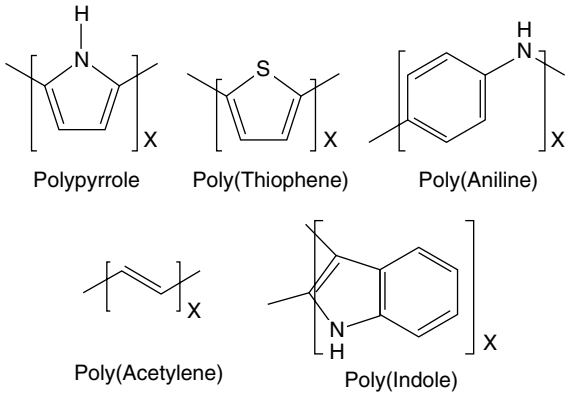


**Figure 1.2** Main classes of conductive polymers [85].

other polymers, such as PANI and polythiophene, PPy can be easily polymerized in a neutral environment, thus proving particularly suitable for biological matrixes [89].

The first example of the use of nanostructured PPy for enzyme immobilization in biosensors was reported in 1992 by Koopal *et al.* [90], who described template synthesis of PPy microtubules inside track-etch membranes for glucose biosensing. GOx was adsorbed within the tubules and glucose was then measured amperometrically. The interesting aspect of this work was the observation that the enzyme was immobilized only inside the tubules and not on the surface of the membrane, because the corrugation of the interior surface of the PPy tubules matched the dimension of GOx, and thus resulted in an intimate connection between the transducer and the bioreceptor.

A nanoporous glucose biosensor was also later developed by Ekanayake *et al.* [91] using platinum plated-alumina substrates. PPy was electrochemically deposited on the top surface as well as inside walls of the platinum nanoholes, thus obtaining a PPy nanotube array and, consequently, a greatly enhanced surface area for GOx immobilization by simple physical adsorption. A significant improvement was demonstrated in the amperometric responses compared to analogous non-nanostructured PPy films created on indium/tin oxide (ITO) electrodes.

Carboxylated PPy monomers were also employed by Shamsipur *et al.* [92] in order to obtain cauliflower-like nanostructures by electropolymerization on platinum disks. Impedance studies of the nanostructured films before and after the immobilization of cytochrome *c* showed good features for the development of a novel $H_2O_2$ biosensor with good sensitivity, dynamic range, detection limit (0.25 μM), and stability.

A higher sensitivity was obtained by Lupu *et al.* [93] using a new sensor platform based on nanoarrays of PPy nanopillars, obtained using nanosphere lithography. Polystyrene beads deposited on a gold surface were reduced in size by plasma etching, covered with an insulating layer, and subsequently removed, thus leaving

nanoholes on the surface. PPy nanopillars were grown into the holes and the redox mediator Prussian blue (ferric ferricyanide) incorporated in the PPy network by electropolymerization ("artificial peroxidase" sensor). In this way, as PPy is conductive in the potential range where the mediator is electroactive, charge propagation across Prussian blue redox centers was enhanced and very low concentrations of HRP ($10^{-9}$ M) was detected using chronoamperometry.

One of the drawbacks of PPy is its poor long-term stability and, in particular, the decrease of electrical conductivity with the increase of temperature and humidity [94]. For this reason, several groups found in polythiophene and derivates, such as polyethylenedioxythiophene (PEDOT), a valid alternative for the realization of nanotubes and nanowires with better environmental stability, and easier control of electrical and optical properties [95]. The first example was reported by Kros *et al.* [96] who reported an amperometric glucose biosensor based on track-etched membranes coated with PEDOT nanotubules. The sensor was designed in order to increase the electrostatic interaction between the negatively charged GOx and the positively charged conducting polymer to obtain a biosensor with a higher response to glucose, due to more efficient electron transfer. In order to obtain a high density of positive charges, polymerization of 3,4-ethylenedioxythiophene was carried out in the presence of the polycation poly-(*N*-methyl-4-pyridine). Subsequently, GOx was immobilized inside the polymer-coated pores and the membranes mounted in a three-electrode cell incorporated in a flow system. A sensitivity of 45 nA $mmol^{-1}l^{-1}$ was achieved with the same sensor over a period of 30 days, thus demonstrating a high stability and suitability for long-term glucose measurements. The influence of nanostructured polythiophene morphology in amperometric glucose sensing was also investigated by Liu *et al.* [97]. They produced nanostructured films by electrochemical copolymerization of 3-methylthiophene and thiophene-3-acetic acid, and found that once the copolymer film grew over a critical thickness, a spontaneous formation of nanostructures occurred, probably depending on changes in the chain length of deposited oligomers and formation of a branched structure as the film thickened.

Another interesting glucose biosensor was demonstrated by Park *et al.* [98] who fabricated a nanotubular array upon electrochemically polymerizing 3,4-ethylenedioxythiophene into a template polycarbonate membrane fixed onto an ITO electrode. Polymer-coated pores formed nanotubes which were loaded with GOx solution, then sealed with a PEDOT/poly(styrenesulfonate) composite cap in order to block the enzyme inside the tubules, but at the same time to allow analytes and oxygen to permeate into the sensing system. In this way the dynamic range of the sensor was enhanced (0–8 mM) and a good selectivity towards interfering compounds (ascorbate and acetaminophen) was achieved.

More recently, a new composite consisting of PEDOT nanofibers and palladium nanoparticles was obtained by a new methodology involving a micellar "soft template" approach [99]. A surfactant (SDS) and an ionic liquid (1-butyl-3-methylimidazolium tetrafluoroborate) were used to form cylindrical micelles that, after monomer addition, were electrodeposited onto the electrode surface, thus obtaining PEDOT nanofibers. Further addition of palladium nanoparticles and

GOx led to the creation of a glucose biosensor, the sensitivity of which was enhanced by the synergistic effect of the nanofibrous PEDOT and the nanoparticles (DL 75 μM). The sensor was also tested with real samples and the results were found to be in good agreement with a reference commercial glucose meter (error 3.24%).

A remarkable *in vivo* study was reported by Rahman *et al.* [100] who developed a PEDOT nanoparticle-based biosensor for monitoring the change in extracellular glutamate levels in response to cocaine exposure. A layer (100 nm) of PEDOT nanoparticles was obtained on a platinum microelectrode by cyclic voltammetry at high scan rate ($1\,V\,s^{-1}$). Subsequently, glutamate oxidase was immobilized in the presence of ascorbate oxidase (to eliminate the ascorbate interference) through the formation of covalent bonds between the carboxylic acid groups of the polymer and the amine groups of the enzymes. The resulting glutamate biosensor was firstly tested *in vitro* with very good results (linear range between 0.2 and 100 μM, DL 0.1 μM), then employed to monitor the extracellular fluctuation of glutamate. For this purpose, the microbiosensor was implanted in a rat's brain and, after repeated injections of cocaine, the increase of basal glutamate levels was monitored.

Among conducting polymers, the class of compounds which recently has been widely investigated for sensing applications is PANI because of its inexpense, easy availability of raw materials for its synthesis, ease of processing, high conductivity, and simple doping process [101]. Despite its extensive application in electrochemical biosensing, mostly as an enzyme or antibody immobilization matrix [86], the performance of conventional PANI films is strongly thickness dependent: the higher the thickness, the poorer the diffusion of analytes towards the sensing element and consequently the sensitivity of measurements decreases [102]. For this reason, considerable attention has been paid to the realization of one-dimensional polymer nanostructures that, due to their greater exposure area, offer the possibility of enhancing the diffusion of analyte towards the transducer. PANI nanofiber sensors have been employed in gas and chemical detection – in all cases, nanostructures performed better than conventional thin films [103, 104].

High-performance composites for bioanalytical applications have been obtained by coupling PANI nanostructures with biologically functional materials (i.e., enzymes, bio- or synthetic receptors). One of the first examples was reported by Morrin *et al.* in 2004 [105], who described the use of PANI nanoparticles for the modification of GC electrode surfaces flowed by immobilization of HRP for $H_2O_2$ sensing. Such nanoparticles were obtained in aqueous media using dodecylbenzene sulfonic acid as doping agent and electrochemically deposited on the electrode surface, thus forming a highly conductive nanostructured film that allowed a uniform electrostatic adsorption of enzyme. Results obtained for $H_2O_2$ biosensing were compared with an analogous non-nanostructured film deposited from bulk monomer solutions. The nanostructured surface proved more efficient, both in terms of protein immobilization (it required a concentration 6-fold lower for homogeneous coverage) and signal-to-noise ratio (3 : 1).

Another interesting nanostructured surface was obtained by Luo *et al.* [106] on carbon SPEs. Polystyrene nanoparticles (diameter 100 nm) were self-assembled on

SPEs and acted as templates for the electropolymerization of a PANI layer (thickness 10–30 nm), which assumed a cauliflower-like nanostructured shape providing a very large immobilization surface. HRP was further deposited using chitosan as immobilization matrix and amperometric determination of $H_2O_2$ was carried out. The biosensor exhibited a fast response time of about 5 s, a detection limit of 0.36 mM, and a high sensitivity of 41.0 mA $mM^{-1}$, due to the benefits of the nanostructured PANI.

Another HRP-based biosensor was recently developed by Du *et al.* [107] using PANI nanofibers synthesized by interface polymerization in the presence 4-toluensulfonic acid as dopant. Nanofibers were dispersed in chitosan together with HRP and cast onto GC electrodes. Good analytical performance (linear range $1 \times 10^{-5}$M to $1.5 \times 10^{-3}$M, DL $5 \times 10^{-7}$M) was obtained due to the highly efficient enzyme loading and rapid electron transfer rate between the active center and electrode, favored by the presence of PANI nanofibers. PANI nanoparticles were also employed by Wang *et al.* [108] for the realization of a new immobilization and detection platform for $H_2O_2$ biosensing based on an Au/Pt-NP/nano-PANI composite on GC electrodes. Au/Pt alloy nanoparticles and nano-PANI exhibited a synergistic effect on electron transfer, thus facilitating a fast response time (below 2 s) and wide linear range (1.0–2200 μM).

A Au-NP/PANI nanorod composite was developed by the Willner group [109] in order to provide a highly enhanced surface area with superior charge transport properties for efficient contacting of GOx with the electrode surface. PANI nanorods were obtained by a template synthesis inside porous alumina templates coated on one side with a gold layer. Au-NPs were further incorporated inside the pores before removing the template and GOx biocatalytic activity was then studied. From the electrochemical characterization of the system a 4-fold increase of anodic currents was observed, in comparison with analogous noncomposite homogeneous PANI layers. The higher bioelectrocatalytic activity of the Au-NP/PANI nanorod assembly was attributed to the enhanced charge transport properties of the Au-NP/polymer matrix.

The enhancement of GOx catalytic activity in the presence of a polymeric nanostructured surface was also investigated by Zhao *et al.* [110]. They reported the creation of PANI nanofibers obtained by interfacial polymerization in the presence of ammonium peroxydisulfate and cast on GC electrodes. The GOx/nano-PANI/GC electrode was fabricated by covalently attaching GOx on the surface of the PANI nanofibers via a carbodiimide coupling reaction. The interesting aspect of this work was a voltammetric study of the biocatalytic activity of GOx immobilized onto the nanostructured composite electrodes, which showed a 6-fold higher electron transfer rate with respect to previous reported GOx-modified electrodes.

A simple and effective new route for PANI nanowire construction and application in glucose biosensing was shown by Horng *et al.* [111]. PANI was directly grown on carbon cloth via electrochemical polymerization, thus obtaining free-standing, template-independent nanowires. Carbon cloth was specifically selected as a support because of its high porosity, chemical stability, high conductivity, cost-effectiveness, and flexible nature, which could be suitable for designing *in*

*vivo* devices. The template-free nanostructure construction consisted of a first nucleation stage, upon applying a proper potential (by linear sweep voltammetry), and subsequent growth under galvanostatic conditions. GOx was electrostatically adsorbed and glucose sensing was performed with excellent sensitivity ($2.5\,mA\,mM^{-1}\,cm^{-2}$) over a detection range claimed to be adequate for clinical monitoring of human glucose levels (0–8 mM).

A way to obtain highly ordered vertical PANI nanotubes was developed by Wang *et al.* [112] using anodic aluminum oxide membrane as template and electropolymerizing the aniline monomers inside the pores by cyclic voltammetry. An amperometric glucose biosensor was then realized by electrostatically incorporating GOx (negatively charged at physiologic pH) in positively charged PANI nanotube inner walls. The biosensor exhibited a good electrocatalytic activity towards the oxidation of glucose and a low detection limit (0.3 μM) in a useful linear range (0.01–5.5 mM) was achieved. Moreover the biosensor resulted selective towards common interfering species (ascorbic acid, uric acid, 4-acetamidophenol).

The kinetics of a different enzyme was studied by Somerset *et al.* [113], who chose AChE in combination with PANI nanorods as an innovative tool for pesticide biosensing. In order to obtain better solubility, PANIs bearing particular substituent groups were synthesized (poly-*o*-methoxy aniline, poly-2,5-dimethoxy aniline) and AChE was encapsulated in the nanopolymeric composite deposited on a gold electrode. The biosensor was applied to the study of the inhibition caused by diazinon and carbofuran pesticides and a detection limit of 0.14 and 0.06 ppb, respectively, was calculated.

PANI nanotubes were fabricated via electrophoretic deposition on ITO electrodes by Dhand *et al.* [114] and utilized for covalent immobilization of lipase for triglyceride detection. From impedimetric investigation they found that charge transfer resistance decreases linearly with increased triglyceride concentration because lipase hydrolyzes tributyrin, thus generating protons and fatty acids in addition to glycerol. The consequent lowering of pH resulted in increased positively charged quinoid moieties on the PANI nanowire backbone, thus enhancing the charge transfer rate (resistance decreased). The biosensor was tested both in pure solution and in serum, and exhibited a discordance of only 5.4%, thus indicating a negligible interference of proteins and other moieties present in the real matrix.

### 1.3.2
### Conductive Polymer Nanostructures Used in Affinity Biosensors

Apart from the more common catalytic enzyme-based biosensors, a number of DNA biosensors have also been developed using PPy and PANI nanostructures. Ozcan *et al.* [115] prepared PPy nanofiber-modified pencil graphite electrodes for the investigation of double-stranded DNA electrochemical oxidation. Nanofibers were obtained by electropolymerization of pyrrole in the presence of $Na_2CO_3$ and $LiClO_4$ upon applying a constant potential. Under the same conditions, but in the absence of carbonate, a PPy film was obtained and results were compared with

those obtained with nanofibers, which exhibited a shift to the more cathodic potential of the guanine and adenine bases as a result of the catalytic effect of nanofiber PPy.

Ko *et al.* [116] reported the formation of carboxylic acid-functionalized PPy nanotubes using aluminum oxide membranes and their application for DNA measurement. After soaking with an oxidant solution (iron chloride), membranes and pyrrole-3-carboxylic acid monomers were placed in a reactor and allowed to polymerize under high pressure. In this way, the authors obtained nanofibers covered with carboxylic groups, which acted as binding sites for amino-tethered oligonucleotides. Conductance changes after the hybridization with different amounts of complementary DNA sequence were measured by depositing functionalized fibers on gold pads and high sensitivity at low analyte concentration was obtained (1 nM). Moreover, this particular sensor design showed promise for future application as a nanosensor and for lab-on-a-chip technology, due the possibility of manipulating and contacting a single nanofiber to act as sensor.

In 2006, Zhu *et al.* [117] fabricated PANI nanowires and modified them with oligonucleotides probes for DNA hybridization detection. Nanowires of a diameter of 80–100 nm were directly synthesized on GC electrodes thorough a three-step electrodeposition of monomer containing solution. In the first polymerization step the polymer was deposited on the electrode surface as small particles, which served as seeds for the growth of nano-frameworks during the following steps, consisting of two continued polymerizations at reduced current density. Oligonucleotides were covalently immobilized through the formation of phosphoramidate bonds between the amino groups of the PANI and phosphate groups at the 5′-end. The hybridization event was measured by DPV, using Methylene blue as indicator. A good discrimination between complementary and non-complementary DNA sequences was achieved, with a detection limit of $1.0 \times 10^{-12}$ mol l$^{-1}$.

Chang *et al.* [118] reported the realization of a PANI nanotube array as platform for immobilization and sensitive detection of oligonucleotide sequences. A good aligned and oriented PANI nanotube array was obtained on graphite electrodes using alumina nanoporous layers as template. As already stated in the case of CNTs, vertical alignment greatly favors orientation and accessibility of DNA probes. Oligonucleotide probes were covalently immobilized on the surface of inner and outer walls of PANI nanotubes, making each PANI nanotube work like a signal amplification nanodevice for the hybridization event. After labeling the hybrid with daunorubicin, the DPV response showed that the PANI nanotube array had a signal enhancement capability, allowing the detection of target oligonucleotides at femtomolar level and a good differentiation between perfect match and one-base mismatched sequences.

PANI nanostructures and metal nanoparticle composites were also used for the development of DNA biosensors. Feng *et al.* [119] created Au-NP/PANI nanotube (diameter around 100 nm) membranes on GC electrodes for the impedimetric investigation of the hybridization event. Also in this case the synergistic effect of the two nanomaterials dramatically enhanced the sensitivity and detection limit ($1 \times 10^{-13}$ mol l$^{-1}$) of specific DNA sequences with respect to other DNA biosensors

realized by the same group. In addition to Au-NPs, Zhou *et al.* [120] also incorporated CNTs in the PANI nanofiber composite in order to further enhance the electron transfer rate and the available surface for oligonucleotide immobilization. PCR amplicons related to transgenically modified products were determined with label-free impedance measurements, achieving a detection limit of $5 \times 10^{-13}$ mol l$^{-1}$.

Another class of polymeric compounds which should be mentioned in the present section consists of nanostructures and nanocomposites of molecularly imprinted polymers (MIPs). MIPs are synthetic polymers with artificial recognition cavities [121]. The imprinting technique consists of using the target molecule as a template for synthesizing polymers. Polymerization of functional monomers occurs in the presence of the template, which directs the positioning and orientation of the material structural components by a self-assembly mechanism. Subsequent removal of the template leaves specific recognition sites in the MIP matrix that are capable of rebinding the target molecules in preference to other closely related molecules. The particular interest this class of compounds has generated is due to three main characteristics: their high affinity and selectivity (similar to those of natural receptors such as enzymes and antibodies), a unique stability, which cannot be found in natural biomolecules, and an ease of preparation, suitable for mass production [122]. The main challenge in designing MIP-based electrochemical sensors is the integration between the recognition and the transduction element. Imprinted polymers, in fact, are mainly based on acrylic or vinylic compounds, which are electrical insulators – this feature could strongly limit their use as receptors in electrochemical sensors, because of the lack of a direct path for conduction from the active sites to the electrode. For this reason, conductive and semiconductive MIPs, such as imprinted PPy, aniline, and aminophenyl boronic acid, have been extensively investigated [123–125]. These MIPs can be directly integrated with the transducer surface using electropolymerization, thus obtaining substrate-selective electrodes (*in situ* imprinting). Moreover, with respect to other immobilization techniques, electropolymerization allows the deposition of receptors at precise spots on the transducer, and the regulation of thickness and polymer density by simply varying electrochemical parameters.

Molecular imprinting technology appears, therefore, a highly promising tool to realize nanosized devices. The advantage can be found not only in the size itself, but also in the increase of equilibrium rate with the analyte and significant enhancement of accessible complementary cavities per material weight [126]. MIP nanofibers and nanowire arrays have been made using the classical approach of template synthesis with alumina nanoporous membranes [127–129]. Another approach to produce polymer nanostructures is electrospinning (ejection of a liquid seed material from a capillary tube at high voltage), which has been employed for the preparation of MIP nanofibers with diameters of 100–300 nm for the recognition of theophylline and estradiol [130, 131].

In order to apply these materials for sensor construction, MIPs have to be patterned on chip surfaces and interfaced with the transducers. Patterning techniques, mainly based on photolithography, soft lithography, and microspotting, have been developed [126], but research in this field is still very challenging and

opens great opportunities for future development of highly sensitive and miniaturized electrochemical devices.

## 1.4 Nanoparticles

Nanoparticles have been employed in an enormous variety of bioanalytical formats; in only the last 5 years, more than 300 papers have been published in the main international scientific journals, illustrating the versatile range of application of nanoparticles as quantification tags, immobilization substrates, for signal amplification, and as carriers. For this reason, this section will present only a brief overview of the fundamental characteristics that have made nanoparticles so interesting for biological sensing, with some examples of the more exciting recent applications.

### 1.4.1 Nanoparticles Used in Catalytic Biosensors

Au-NP/enzyme hybrid systems have been widely investigated by the Willner group [132, 133] in order to overcome the lack of electrical communication often observed between redox enzymes and an electrode surface. Biocatalytic electrodes were prepared by conjugation of apo-GOx (apoprotein form) with Au-NPs functionalized with a flavin adenine dinucleotide cofactor unit extracted from active GOx and self-assembled on a dithiol-modified gold electrode. In this way, nanoparticles were implanted in intimate contact with the active site of the enzyme, thus forming a hybrid architecture that facilitated the electrocatalytic oxidation of glucose, thanks to highly efficient electron transport.

Other Au-NP–enzyme composites were investigated by the Pingarròn group [134, 135]. A xanthine oxidase biosensor for hypoxanthine detection was realized using carbon paste electrodes modified with electrodeposited Au-NPs, onto which the enzyme was cross-linked with glutaraldehyde and bovine serum albumin [134]. This format allowed the determination of hypoxanthine at lower potential (0 V) thus minimizing interference by ascorbic acid. Another enzyme biosensor was fabricated using graphite/Teflon electrodes in which tyrosinase and Au-NPs were incorporated [135]. The presence of colloidal gold particles enhanced kinetics of both the enzyme reaction and the electrochemical reduction of the analyte (*o*-quinones) at the electrode, thus providing a high sensitivity for catechol and other phenolic compounds detection (20 nM).

Orozco *et al*. [136] demonstrated the role of Au-NPs in enhancing the voltammetric performance of ultra-microelectrodes-based biosensors through a comparative study of bare and nanoparticle-modified surfaces using HRP as a model recognition element. HRP was covalently immobilized by means of a thiol self-assembled monolayer used for the amperometric detection of catechol. The use of Au-NPs increased the sensitivity of the developed biosensor 3-fold with respect

to bare microelectrodes. A mediator-less HRP-based biosensor was developed by Chico *et al.* [137] by exploiting the electron transfer activity of Au-NPs. The enzyme was cross-linked with cysteamine-capped Au-NPs and further immobilized on a sodium alginate-coated gold electrode through polyelectrostatic interactions. The resulting biosensor showed linear response towards $H_2O_2$ between 20 and 13.7 μM and a detection limit of 3 μM. A composite of Au-NPs and silk fibroin was employed by Yin *et al.* [138] for the modification of platinum electrodes and the construction of a biosensor for monitoring carbamate and organophosphate pesticides, based on the inhibition AChE activity. In this way silk fibroin provided a biocompatible microenvironment for AChE immobilization and preservation of its biological activity, while Au-NPs promoted electron transfer reaction at a lower potential and catalyzed the enzymatic reaction, thus increasing the sensitivity of the sensor.

Magnetic nanoparticles have also been involved in the construction of composite biocatalytic assays. A biosensor based on a $Fe_3O_4$ nanoparticle/chitosan nanocomposite was developed for the determination of phenolic compounds [139]. The large surface area of nanoparticles and the porous morphology of chitosan allowed a better loading of enzyme without compromising its bioactivity. The biosensor exhibited a linear range from $8.3 \times 10^{-8}$ to $7.0 \times 10^{-5}$ mol l$^{-1}$, and a detection limit of $2.5 \times 10^{-8}$ mol l$^{-1}$ for catechol detection. Mavré *et al.* [140] prepared self-assembled aggregates of iron oxide nanoparticles, avidin, and a biotinylated diaphorase oxidoreductase for bioelectrocatalytic oxidation of NADH. This method represented a very simple, fast, and efficient route for the construction of highly loaded enzyme electrodes. Upon applying a magnet, the magnetic enzyme aggregate was collected on a carbon SPE and catalytic currents recorded by cyclic voltammetry. The response obtained was much higher than that measured at an electrode directly coated with a packed film of diaphorase.

Further advantages have been demonstrated to arise from the combination of Au-NPs with CNTs [44] or conductive polymers such as PPy and PANI [141].

### 1.4.2
### Nanoparticles Used in Affinity Biosensors

Many particle-based routes have been investigated for gene detection and immunosensing. These protocols are based on colloidal gold tags but also on polymer carrier beads and quantum dot (QD) tracers (semiconductor nanocrystals ranging from 2 to 10 nm in diameter). With respect to traditional labeling techniques, nanoparticles offer several advantages: higher stability (enzyme label and isotope lifetime is limited), possible combination of different tags for simultaneous analysis of various analytes, and suitability for multiplexed array construction.

The most effective approaches, especially for DNA sensing, rely on the voltammetric or potentiometric stripping of nanometal/semiconductor tracers. This method, as extensively reviewed by Merkoci *et al.* [142–144], consists of different strategies, as illustrated in Figure 1.3. One possibility is monitoring the enhancement of conductivity after accumulation of silver or gold on Au-NPs anchored to conventional genosensors (Figure 1.3a). Another strategy has been the stripping

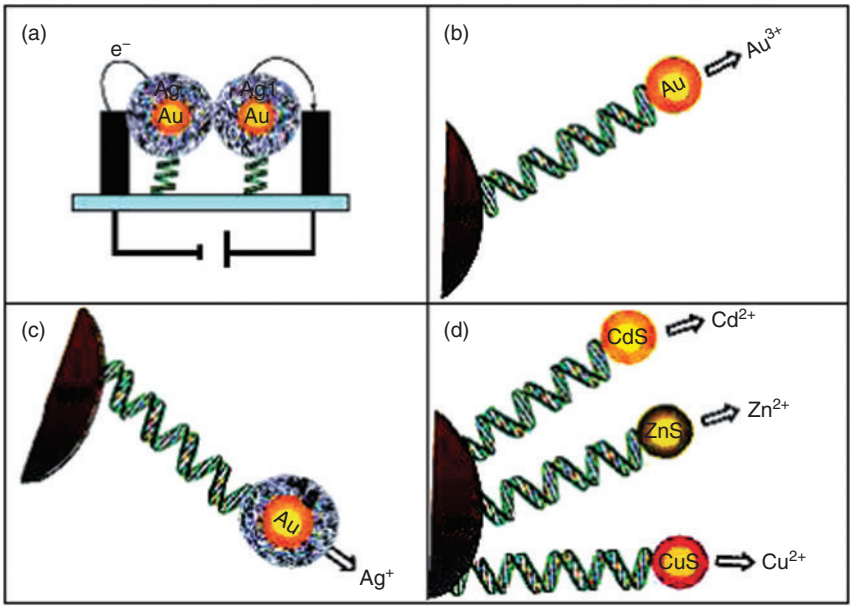


**Figure 1.3** Schematic representation of four different nanoparticle-based labeling routes: (a) conductimetric detection; (b) gold dissolving and Au(III) stripping accumulation and detection; (c) silver precipitation, dissolution (with $HNO_3$), and $Ag^+$ stripping; and (d) multilabeling with different QDs and detection of the corresponding ions [141].

analysis of gold directly, as well as Au(III) ions released after acid treatment with $HBr/Br_2$ (Figure 1.3b) or of silver, previously deposited un Au-NPs (Figure 1.3c). Finally, multilabeling with three different QDs and simultaneous detection of the released different metals (Figure 1.3d) has been found to be useful for simultaneous analyzes of different compounds. Usually, the DNA probe is immobilized directly on the transduction platform as well as on paramagnetic beads and successively magnetically confined on the electrode surface. Labeling with nanoparticles is performed upon hybridization of target DNA in the presence of nanoparticle-modified secondary probes (sandwich hybridization assay), previously prepared. Thiol–gold covalent binding and streptavidin–biotin affinity reactions are the most common procedures for the immobilization of biological molecules, such as oligonucleotides and antibodies, on nanoparticles.

One of the first examples of this type of technology was reported by the Wang group in 2001 [145], who described the immobilization of a DNA probe on streptavidin-coated magnetic beads and hybridization with a biotinylated target, which was able to bind streptavidin-coated Au-NPs (5 nm in diameter). Dissolved gold was quantified by potentiometric stripping analysis on carbon electrodes, obtaining a detection limit of 4 nM for segments related to breast cancer. A better detection limit (femtomolar level) was achieved by the same group [146] by using the silver enhancement method, based on the precipitation on gold on Au-NPs,

its dissolution with $HNO_3$ and potentiometric detection. An analog silver electrodeposition on Au-NPs was also developed in the Merkoci group [147] in order to enhance the sensitivity of immunosensor based on a sandwich assay performed on magnetic beads, thus obtaining low protein detection limits in the femtogram per milliliter range.

The same group [148] reported a nanoparticle-based system using magnetically induced direct electrochemical detection of gold QD tracers (Au67, diameter 1.4 nm) linked to the DNA target in 1 : 1 ratio. The assay was performed on paramagnetic beads, further collected on magnetic graphite/epoxy composite electrodes, and Au67 was directly quantified by DPV, achieving a nanomolar detection limit. The two main advantages of this platform were: the direct detection of QDs, without the need for dissolution and absence of an interconnected three-dimensional network of Au–DNA duplex paramagnetic beads, which may decrease the sensitivity because of the sharing of one gold tag by several DNA strands.

Rochelet-Dequaire *et al.* [149] investigated a new route for DNA detection avoiding previous PCR amplification, by realizing a new genosensor for the determination a 35-base human cytomegalovirus nucleic acid target. Target was adsorbed in polystyrene microwells and hybridized with an Au-NP-modified detection probe, to be detected by anodic stripping of the chemically oxidized gold label at SPEs. Further enhancement of the hybridization signal was obtained upon incubating with mixture of Au(III) and hydroxylamine, which induced the autocatalytic reductive deposition of ionic gold on the surface of the Au-NPs labels. This strategy allowed the detection of DNA concentrations as low as 600 aM. A singular signal amplification was more recently achieved by Du *et al.* [150] who realized a sandwich hybridization assay in which gold nanotags were further linked to DNA-modified PbS nanospheres ("bio-barcode") and lead ions were detected using anodic stripping voltammetry, thus achieving a detection of $5 \times 10^{-15}$ M for oligonucleotide target.

Metal sulfide QDs were employed by Liu *et al.* [151] for the simultaneous detection of different single-nucleotide polymorphisms. The format consisted of linking ZnS, CdS, PbS, and CuS NPs to adenosine, cytidine, guanosine, and thymidine mononucleotides, respectively. Monobase-conjugated nanocrystals were then incubated with the hybrid-coated magnetic bead solution and each mutation captured different nanocrystal mononucleotides. In this way, for each single-nucleotide polymorphism, distinct voltammetric stripping signals were obtained.

A similar approach was also reported by the same authors for simultaneous immunosensing of $\beta_2$-microglobulin, IgG, bovine serum albumin, and C-reactive protein [152]. The multianalyte sandwich immunoassay involved a dual-binding event of primary and secondary antibodies onto QDs tags (ZnS, CdS, PbS, and CuS) and magnetic beads, respectively. A carbamate-base linkage was used for conjugating the hydroxyl-terminated nanocrystals with the secondary antibodies. Each biorecognition event generated a distinct voltammetric peak, the position and size of which was specific of the type and concentration of the corresponding antigen. CdS QDs were also used as tags [153] for the realization of an immunosensor for CEA detection in combination with carbon nanobeads able enhance the

electrode surface. The low detection limit obtained (32 pg $ml^{-1}$) with this format suggested that the method could be suitable also for urinary CEA detection, a marker for early diagnosis of urothelial carcinoma.

Other immunoassays were developed exploiting Au-NP labeling. Liao *et al.* [154] reported a highly sensitive assay based on the autocatalytic deposition of Au(III) onto Au-NPs for the determination of rabbit IgG with square-wave stripping voltammetry (detection limit 1.6 fM). Chu *et al.* [155] were able to detect a concentration of 1 ng $ml^{-1}$ of human IgG using the method based on the precipitation of silver on colloidal gold labels. Direct electrical detection of gold was instead employed by Idegami *et al.* [156] for the design of an immunosensor for the detection of a pregnancy marker (human chorionic gonadotropin hormone). Primary antibody was immobilized on screen-printed carbon strips and the captured antigen was sandwiched with Au-NP-labeled secondary antibody. Gold nanoparticles were exposed to a preoxidation process and then reduced via DPV. Urine samples of pregnant and nonpregnant adults were tested, and results compared with a standard enzyme-linked immunosorbent assay test with good agreement, as evidenced by the fact that both tests were not able to detect any human chorionic gonadotropin hormone in the urine sample of nonpregnant women.

Au-NPs have been not only employed for labeling, but also for the enhancement of electrical properties. An example is the label-free immunoassay based on impedimetric measurements developed by Tang *et al.* [157] for the detection of CEA tumor marker. Carcinoembryonic antibody was covalently attached to Au-NPs and the composite immobilized on a gold electrode by electrocopolymerization with *o*-aminophenol. Electrochemical impedance spectroscopy studies demonstrated that the formation of antibody–antigen complexes increased the electron transfer resistance of $[Fe(CN)_6]^{3-/4-}$ redox probe at the poly-*o*-aminophenol/carcinoembryonic antibody/Au-NP/Au electrode, thus monitoring of CEA concentration could be performed (detection limit 0.1 ng $ml^{-1}$).

An alternative application of Au-NPs was also reported by He *et al.* [158] for the development of label-free sensors for thrombin detection using aptamers. Aptamers are DNA (or RNA) oligonucleotides, able to recognize a variety of targets such as proteins, peptides, and small molecules [159]. Antithrombin antibodies were immobilized on the microtiter plates to bind thrombin and the complex was sandwiched with aptamers conjugated to Au-NPs ("bio-barcode"). After washing, a basic treatment allowed the collection of the "barcode" aptamers, which were further degraded and the amount of adenine (proportional to the amount of bound thrombin) quantified by DPV. This assay takes advantage of the amplification potential of Au-NPs carrying numerous aptamer tags. An analog approach was also developed by Zhang *at al.* [160] for the determination of DNA sequences.

Another important use of nanoparticles is their employment as platforms for the immobilization of biological elements. Their large surface area greatly increases biomolecule loading. Moreover, with respect to confinement on an electrode surface, the higher mobility achieved favors delivering of reactants and recognition reactions. Due to the ease of functionalization with thiol groups, Au-NPs have also been widely employed in this field, both for immunosensing and genosensing

[161, 162]. The greatest contribution to the improvement of sensitivity and reliability of electrochemical biosensors has been provided by magnetic micro and nanoparticles (or beads). A recurring problem in electrochemical biosensing is the background interference due to aspecific adsorption of ligands or enzymatic/chemical labels at the electrode surface. Moreover, passivation and fouling of electrodes is the most important problem in all electroanayltical techniques [163]. To overcome these obstacles, in the last decade, magnetic beads have represented a very elegant and effective solution. Many groups exploited the possibility of performing the recognition event on the surface of paramagnetic micro- and nanobeads, thus realizing highly sensitive electrochemical immunosensors [164–167] and genosensors [168–176], which are also called immunomagnetic and genomagnetic sensors, respectively. This approach offers several advantages. Firstly, by performing the biorecognition and the transduction step at different surfaces (i.e., magnetic beads and unmodified electrodes), the nonspecific adsorption of analytes and other reagents can be significantly reduced. Moreover, upon employing receptor-modified particles freely moving in solution, random collisions between reagents are favored and the efficiency of coupling rises. Finally, magnetic separation of the particles from the solution facilitates washing steps, thus improving the removal of nonspecifically adsorbed reagents.

Centi *et al.* [164–166] reported several interesting immunosensors and aptasensors in which the analytical performances of the assay were significantly improved by immobilizing antibodies (or aptamers) on paramagnetic beads rather than directly onto the working electrode surface. As demonstrated also by Sarkar *et al.* [167] in the determination of free PSA, this method has great potential to be used as a diagnostic tool because, after binding with the analyte, particles can be magnetically separated from the sample medium (blood, serum) and thus the electrode can be preserved from fouling or interference problems.

Palacek and Wang can be considered the pioneers of genomagnetic assays with tens of papers and reviews published over the last decade, exploring both label-free and enzyme-linked methods [168–171]. An interesting combination of magnetic, polymeric, and Au-NPs was reported by Kawde and Wang [172], who achieved a detection limit of 0.1 ng $ml^{-1}$ using oligonucleotides functionalized with polymeric beads carrying Au-NPs. This strategy involved the hybridization of the oligonucleotide probe (captured on magnetic beads) to the DNA target labeled with the gold-loaded sphere, and subsequent dissolution and stripping-potentiometric detection of the gold tracer. Lermo *et al.* [173] developed a genomagnetic assay for the detection of food pathogens based on a graphite/epoxy composite magneto electrode as electrochemical transducer. The assay was performed in a sandwich format by double labeling the amplicon ends during PCR, with a biotinylated capture probe, to achieve the immobilization on streptavidin-coated magnetic beads and with a digoxigenin signaling probe, to achieve further labeling with the enzyme marker (antidigoxigenin HRP). Erdem *et al.* [174] proposed a genomagnetic assay based on label-free electrochemical detection of hepatitis B virus DNA in PCR amplicons, using pencil graphite electrodes as transducers. They obtained a detection limit in the femtomolar range. The same group reduced the magnetic

bead dimension to the nanoscale to further increase the sensitivity of the assay [175]. The magnetite ($Fe_3O_4$) nanoparticles (average dimension of 125 and 225 nm) were prepared by coprecipitation technique and functionalized for coating with streptavidin. A label-free DNA hybridization assay was developed by immobilizing guanine-free biotinylated probe and monitoring the guanine oxidation peak after hybridization. Very small diameter magnetic beads (18 nm) were also prepared by Zhu *at al.* [176]. After immobilization of DNA, probe nanoparticles were deposited on pyrolitic graphite electrodes, incubated with target, and the hybridization event was monitored by cyclic voltammetry using the redox couple $K_3[Fe(CN)_6]$/$K_4[Fe(CN)_6]$ as indicator (redox peaks decreased after base- pair coupling). Over the whole hybridization period, a magnetic field was applied over or below the electrode. NPs were either repelled or attracted from or to the surface of the electrode, thus working as a magneto-switch as NPs were released once hybridization occurred.

Other applications of magnetic NPs have involved the construction of composite or layer-by-layer films for immunomagnetic assay design. Three-layer nanoparticles composed of a ferrite magnetic core covered with Prussian blue and gold were realized by Zhuo *et al.* [177] to be applied as a mobile platform for the immobilization of a secondary antibody and a bienzyme labeling system (HRP and GOx) for immunosensing. Primary antibodies were immobilized on a hydrogel composite gold electrode and, after incubation with CEA, labeling could be easily performed with the multifunctionalized nanoparticles. In this way the immunosensor could be regenerated by simply applying an external magnetic field, thus obtaining a dramatic improvement in reproducibility.

A different type of magnetic composite nanobead was developed by Pal *et al.* [178] to act as an immunomagnetic concentrator of *Bacillus anthracis* spores from food samples as well as an electrical transducer. Magnetic iron oxide nanoparticles (100 nm in diameter) were coated with a conductive PANI layer, linked to a detector antibody, and added to the contaminated food sample. After binding the spores, beads were magnetically removed and deposited on a pad, placed between silver electrodes, where a secondary antibody had been previously immobilized. The presence of conductive particles increases conduction between the two silver electrodes and was proportional to the amount of analyte, which could be detected at concentrations as low as $4.2 \times 10^2$ spores $ml^{-1}$.

These examples show attractive features, especially for automation of analytical biosystems. Magnetic beads, in fact, also offer great advantages in flow systems where magnetic properties may facilitate the delivery and removal of reagents through the channels and help in the miniaturization of the whole sensing apparatus. Several genosensors based on this highly promising combination were developed by Baeumner's group [179, 180] who realized a microfluidic device comprising disposable microchannels made of polydimethylsiloxane integrated in a glass chip and a sandwich assay based on paramagnetic beads for probe immobilization and a secondary probe labeled with dye-loaded liposome. This was achieved by integrating an interdigitated ultramicroelectrode array in the glass chip, downstream of the capturing magnet and labeling the hybrid with liposomes

filled with an electrochemical marker, which could be oxidized or reduced at the electrode surface. A similar approach, based on silicon electrical chip arrays coupled to interdigitated ultramicroelectrodes, was reported by Gabig *et al.* [181] for the recognition of the RNA of infectious bacteria. In this case, the DNA probe was captured on streptavidin-coated beads and labeled with a secondary probe functionalized with digoxigenin. After incubation with an antidigoxigenin antibody conjugated with alkaline phosphatase, an enzyme-amplified detection of the hybridization event was performed. Berti *et al.* [182] combined genomagnetic assay based on paramagnetic beads with a microelectroanalytical device that combined a special cartridge containing gold microelectrodes embedded in eight polymer microchannels, with a computer-controlled instrument for the control of fluidics. This format allowed the simultaneous detection of eight different PCR samples with a detection limit of 0.2 nM.

## 1.5 Conclusions

The main intent of this chapter was to highlight the exceptional potential of nanomaterials for the design of novel sensing technologies and to enhance the analytical performance of biosensing systems. One of most challenging problems for achieving the total miniaturization of analytical systems remains the preliminary operations (sampling, sample introduction, and treatment). By contrast, detection and signal transduction, as well as data acquisition and processing, can achieve a high degree of miniaturization [183]. Thus, coupling new micro and nanotechnologies with emerging nanostructures, "smart" nanosensors able of electrochemical coding could be the basis for the construction of a tiny "chemical lab" (lab-on-a-bead) [142] able to detect and analyze a unique ligand in a complex mixture.

## References


1 Wang, J. (2005) *Analyst*, **130**, 421–426.
2 Xu, T., Zhang, N., Nichols, H.L., Shi, D., and Wen, X. (2007) *Mater. Sci. Eng. C*, **27**, 579–594.
3 Fortina, P., Kricka, L.J., Surrey, S., and Grodzinski, P. (2005) *Trends Biotechnol.*, **23**, 168–173.
4 Suni, I.I. (2008) *Trends Anal. Chem.*, **27**, 604–611.
5 Iijima, S. (1991) *Nature*, **354**, 56–58.
6 Baughman, R.H., Zakhidov, A., and De Heer, W.A. (2002) *Science*, **297**, 787–792.
7 Valentini, F., Orlanducci, S., Terranova, M.L., Amine, A., and Palleschi, G. (2004) *Sens. Actuators B*, **100**, 117–125.
8 Rivas, G.A., Rubianes, M.D., Rodrìguez, M.C., Ferreyra, N.F., Luque, G.L., Pedano, M.L., Miscoria, S.A., and Parrado, C. (2007) *Talanta*, **74**, 291–307.
9 Merkoci, A., Pumera, M., Leopis, X., Péres, B., Del Valle, M., and Alegret, S. (2005) *Trends Anal. Chem.*, **4**, 826–838.
10 Iijima, S. and Ichihashi, T. (1993) *Nature*, **363**, 603–605.
11 Guo, T., Nikolaev, P., Thess, A., Colbert, D.T., and Smalley, R.E. (1995) *Chem. Phys. Lett.*, **243**, 49–54.
12 Che, G., Lakshmi, B.B., Martin, C.R., and Fisher, E.R. (1998) *Chem. Mater.*, **10**, 260–267.

**13** Banks, C.E., Davies, T.J., Wildgoose, G.G., and Compton, R.G. (2005) *Chem. Commun.*, 829–841.

**14** Britto, P.J., Santhanam, K.S.V., Rubio, A., Alonso, J.A., and Ajayan, P.M. (1999) *Adv. Mater.*, **11**, 154–157.

**15** Sotiropoulou, S. and Chaniotakis, N.A. (2003) *Anal. Bioanal. Chem.*, **375**, 103–105.

**16** Hirsch, A. (2002) *Angew. Chem. Int. Ed.*, **41**, 1853–1859.

**17** Bidan, G. (1992) *Sens. Actuators B*, **6**, 45–56.

**18** Lange, U., Roznyatovskaya, N.V., and Mirsky, V.M. (2008) *Anal. Chim. Acta*, **614**, 1–26.

**19** Palaniappan, S. and John, A. (2008) *Prog. Polym. Sci.*, **33**, 732–758.

**20** Yoon, H. and Jang, J. (2009) *Adv. Funct. Mater.*, **19**, 1567–1576.

**21** Kuchibhatla, S.V.N., Karakoti, A.S., Bera, D., and Seal, S. (2007) *Prog. Mater. Sci.*, **52**, 699–913.

**22** Cho, S. and Lee, S.B. (2008) *Acc. Chem. Res.*, **41**, 699–707.

**23** Cao, G. and Liu, D. (2008) *Adv. Colloid Interface Sci.*, **136**, 45–64.

**24** Martin, C.R. (1996) *Chem. Mater.*, **8**, 1739–1746.

**25** Chen, J., Xu, Y., Zheng, Y., Dai, L., and Wu, H. (2008) *Compt. Rend. Chim.*, **11**, 84–89.

**26** Katz, E., Willner, I., and Wang, J. (2004) *Electroanalysis*, **16**, 19–42.

**27** Guo, S. and Wang, E. (2007) *Anal. Chim. Acta*, **598**, 181–192.

**28** Gupta, A.K. and Gupta, M. (2005) *Biomaterials*, **26**, 3995–4021.

**29** Carpani, I., Scavetta, E., and Tonelli, D. (2008) *Electroanalysis*, **1**, 84–90.

**30** Radoi, A., Compagnone, D., Valcarcel, M.A., Placidi, P., Materazzi, S., Moscone, D., and Palleschi, G. (2008) *Electrochim. Acta*, **53**, 2161–2169.

**31** Tasca, F., Gorton, L., Wagner, J.B., and Noll, G. (2008) *Biosens. Bioelectron.*, **24**, 272–278.

**32** Jeykumari, D.R.S. and Narayanan, S.S. (2008) *Biosens. Bioelectron.*, **23**, 1404–1411.

**33** Jeykumari, D.R.S. and Narayanan, S.S. (2009) *Carbon*, **47**, 957–996.

**34** Tsai, Y. and Chiu, C. (2007) *Sens. Actuators B*, **125**, 10–16.

**35** Deo, R.P., Wang, J., Block, I., Mulchandani, A., Joshi, K.A., Trojanowicz, M., Scholz, F., Chen, W., and Lin, Y. (2005) *Anal. Chim. Acta*, **530**, 185–189.

**36** Luo, X., Xu, J., Wang, J., and Chen, H. (2005) *Chem. Commun.*, 2169–2171.

**37** Qian, L. and Yang, X. (2006) *Talanta*, **68**, 721–727.

**38** Rubianes, M.D. and Rivas, G.A. (2007) *Electrochem. Commun.*, **9**, 480–484.

**39** Laschi, S., Bulukin, E., Palchetti, I., Cristea, C., and Mascini, M. (2008) *ITBM-RBM*, **29**, 202–207.

**40** Sanchez, S., Pumera, M., Cabrujac, E., and Fabregas, E. (2007) *Analyst*, **132**, 142–147.

**41** Bareket, L., Rephaeli, A., Berkovitch, G., Nudelman, A., and Rishpon, J. (2010) *Bioelectrochemistry*, **77**, 94–99.

**42** Rivas, G.A., Rubianes, M.D., Pedano, M.L., Ferreyra, N.F., Luque, G.L., Rodriguez, M.C., and Miscoria, S.A. (2007) *Electroanalysis*, **19**, 823–831.

**43** Perez-Lopez, B., Sola, J., Alegret, S., and Merkoci, A. (2008) *Electroanalysis*, **20**, 603–610.

**44** Manso, J., Mena, M.L., Yanez-Sedeno, P., and Pingarron, J. (2007) *J. Electroanal. Chem.*, **603**, 1–7.

**45** Aguì, L., Eguìlaz, M., Pena-Farfal, C., Yanez-Sedeno, P., and Pingarron, J.M. (2009) *Electroanalysis*, **21**, 386–391.

**46** Ammam, M. and Fransaer, J. (2010) *Biosens. Bioelectron.*, **25**, 1597–1602.

**47** Ozoner, S.K., Yalvac, M., and Erhan, E. (2010) *Curr. Appl. Phys.*, **10**, 323–328.

**48** Zeng, X., Li, X., Liu, X., Liu, Y., Luo, S., Kong, B., Yang, S., and Wei, W. (2009) *Biosens. Bioelectron.*, **25**, 896–900.

**49** Wang, J. and Lin, Y. (2008) *Trends Anal. Chem.*, **27**, 619–626.

**50** Zhang, Y., Liu, L., Xi, F., Wu, T., and Lin, X. (2010) *Electroanalysis*, **22**, 277–285.

**51** Yan, X.B., Chen, X.J., Tay, B.K., and Khor, K.A. (2007) *Electrochem. Commun.*, **9**, 1269–1275.

**52** Liu, G. and Lin, Y. (2006) *Anal. Chem.*, **78**, 835–843.

**53** Viswanathan, S., Radecka, H., and Radecki, J. (2009) *Biosens. Bioelectron.*, **24**, 2772–2777.

**54** Lin, Y., Lu, F., Tu, Y., and Ren, Z. (2004) *Nano Lett.*, **4**, 191–195.

**55** Withey, G.D., Lazareck, A.D., Tzolov, M.B., Yina, A., Aich, P., Yeh, J.I., and Xua, J.M. (2006) *Biosens. Bioelectron.*, **21**, 1560–1565.

**56** Maghsoodi, S., Gholami, Z., Chourchian, H., Mortazavi, Y., and Khodadadi, A.A. (2009) *Sens. Actuators B*, **141**, 526–531.

**57** Boo, H., Jeong, R., Park, S., Kim, K.S., An, K.H., Lee, Y.H., Han, J.H., Kim, H.C., and Chung, T.D. (2006) *Anal. Chem.*, **78**, 617–620.

**58** Sanchez, S., Pumera, M., and Fabregas, E. (2007) *Biosens. Bioelectron.*, **23**, 332–340.

**59** Buch, M. and Rishpon, J. (2008) *Electroanalysis*, **20**, 2592–2594.

**60** Viswanathana, S., Rani, C., Anand, A.V., and Ho, J.A. (2009) *Biosens. Bioelectron.*, **24**, 1984–1989.

**61** Panini, N.V., Messina, G.A., Salinas, E., Fernandez, H., and Raba, J. (2008) *Biosens. Bioelectron.*, **23**, 1145–1151.

**62** He, P., Wang, Z.I., Zhang, L., and Yan, W. (2009) *Food Chem.*, **112**, 707–714.

**63** Okuno, J., Maehashi, K., Matsumoto, K., Kerman, K., Takamura, Y., and Tamiya, E. (2007) *Electrochem. Commun.*, **9**, 13–18.

**64** Okuno, J., Maehashi, K., Kerman, K., Takamura, Y., Matsumoto, K., and Tamiya, E. (2007) *Biosens. Bioelectron.*, **22**, 2377–2381.

**65** Yun, Y., Bange, A., Heineman, W.R., Halsall, H.B., Shanov, V.N., Dong, Z., Pixley, S., Behbehani, M., Jazieh, A., Tu, Y., Wong, D.K.Y., Bhattacharya, A., and Schulz, M.J. (2007) *Sens. Actuators B*, **123**, 177–182.

**66** Yun, Y., Dong, Z., Shanov, V.N., Doepke, A., Heineman, W.R., Halsall, H.B., Bhattacharya, A., Wong, D.K.Y., and Schulz, M.J. (2008) *Sens. Actuators B*, **133**, 208–212.

**67** Yu, X., Kim, S.N., Papadimitrakopoulos, F., and Rusling, J.F. (2005) *Mol. Biosyst.*, **1**, 70–78.

**68** Yu, X., Munge, B., Patel, V., Jensen, G., Bhirde, A., Gong, J.D., Kim, S.N., Gillespie, J., Gutkind, J.S., Papadimitrakopoulos, F., and Rusling, J.F. (2006) *J. Am. Chem. Soc.*, **128**, 11199–11205.

**69** Rusling, J.F., Sotzing, G., and Papadimitrakopoulos, F. (2009) *Bioelectrochemistry*, **76**, 189–194.

**70** Erdem, A. (2007) *Talanta*, **74**, 318–325.

**71** Erdem, A., Papakonstantinou, P., and Murphy, H. (2006) *Anal. Chem.*, **78**, 6656–6659.

**72** Erdem, A., Karadeniz, H., and Caliskan, A. (2009) *Electroanalysis*, **21**, 464–471.

**73** Yang, Y., Wang, Z., Yang, M., Li, J., Zheng, F., Shen, G., and Yu, R. (2007) *Anal. Chim. Acta*, **584**, 268–274.

**74** Yang, T., Zhou, N., Zhang, Y., Zhang, W., Jiao, K., and Li, G. (2009) *Biosens. Bioelectron.*, **24**, 2165–2170.

**75** Wei, H., Du, Y., Kang, J., and Wang, E. (2007) *Electrochem. Commun.*, **9**, 1474–1479.

**76** Jiang, C., Yang, T., Jiao, K., and Gao, H. (2008) *Electrochim. Acta*, **53**, 2917–2924.

**77** Xu, Y., Ye, X., Yang, L., He, P., and Fang, Y. (2006) *Electroanalysis*, **18**, 1471–1478.

**78** Huska, D., Hubalek, J., Adam, V., and Kizek, R. (2008) *Electrophoresis*, **29**, 4964–4971.

**79** He, P., Li, S., and Dai, L. (2005) *Synth. Met.*, **154**, 17–20.

**80** Berti, F., Lozzi, L., Palchetti, I., Santucci, S., and Marrazza, G. (2009) *Electrochim. Acta*, **54**, 5035–5041.

**81** Nguyen, C.V., Delzeit, L., Cassell, A.M., Li, J., Han, J., and Meyyappan, M. (2002) *Nano Lett.*, **2**, 1079–1081.

**82** Li, J., Ng, H.T., Cassell, A., Fan, W., Chen, H., Ye, Q., Koehne, J., Han, J., and Meyyappan, M. (2003) *Nano Lett.*, **3**, 597–602.

**83** Koehne, J., Chen, H., Li, J., Cassell, A.M., Ye, Q., Ng, H.T., Han, J., and Meyyappan, M. (2003) *Nanotechnology*, **14**, 1239–1245.

**84** Arumugam, P.U., Chen, H., Siddiqui, S., Weinrich, J.A.P., Jejelowo, A., Li, J., and Meyyappan, M. (2009) *Biosens. Bioelectron.*, **24**, 2818–2824.

**85** Ahuja, T., Mir, I.A., and Rajesh, D.K. (2007) *Biomaterials*, **28**, 791–805.

**86** Cosnier, S. (1999) *Biosens. Bioelectron.*, **14**, 443–456.

**87** Teles, F.R.R. and Fonseca, L.P. (2008) *Mater. Sci. Eng. C*, **28**, 1530–1543.

**88** Lahiff, E., Woods, T., Blau, W., Wallace, G.G., and Diamond, D. (2009) *Synth. Met.*, **159**, 741–748.

**89** Ramanavicius, A., Ramanaviciene, A., and Malinauskas, A. (2006) *Electrochim. Acta*, **51**, 6025–6037.

**90** Koopal, C.G.J., Feiters, M.C., Nolte, R.J.M., de Ruiter, B., and Schasfoort, R.B.M. (1992) *Biosens. Bioelectron.*, **7**, 461–471.

**91** Ekanayake, E.M.I.M., Preethichandra, D.M.G., and Kaneto, K. (2007) *Biosens. Bioelectron.*, **23**, 107–113.

**92** Shamsipur, M., Kazemi, S.H., and Mousavi, M.F. (2008) *Biosens. Bioelectron.*, **24**, 104–110.

**93** Lupu, A., Lisboa, P., Valsesia, A., Colpo, P., and Rossi, F. (2009) *Sens. Actuators B*, **137**, 56–61.

**94** Kros, A., Nolte, R.J.M., and Sommerdijk, N.A.J.M. (2002) *Adv. Mater.*, **14**, 1779–1782.

**95** Park, D.H., Kim, B.H., Jang, M.K., Bae, K.Y., Lee, S.J., and Joo, J. (2005) *Synth. Met.*, **153**, 341–334.

**96** Kros, A., van Hövell, S.W.F.M., Sommerdijk, N.A.J.M., and Nolte, R.J.M. (2001) *Adv. Mater.*, **13**, 1555–1557.

**97** Liu, C., Kuwahara, T., Yamazaki, R., and Shimomura, M. (2007) *Eur. Polym. J.*, **43**, 3264–3276.

**98** Park, J., Kim, H.K., and Son, Y. (2008) *Sens. Actuators B*, **133**, 244–250.

**99** Santhosh, P., Manesh, K.M., Uthayakumar, S., Komathi, S., Gopalan, A.I., and Lee, K.P. (2009) *Bioelectrochemistry*, **75**, 61–66.

**100** Rahman, M.A., Kwon, N., Won, M., Choe, E.S., and Shim, Y. (2005) *Anal. Chem.*, **77**, 4854–4860.

**101** Ding, S., Chao, D., Zhang, M., and Zhang, W. (2008) *J. Appl. Polym. Sci.*, **107**, 3408–3412.

**102** Zhang, D. and Wang, Y. (2006) *Mater. Sci. Eng. B*, **134**, 9–19.

**103** Virji, S., Huang, J., Kaner, R.B., and Weiller, B.H. (2004) *Nano Lett.*, **4**, 491–496.

**104** Huang, J., Virji, S., Weiller, B.H., and Kaner, R.B. (2004) *Chem. Eur. J.*, **10**, 1314–1319.

**105** Morrin, A., Ngamna, O., Killard, A.J., Moulton, S.E., Smyth, M.R., and Fallace, G.G. (2005) *Electroanalysis*, **17**, 423–430.

**106** Luo, X., Vidal, G.D., Killard, A.J., Morrin, A., and Smyth, M.R. (2007) *Electroanalysis*, **19**, 876–883.

**107** Du, Z., Li, C., Li, L., Zhang, M., Xu, S., and Wang, T. (2009) *Mater. Sci. Eng. C*, **29**, 1794–1797.

**108** Wang, X., Yang, T., Feng, Y., Jiao, K., and Li, G. (2009) *Electroanalysis*, **21**, 819–825.

**109** Granot, E., Katz, E., Basner, B., and Willner, I. (2005) *Chem. Mater.*, **17**, 4600–4609.

**110** Zhao, M., Wu, X., and Cai, C. (2009) *J. Phys. Chem. C*, **113**, 4987–4996.

**111** Horng, Y., Hsu, Y., Ganguly, A., Chen, C., Chen, L., and Chen, K. (2009) *Electrochem. Commun.*, **11**, 850–853.

**112** Wang, Z., Liu, S., Wu, P., and Cai, C. (2009) *Anal. Chem.*, **81**, 1638–1645.

**113** Somerset, V., Klink, M., Akinyeye, R., Michira, I., Sekota, M., Al-Ahmed, A., Baker, P., and Iwuoha, E. (2007) *Macromol. Symp.*, **255**, 36–49.

**114** Dhand, C., Solanki, P.R., Sood, K.N., Datta, M., and Malhotra, B.D. (2009) *Electrochem. Commun.*, **11**, 1482–1486.

**115** Ozcan, A., Sahin, Y., Ozsoz, M., and Turan, S. (2007) *Electroanalysis*, **19**, 2208–2216.

**116** Ko, S. and Jang, J. (2008) *Ultramicroscopy*, **108**, 1328– 1333.

**117** Zhu, N., Chang, Z., Heb, P., and Fang, Y. (2006) *Electrochim. Acta*, **51**, 3758–3762.

**118** Chang, H., Yuan, Y., Shi, N., and Guan, Y. (2007) *Anal. Chem.*, **79**, 5111–5115.

**119** Feng, Y., Yang, T., Zhang, W., Jiang, C., and Jiao, K. (2008) *Anal. Chim. Acta*, **616**, 144–151.

**120** Zhou, N., Yang, T., Jiang, C., Du, M., and Jiao, K. (2009) *Talanta*, **77**, 1021–1026.

**121** Mosbach, K. (1994) *Trends Biochem. Sci.*, **19**, 9–14.

**122** Piletsky, S., Turner, N.W., and Laitenberger, P. (2006) *Med. Eng. Phys.*, **28**, 971–977.

**123** Deore, B., Chen, Z., and Nagaoka, T. (1999) *Anal. Sci.*, **15**, 827–828.

**124** Sreenivasan, K. (2007) *J. Mater. Sci.*, **42**, 7575–1578.

**125** Deore, B. and Freund, M.S. (2003) *Analyst*, **128**, 803–806.

**126** Tokonami, S., Shiigi, H., and Nagaoka, T. (2009) *Anal. Chim. Acta*, **641**, 7–13.

**127** Li, Y., Yin, X.F., Chen, F.R., Yang, H.H., Zhuang, Z.X., and Wang, X.R. (2006) *Macromolecules*, **39**, 4497–4499.

**128** Xie, C., Zhang, Z., Wang, D., Guan, G., Gao, D., and Liu, J. (2006) *Anal. Chem.*, **78**, 8339–8346.

**129** Vandevelde, F., Belmont, A.S., Pantigny, J., and Haupt, K. (2007) *Adv. Mater.*, **19**, 3717–3720.

**130** Agarwal, S., Wendorff, J.H., and Greiner, A. (2008) *Polymer*, **49**, 5603–5621.

**131** Chronakis, S., Jakob, A., Hagstrom, B., and Ye, L. (2006) *Langmuir*, **22**, 8960–8965.

**132** Willner, I., Basnar, B., and Willner, B. (2007) *FEBS J.*, **274**, 302–309.

**133** Yan, Y., Tel-Vered, R., Yehezkeli, O., Cheglakov, Z., and Willner, I. (2008) *Adv. Mater.*, **20**, 2365–2370.

**134** Aguì, L., Manso, J., Yanez-Sedeno, P., and Pingarron, J.M. (2006) *Sens. Actuators B*, **113**, 272–280.

**135** Carralero, C., Mena, M.L., Gonzalez-Cortes, A., Yanez-Sedeno, P., and Pingarron, J.M. (2006) *Biosens. Bioelectron.*, **22**, 730–736.

**136** Orozco, J., Jiménez-Jorquera, C., and Fernández-Sánchez, C. (2009) *Bioelectrochemistry*, **75**, 176–181.

**137** Chico, B., Camacho, C., Pérez, M., Longo, M.A., Sanromán, M.A., Pingarrón, J.M., and Villalonga, R. (2009) *J. Electroanal. Chem.*, **629**, 126–132.

**138** Yin, H., Ai, S., Xu, J., Shi, W., and Zhu, L. (2009) *J. Electroanal. Chem.*, **637**, 21–27.

**139** Wang, S., Tan, Y., Zhao, D., and Liu, G. (2008) *Biosens. Bioelectron.*, **23**, 1781–1787.

**140** Mavré, F., Bontemps, M., Ammar-Merah, S., Marchal, D., and Limoges, B. (2007) *Anal. Chem.*, **79**, 187–194.

**141** Pingarron, J.M., Yanez-Sedeno, P., and Gonzalez-Cortes, A. (2008) *Electrochim. Acta*, **53**, 5848–5866.

**142** Merkoci, A. (2007) *FEBS J.*, **274**, 310–316.

**143** Castaneda, M.T., Alegret, S., and Merkoci, A. (2007) *Electroanalysis*, **19**, 743–753.

**144** Merkoci, A., Aldavert, M., Marìn, S., and Alegret, S. (2005) *Trends Anal. Chem.*, **24**, 341–350.

**145** Wang, J., Xu, D., Kawde, A., and Polsky, R. (2001) *Anal. Chem.*, **73**, 5576–5581.

**146** Wang, J., Xu, D., and Polsky, R. (2002) *J. Am. Chem. Soc*, **124**, 4208–4209.

**147** de la Escosura-Muniz, A., Maltez-da Costa, M., and Merkoci, A. (2009) *Biosens. Bioelectron.*, **24**, 2475–2482.

**148** Pumera, M., Castaneda, M.T., Pividori, M.I., Eritja, R., Merkoci, A., and Alegret, S. (2005) *Langmuir*, **21**, 9625–9629.

**149** Rochelet-Dequaire, M., Limoges, B., and Brossier, P. (2006) *Analyst*, **131**, 923–929.

**150** Du, P., Li, H., and Cao, W. (2009) *Biosens. Bioelectron.*, **24**, 3223–3228.

**151** Liu, G., Lee, T.M.H., and Wang, J. (2005) *J. Am. Chem. Soc*, **127**, 38–39.

**152** Liu, G., Wang, J., Kim, J., and Jan, M.R. (2004) *Anal. Chem.*, **76**, 7126–7130.

**153** Ho, J.A., Lin, Y., Wang, L., Hwang, K., and Chou, P. (2009) *Anal. Chem.*, **81**, 1340–1346.

**154** Liao, K.T. and Huang, H.J. (2005) *Anal. Chim. Acta*, **538**, 159–164.

**155** Chu, X., Fu, X., Chen, K., Shen, G.L., and Yu, R.Q. (2005) *Biosens. Bioelectron.*, **20**, 1805–1812.

**156** Idegami, K., Chikae, M., Kerman, K., Nagatani, N., Yuhi, T., Endo, T., and Tamiya, E. (2008) *Electroanalysis*, **20**, 14–21.

**157** Tang, H., Chen, J.H., Nie, L.H., Kuang, Y.F., and Yao, S.Z. (2007) *Biosens. Bioelectron.*, **22**, 1061–1067.

**158** He, P., Shen, L., Cao, Y., and Li, D. (2007) *Anal. Chem.*, **79**, 8024–8029.

**159** Tombelli, S., Minunni, M., and Mascini, M. (2005) *Biosens. Bioelectron.*, **20**, 2424–2434.

**160** Zhang, X., Su, H., Bi, S., Li, S., and Zhang, S. (2009) *Biosens. Bioelectron.*, **24**, 2730–2734.

**161** Mani, V., Chikkaveeraiah, B.V., Patel, V., Gutkind, J.S., and Rusling, J.F. (2009) *ACS Nano.*, **3**, 585–594.

**162** Zhang, K. and Zhang, Y. (2010) *Electroanalysis*, **22**, 673–679.
**163** Solé, S., Merkoci, A., and Alegret, S. (2001) *Trends Anal. Chem.*, **20**, 102–110.
**164** Centi, S., Laschi, S., and Mascini, M. (2007) *Talanta*, **73**, 394–399.
**165** Centi, S., Tombelli, S., Minunni, M., and Mascini, M. (2007) *Anal. Chem.*, **79**, 1466–1473.
**166** Centi, S., Bonel Sanmartin, L., Tombelli, S., Palchetti, I., and Mascini, M. (2009) *Electroanalysis*, **21**, 1309–1315.
**167** Sarkar, P., Ghosh, D., Bhattacharyay, D., Setford, S.J., and Turner, A.P.F. (2008) *Electroanalysis*, **20**, 1414–1420.
**168** Wang, J., Kawde, A., Erdem, A., and Salzar, M. (2001) *Analyst*, **126**, 2020–2024.
**169** Wang, J., Xu, D., Erdem, A., Polsky, R., and Salazar, M.A. (2002) *Talanta*, **56**, 931–938.
**170** Palecek, E., Billovà, S., Havran, L., Kizek, R., Miculkova, A., and Jelen, F. (2002) *Talanta*, **56**, 919–930.
**171** Palecek, E. and Fojta, M. (2007) *Talanta*, **74**, 276–290.
**172** Kawde, A.N. and Wang, J. (2004) *Electroanalysis*, **16**, 101–107.
**173** Lermo, A., Campoy, S., Barbè, J., Hernadez, S., Alegret, S., and Pividori, M.I. (2007) *Biosens. Bioelectron.*, **22**, 2010–2017.
**174** Erdem, A., Ariksoysal, D.O., Karadeniz, H., Kara, P., Sengonul, A., Sayiner, A.A., and Ozsoz, M. (2005) *Electrochem. Commun.*, **7**, 815–820.
**175** Erdem, A., Sayar, F., Karadeniz, H., Guven, G., Ozsoz, M., and Piskin, E. (2007) *Electroanalysis*, **19**, 798–804.
**176** Zhu, X., Han, K., and Li, G. (2006) *Anal. Chem.*, **78**, 2447–2449.
**177** Zhuo, Y., Yuan, P., Yuan, R., Chai, Y., and Hong, C. (2009) *Biomaterials*, **30**, 2284–2290.
**178** Pal, S. and Alocilja, E.C. (2009) *Biosens. Bioelectron.*, **24**, 1437–1444.
**179** Kwakye, S., Goral, V.N., and Baeumner, A.J. (2006) *Biosens. Bioelectron.*, **21**, 2217–2223.
**180** V.N. Goral, N.V. Zaytseva, and Baeumner A.J. (2006) *Lab Chip.*, **6**, 414–421.
**181** Gabig-Ciminska, M., Holmgren, A., Andresen, H., Bundvig Barken, K., Wümpelmann, M., J. Albers, R. Hintsche, Breitenstein A., Neubauer, P., Lose, M., Czyzf, A., Wegrzyn, G., Silfversparre, G., Jürgen, B., Schweder, T., and Enfors, S.O. (2004) *Biosens. Bioelectron.*, **19**, 537–546.
**182** Berti, F., Laschi, S., Palchetti, I., Rossier, J.S., Reymond, F., Mascini, M., and Marrazza, G. (2009) *Talanta*, **3**, 971–978.
**183** Rìos, A., Escarpa, A., Gonzàlez, M.C., and Crevillén, G.A.G. (2006) *Trends Anal. Chem.*, **25**, 467–479.

# 2
# Advanced Nanoparticles in Medical Biosensors

*Dan Fei, Songjun Li, Christian Cimorra, and Yi Ge*

## 2.1
## Introduction

Nanotechnology is redefining fields like imaging, diagnosis, drug delivery, regenerative medicine, and biomaterials as well as underpinning the development of new generations of medical products. Many of these advances could offer vastly improved outcomes for patients, therapies for hitherto difficult-to-treat diseases or conditions, improved manufacturing efficiency, or better use of valuable medical professional resources. The technology has already found its way into multifarious applications, including diagnostic imaging agents, drug delivery systems, body sensors, displays, high performance X-ray tubes, tissue engineering, microfluidics, lab-on-a-chip, pathogen detection systems, and compact electronic systems [1].

What makes nanotechnology so important and attractive is its ability to help researchers and scientists disclose and understand many diseases on the molecular and cellular level, leading to new insights in diagnostics and therapy. This unique capability is invigorating the demand for nanotechnology in medicine to help solve many of today's challenges in healthcare.

Nanotechnology has impacted vastly in the detection of disease, mainly by electrochemical, electromechanical, resonance, thermal, magnetic, and optical strategies. The formulation of medical biosensors has improved the clinician's and researcher's ability to identify specific analytes and infer knowledge to detail biomolecular profiles of disease. The recognition of specific biomarkers and their proportional expressions has led to the development of integrated detection systems capable of "sensing" microenvironmental fluctuations, thus providing an indication of disease, disease progression, and therapeutic efficacy assessment.

For example, cancerous and tumoral references have been reported throughout the centuries, making this complex and varied disease state a major burden on the quality of life and life expectancy throughout the human population. Diagnosis usually could only be preformed when a clear solid tumor mass progression or pathophysiology was apparent, thereby reducing the possibility for optimal prognosis. Concomitant to the evolution of disease, medical nanotechnologies have elucidated the biological origins of many pathological states and are gaining

*Biosensor Nanomaterials*. Edited by Songjun Li, Jagdish Singh, and Ipsita A. Banerjee

ISBN: 978-3-527-32841-3

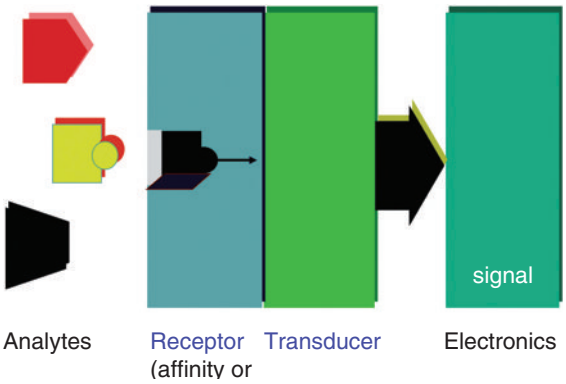


**Figure 2.1** Schematic representation of a biosensor.

momentum in early disease detection procedures utilizing advanced biosensing technologies.

As illustrated in Figure 2.1, biosensors are analytical devices incorporating a biological material (e.g., tissue, microorganisms, organelles, cell receptors, enzymes, antibodies, nucleic acids, natural products), a biologically derived material (e.g., recombinant antibodies, engineered proteins, aptamers), or a biomimic (e.g., synthetic catalysts, combinatorial ligands, imprinted polymers) intimately associated with or integrated within a physicochemical transducer or transducing microsystem, which may be optical, electrochemical, thermometric, piezoelectric, magnetic, or micromechanical [2]. Biosensors usually yield a digital electronic signal that is proportional to the concentration of a specific analyte or group of analytes. While the signal may in principle be continuous, devices can be configured to yield single measurements to meet specific market requirements [2].

The sensing component of a biosensor can be made from a variety of materials, commonly chosen by their selectivity and specificity to the sought analyte. The most widely used sensing elements are antibodies and antigens due to their highly selective binding to homologous antibodies/antigens (monoclonal/polyclonal) and the ease of identification from within a library derived from phage display technologies (immunosensor). However, many other biomolecule receptors have been described (biosensor), including peptides derived from combinatorial library screening, synthetic receptors fabricated by molecularly imprinted polymers (MIPs) [3–5], and synthetic nucleic acid receptors termed aptamers [6], which are determined by stochastic synthetic evolution of ligands. The choice of the element depends on the applied use and the relevant transductor mechanism utilized; it is therefore necessary to determine the available biosensor system that will most optimally function under the microenvironmental conditions desired.

The exploitation of nanosized materials for sensor fabrication has attracted increasing interest during the past decade mainly due to the highly tunable size- and shape-dependent chemical and physical properties of nanomaterials. They

exhibit unique surface chemistry, high surface area, large pore volume per unit mass, and thermal stability, offering excellent prospects for designing novel sensing systems and enhancing the performance of the sensing. The main nanosized materials utilized by medical diagnostic tactics include nanoparticles, carbon nanotubes, nanocantilevers, nanopores, quantum dots (QDs), dendrimers, nanotubes/wires/rods/shells, fullerenes, and so on. Receptors can be immobilized onto these structured surfaces and elicit a change in the physicochemical properties of the structure, thereby causing a measurable "change." These engineered nanostructures could even integrate sensory and transductor components into a single functional system (self-sensing and reporting). In other words, by utilizing those advanced nanosized materials, biosensors could be miniaturized into nanodimensions and multiplex biosensor (micro)systems could be fabricated. Nanobiosensors could further offer great promise for the attainment of multiple goals (e.g., faster, cheaper, less complex, and more easy to centralize) in medical diagnostics, such as the detection of microorganisms in various samples, monitoring of metabolites in body fluids, and detection of tissue pathology such as cancer.

## 2.2 Nanoparticles

In nanotechnology, in terms of diameter, a nanoparticle (or nanopowder or nanocluster or nanocrystal) usually is a microscopic particle sized between 1 and 100 nm. They may or may not exhibit size-related properties that differ significantly from those observed in fine particles or bulk materials. Nanoparticle research is currently an area of intense scientific research, due to a wide variety of potential applications in biomedical, optical, and electronic fields. Nanoparticles are of great scientific interest for medical biosensors as they have some unique properties (e.g., mechanical, optical, electrochemical, and magnetic properties) that can be applied to and facilitate sensor applications. Furthermore, the functionalization of the periphery of nanoparticles, such as encapsulation of nanoparticles with biological species and coating of nanoparticles with biodegradable polymers, offers distinct advantages in term of biocompatibility, solubility, and special targeting in sensor applications.

The preparation and properties of nanoparticles have been comprehensively reviewed [7–9] and they are commonly synthesized by chemical reduction. Novel synthetic methods have already led to precise control over particle size, shape, and stability, thus allowing further modification of a wide variety of ligands on the particle surfaces.

### 2.2.1 Gold Nanoparticles

Gold nanoparticles (Au-NPs) are among the most utilized nanoparticles in the fabrication of a broad range of medical biosensors. Mirkin *et al.* invented an

elegant ultrasensitive assay, namely the bio-barcode assay, for detecting protein analytes [10], which demonstrated its capability to detect protein concentrations as low as attomolar in solution using DNA-functionalized Au-NPs. The bio-barcode assay is a powerful amplification and detection system for nucleic acids and proteins [11–13]. Later, a single disposable chip sensor that realizes the optimized bio-barcode assay was developed for screening protein biomarkers, such as prostate-specific antigen (PSA) [14]. As can been seen in Figure 2.2, the general protocol of a bio-barcode assay can be divided into two stages: target protein separation and barcode DNA detection. The enhanced nanoparticles after silver staining are visible to the naked eye and can be thus detected by the commercially available scanners.

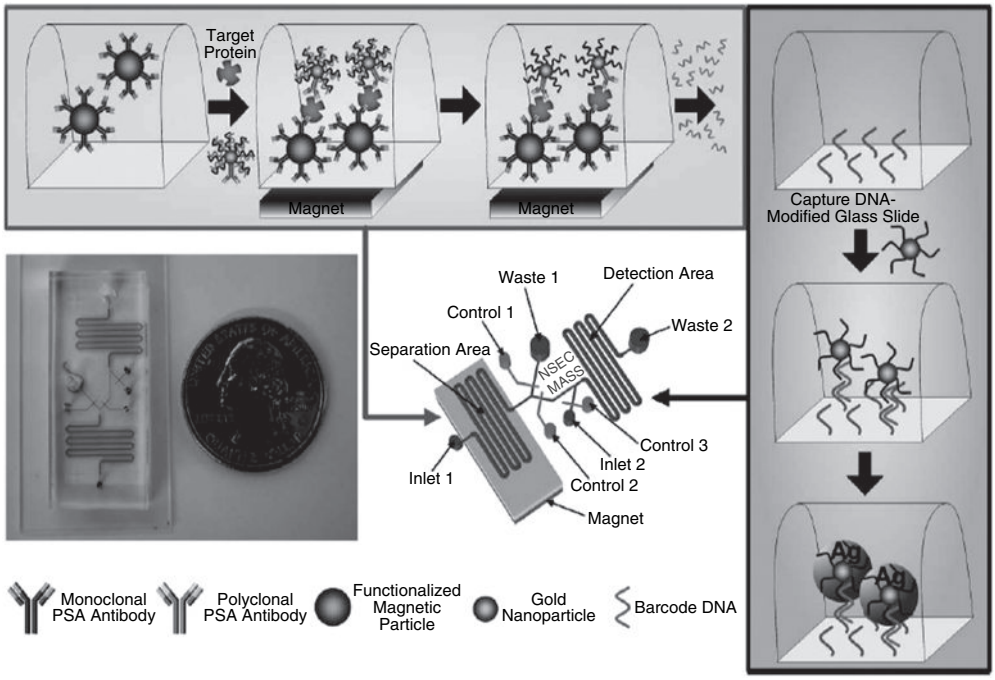


**Figure 2.2** Implementation of the bio-barcode assay within a microfluidic device. First, magnetic particles functionalized with monoclonal PSA antibodies are introduced into the separation area of the chip. The particles are then immobilized by placing a permanent magnet under the chip, followed by introduction of the sample and Au-NPs that are decorated with both polyclonal antibodies and barcode DNA. The barcode DNA is then released from the Au-NPs and is transported to the detection area of the chip. The detection area of the chip is patterned with capture DNA. Salt and a second set of Au-NPs functionalized with complementary barcode DNA sequences are introduced into the detection area to allow hybridization. Finally, the signal from the Au-NPs is amplified using silver stain. (Adapted from [14].)

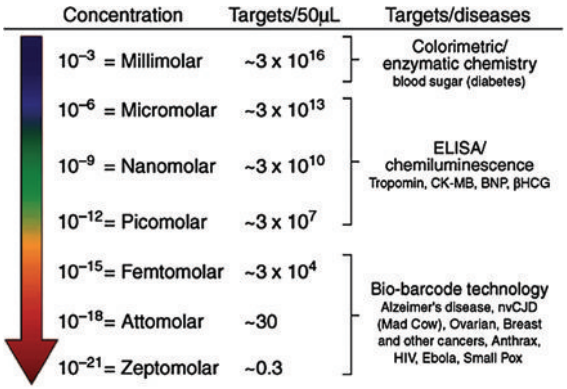


**Figure 2.3** Biomolecule detection technology. The bio-barcode assay provides access to a target concentration range well below that of conventional ELISAs. This ultrasensitivity provides the ability to utilize new markers for disease screening in biodiagnostics. CK-MB = creatine kinase MB isoenzyme; BNP = B-type natriuretic peptide; β-HCG = β-human chorionic gonadotrophin; HIV = human immunodeficiency disease; nvCJD = new variant Creutzfeldt–Jakob. disease (Adapted from [15].)

In medical diagnostics and clinical practice, this bio-barcode detection system offers great advantages to detect nucleic acids close to the sensitivity of polymerase chain reaction (PCR) without the need for complicated enzymatic processes, such as enzyme-linked immunosorbent assay (ELISA). In comparison to the ELISA-based technologies, the bio-barcode assay is up to $10^6$ times more sensitive, and this technology has been successfully applied to the screening and diagnostics of Alzheimer's disease, mad cow disease, prostate cancer, and so on, by utilizing and detecting new biomarkers [15] (Figure 2.3).

Introducing molecular recognition motifs (i.e., biofunctional groups) to the nanoparticles has attracted increasing interest since it provides new tools to control the bottom-up assembly of nanostructures and facilitates novel bioanalytical applications. After the functionalization, nanoparticles could be integrated with biomolecules (e.g., enzymes, antigens/antibodies, and DNA) to form hybrids, which may reveal new materials functions. A novel enzyme–nanoparticle hybrid system was successfully developed by Willner *et al.* for an advanced glucose biosensor [16]. An electrical wiring of the cofactor flavin adenine dinucleotide (FAD)-dependent glucose oxidase (GOx) was constructed on an electrode using a 1.4-nm FAD-functionalized Au-NP as the electrical nanoconnector [17] (Figure 2.4). This system showed exceptional electrical contact with the electrode support, where the electron transfer turnover rate is about 5000 $s^{-1}$, compared with the rate at which molecular oxygen, the natural cosubstrate of the enzyme, accepts electrons (around 700 $s^{-1}$). The Au-NP acts as an electron relay or "electrical nanoplug" for the alignment of the enzyme on the conductive support and for the electrical wiring of its redox-active center. Willner *et al.* later reported the reconstitution of apo-glucose dehydrogenase to a pyrroloquinoline quinine-functionalized Au-NP

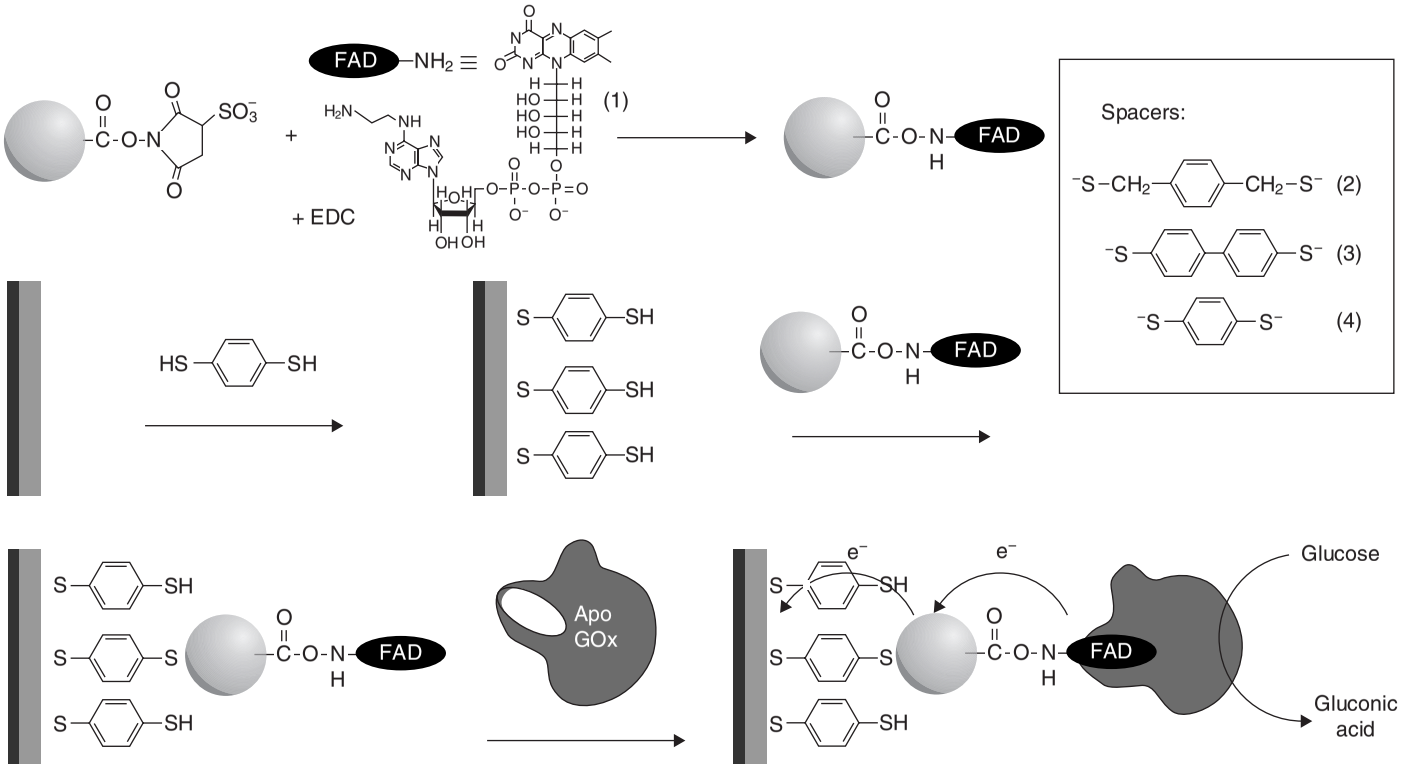


**Figure 2.4** Assembly of a Au-NP-reconstituted GOx electrode. EDC = 1-ethyl-3-(3-dimethylaminopropyl)-carbodiimide. (Adapted from [17].)

linked to the electrode by dithiolate [18]. The electron transfer turnover rate was also exceptionally high (around 11 800 $s^{-1}$). Some other enzymes, such as alcohol dehydrogenase ($NAD(P)^+$-dependent enzyme) [19, 20], acetylcholinesterase [21], and tyrosinase [22], have been successfully applied to the enzyme/nanoparticle hybrid system.

The detection and determination of enzymatic activities and kinetic parameters play an important role in the fabrication of advanced medical diagnostic devices. Except for the electrochemical biosensors for probing enzyme activities by using the enzyme/nanoparticle hybrid systems, the colorimetric indicators using Au-NPs have been developed towards the evaluation of enzyme activity and screening of enzyme inhibitors [23]. This technology can be applied to screen libraries of inhibitors of endonucleases in a high-throughput fashion by either the naked eye or a simple colorimetric reader. In addition, single-base gene variations can be disease cause (e.g., cancer), but most established methods rely on melting point analysis of double-stranded DNA. By using DNA-linked Au-NPs, improved assay performance with a precise discrimination of single-base mismatch could be achieved at an extremely narrow melting range (1–2 °C) [24]. This system provides a novel platform for DNA detection with impressively high sensitivity and selectivity. Another good example of a nanobiosensor with improved sensitivity was reported by Wang *et al.* [25]. They developed an Au-NP-amplified quartz crystal microbalance (QCM) sensor for *Escherichia coli* O157:H7 detection. The limit of detection is as low as $2 \times 10^3$ CFU $ml^{-1}$, demonstrating a significantly improvement compared to traditional QCM.

### 2.2.2
### Magnetic Nanoparticles

Magnetic nanoparticles (MNPs) are a class of nanoparticles that can be manipulated under the influence of an external magnetic field. They are usually composed of magnetic elements, such as iron, nickel, cobalt, and their oxides, and are widely applied in magnetic resonance imaging, targeted drug and gene delivery, tissue engineering, cell tracking, and bioseparation. Recently, MNPs have been used as labels in medical biosensors [26, 27]. Koets *et al.* demonstrated a magneto-resistant biosensor using superparamagnetic particles as detection labels for *E. coli* and *Salmonella* [28]. In their work, the purified genomic bacterial DNA was used as a template for PCR using a 5′-biotin forward primer and a 5′-fluorescein reverse primer. The double-stranded PCR product was then mixed with streptavidin-coated superparamagnetic particles. As a result, the particle complexes could be captured by antifluorescein antibodies at the sensor surface and detected by the giant magneto resistance (GMR) biosensor platform (Figure 2.5). Since the magnetic particles speed up the assay by reducing diffusion limitations, the modified GMR biosensor was demonstrated to be very powerful. This technology resulted in a very fast (one-step format with total assay times of less than 3 min) and highly sensitive (4–250 pM amplicon concentrations) biosensing system. Another GMR biochip based on a spin-valve sensor array and magnetic nanoparticle labels was

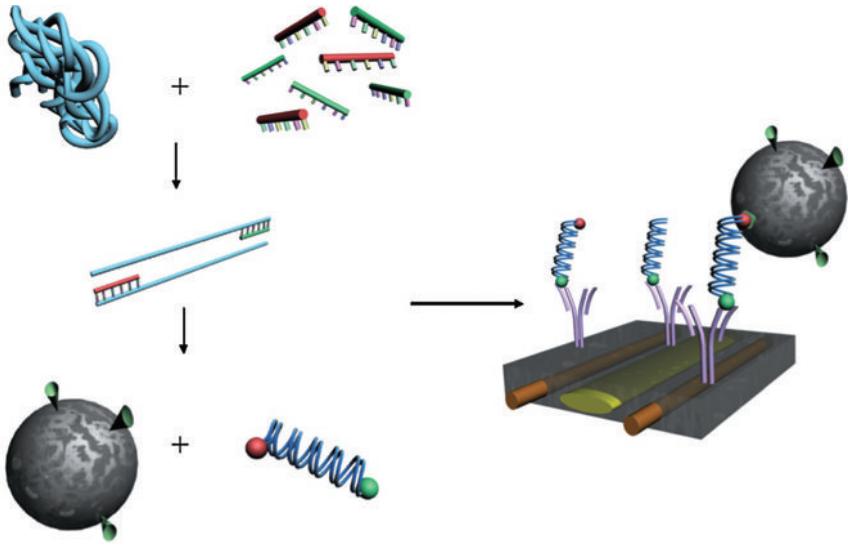

**Figure 2.5** Detection of double-tagged PCR product on a GMR sensor using magnetic particles in a one-step assay format. Amplification of an *E. coli*-specific DNA product is performed by PCR on genomic DNA using a 5′-biotin forward primer and a 5′-fluorescein reverse primer. The double-stranded PCR product is mixed with streptavidin-coated superparamagnetic particles and applied to the cartridge. Amplicon–particle complexes are captured by antifluorescein antibodies at the sensor surface and detected by the GMR sensor. (Adapted from [28].)

recently reported by Wang *et al.* for inexpensive, sensitive, and reliable DNA detection [29, 30]. The real-time measurement results showed that the magnetic biochips are sensitive to a wide range of target DNA concentration, ranging from 10 pM to 10 nM.

Other immunomagnetic biosensors utilizing MNPs have been described for the detection of *E. coli* [31, 32], *Salmonella* [33] and *Staphylococcus aureus* [34]. Very recently, Wan *et al.* reported a fast, sensitive and reliable QCM biosensor for the selective detection of the marine pathogenic sulfate-reducing bacterium, D. desulfotomaculum [35]. In summary, the applications of MNPs in biosensing showed great potentials in developing fast, sensitive, and reliable medical diagnostic devices.

### 2.2.3 Quantum Dots

A quantum dot (QD) is a semiconductor whose excitons are confined in all three spatial dimensions. As a result, they have properties that are between those of bulk semiconductors and those of discrete molecules. The most important properties involve the ability to emit light with an extremely narrow spectrum emission

proportional to the particle size. They are normally made of copper, zinc, and lead sulfides, selenides, and tellurides with a dimension between 5 and 50 nm, and they have already been applied in transistors, solar cells, LEDs, diode lasers, medical imaging, and so on.

Intensive investigations have been conducted applying QDs to medical biosensors due to their unique photoluminescent properties. Compared with conventional optical biosensors based on the measurement of protein-based fluorophores [36] and fluorescence emission of organic dyes [37], QDs exhibits excellent photostability and high quantum yield (i.e., high intensity). More importantly, unlike traditional fluorescent biosensors, which are usually not applicable for multicolor applications, QDs show size- and composition-tunable emission spectra, thus allowing the simultaneous identification of multiple samples.

Nie *et al*. presented a novel work on multicolor optical coding for biological assays by embedding different sized QDs (zinc sulfide-capped cadmium selenide nanocrystals) into polymeric microbeads at precisely controlled ratios [38]. The imaging and spectroscopic measurements indicated that the QD-tagged beads are highly uniform and reproducible, yielding bead identification accuracies as high as 99.99% under favorable conditions. It was found that the use of 10 intensity levels and six colors could theoretically code 1 million nucleic acid or protein sequences, and the coding and target signals could be simultaneously read at the single-bead level. New opportunities in medicine and biology, such as medical diagnostics, gene expression studies, and high-throughput screening, could be expected to be offered. Nie's group recently successfully coated the surfaces of QDs with a copolymer of polyethylene glycol (PEG) and polyethylenimine (PEI), so that they are able to be introduced into cells [39]. PEI is widely used as a gene delivery vector since it can cross the cell membrane and disrupt intracellular organelles, giving the QDs access to a myriad of cellular targets, while PEG improves the QDs' solubility and stability, and dramatically reduces the cytotoxic effects of the PEI. Their work greatly facilitates the introduction of nontoxic QDs into the cytosol where they can act as signal transducers in sensing schemes. Recently, Liu *et al*. developed a biosensor system based on a flowing chamber with a microporous immunofilter for capturing *E. coli* O157:H7 and used QD dendron nanocrystals as fluorescent labels [40].

Apart from fluorescent detection in medical biosensing applications, QDs have also been utilized for electrochemical detection. Wang *et al*. described an electrochemical coding technology for simultaneous detection of multiple DNA targets by electrochemical stripping analysis [41]. They developed a new multitarget sandwich hybridization assay involving a dual-hybridization approach, where multiple different probes are attached to the magnet beads and another set of probes for specific targets (e.g., multiple DNA targets) is immobilized on three different QDs (CdS, PdS, and ZnS QDs). As can be seen in Figure 2.6, probe-modified magnetic beads were first incubated with targets (i.e., the first hybridization). The second hybridization with probe-modified QDs then produced functional magnetic beads with multiple QD labels. Finally, following a magnetic separation step and dissolution of the QDs, the stripping voltammetry was able to reveal

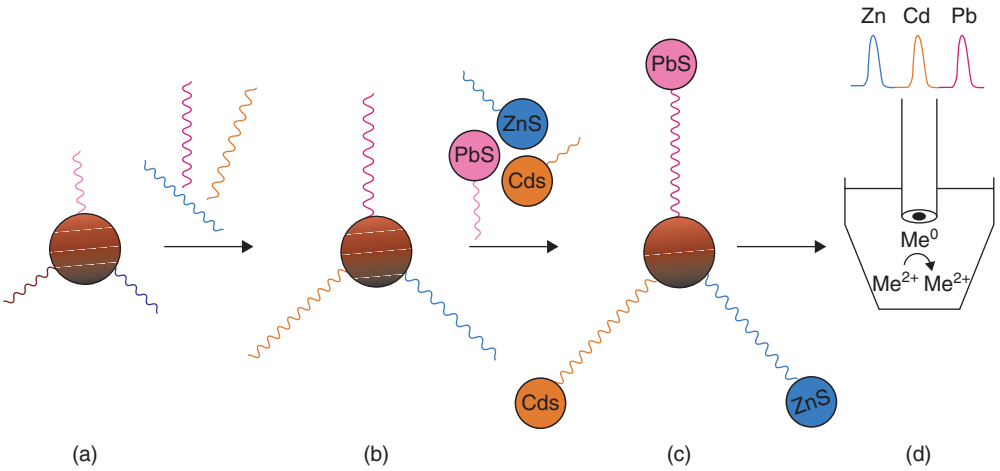


**Figure 2.6** Multitarget electrical DNA detection protocol based on different inorganic colloid nanocrystal tracers. (a) Introduction of probe-modified magnetic beads. (b) Hybridization with the DNA targets. (c) Second hybridization with the QD-labeled probes. (d) Dissolution of QDs and electrochemical detection. (Adapted from [41].)

the amount of target molecules present in a sample since the metals ions from the dissolved QDs strip from the voltammetric electrode at different potentials. The reported limit of detection is 13 fmol in 50-µl samples, corresponding to 270 pM, and up to five different types of QDs could be present in a single assay, thus allowing the simultaneous detection of up to five different targets. Wang *et al.* further reported a simultaneous detection of multiple protein targets in a similar way [42] and in one of their recent works they immobilized aptamer capture probes on a gold surface for the detection of lysozyme and thrombin via a single-step displacement protocol [43].

Although stripping analysis is a very sensitive technique for the detection of metal ions in solution, it requires the ions in solution to be transiently deposited on the electrode. In contrast, potentiometry with ion-selective electrodes is able to detect the presence of femtomolar amounts of ions in microliter volumes without the need for preconcentration deposition on the electrode. This technique has a direct relationship between sample activity and observed electromotive force, thus it is independent of the volume of the sample or electrode surface. A potentiometric immunoassay of mouse IgG via CdSe QD labels was recently described, on a secondary antibody according to a sandwich immunoassay protocol in a microtiter plate format reported, for the detection of cadmium ions [44]. This immunoassay showed a detection limit of less than 10 fmol in 150-µl sample wells and the CdSe QDs were found to help the maintenance of pH at a near-neutral value since they are easy to be dissolved/oxidized in a matter of minutes with $H_2O_2$.

### 2.2.4
### Silica-Based Nanoparticles

Silica-based nanoparticles (SNPs) are usually prepared by two approaches: the Stöber method and the reverse microemulsion method. They are both "bottom-up" methods and the particles are formed by self-assembly. SNPs have been investigated intensively in recent years since they are highly chemically and thermally stable, have a large surface area and a fine suspension ability in aqueous solution, and are relatively environmentally inert [45]. Moreover, SNPs have a high surface silanol concentration that greatly facilitates a broad variety of surface reactions/modifications and the consequent binding of biomolecules, such as biotin–avidin, antigen–antibodies, peptides, proteins, and DNA. In addition, SNPs could be simply modified and functionalized by doping/mixing with different materials (e.g., organic dyes, magnetite, biomolecules, and QDs) for many applications, such as biosensing, labeling, and biomedical imaging.

Glutamate dehydrogenase- and lactate dehydrogenase-immobilized/conjugated SNPs were reported in 2001 [46]. The results showed that SNPs are a good biocompatible solid support for enzyme immobilization, and the immobilized enzymes retains their activities in their respective enzymatic reactions. Thus, the application of biosensing using such kinds of functionalized system is feasible. More enzyme-based biosensors using SNPs have been developed in recent years [47–51]. They showed great specificity and low concentration detection limits; however, they suffer from the problems of denaturation and inactivation, and are lack high porosity and optical transparency. Mesoporous silicas provide a solution towards the last two defects: (i) they have high porosity and large surface areas that benefit the immobilization of the sensing molecules not only on the external surface of the material, but also inside the pores, giving fast responses and low detection limits; and (ii) they have good optical transparency, which permits optical detection through the layers of molecules.

Lin *et al*. successfully developed novel mesoporous SNP-based selective sensory systems by controlling the diffusional penetration of analytes into the surface-functionalized mesopores [52]. They later described a work on a poly(lactic acid) (PLA)-coated mesoporous silica nanosphere-based fluorescence probe for the detection of amino-containing neurotransmitters [53]. As can been seen in Figure 2.7, the exterior surface of *o*-phthalic hemithioacetal (OPTA)–mesoporous SNP was selectively functionalized with PLA. The PLA layer acts as a gatekeeper controlling the diffusion of neurotransmitters to the inside of the pores where they react with the surface-anchored OPTA groups. The probe is able to distinguish between several structurally similar neurotransmitters, such as dopamine, tyrosine, and glutamic acid. Martinez-Manez *et al*. reported another similar biosensing system by grafting aminomethylanthracene groups onto mesoporous SNPs for the recognition and detection of anions [54].

In addition to the biomolecule immobilized/conjugated SNPs, the technique of sol–gel-based entrapment of biomolecules has also been extensively applied to the preparation of medical biosensors. The resulting systems could provide high

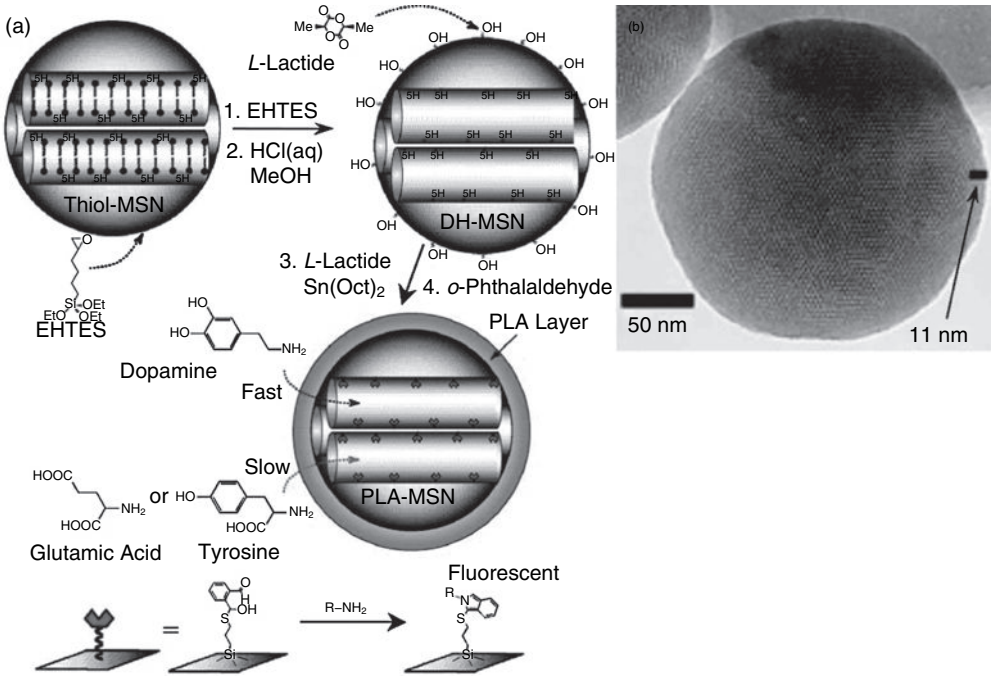


**Figure 2.7** (a) Schematic representation of the synthesis of PLA-coated mesoporous SNP (MSN)-based fluorescence sensor system for detection of amine-containing neurotransmitters (i.e., dopamine, glutamic acid, and tyrosine ($R\text{-}NH_2$)). EHTES = 5,6-epo xyhexyltriethoxysilane; cetyltrimethylammonium bromide surfactant shown in schematic head–tail representation. (b) Transmission electron micrograph of an ultramicrotomed PLA–mesoporous SNP material. The layer of PLA can be visualized by the rim of amorphous structure surrounding the MCM-41 type mesoporous SNP core with mesopores packed in a hexagonal symmetry. (Adapted from [53].)

loading capacities for biomolecular immobilization, which have high volumetric activity and enhanced mechanical stability. A fast amperometric biosensor was constructed by horseradish peroxidase (HRP)-encapsulated silica colloids to detect $H_2O_2$ [55]. Other hybrid materials, such as alginate [56], ferrocene [57], chitosan [58], and hydroxyapatite [59], have also been doped into silica sol–gel for the fabrication of biosensors. Electrochemiluminescent tris(2,2′-(bipyridyl)ruthenium(II) ($Ru(bpy)_3^{2+}$) ion-doped SNPs have been utilized for biosensors for a variety of medical analytes, such as DNA, peptides, and proteins [40], and silica-coated QD nanoparticles were further used for the electrochemical and optical detection of glucose [60].

### 2.2.5 Dendrimers

Dendrimers, which are spheroid or globular nanostructures, have been extensively exploited for applications in medical biosensing. They are very uniform with

extremely low polydispersities and are commonly created with dimensions incrementally grown in approximately nanometer steps from 1 to over 10 nm. Dendrimers are precisely engineered and are capable of carrying molecules encapsulated in their interior void spaces or attached to the surface. The control over size, shape, and surface functionality makes dendrimers one of the "smartest" or customizable nanotechnologies available.

In early 2000, Yoon *et al.* reported an affinity biosensor system based on avidin–biotin interaction on a gold electrode [61]. A fourth-generation (G4) poly(amidoamine) dendrimer with partial ferrocenyl-tethered surface groups was synthesized following by a covalent immobilization on a gold electrode. The unmodified surface amine groups from the dendritic monolayer were then functionalized with biotinamidocaproate before an affinity-sensing surface interacting with avidin. The detection limit of avidin was about 4.5 pM and the sensor signal was linear ranging from 1.5 pM to 10 nM under optimized conditions. Another electrochemical biosensor utilizing dendrimers was described by Chang *et al.* for the detection of live *Pseudomonas aeruginosa* [62]. A sensing film containing a G4 hydroxy-terminated polyamidoamine (PAMAM) dendrimer (i.e., G4-OH) and SYTOX Green fluorescent nucleic acid stain was developed, and configured on simple, disposable plastic coupons or optical fibers. The resulting system was interrogated by a miniature fiber-optic spectrometer. Dendrimers were found to dramatically increase the sensitivity and stability of the sensing film. Frasconi *et al.* applied ferrocenyl-tethered dendrimers as an electrode modifier supported by a self-assembled monolayer-coated gold surface [63]. GOx was further covalently attached to the dendrimers. The resulting integrated hybrid system provides electrical contact between the redox center of the GOx and the electrode, thus improving the overall bioelectrocatalyzed oxidation of glucose.

Recently, dendrimers in conjugation with other nanoparticles have been extensively investigated. A penicillamine biosensor based on tyrosinase immobilized on Au-NP/PAMAM dendrimer-modified gold electrode was successfully developed [64](Figure 2.8). The gold electrodes were modified with submonolayers of 3-mercaptopropionic acid and further reacted with PAMAM dendrimers to obtain thin films. The high affinity of PAMAM dendrimer for Au-NPs with its amine groups was used to realize the role of nano-gold as an intermediator to immobilize tyrosinase, which can effectively catalyze the oxidation of catechol to *o*-benzoquinone. Since penicillamine could react with *o*-benzoquinone to form the corresponding thioquinone derivatives, a decrease of the reduction current of *o*-benzoquinone would be electrochemically detected. The prepared biosensor showed a good performance in terms of sensitivity, operational stability, and nice reproducibility.

Yao *et al.* presented a work on an enzyme-linked field-effect transistor (ENFET) biosensor using dendrimer-encapsulated platinum nanoparticles for direct glucose concentration analysis [65]. The fabricated glucose-sensitive ENFETs biosensor showed dramatically enhanced sensitivity and extended lifetime compared with conventional biosensors. The sensor has a linear range of 0.25–2.0 mM and a detection limit of around 0.15 mM. When stored in a dry state at 4 °C, it could be well used for detecting glucose samples at intervals for at least 1 month.

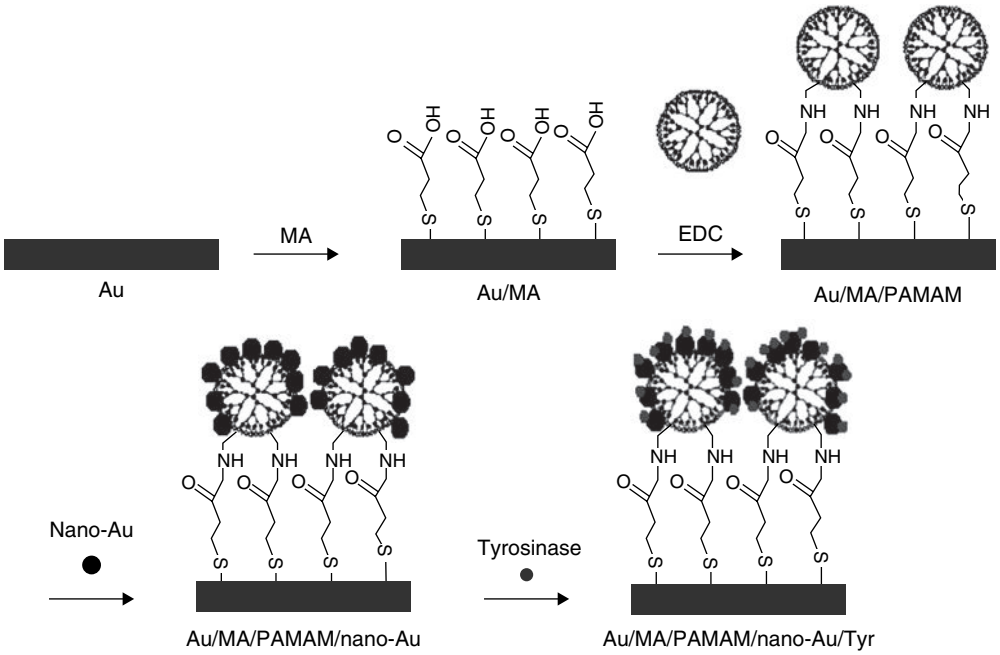


**Figure 2.8** Schematic representation of the surface modification process and fabrication of a tyrosinase biosensor. MA = 3-mercaptopropionic acid. EDC = 1-ethyl-3-(3-dimethylaminopropyl)-carbodiimide. (Adapted from [64].)

### 2.2.6
### Fullerenes

Fullerenes molecules consist of 60, 70, or more carbon atoms, unlike diamond and graphite – the more familiar forms of carbon. Since their discovery in 1985 [66], fullerenes have attracted considerable interest in many fields of research including material science and biomedical applications because of their unique physical and chemical properties. In recent years, studies on functionalized fullerenes for various applications in the field of biomedical sciences have seen a significant increase. The ultimate goal is towards employing these functionalized fullerenes in the diagnosis and therapy of human diseases. Functionalized fullerenes are one of many different classes of compounds that are currently being investigated in the rapidly emerging field of nanomedicine.

For example, fullerene is a very promising family of electroactive compounds. This new type of compound has been found very promising as electrochemical mediators in amperometric biosensors, since it has multiple redox states in a wide range of potentials, very low solubility in aqueous solutions, and is stable in many redox forms. Mediators in biosensors are usually employed to shuttle electrons between the redox protein and conducting support (e.g., electrode). It was reported that a buckminsterfullerene ($C_{60}$) could undergo six distinct one-electron reversible

reductions forming stable intermediates [67]. Furthermore, the possibility of achieving electron transfer between soluble enzymes and electrode by $C_{60}$ was demonstrated by Willner *et al*. [68].

Back to 2000, a first successful prototype of fullerene-mediated amperometric biosensor for glucose detection was described by Gavalas *et al*. [69]. In their work, different amounts of fullerene ($C_{60}$) were immobilized by adsorption into a porous electrode prior to the introduction of GOx. The use of fullerene as an electrochemical mediator allows for lower optimum operation potentials, while higher loading of fullerene results in faster response times and good overall analytical characteristics. The operational stability of this amperometric biosensor, as well as the immobilization procedure, was further investigated [70]. It was found that mesoporous carbon materials with surface oxygen groups are the most suitable electrochemical transducers. These materials also showed the best sensitivity to $H_2O_2$, and provided a very good matrix for enzyme adsorption and immobilization. The combination of it and fullerenes thus could generate a versatile biosensor.

Unlike Gavalas's system, Carano *et al*. later demonstrated a glutathione amperometric biosensor using a functionalized amphiphilic fullerene [71], where the functionalized fullerene and redox enzyme were covalently immobilized within the an amphiphilic polypyrrole film to prevent the leakage that may occurs. The film was then cast onto a glassy carbon electrode to realize a fast and reproducible biosensor for glutathione. Very recently, a synergistic glucose biosensor employing not only fullerene but also ferrocene, chitosan, and ionic liquid was reported [72]. In such system, the electrochemical activity of fullerene ($C_{60}$) and ferrocene could greatly accelerate the electrochemical reaction and improve the electron relays for activating the oxidation of glucose. Meanwhile, the network of a chitosan–ionic liquid would provide a favorable microenvironment to keep the bioactivity of GOx, and the electron conduction pathways for GOx through fullerene ($C_{60}$) and ferrocene. Due to these synergetic contributions, a novel glucose biosensor was fabricated with excellent sensitivity, selectivity, stability, and fast response time. Moreover, it has other attractive advantages such as ease of preparation, low cost, and acceptable accuracy for sample determination, which all make this sensor ideal for the detection of glucose in real samples such as blood serum samples. In addition, due to its low operating potential (100 mV), the resulting biosensor is relatively insensitive to electroactive interfering species in human blood, such as ascorbic acid and uric acid, which are commonly found in blood samples.

Apart from the popular electrochemical biosensors, Shih demonstrated a piezoelectric crystal immunobiosensor based on immobilized fullerene ($C_{60}$)–antibodies [73]. As illustrated in Figure 2.9, the fullerene–antihuman IgG-coated piezoelectric crystals were prepared and applied in a piezoelectric quartz crystal immunobiosensor for detecting human IgG. As it is well know, the fullerene ($C_{60}$) molecule with a conjugate π-electron structure [66, 74–76], like olefin molecules, can be electrophilically attacked by electron-releasing molecules such as amines, proteins, and enzymes [77–80]. Thus NH group-containing amines and enzymes (e.g.,

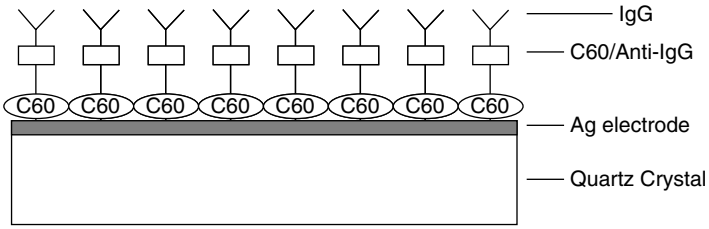


**Figure 2.9** Fullerene–antihuman IgG-coated quartz crystal electrode for sensing human IgG. (Adapted from [73].)

antihuman IgG and antihemoglobin) could be chemically attached to the fullerene ($C_{60}$) molecule, resulting in the formation of immobilized fullerene–antibodies such as fullerene–antihuman IgG and fullerene–antihemoglobin. The resulting biosensor exhibited good sensitivity with detection limits of below $10^{-4}$ mg ml$^{-1}$ for both of IgG and hemoglobin, and good selectivity for these biomolecules in aqueous solutions. Furthermore, the interference of various common species in human blood (e.g., urea, uric acid, cysteine, tyrosine, ascorbic acid, and metal ions) to the IgG piezoelectric crystal biosensor was investigated and nearly no interference was found.

## 2.3 Conclusions and Outlook

In summary, advanced nanomaterials have been extensively explored in recent years to create state-of-the-art sensor products, displaying high performance (high sensitivity and selectivity in particular) together with some great advantages such as miniaturization, fast response time, and cost-effectiveness, for the detection and quantification of bioanalytes in clinical practice (e.g., routine blood testing), home healthcare (e.g., glucose monitoring), manufacturing (e.g., worker health), and so on.

Among multifarious nanomaterials, nanoparticles hold immense promise as versatile materials for realizing a new generation of medical biosensors because of their characteristic properties (e.g., unique mechanical, electrochemical, optical, and magnetic properties) and capability of flexible modification/functionalization (e.g., coupling of electroactive compounds and/or biomolecules). For example, protein- and nucleic acid-functionalized SNPs have been successfully developed as labels for the amplified transduction of biorecognition events.

Striking progress in this emerging field has been made and it has been underpinned by the rapid expansion of nanotechnology; however, more investigations with respect to the toxicity, ethics, and regulation of nanoparticles are further required, especially in their biomedical applications such as medical devices, diagnostics, biological assays, and drug delivery. Nevertheless, in light of the current

healthy status of nanoparticle development, it could be foreseen that nanoparticle-based medical biosensors will keep evolving rapidly, and have great potential to rival and eventually replace our existing conventional medical biosensors.

## References


**1** Jain, K.K. (2008) *Med. Princ. Pract.*, **17**, 89–101.
**2** Eggins, B.R. (2002) *Chemical Sensors and Biosensors*, John Wiley & Sons, Ltd, Chichester.
**3** Yano, K. and Karube, I. (1999) *Trends Anal. Chem.*, **18**, 199–204.
**4** Ge, Y. and Turner, A.P.F. (2008) *Trends Biotechnol.*, **26**, 218–224.
**5** Ge, Y. and Turner, A.P.F. (2009) *Chem. Eur. J.*, **15**, 8100–8107.
**6** Lee, J., So, H., Jeon, E., Chang, H., Won, K., and Kim, Y.H. (2008) *Anal. Bioanal. Chem.*, **390**, 1023–1032.
**7** Niemeyer, C.M. (2001) *Angew. Chem. Int. Ed.*, **40**, 4128–4158.
**8** Bönnemann, H. and Richards, R.M. (2001) *Eur. J. Inorg. Chem.*, 2455–2480.
**9** Wang, Z. and Ma, L. (2009) *Coord. Chem. Rev.*, **253**, 1607–1618.
**10** Nam, J.M., Thaxton, C.S., and Mirkin, C.A. (2003) *Science*, **301**, 1884–1886.
**11** Nam, J.M., Stoeva, S.I., and Mirkin, C.A. (2004) *J. Am. Chem. Soc.*, **126**, 5932–5933.
**12** Thaxton, C.S., Hill, H.D., Georganopoulou, D.G., Stoeva, S.I., and Mirkin, C.A. (2005) *Anal. Chem.*, **77**, 8174–8178.
**13** Georganopoulou, D.G., Chang, L., Nam, J.M., Thaxton, C.S., Mufson, E.J., Klein, W.L., and Mirkin, C.A. (2005) *Proc. Natl. Acad. Sci. USA*, **102**, 2273–2276.
**14** Goluch, E.D., Nam, J.M., Georganopoulou, D.G., Chiesl, T.N., Shaikh, K.A., Ryu, K.S., Barron, A.E., Mirkin, C.A., and Liu, C. (2006) *Lab Chip*, **6**, 1293–1299.
**15** Cheng, M.M.C., Cuda, G., Bunimovich, Y.L., Gaspari, M., Heath, J.R., Hill, H.D., Mirkin, C.A., Nijdam, J., Terracciano, R., Thundat, T., and Ferrari, M. (2006) *Curr. Opin. Chem. Biol.*, **10**, 11–19.
**16** Xiao, Y., Patolsky, F., Katz, E., Hainfeld, J.F., and Willner, I. (2003) *Science*, **299**, 1877–1881.
**17** Willner, I., Baron, R., and Willner, B. (2007) *Biosens. Bioelectron.*, **22**, 1841–1852.
**18** Zayats, M., Katz, E., Baron, R., and Willner, I. (2005) *J. Am. Chem. Soc.*, **127**, 12400–12406.
**19** Xiao, Y., Pavlov, V., Levine, S., Niazov, T., Markovitch, G., and Willner, I. (2004) *Angew. Chem. Int. Ed.*, **43**, 4519–4622.
**20** Shlyahovsky, B., Katz, E., Xiao, Y., Pavlov, V., and Willner, I. (2005) *Small*, **1**, 213–216.
**21** Xiao, Y., Pavlov, V., Shlyahovsky, B., and Willner, I. (2005) *Chem. Eur. J.*, **11**, 2698–2704.
**22** Baron, R., Zayats, M., and Willner, I. (2005) *Anal. Chem.*, **77**, 1566–1571.
**23** Xu, X., Han, M.S., and Mirkin, C.A. (2007) *Angew. Chem. Int. Ed.*, **46**, 3468–3470.
**24** Jin, R., Wu, G., Li, Z., Mirkin, C.A., and Schatz, G.C. (2003) *J. Am. Chem. Soc.*, **125**, 1643–1654.
**25** Wang, L.J., Wei, Q.S., Wu, C.S., Hu, Z.Y., Ji, J., and Wang, P. (2008) *Chin. Sci. Bull.*, **53**, 1175–1184.
**26** Shen, W., Schrag, B.D., Carter, M.J., and Xiao, G. (2008) *Appl. Phys. Lett.*, **93**, 033903.
**27** Lowery, T.J., Palazzolo, R., Wong, S.M., Prado, P.J., and Taktak, S. (2008) *Anal. Chem.*, **80**, 1118–1123.
**28** Koets, M., van der Wijk, T., van Eemeren, J.T.W.M., van Amerongen, A., and Prins, M.W.J. (2009) *Biosens. Bioelectron.*, **24**, 1893–1898.
**29** Xu, L., Yu, H., Akhras, M.S., Han, S.J., Osterfeld, S., White, R.L., Pourmand, N., and Wang, S.X. (2008) *Biosens. Bioelectron.*, **24**, 99–103.
**30** Han, S.J. and Wang, S. (2010) *J. Ass. Lab. Auto.*, **15**, 93–98.

**31** Maalouf, R., Hassen, W.M., Fournier-Wirth, C., Coste, J., and Jaffrezic-Renault, N. (2008) *Microchim. Acta*, **163**, 157–161.

**32** Mujika, M., Arana, S., Castan, E., Tijero, M., Vilares, R., Ruano-López, J.M., Cruz, A., Sainz, L., and Berganza, J. (2009) *Biosens. Bioelectron.*, **24**, 1253–1258.

**33** Liébana, S., Lermo, A., Campoy, S., Barbe, J., Alegret, S., and Pividori, M.I. (2009) *Anal. Chem.*, **81**, 5812–5820.

**34** Lee, H., Sun, E., Ham, D., and Weissleder, R. (2008) *Nat. Med.*, **14**, 869–874.

**35** Wan, Y., Zhang, D., and Hou, B. (2010) *Biosens. Bioelectron.*, **25**, 1847–1850.

**36** Simpson-Stroot, J.M., Kearns, E.A., Stroot, P.G., Magan, S., and Lim, D.V. (2008) *J. Microbiol. Methods*, **72**, 29–37.

**37** Curtis, T., Naal, R.M., Batt, C., Tabb, J., and Holowka, D. (2008) *Biosens. Bioelectron.*, **23**, 1024–1031.

**38** Han, M., Gao, X., Su, J.Z., and Nie, S. (2001) *Nat. Biotechnol.*, **19**, 631–635.

**39** Duan, H. and Nie, S. (2007) *J. Am. Chem. Soc.*, **129**, 3333–3338.

**40** Liu, Y., Brandon, R., Cate, M., Peng, X., Stony, R., and Johnson, M. (2007) *Anal. Chem.*, **79**, 8796–8802.

**41** Wang, J., Liu, G.D., and Mercoki, A. (2003) *J. Am. Chem. Soc.*, **125**, 3214–3215.

**42** Liu, G., Wang, J., Kim, J., Jan, M.R., and Collins, G.E. (2004) *Anal. Chem.*, **76**, 7126–7130.

**43** Hansen, J.A., Wang, J., Kawde, A.N., Xiang, Y., Gothelf, K.V., and Collins, G. (2006) *J. Am. Chem. Soc.*, **128**, 2228–2229.

**44** Thurer, R., Vigassy, T., Hirayama, M., Wang, J., Bakker, E., and Pretsch, E. (2007) *Anal. Chem.*, **79**, 5107–5110.

**45** Tang, D., Yuan, R., and Chai, Y. (2007) *Clin. Chem.*, **53**, 1323–1329.

**46** Qhobosheane, M., Santra, S., Zhang, P., and Tan, W. (2001) *Analyst*, **126**, 1274–1278.

**47** Zong, S., Cao, Y., Zhou, Y., and Ju, H. (2006) *Langmuir*, **22**, 8915–8919.

**48** Shan, W., Yu, T., Wang, B., Hu, J., Zhang, Y., Wang, X., and Tang, Y. (2006) *Chem. Mater.*, **18**, 3169–3172.

**49** Shan, D., Zhu, M., Xue, H., and Cosnier, S. (2007) *Biosens. Bioelectron.*, **22**, 1612–1617.

**50** Betancor, L., Luckarift, H., Seo, J., Brand, O., and Spain, J. (2008) *Biotechnol. Bioeng.*, **99**, 261–267.

**51** Wu, Y., Chen, C., and Liu, S. (2009) *Anal. Chem.*, **81**, 1600–1607.

**52** Lin, V.S.Y., Lai, C.Y., Huang, J., Song, S.A., and Xu, S. (2001) *J. Am. Chem. Soc.*, **123**, 11510–11511.

**53** Radu, D.R., Lai, C.Y., Wiench, J.W., Pruski, M., and Lin, V.S.Y. (2004) *J. Am. Chem. Soc.*, **126**, 1640–1641.

**54** Descalzo, A.B., Marcos, M.D., Martinez-Manez, R., Soto, J., Beltran, D., and Amoros, P. (2005) *J. Mater. Chem.*, **15**, 2721–2731.

**55** Wang, G. and Zhang, L. (2006) *J. Phys. Chem. B*, **110**, 24864–24868.

**56** Lei, C., Shen, G., and Yu, R. (2007) *Chin. J. Anal. Chem.*, **35**, 273.

**57** Ballarin, B., Cassani, M., Mazzoni, R., Scavetta, E., and Tonelli, D. (2007) *Biosens. Bioelectron.*, **22**, 1317–1322.

**58** Kang, X., Mai, Z., Zou, X., Cai, P., and Mo, J. (2008) *Talanta*, **74**, 879–886.

**59** Wang, B., Zhang, J., Pan, Z., Tao, X., and Wang, H. (2009) *Biosens. Bioelectron.*, **24**, 1141–1145.

**60** Cavaliere-Jaricot, S., Darbandi, M., Kuçur, E., and Nann, T. (2008) *Microchim. Acta*, **160**, 375–383.

**61** Yoon, H.C., Hong, M., and Kim, H. (2000) *Anal. Biochem.*, **282**, 121–128.

**62** Chang, A., Gillespie, J.B., and Tabacco, M.B. (2001) *Anal. Chem.*, **73**, 467–470.

**63** Frasconi, M., Deriu, D., Dannibale, A., and Mazzei, F. (2009) *Nanotechnology*, **20**, 505501.

**64** Li, N.B., and Kwak, J. (2007) *Electroanalysis*, **19**, 2428–2436.

**65** Yao, K., Zhu, Y., Yang, X., and Li, C. (2008) *Mater. Sci. Eng. C*, **28**, 1236–1241.

**66** Kroto, H.W., Heath, J.R., O'Brien, S.C., Curl, R.F., and Smalley, R.E. (1985) *Nature*, **318**, 162–163.

**67** Dresselhaus, M.S., Dresselhaus, G., and Eklund, P.C. (1995) *Science of Fullerenes and Carbon Nanotubes*, Academic Press, San Diego, CA.

**68** Patolsky, F., Tao, G., Katz, E., and Willner, I. (1998) *J. Electroanal. Chem.*, **454**, 9–13.

**69** Gavalas, V.G. and Chaniotakis, N.A. (2000) *Anal. Chim. Acta*, **409**, 131–135.
**70** Sotiropoulou, S., Gavalas, V., Vamvakaki, V., and Chaniotakis, N.A. (2003) *Biosens. Bioelectron.*, **18**, 211–215.
**71** Carano, M., Cosnier, S., Kordatos, K., Marcaccio, M., Margotti, M., Paolucci, F., Prato, M., and Roffia, S. (2002) *J. Mater. Chem.*, **12**, 1996–2000.
**72** Wei, Z., Li, Z., Sun, X., Fang, Y., and Liu, J. (2010) *Biosens. Bioelectron.*, **25**, 1434–1438.
**73** Pan, N. and Shih, J. (2004) *Sens. Actuator B*, **98**, 180–187.
**74** Kraetschmer, W., Lamb, L.D., Fostiropoules, K., and Huffman, D.R. (1990) *Nature*, **347**, 354–358.
**75** Hawkins, J.M., Meyer, A., Lewis, T.A., Loren, S., and Hollander, F.J. (1991) *Science*, **252**, 312–313.
**76** Scrivens, W.A. and Tour, J.M. (1992) *J. Am. Chem. Soc.*, **114**, 7917–7919.
**77** Wei, L.F. and Shih, J.S. (2001) *Anal. Chim. Acta*, **437**, 77–85.
**78** Chao, Y.C. and Shih, J.S. (1998) *Anal. Chim. Acta*, **374**, 39–46.
**79** Hung, C.H. and Shih, J.S. (2000) *J. Chin. Chem. Soc.*, **47**, 1095–1104.
**80** Chuang, W. and Shih, J.S. (2001) *Sens. Actuator.*, **81**, 1–8.

# 3
# Smart Polymeric Nanofibers Resolving Biorecognition Issues

*Ashutosh Tiwari, Ajay K. Mishra, Shivani B. Mishra, Rajeev Mishra, and Songjun Li*

## 3.1
## Introduction

Smart materials are a class of materials having one or more properties that can be significantly changed in a controlled manner by changing the external stimuli, such as stress, temperature, moisture, pH, electric, and magnetic fields. There are numerous types of smart materials; however, we can categorize them on the basis of their responsive behaviors during the stimuli. "Piezoelectric materials" are ceramics or polymers characterized by a swift, linear shape change in response to an electric field. The electricity makes the material expand or instantly contract. This class of materials has potential applications in actuators to control chatter in precision machine tools, improve robotic parts for faster and accurate movement, microelectronic circuits in machines (e.g., computers, photolithography printers, etc.), and also in integrity-monitoring fibers for bridges, buildings, and wood utility poles [1]. "Electrostrictive and magnetostrictive materials" show a change in material size with response to either an electric or magnetic field, and conversely produce a voltage when stretched. These materials show promising applications for the manufacturing of pumps and valves, aerospace wind tunnels, shock-tube instrumentation, landing gear hydraulics, and further biomechanics force measurement of orthopedic gait and posturography, sports, ergonomics, neurology, cardiology, and rehabilitation [2]. "Rheological materials" are smart materials that include not only solids, but also fluids like electrorheological and magnetorheological fluids that can change state instantly using an electric or magnetic field [3]. These types of fluids being used as dampers for vehicle seats, shock absorbers, exercise equipment, and optical finishing. "Thermo-responsive materials," such as shape memory alloys, show a change in shape in response to heat and/or cold. Nitinol or nickel and titanium are usually combined to form such intelligent materials. The rarely used materials for this class are Au/Cd, Ag/Cd, Cu/Al/Ni, Cu/Sn, and Cu/Zn/Al [4]. They are frequently used in couplers, thermostats, and automobile, plane and helicopter parts. "pH-sensitive" materials are used as indicators and can change color as a function of pH. This type of smart material shows promise in paints

*Biosensor Nanomaterials*. Edited by Songjun Li, Jagdish Singh, and Ipsita A. Banerjee

ISBN: 978-3-527-32841-3

that change color when the metal beneath begins to corrode [5]. "Electrochromic materials" demonstrate the phenomenon of being able to change their optical properties when a voltage is applied across them. These materials are used as antistatic layers, electrochrome layers in liquid crystal displays, and cathodes in lithium batteries. "Smart gels" are gels engineered to respond by shrinking or swelling by a factor of 1000, and that can be programmed to absorb or release fluids in response to chemical or p hysical stimulus. These gels are used for agriculture, food, drug delivery, prostheses, cosmetics, and chemical processing applications [5].

In general, smart polymers undergo fast and reversible changes in the microstructure from a hydrophilic to a hydrophobic state that are triggered by small stimuli in the environment. The changes are apparent at the macroscopic level as order of magnitude changes in hydrogel size [6]. It is a reversible process – the system returns to the initial stage after removal of the trigger, including neutralization of charged groups either by a pH change or adding oppositely charged polymer, changing the efficiency of hydrogen bonding with an increase in temperature or ionic strength, and by breaking up hydrogels. Electrical-, magnetic- and radiation-induced reversible phase transitions are also known, and have found various biological applications [7].

Further, smart materials respond to environmental stimuli with particular changes in some variables and because of this these types of materials are often also called responsive materials. Depending on the changes in some external conditions, "smart" materials change their properties, such as mechanical, electrical, appearance, and/or structure and/or composition and/or function. Mostly, "smart" materials are embedded in systems whose inherent properties can be favorably changed to meet the desirable performance. It is well known that polymeric materials can be significantly changed in one or more properties in a controlled fashion under external stimuli, including stress, temperature, moisture, pH, electric, or magnetic fields. These materials could be piezoelectric materials, shape memory alloys and polymers, magnetic shape memory alloys, pH- and temperature-responsive polymers, halochromic and chromogenic materials, and non-Newtonian fluids [8].

The piezoelectric effect mainly occurs in the case of nonconducting materials such as crystals (i.e., quartz, burlinit, and tourmaline) and ceramics (i.e., barium titanate and lead zirconium titanate). Such materials can convert the applied mechanical stress into electrical voltage and vice versa. Therefore, they could be promising for sensors, ultrasonics, transducers, piezoelectric motors, and many other applications. Shape memory alloys such as Cu/Zn/Al/Ni, Cu/Al/Ni, Ni/Ti, and polymers (i.e., thermoplastics and thermosets) are sensitive to temperature changes, and are used in medical and industrial applications. A magnetic shape memory, Heusler alloy (i.e., $Ni_2MnGa$), can undergo large reversible deformations in an applied magnetic field. These types of materials can be used as sensors and actuators. Figure 3.1 shows the chemical structure of poly(*N*-isopropylacrylamide) (PNIPAm). It is a temperature-responsive polymer, which undergoes a reversible phase transition when heated above 33 °C in water. Hydrogels based on *N*-

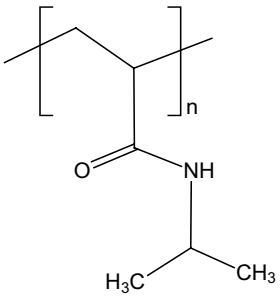


**Figure 3.1** Chemical structure of PNIPAm.

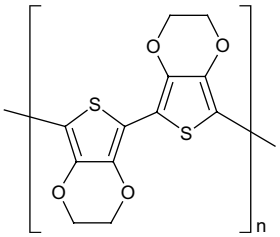


**Figure 3.2** Chemical structure of PEDOT.

isopropylacrylamide and sodium acrylate are both sensitive towards pH and temperature.

Polychromic, chromogenic, and halochromic materials are materials that change color due to external influences, including pH, temperature, light, and electricity. Thermochromic materials change color due to an increase or decrease in temperature, whereas photochromic materials alter because of a change in light intensity. Similarly, halochromic substances may be used as indicators to determine the pH of unknown substance. Poly(3,4-ethylene-dioxythiophene) (PEDOT, Figure 3.2) is an example of a polychromic material that can change its color from purple red at neutral state to blue and transparent in the oxidized state. Such materials are used as stress testers, forehead thermometers, and also in product labeling, and medical and security applications. Non-Newtonian fluids are liquids that change their viscosity in response of some sort of pressure or force. Unlike Newtonian fluids, non-Newtonian fluids show a nonlinear relationship between the shear stress and the strain rate. However, their viscosity is variable based on the applied stress. Ketchup, starch suspensions, paint, and shampoo are commonly used non-Newtonian fluids.

It is well known that response to stimulus is a basic principle of living systems. Life is made up of biopolymers such as carbohydrates, proteins, and nucleic acids, and the functions of living cells are regulated by these polymeric materials, which

form the basis of all natural processes. Based on lessons from nature, polymer scientists have been designing useful materials that respond to external stimuli such as light, temperature, pH, chemicals, and electrical field. Polymeric materials that respond by large changes due to small changes in the environments are referred to as "stimuli-responsive polymers," "smart polymers," "intelligent polymers, " or "environmentally sensitive polymers" [9–14]. Accordingly, smart polymers have promising applications in the area of biomedicine, such as in delivery systems for therapeutic agents, tissue engineering scaffolds, cell culture supports, bioseparation devices, and sensor or actuator systems. The environmental trigger behind these transitions can be changed either with a temperature or pH shift, increase in ionic strength, presence of certain metabolic chemicals, addition of an oppositely charged polymer, and polycation–polyanion complex formation [14–19]. More recently, changes in electric and magnetic field, light, or radiation have also been reported as stimuli for these polymers [20–22]. Among the above, the pH- and temperature-responsive polymers are the main focus of polymer scientists.

In this context, the use of nanomaterials to fabricate smart materials is one of the most exciting approaches because nanomaterials have a unique structure and high surface-to-volume ratio [23]. The surfaces of nanomaterials can also be tailored at the molecular scale in order to achieve various desirable properties [24]. Many attempts have been made to fabricate smart polymeric nanomaterials with self-assembly technology [25–30]; however, these approaches were based on planar self-assembly that may only offer limited available surface area for the stimulus, which can compromise the performance of the applications. Currently, polymeric nanofibers obtained by electrospinning have gained much attention; the surface-to-volume ratio of the fibers is significantly high. Also, nonwoven mats formed from such nanofibers have very small pore sizes. However, the total porosity of the mats will still be very high. Hence, smart polymeric nanofibers can provide better biosensing performance with biological macromolecules (i.e., enzymes, DNA, antigens, etc.) and retain their recognition activity after immobilizing onto the nanofiber surface. Nanofibers are particularly attractive for biosensor fabrication because they can be prepared under ambient conditions, and they exhibit tunable porosity, high stability, and chemical inertness. In this chapter, a successful attempt has been made toward the fabrication of nanofibers, and we show the properties and applications of nanofibers as potential biosensors.

## 3.2 Nanofibers

Nanofibers are one-dimensional thread-like structures with a diameter in the range of above 100 nm. They can be processed by a number of techniques, such as self-assembly, drawing, template synthesis, interfacial polymerization, and electrospinning. In this chapter, mainly electrospun fiber manufacturing technology is reviewed. Typically, the following categories of smart nanofibers can be applied for biosensor applications.

### 3.2.1 pH-Sensitive Nanofibers

pH-sensitive polymeric nanofibers usually consist of pendant acidic (i.e., carboxylic and sulfonic acids) or basic (e.g. ammonium salts) groups that either accept or release protons in response to changes in environmental pH [23]. Polyacrylic acid, poly(methacrylic acid), poly(2-ethylacrylic acid), poly(2-propylacrylic acid), and polysulfonamides (derivatives of *p*-aminobenzenesulfonamide) are a few examples of poly acids (anionic polymers). Similarly, poly(*N*,*N*-diakylaminoet hylmethacrylates), poly(L-ysine), poly(ethylenimine), and chitosan represent cationic polyelectrolytes. The pH-sensitive macromolecules dissociate to give polymeric ions after dissolving in ionizing solvent. Repulsion between similar charges on the polymeric chains results in chain expansion when ionized in a suitable solvent. However, when unionized in the case of a poor solvent and hydrophobic polymer, they collapse into globules and precipitate from solution. The interplay between hydrophobic surface energy and electrostatic repulsion between charges dictates the behavior of the polyelectrolytes. The degree of ionization of weak polyelectrolytes is controlled by the pH value and ionic composition of an aqueous medium; therefore, the smart polymers dramatically change conformation in response to minute changes in the pH of an aqueous environment.

Various works have been performed on poly(methylmethacrylate)-based polymers. Microparticles prepared from poly(methacrylic acid-*g*-ethylene glycol) loaded with insulin exhibited unique pH-responsive characteristics in which interpolymer complexes were formed in acidic media and dissociated in neutral/basic environments. As a result, insulin release from the gel was significantly retarded in acidic media while rapid release occurred under neutral/basic conditions. Copolymer networks of poly(methacrylic acid) grafted with poly(ethylene glycol) with reversible pH-dependent swelling behavior, due to the formation of interpolymer complexes between protonated pendant acid groups and the etheric groups on the graft chains, were developed. Gels containing equimolar amounts of methacrylic acid/ethylene glycol exhibited less swelling at lower pH. The pH of the swelling solution affected the average network mesh size. *In vitro* release of insulin from poly(methacrylic acid-*g*-ethylene glycol) gels containing poly(ethylene glycol) grafts indicated a significant release of insulin as the gel decomplexed. Composite membranes made from nanoparticles of poly(*N*-isopropylacrylamide-*co*-methacrylic acid) of various *N*-isopropylacrylamide : methacrylic acid ratios dispersed in a matrix of a hydrophobic polymer were investigated [45].

### 3.2.2 Temperature-Responsive Nanofibers

Polymers sensitive to temperature changes are the most studied class of environmentally sensitive polymers as they have potential applications in the biomedical field. This type of system exhibits a critical solution temperature (typically in water) at which the phase of polymer and solution is changed in accordance with their

composition [24]. Those systems exhibiting one phase above a certain temperature and a phase separation below it possess an upper critical solution temperature. However, polymer solutions that appear as monophasic below a specific temperature and biphasic above it generally exhibit the so-called lower critical solution temperature (LCST; "cloud point"). LCST polymers have a number of applications. The typical example is PNIPAm that presents a LCST at 32 °C in water solution. Fu *et al*. prepared thermal-responsive poly(4-vinylbenzyl chloride)-*b*-poly(glycidyl methacrylate)-*g*-PNIPAm (PVBC-*b*-PGMA-*g*-PNIPAm) nanofibers by the combined technology of reversible addition-fragmentation chain transfer polymerization, atom transfer radical polymerization, electrospinning, and "click chemistry" [25]. PVBC-*b*-PGMA-*g*-PNIPAM nanofibers exhibit a good resistance to solvents and a thermal-responsive character to the environment, having a hydrophobic surface at 45 °C (water contact angle 140°) and a hydrophilic surface at 20 °C (water contact angle 30°). Below that temperature the polymer is soluble as the hydrophilic interactions, due to hydrogen bonding, are predominant, whereas a phase separation occurs above the LCST due to the predominance of hydrophobic interactions. LCST values of polymers are found to be controlled by the alkyl group bound to the nitrogen atom. Another type of temperature sensitivity is based on intermolecular association, as in the case of pluronics or poloxamers (triblock poly(ethylene oxide)--> (PEO) and poly(propylene oxide) (PPO)-based systems (PEO–PPO–PEO)), where hydrophobic association of PPO blocks leads to the formation of micelle structures above the critical micellar temperature .

*N*-Alkylacrylamide monomers are mostly employed to obtain temperature-sensitive polymers. These monomers are synthesized by the nucleophilic substitution reaction of acryloyl chloride with the suitable amine. Some examples of *N*-alkylacrylamide monomers are *N*-isopropylacrylamide, *N*-isopropylmethacrylamide, isopropylmethacrylamide, diethylacrylamide, methylpropylacrylamide, cyclopropylacrylamide, propylacrylamide, ethylpropylacrylamide, *n*- and *tert*-butylacrylamide, and ethoxyethylacrylamide. LCST values of polymers are found to be controlled by the alkyl group bound to the nitrogen atom. The polymers prepared by the polymerization of *N*-isopropylacrylamide generally exhibit LCST values in the range of 30–32 °C depending upon the synthesis method. In biotechnological applications, some chemical modifications can be necessary in the structure of PNIPAm. These modifications are usually made for introducing some functional groups or improving the mechanical properties of the gel matrices.

## 3.3 Electrospinning of Nanofibers

In recent years, polymers have been processed by various techniques such as drawing, template synthesis, phase separation, self-assembly, electrospinning, and so on, to prepare polymer nanofibers from the micron to nanometer scale [26–31]. The main idea is to reduce the diameter of the polymeric fibers so as to achieve

outstanding characteristics such as very large surface area-to-volume ratio, flexibilities in surface functionalities, and superior mechanical properties.

The drawing-in process is similar to dry spinning. The drawing method can be used to make one-by-one and very long single nanofibers. However, this method is possible only for viscoelastic polymers that can undergo strong deformations while being cohesive enough to support the stresses developed during pulling. Similarly, in the case of template synthesis, a nanoporous membrane is used as a template to make nanofibers of solid (i.e., fibril) or hollow (i.e., tubule) shape. Using this method, nanometer tubules and fibrils of various raw materials such as electronically conducting polymers, metals, semiconductors, and carbons can be fabricated. This method cannot, however, make one-by-one continuous nanofibers.

Phase separation is a complex process consisting of dissolution, gelation, extraction using a different solvent, freezing, and drying, resulting in nanoscale porous foam. This process takes a longer time to transfer the solid polymer into the nanoporous foam. On the other hand, self-assembly is a process in which individual, pre-existing components organize themselves into desired patterns and functions. However, self-assembly is also a time-consuming process similar to phase separation.

In this context, the electrospinning process seems to be the only method that can be further developed for mass production of one-by-one continuous nanofibers from various polymers. The term "electrospinning" has been derived from "electrostatic spinning." The innovative setup to produce fibers dates back from 1934, when Formhals published a patent describing an experimental setup for the production of polymer filaments [32]. In 1952, Vonnegut and Neubauer were able to produce streams of highly electrified uniform droplets of about 0.1 mm in diameter using a capillary with a diameter of the order of a few tenths of a millimeter [33]. In 1955, Drozin investigated the dispersion of a series of liquids into aerosols under high electric potentials [34]. He used a glass tube ending in a fine capillary similar to the one employed by Vonnegut and Neubauer. In 1966, Simons patented an apparatus for the production of ultrathin, very lightweight nonwoven fabrics with different patterns using electrical spinning [35]. The positive electrode was immersed into the polymer solution and the negative electrode was connected to a belt where the nonwoven fabric was collected. He found that the fibers from low-viscosity solutions tended to be shorter and finer, whereas those from more viscous solutions were relatively continuous. In 1971, Baumgarten made an apparatus to electrospin acrylic fibers with diameters in the range of 0.05–1.1 nm [36]. A schematic representation of an electrospinning assembly is as shown in Figure 3.3.

The spinning drop was suspended from a stainless steel capillary tube and maintained at constant size by adjusting the feed rate of an infusion pump. A high-voltage DC current was connected to the capillary tube and the fibers were collected on a grounded metal screen. Since the 1980s, and especially in recent years, the electrospinning process essentially similar to that described by has regained more attention, probably in part due to the surging interest in

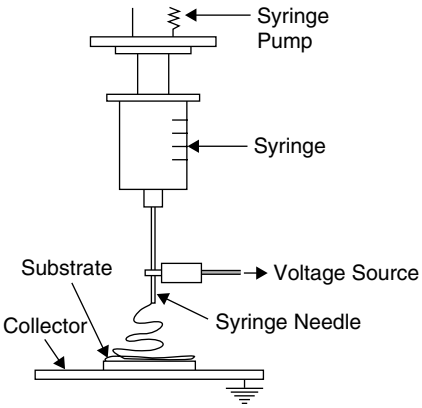


**Figure 3.3** Schematic illustration of the setup for electrospinning.

nanotechnology, as ultrafine fibers or fibrous structures of various polymers with diameters down to submicrons or nanometers can be easily fabricated with this process [31]. Strangely enough, although the electrospinning process has shown promising potential and has existed in the literature for several decades, our understanding of it is still very limited.

In summary, the formation of nanofibers through electrospinning is based on the uniaxial stretching of a viscoelastic solution. Although all spinning processes (dry-spinning, melt-spinning, and electrospinning) utilize the drawing of the solution to form the fiber, electrospinning makes use of electrostatic forces to stretch the solution as it solidifies. Thus, without any disruption to the electrospinning jet the formation of the fiber will be continuous. During the process a viscous solution is first fed through the spinneret. A high voltage (typically more than 5 kV) is applied to the solution. When the repulsive force within the charged solution is larger than its surface tension, a jet erupts from the tip entering a bending instability stage. Various parameters affecting fiber formation include solution viscosity, conductivity, applied voltage, spinneret tip-to-collector distance, and humidity.

## 3.4 Biorecognition Devices

A biorecognition device, a so-called "biosensor, " is an analytical device that converts a biological response into an electrical signal. Biosensors are used to determine the concentration of substances and other parameters of biological interest. A successful biosensor must possess a number of important properties: it should be specific; stable under normal storage conditions; produce an accurate, precise, reproducible, and linear response over the useful analytical range; be economical; and be portable and capable of being used by semiskilled persons. The biocatalyst (a) converts the substrate (S) to product (P). This reaction is determined by the

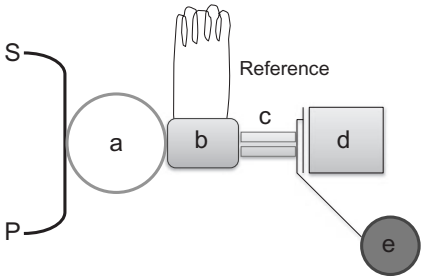


**Figure 3.4** Schematic diagram of a biosensor.

transducer (b) that converts it to an electrical signal. The output from the transducer is amplified (c), processed (d), and displayed (e) as shown in Figure 3.4.

The transducer has a key role in a biosensor that makes use of a physical change accompanying the reaction. This may be the heat output (or absorbed) by the reaction (calorimetric biosensors) [37], changes in the distribution of charges causing an electrical potential to be produced (potentiometric biosensors), movement of electrons produced in a redox reaction (amperometric biosensors), light output during the reaction or a light absorbance difference between the reactants and products (optical biosensors), or effects due to the mass of the reactants or products (piezoelectric biosensors).

There are three so-called "generations" of biosensors: first-generation biosensors where the normal product of the reaction diffuses to the transducer and causes the electrical response; second-generation biosensors that involve specific "mediators" between the reaction and the transducer in order to generate an improved response; and third-generation biosensors where the reaction itself causes the response and no product or mediator diffusion is directly involved.

The electrical signal from the transducer is often low and superimposed upon a relatively high and noisy signal (i.e., containing a high-frequency signal component of an apparently random nature, due to electrical interference or noise generated within the electronic components of the transducer baseline). The signal processing normally involves subtracting a "reference" baseline signal, derived from a similar transducer without any biocatalytic membrane, from the sample signal and amplifying the result. The analog signal produced at this stage may be output directly, but is usually converted to a digital signal and passed to a microprocessor stage where the data is processed, converted to concentration units, and output to a display device.

Many enzyme-catalyzed reactions are exothermic (i.e., evolving heat) [38] (Table 3.1), which may be used as a basis for measuring the rate of reaction and, hence, the analyte concentration. This represents the case with calorimetric biosensors. Thermistors are usually used to measure the temperature changes incorporated at the entrance and exit of small packed bed columns containing immobilized enzymes within a constant temperature environment. Under such closely controlled conditions, up to 80% of the heat generated in the reaction may be registered

**Table 3.1** Molar heat enthalpies of enzyme-catalyzed reactions [29].

| Reactant | Enzyme | Molar heat enthalpies $-\Delta H$ (kJ mol$^{-1}$) |
|---|---|---|
| Cholesterol | Cholesterol oxidase | 53 |
| Esters | Chymotrypsin | 4–16 |
| Glucose | GOx | 80 |
| $H_2O_2$ | Catalase | 100 |
| Penicillin G | Penicillinase | 67 |
| Peptides | Trypsin | 10–30 |
| Starch | Amylase | 8 |
| Sucrose | Invertase | 20 |
| Urea | Urease | 61 |
| Uric acid | Uricase | 49 |

as a temperature change in the sample stream. This may be simply calculated from the enthalpy change and the amount reacted. If 1 mM of reactant is completely converted to product in a reaction generating 100 kJ mol$^{-1}$ then each milliliter of solution generates 0.1 J of heat. At 80% efficiency, this will cause a change in temperature of the solution amounting to approximately 0.02 °C. This is about the temperature change commonly encountered and necessitates a temperature resolution of 0.0001 °C for the biosensor to be generally useful.

The sensitivity ($10^{-4}$ M) and range ($10^{-4}$ to $10^{-2}$ M) are both quite low for the majority of applications with biosensors using thermistor. The sensitivity can be increased by using more exothermic reactions (e.g., catalase). The low sensitivity of the system can be increased substantially by increasing the heat output by the reaction. In the simplest case this can be achieved by linking together several reactions in a reaction pathway, all of which contribute to the heat output. Thus, the sensitivity of the glucose analysis using glucose oxidase (GOx) can be more than doubled by the coimmobilization of catalase within the column reactor in order to disproportionate the $H_2O_2$ produced [39].

Potentiometric biosensors use ion-selective electrodes to transduce the biological reaction into an electrical signal. These consist of an immobilized enzyme membrane surrounding the probe from a pH meter [40], where the catalyzed reaction generates or absorbs hydrogen ions. There are three types of ion-selective electrodes are used in biosensors:

- Glass electrodes for cations (e.g., normal pH electrodes) in which the sensing element is a very thin hydrated glass membrane that generates a transverse electrical potential due to the concentration-dependent competition between the cations for specific binding sites. The selectivity of this membrane is determined by the composition of the glass. The sensitivity to $H^+$ is greater than that achievable for $NH_4^+$.
- Glass pH electrodes coated with a gas-permeable membrane selective for $CO_2$, $NH_3$, or $H_2S$. The diffusion of the gas through this membrane causes a change

in pH of a sensing solution between the membrane and the electrode, which is then determined.

- Solid-state electrodes where the glass membrane is replaced by a thin membrane of a specific ion conductor made from a mixture of silver sulfide and a silver halide. The iodide electrode is useful for the determination of $I^-$ in the peroxidase reaction and also responds to cyanide ions [41].

Reactions involving the release or absorption of ions may be utilized in potentiometric biosensors:

- H+ cation

  *GOx $H_2O$:*

  $$\text{D-glucose} + O_2 \rightarrow \text{D-glucono-1,5-lactone} + H_2O_2 \rightarrow \text{D-gluconate} + H^+$$

  *Penicillinase:*

  $$\text{penicillin} \rightarrow \text{penicilloic acid} + H^+$$

  *Urease (pH 6.0):*

  $$H_2NCONH_2 + H_2O + 2H^+ \rightarrow 2NH_4^+ + CO_2$$

  *Urease (pH 9.5):*

  $$H_2NCONH_2 + 2H_2O \rightarrow 2NH_3 + HCO_3^- + H^+$$

  *Lipase:*

  $$\text{neutral lipids} + H_2O \rightarrow \text{glycerol} + \text{fatty acids} + H^+$$

- $NH_4^+$ cation

  L-*Amino acid oxidase:*

  $$\text{L-amino acid} + O_2 + H_2O \rightarrow \text{keto acid} + NH_4^+ + H_2O_2$$

  *Asparaginase:*

  $$\text{L-asparagine} + H_2O \rightarrow \text{L-aspartate} + NH_4^+$$

  *Urease (pH 7.5):*

  $$H_2NCONH_2 + 2H_2O \rightarrow H^+ + 2NH_4^+ + HCO_3^-$$

- $I^-$ anion

  *Peroxidase:*

  $$H_2O_2 + 2H^+ + 2I^- \rightarrow I_2 + 2H_2O$$

- $CN^-$ anion

  *Glucosidase:*

  $$\text{amygdalin} + 2H_2O \rightarrow 2\text{glucose} + \text{benzaldehyde} + H^+ + CN^-$$

It can also be used in $NH_4^+$ and $CO_2$ (gas) potentiometric biosensors. It is further utilized as a $NH_3$ (gas) potentiometric biosensor.

Amperometric biosensors function by the generation of a current when a potential is applied between two electrodes [42]. They generally have response times, dynamic ranges, and sensitivities similar to the potentiometric biosensors. The simplest amperometric biosensors in common usage involve the Clark oxygen electrode. It consists of a platinum cathode at which oxygen is reduced and a Ag/AgCl reference electrode. When a potential of –0.6 V relative to the Ag/AgCl electrode is applied to the platinum cathode, a current proportional to the oxygen concentration is produced. Normally both electrodes are bathed in a solution of saturated potassium chloride and separated from the bulk solution by an oxygen-permeable plastic membrane (e.g., Teflon, polytetrafluoroethylene). The following reactions occur:

- Silver anode:

$$4Ag^0 + 4Cl^- \rightarrow 4AgCl + 4e^-$$

- *Platinum cathode:*

$$O_2 + 4H^+ + 4e^- \rightarrow 2H_2O$$

The efficient reduction of oxygen at the surface of the cathode causes the oxygen concentration there to be effectively zero. The rate of this electrochemical reduction therefore depends on the rate of diffusion of the oxygen from the bulk solution, which is dependent on the concentration gradient and hence the bulk oxygen concentration. Thus, a small, but significant, proportion of the oxygen present in the bulk is consumed by this process; the oxygen electrode measures the rate of a process that is far from equilibrium, whereas ion-selective electrodes are used close to equilibrium conditions. This causes the oxygen electrode to be much more sensitive to changes in temperature than potentiometric sensors. A typical application for this simple type of biosensor is the determination of glucose concentrations by the use of an immobilized GOx membrane. The reaction results in a reduction of the oxygen concentration as it diffuses through the biocatalytic membrane to the cathode, this being detected by a reduction in the current between the electrodes [43]. Other oxidases may be used in a similar manner for the analysis of their substrates (e.g., alcohol oxidase, D- and L-amino acid oxidases, cholesterol oxidase, galactose oxidase, and urate oxidase).

A potential is applied between the central platinum cathode and the annular silver anode. This generates a current ($I$) that is carried between the electrodes by means of a saturated solution of KCl. This electrode compartment is separated from the biocatalyst (e.g., GOx) by a thin plastic membrane, permeable only to oxygen. The analyte solution is separated from the biocatalyst by another membrane, permeable to the substrate(s) and product(s).

There are two main areas of development in optical biosensors. These involve determining changes in light absorption between the reactants and products of a reaction, and measuring the light output by a luminescent process [44]. The former

usually involves the widely established, if rather low technology, use of colorimetric test strips. These are disposable single-use cellulose pads impregnated with enzyme and reagents. The most common use of this technology is for whole-blood monitoring in diabetes control. In this case, the strips include GOx, horseradish peroxidase (EC 1.11.1.7), and a chromogen (e.g., *o*-toluidine or 3,3′,5,5′-tetramethylbenzidine). The $H_2O_2$ is produced by the aerobic oxidation of glucose and oxidizes the weakly colored chromogen to a highly colored dye.

$$\text{D-glucose} + \text{oxygen} \rightarrow \text{D-glucono-1,5-lactone} + H_2O_2$$

*Peroxidase:*

$$\text{chromogen}(2H) + H_2O_2 \rightarrow \text{dye} + 2H_2O$$

The evaluation of the dyed strips is best achieved by the use of portable reflectance meters, although direct visual comparison with a colored chart is often used. A wide variety of test strips involving other enzymes are commercially available at the present time. A most promising biosensor involving luminescence uses firefly luciferase (*Photinus* luciferin 4-monooxygenase (ATP-hydrolyzing), EC 1.13.12.7) to detect the presence of bacteria in food or clinical samples. Bacteria are specifically lysed and the ATP released (roughly proportional to the number of bacteria present) reacted with D-luciferin and oxygen in a reaction that produces yellow light in high quantum yield.

*Luciferase:*

$$\text{ATP} + \text{D-luciferin} + O_2 \rightarrow \text{oxyluciferin} + \text{AMP} + \text{pyrophosphate} + CO_2 + \text{light (562 nm)}$$

The light produced may be detected photometrically by use of high-voltage, expensive photomultiplier tubes or low-voltage, cheap photodiode systems.

In general, biosensors are easy to operate, analyze over a wide range of useful analyte concentrations, and give reproducible results. The diffusion limitation of substrate(s) may be an asset to be encouraged in biosensor design due to the consequent reduction in the effects of analyte pH, temperature, and inhibitors on biosensor response. The one-dimensional polymer structural design (i.e., polymeric nanofibers) as a substrate may have potential to provide a new era of advanced biosensors.

## 3.5 Conclusions

This chapter provides only a glimpse into the design complexities, behavior, and utility of smart polymeric materials, introducing smart nanofibers and their fabrication using electrospinning method; however, with this snapshot we have tried to illustrate the versatility and potential of these materials. It seems to be the beginning of the application of smart polymeric nanofibers into biological

recognition. The applications of these materials are limited by our imagination. It will not be long before we can really utilize their application in our biosensing devices.

## References


1 Stuart, M.A.C., Huck, W.T.S., Genzer, J., Müller, M., Ober, C., Stamm, M., Sukhorukov, G.B., Szleifer, I., Tsukruk, V.V., Urban, M., Winnik, F., Zauscher, S., Luzinov, I., and Minko, S. (2010) *Nat. Mater.*, **9**, 101–113.
2 Fu, Y., Du, H., Huang, W., Zhang, S., and Hu, M. (2004) *Sens. Actuators A*, **112**, 395.
3 Rousseau, I.A. (2008) *Polym. Eng. Sci.*, **48**, 2075.
4 Manosa, L., Moyaa, X., Planes, A., Krenke, T., Acet, M., and Wassermann, E.F. (2008) *Mater. Sci. Eng. A*, **481**, 49.
5 Schmaljohann, D. (2006) *Adv. Drug Deliv. Rev.*, **58**, 1655.
6 Reichardt, C. (1994) *Chem. Rev.*, **94**, 2319.
7 Seeboth, A., Kriweknek, J., Lotzsch, D., and Patzak, A. (2002) *Polym. Adv. Technol.*, **13**, 507.
8 De-Silva, A.K., Kobayashi, M.H., and Coimbra, C.F.M. (2007) *Biotechnol. Bioeng.*, **96**, 37.
9 Jeong, B. and Gutowska, A. (2002) *Trends Biotechnol.*, **20**, 305.
10 Hoffman, A.S., Stayton, P.S., Bulmus, V., Chen, G., Jinping, C., and Chueng, C. (2000) *J. Biomed. Mater. Res.*, **52**, 577–586.
11 Galaev, I.Y. and Mattiasson, B. (2000) *Trends Biotechnol.*, **17**, 335.
12 Kikuchi, A. and Okan, O.T. (2002) *Prog. Polym. Sci.*, **27**, 1165.
13 Qiu, Y. and Park, K. (2001) *Adv. Drug Deliv. Rev.*, **53**, 321.
14 Unno, H., Huang, X., Akehata, T., and Hirasa, O. (1993) *Responsive Gels: Volume Transitions II* (ed. K. Dusek), Springer, Berlin, pp. 180–197.
15 Twaites, B.R., Alarcon, C.H., Cunliffe, D., Lavigne, M., Pennadam, S., and Smith, J.R. (2004) *J. Control. Rel.*, **97**, 551.
16 Lomadze, N. and Schneider, H.J. (2005) *Tetrahedron Lett.*, **46**, 751.
17 Kabanov, V.A. (1994) *Polym. Sci.*, **36**, 143.
18 Leclercq, L., Boustta, M., and Vert, M.A. (2003) *J. Drug Target.*, **11**, 129.
19 Filipcsei, G., Feher, J., and Zrinyi, M. (2000) *J. Mol. Struct.*, **554**, 109.
20 Zrinyi, M. (2000) *Colloid Polym. Sci.*, **278**, 98.
21 Juodkazis, S., Mukai, N., Wakaki, R., Yamaguchi, A., Matsuo, S., and Misawa, H. (2000) *Nature*, **408**, 178.
22 Galaev, I.Y., Gupta, M.N., and Mattiasson, B. (1996) *Chemtech*, **26**, 19.
23 Vorotyntsev, M.A. and Vasilyeva, S.V. (2008) *Adv. Colloid Interface Sci.*, **139**, 97.
24 Gil, E.S. and Hudson, S.M. (2004) *Prog. Polym. Sci.*, **29**, 1173.
25 Fu, G.D., Xu, L.Q., Yao, F., Zhang, K., Wang, X.F., and Zhu, M.F. (2009) *Mater. Sci.*, **1**, 239.
26 Ondarcuhu, T. and Joachim, C. (1998) *Europhys. Lett.*, **42**, 215.
27 Martin, C.R. (1996) *Chem. Mater.*, **8**, 1739.
28 Ma, P.X. and Zhang, R. (1999) *J. Biomed. Mat. Res.*, **46**, 60.
29 Liu, G.J., Ding, J.F., Qiao, L.J., Guo, A., Dymov, B.P., and Gleeson, J.T. (1999) *Chem. Eur. J.*, **5**, 2740.
30 Burger, C., Hsiao, B.S., and Chu, B. (2006) *Annu. Rev. Mater. Res.*, **36**, 333–368.
31 Deitzel, J.M., Kleinmeyer, J., Hirvonen, J.K., and Beck, T.N.C. (2001) *Polymer*, **42**, 8163.
32 Formhals, A. (1934) US Patent 1975504.
33 Vonnegut, B. and Neubauer, R.L. (1952) *J. Colloid Sci.*, **7**, 616.
34 Drozin, V.G. (1955) *J. Colloid Sci.*, **10**, 158.
35 Simons, H.L. (1966) US Patent 3280229.
36 Baumgarten, P.K. (1971) *J. Colloid Interface Sci.*, **36**, 71.
37 Hundeck, H.G., Weiss, M., Scheper, T., and Schubert, F. (1993) *Biosens. Bioelec.*, **8**, 205–208.

**38** Scheller, F. and Schubert, F. (1992) *Biosensors*, Elsevier, Amsterdam, pp. 3–12.
**39** Godjevargova, T., Dayal, R., and Marinov, I. (2004) *J. Appl. Sci.*, **91**, 4057–4063.
**40** Situmorang, M., Gooding, J., Hibbert, D.B., and Barnett, D. (2001) *Electroanalysis*, **13**, 1469–1474.
**41** Walker, M. and Rapley, R. (2008) *Molecular Biology and Biotechnology*, Royal Society of Chemistry, London, pp. 539–541.
**42** Heller, A. (1996) *Curr. Opin. Biotechnol.*, **7**, 50–55.
**43** Rubio, R.J., Lopez, C.E., Mecerreyes, D., and Lopez-Ruiz, B. (2004) *Biosens. Bioelectron.*, **20**, 1111–1117.
**44** Vittorio, M.N.P., Francesco, D., Biagio, C., and Francesco, D.L. (2007) *Sensors*, **7**, 508–536.
**45** Zhang, K., Xiao, X.Y., and Wu, Y. (2004) *Biomaterials*, **25**, 2004, 5281–5291.

# 4
# Fabrication and Evaluation of Nanoparticle-Based Biosensors

*Rhishikesh Mandke, Buddhadev Layek, Gitanjali Sharma, and Jagdish Singh*

## 4.1
## Introduction

Nanotechnology can be defined as "a technology concerning the application of nanomaterials as well as the use of nanostructuring methods" [1]. A combined effort in the field of nanotechnology, biology, advanced materials, and photonics has resulted in the evolution of nanobiosensors as diagnostic agents. A biosensor is a device that uses specific biochemical reactions mediated by isolated enzymes, immunosystems, tissues, organelles, or whole cells to detect chemical compounds, usually by electrical, thermal, or optical signals [2]. For a basic understanding, a biosensor can be defined as a measurement system used for the detection of an analyte, usually combining a biological component with a physicochemical detector. A nanobiosensor is a biosensor on a nanoscale size [3, 4].

A biosensor usually comprises three structural elements: a recognition element, a transducer, and an amplifier [4]. The recognition element, which is any element sensitive to the analyte of interest, includes biological elements, ranging from tissues, cells, and organelles to antibodies, enzymes, receptors, and nucleic acids, biologically derived or biomimetic materials. The transducer acts as an interface between the biological element and the amplifier, thereby performing a detector function. The main role of the transducer is to transform the signal originating from the interaction between the analyte and the recognition element into a recognizable and/or quantifiable output. Major types of transducers include electrochemical, optical, piezoelectric, and calorimetric transducers, which measure the changes in electric distribution, optical properties, mass, and thermal properties, respectively. Finally, the amplifier amplifies the transducer signal, which is displayed in a user-friendly way (Figure 4.1) [5].

Nanomaterials have promising roles in chemical sensing and biochemical analysis due to the following characteristics: their physicochemical properties are highly tunable depending on their size and shape; their unique surface chemistry, thermal stability, high surface area, and large pore volume per unit mass makes them highly suitable for sensor fabrication; they can measure nonpolar molecules that do not respond to most measurement devices; immobilization systems used

*Biosensor Nanomaterials*. Edited by Songjun Li, Jagdish Singh, and Ipsita A. Banerjee

ISBN: 978-3-527-32841-3

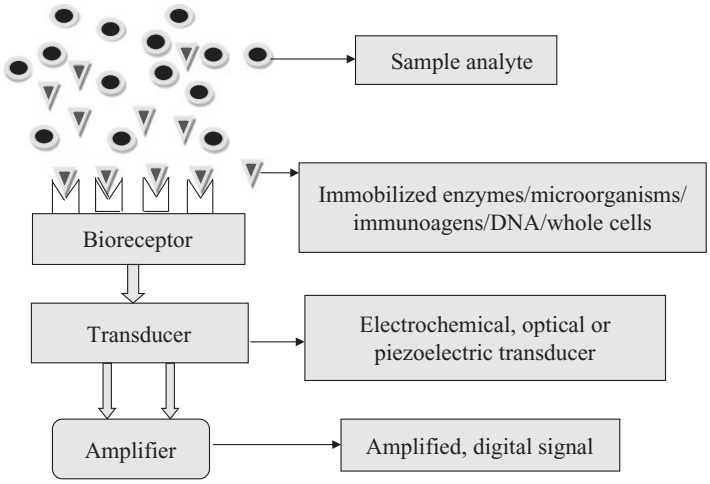


**Figure 4.1** Schematics of a biosensor.

in their fabrication amplify their specificity; and rapid and continuous monitoring of response signals can be performed using these sensors. These unique properties have been utilized for the fabrication of biosensors with elevated specificity and sensitivity [6].

Ideally, a biosensor should have an optimum balance of specificity, stability, linearity, sensitivity, and response time. Additionally, a biosensor should be cheap, small, portable, and capable of being used by semiskilled operators. Furthermore, biosensors used for invasive monitoring in clinical situations should be biocompatible, nontoxic, nonantigenic, portable, and stable under physiological conditions.

This chapter focuses on the fabrication and evaluation of nanoparticle-based biosensors, and is broadly divided in three parts: nanoparticle-based biosensors and their fabrication, the structural and functional evaluation of these biosensors, and finally a brief survey of reported applications of nanoparticle-based biosensors.

## 4.2
## Nanoparticle-Based Biosensors and their Fabrication

### 4.2.1
### Types of Nanobiosensors

Nanobiosensors can be classified according to their method of signal transduction or their structural elements. Keeping the diversity of structural elements in context, it is difficult to classify the newer biosensors on a strictly structural basis. There-

fore, in this chapter, we will consider the methods of signal transduction for biosensor classification. Accordingly, biosensors can be broadly classified into the following categories.

#### 4.2.1.1 Electrochemical Biosensors

Electrochemical biosensors are the most widely used class of biosensors [4]. The first amperometric enzyme electrode for the determination of glucose was reported by Clark and Lyons in 1962 [7]. Clark's work and the subsequent transfer of his technology to Yellow Springs Instrument Company led to the successful commercial launch of the first dedicated glucose biosensor in 1975 [8]. Since then, various forms of electrochemical biosensors have been developed due to their high sensitivity, selectivity, ability to operate in turbid solutions, and amenability to miniaturization. In an electrochemical biosensor, an electrochemical transducer is intimately coupled with a biological element to measure the electrochemical signal produced as a result of electron generation or consumption during a biomolecular reaction. Most often, enzymes are used as biorecognition elements because of their specific binding capabilities and biocatalytic activity [9–11]. The other types of biorecognition elements are antibodies, antigens, antibody fragments, cells, and microorganisms [5, 8].

Depending upon the detection or measurement mode, electrochemical biosensors are further classified into the three main categories: amperometric (measure current), potentiometric (measure potential difference or charge accumulation), and conductometric (measure conductance) biosensors [12]. Other types of electrochemical biosensors include impedimetric [13] and field-effect, which measure current as a result of a potentiometric effect at a gate electrode using transistor technology [14].

**Amperometric Biosensors** Amperometric biosensors are based on the continuous measurement of current of the working electrode resulting from the oxidation or reduction of an electroactive species in a biochemical reaction [12]. The resulting current measured within a linear potential range is directly proportional to the bulk concentration of the electroactive species or its consumption or production rate in the adjacent biocatalytic layer [14]. The glucose biosensor is an excellent example of an amperometric device that is based on amperometric detection of $H_2O_2$. Amperometric biosensors are used in combination with immunosensing techniques to determine the levels of human chorionic gonadotropin β-subunit for pregnancy testing [15].

**Potentiometric Biosensors** Potentiometric biosensors measure the potential difference between the working electrode and reference electrode in an electrochemical cell when there is zero or no significant current flowing between them [5, 6, 8]. Therefore, potentiometry is used to monitor the ion activity in an electrochemical reaction [16]. Ion-selective electrodes are used to detect ions such as $H^+$, $Na^+$, $K^+$, $Ca^{2+}$, $NH_4^+$, $I^-$, or $CN^-$ in complex biological matrices by measuring changes in electrode potential [12].

Potentiometry is also used to electrically determine the end-point of a titration involving two oppositely charged ions [17]. Potentiometric devices based on various forms of field-effect transistor (FET) are often used to measure pH changes, selective ion concentration, and kinetics of enzyme-catalyzed reaction [18]. Lud *et al.* [19] developed a label-free and direct potentiometric biosensor for the detection of small peptides and proteins due to their intrinsic charges using biofunctionalized ion-sensitive FETs. Recently, a silver nanoparticle redox marker-based glucose biosensor has been described by Ngeontae *et al.* [20], which is able to measure glucose in the linear range of 0.1–3 mM in magnesium acetate buffer at pH 6.0.

**Conductometric Biosensors** Conductometric devices are based on the measurement of changes in conductance between two metal electrodes as a result of a biochemical reaction [21]. Hence, conductometric biosensors can be used to study enzyme-catalyzed reactions where the ionic strength and thus the conductivity of a solution changes as a consequences of an enzymatic reaction [10]. The conductometric measurements of enzymatic reactions are limited by several factors such as variable ionic background of clinical samples, requirement of measuring small conductivity changes, high ionic strength of the medium, and so on [17]. The changes in conductivity can be monitored directly by immobilizing the enzymes onto the electrode surface. Recently, there has been a trend to use conductometric biosensors in combination with nanowires for biosensing [22, 23]. The conductometric devices have been successfully used for practical purposes such as pollutant detection in river samples [24], lactose detection in milk [25], and drug detection in urine [26].

#### 4.2.1.2 Calorimetric Biosensors

Calorimetric biosensors are based on the principle of change in heat content (i.e., absorption or evolution of heat during a biochemical reaction, resulting in a change in temperature of the reaction medium) [27]. The temperature change of the solution is usually measured by thermistors at the entrance and exit of the small packed bed column containing immobilized enzyme at a constant temperature. The peak height of the thermometric recording is proportional to the enthalpy change corresponding to a specific substrate concentration. The heat capacity of organic solvents is generally 2 or 3 times lower than that of aqueous solvents [28], ensuring better sensitivities and detection limits in the organic solvents for the same value of enthalpy change per mole. A further improvement in the sensitivity can be achieved by recycling the coenzyme or the substrate [29].

#### 4.2.1.3 Optical Biosensors

Optical biosensors have been widely employed in healthcare, biomedical research, pharmaceuticals, environmental monitoring, homeland security, and the battlefield as a powerful detection and analytical tool [30]. The key advantages of optical biosensors are their speed, high sensitivity, simplicity, and the immunity of the signal to electromagnetic interference. They are readily multiplexed, capable of

performing remote sensing, and samples can be simultaneously interrogated at different wavelengths without interfering with one another. Optical measurement can be based on the changes in absorbance, fluorescence/phosphorescence, chemiluminescence, reflectance, light scattering, or refractive index. However, the two most commonly used detection protocols are fluorescence-based detection and label-free detection [31, 32].

**Fluorescence-Based Detection** Fluorescence is a widely used optical method for biosensing due to its selectivity and sensitivity, with the detection limit down to a single molecule [33]. The major types of fluorescence biosensing are direct, indirect, and fluorescence resonance energy transfer (FRET) [34]. In direct sensing, a specific molecule is detected before and after the reaction takes place, whereas indirect sensing involves the addition of a dye to the sample from the outside that will optically transduce the presence of a specific target molecule. Green Fluorescent Protein is frequently used as a fluorescence tag to study the location, structure, and dynamics of molecular events within the living cells [34]. In FRET, two fluorophores are paired in such a way that the emission wavelength of one fluorophore (donor) overlaps with the excitation wavelength of the other (acceptor). The donor fluorophore transfers energy to the acceptor fluorophore through nonradiative dipole–dipole coupling, if they reside in close proximity. The most popular FRET pair for biological use is a Cyan Fluorescent Protein and Yellow Fluorescent Protein pair.

A fourth type of fluorescence biosensing technique is based on recently developed molecular beacons that use electronic energy transfer between a fluorescent molecule and a fluorescent quencher [35]. Molecular beacons are single-stranded oligonucleotide hybridization probes that can report the presence of specific nucleic acids in homogenous solutions.

**Label-Free Detection** In case of label-free detection, the biomolecules remain unlabeled or unmodified and are detected in their natural forms. Label-free optical biosensors measure the small changes of refractive index near the transducer surface as the sensing signal. The sensor is usually composed of a glass substrate coated with a thin film of a noble metal (gold, silver, or platinum). Light passes through the substrate and is reflected off the metal surface. When this metal surface is irradiated by light of certain wavelength at a specific angle (surface plasmon resonance (SPR) angle), a portion of the light energy couples through the metal coating, and creates a surface plasmon wave at the sample and metal surface interface. The SPR angle is very sensitive to changes in refractive index at the surface, and these changes are used to detect and monitor the association and dissociation of biomolecules, such as the binding of antibodies to antigens, immobilized at the sensor surface [36]. SPR-based biosensors are successfully used for the rapid detection of pathogens [37]. Other types of label-free evanescent wave optical biosensors include dual polarization interferometery, which uses a buried waveguide as a reference against which the change in propagation constant is measured.

#### 4.2.1.4 Piezoelectric Biosensors

A piezoelectric biosensor is an analytical device that uses the piezoelectric effect to measure the mass changes on a piezoelectric crystal. Piezoelectricity is defined as the ability of some materials including crystals (most commonly quartz) and certain ceramics to generate an electric field or electric potential in response to applied mechanical stress [38]. The piezoelectric transducer works by sending an electrical signal through the piezoelectric crystal, which causes vibration at some resonant frequency depending on its chemical nature, size, shape, and mass. By placing the crystal in an oscillating circuit and keeping the other influencing parameters constant, the frequency can be measured as a function of the mass. The mass change due to the adsorption of the analyte on the crystal surface is used to measure the specific biological activity [39]. A modified piezoelectric immunosensor based on single-fragment antibodies and single-domain recombinant antibodies was developed by Encarnação *et al.* [40] to recognize human immunodeficiency virus-1 viral infective factor and its binding kinetics to recombinant antibodies.

### 4.2.2 Fabrication of Biosensors

#### 4.2.2.1 Immobilization of Biomolecules

Immobilization techniques have been used in the fabrication of many nanoparticle-based biosensors. The method of immobilization is a critical factor in the construction of the biosensor and can greatly affect its performance. Commonly used techniques for biomolecule immobilization include physical adsorption, covalent binding, cross-linking, and physical entrapment in gels or membranes. These conventionally used methods have resulted in low reproducibility and poor spatially controlled deposition [41]. Irrespective of the immobilization method to be used, it should be simple to carry out, highly reproducible, should avoid nonspecific binding, and should be stable under extreme environmental conditions [17, 41, 42].

Physical adsorption, a commonly used immobilization technique, involves binding forces that include hydrogen bonds, multiple salt bridges, electrostatic interactions, and van der Waals forces [43], making the binding susceptible to changes in pH. Moreover, adsorption of the biomolecule onto the matrix results in a weak binding that may lead to desorption and leaching of the biomolecule to the sample solution during measurements. The surface of the immobilization matrix usually consists of an organic polymer with or without an inorganic conjugate (e.g., chitosan/ZnO matrix) [44]. Newer biosensing technologies have replaced glass or ceramic adsorption surfaces by polymeric surfaces that offer certain advantages like being lightweight, flexible, corrosion-resistant, highly chemically inert, and easy to process [41, 45].

Immobilization may also include entrapment through cross-linking wherein the biomolecule is entrapped within a matrix by cross-linking of the matrix molecules. The most commonly used gel matrices for the entrapment of biomolecules include polyacrylamide, glutaraldehyde, or gelatin, which undergo cross-linking in the

presence of the probe to be immobilized (e.g., coimmobilization of acetylcholine esterase and choline oxidase by cross-linking with glutaraldehyde onto a platinum surface [46]). The degree of cross-linking is a critical factor in affecting the functionality of the biosensor. An excessive degree of cross-linking of the matrix can hamper the analyte transport whereas, low cross-linking causes leaching of the biomolecule [42]. Covalent binding is a preferred immobilization technique as it is stronger and therefore less prone to detachment of the biomolecule that leads to increased stability of the linkage (e.g., coupling of glucose oxidase via acyl azide derivatives with polyacrylamide for glucose detection [41, 47]). However, covalent linkage can lead to partial or complete loss of activity.

In the mid-1970s, the conductive nature of some polymers was assessed after the discovery of polyacetylene. These conductive polymers were termed "synthetic metals" as they possessed a conjugated $\pi$-electron backbone in their chemical composition that imparted them with usual electrochemical characteristics like low ionization potential, high electrical conductivity, and high electronic affinity [43]. The examples of such polymers include polyaniline, polypyrrole, and polythiophene. These polymers can be electrochemically polymerized to form films that entrap the biomolecules. The method of electrochemical deposition offers the enhanced advantage of precisely electrogenerating a polymer coating over conductive microsurfaces of a complex geometry [48].

Another interesting approach, called liquid crystals, used in the fabrication of nanobiosensors involves oriented immobilization of biomolecules in a matrix. The phospholipids, by virtue of their amphipathic nature, assemble spontaneously at planar interfaces between thermotropic liquid crystals and aqueous phases. This gives rise to patterned orientations of the liquid crystals that reflect the spatial and temporal organization of the phospholipids. The proteins specifically bind at these interfaces and drive the reorganization of the phospholipids that triggers orientational transitions in the liquid crystals [1].

Holographic polymeric structures have been used to create biosensors. Using this approach, a holographic image can be changed by varying external parameters like humidity or by antibody–antigen immunoreactions [1, 49]. However, a disadvantage of this immobilization method is the lack of site-directed action, which often results in a partial or full loss of the function of the biomolecule.

In recent years, there has been a shift in the focus to develop biosensors for targeting and rapid detection of pathogens. Optical biosensors involve the use of SPR, which has been successfully used for the rapid detection of different pathogens [50, 51]. SPR-based assays have the advantage of being label-free and rapid. The antibodies against the pathogen to be detected are immobilized on the surface of gold. The main component in SPR biosensors is usually gold, which is predominantly used by virtue of being a free electron metal [50–52]. SPR-based immunoassays have been used for the detection of bacteria, including *Salmonella*. This immunoassay strategy either uses direct adsorption of the antibodies on the gold surface [50, 53, 54] or surfaces having standard alkylthiol chemistry [50, 55–57], or the carboxymethyl-dextran [50, 58, 59] surface. All these surfaces have been used for the capture of antibodies.

#### 4.2.2.2 Conjugation of Biomolecules and Nanomaterials

The biological functionality and the stability of a nanobiosystem are affected by the method of conjugation used. Three broad classifications of these methods of conjugation between the nanocrystals and biomolecules have been illustrated. In the first category, the biomolecules are noncovalently bound to the nanoparticles. The surfaces of these nanoparticles are made hydrophobic by derivatizing with a chemisorbed monolayer or the capping agent from the synthesis. Following this, these hydrophobic nanoparticles are precipitated and redissolved in water within tensidic micelles. The common micelle building agents that have been used include phospholipids, sodium dodecylsulfate, and Triton X-100. Finally, the biomolecules are coupled covalently to the functional groups at the outer sphere of the micelles. In this case, the interaction between the nanoparticles and the biomolecules depends on the hydrophobic interactions within the micelles. This enables the conjugate to disintegrate relatively easily.

A number of biological experiments involve the use of detergents that may lead to fusion of the micelles and coagulation of the nanoparticles. A recent improvement in this method involves the derivatization of the nanoparticles with charged surface molecules and attachment of the biomolecules to polyelectrolytes of opposite charge.

In the second category, the biomolecules are chemisorbed onto nanoparticles by means of a "linker." Either the biomolecule contains surface active groups like thiols that can be directly chemisorbed onto the nanoparticles or a bifunctional molecule may be chemisorbed onto the nanoparticles followed by the coupling of the biomolecule to these molecules. These conjugates do not generally disintegrate easily and, therefore, can be used in long-term experiments.

The third category of the conjugation methods involves covalent linking between the biomolecule and the nanoparticles. In such case, the nanoparticles are derivatized with cross-linked surface shells like functionalized polymers or inorganic conjugates like silica. These cross-linked surface shells contain binding sites for biomolecules where the biomolecules can be coupled. This method, although is difficult and expensive to prepare, results in the formation of stable covalent conjugates that may be useful in long-term experiments [1].

#### 4.2.2.3 Newer Nanobiosensing Technologies

A recent advancement in the area of nanobiosensing technologies has been the development of hybrid structures, which include either a single nanoparticle or an array of nanoparticles that play the role of the main functional element of a device. These nanoparticles have been widely used for making single electron transistors, memory storage devices, nanoscale photodetectors, nanoantennas, nanophotonic/plasmonic waveguides, and integrated circuits such as immobilization of 200- to 350-nm Co/Ni nanoparticles on a substrate using electron-beam induced deposition [60].

Over recent years, semiconducting nanocrystals have become potential biosensors. These crystals have optoelectronic properties that offer significant advantages compared with the conventionally used organic fluorophores. They show high

brilliance, the emission maxima of these crystals are continuously tunable due to quantum size effects, they have broad absorption characteristics, the emission has a narrow spectral linewidth, and, finally, they do not show photobleaching [1]. However, these luminescent nanocrystals have some limiting properties and, therefore, cannot be used in certain applications. These crystals show a higher luminescence on initial excitation. This effect has been attributed to a number of traps that include the surface properties and intrinsic impurities in the nanocrystal. The excitation of these crystals leads to a competition between the band edge luminescence and the alternative decay paths over the traps. This phenomenon gradually saturates the traps and makes the band edge luminescence more preferred than other modes of luminescence. When all the traps are saturated, it implies that there is equilibrium between the band edge luminescence and other forms of recombination. At this time, the luminescence remains constant. Another disadvantage of these nanocrystals is thermoquenching, which means that the luminescence of a nanocrystal can decrease with an increase in temperature. Also, the spherical semiconductor nanocrystals usually have a mean size of about 4 nm, being the same as those of large proteins. This may potentially become an important parameter in affecting the biological functionality of the process under study and any transport through cell membranes.

A recent advancement in this area includes the development of metal nanocrystals that offer the potential advantage of being detected by means of optical absorbance, Mie scattering, spectral shift, or SPR imaging. Noble metals that have been used for the synthesis of metal nanocrystals include silver, gold, platinum, and palladium. Silver and gold are the most commonly used nanocrystals. These crystals have different shapes and possess unique optical scattering responses. Highly symmetric spherical particles exhibit a single scattering peak, whereas other anisotropic shapes like rods [61], triangular prisms [62], and cubes [63] exhibit multiple scattering peaks in the visible wavelengths. This phenomenon primarily occurs due to highly localized charge polarizations at the corners and edges [64]. The colloidal methods have been widely used for the synthesis of these metal nanoparticle systems, and they offer a crystallographic control over the nucleation and growth of nanoparticles. These methods generally involve a metal salt precursor that is reduced in an aqueous or a nonaqueous solution in the presence of a stabilizing agent, which prevents aggregation and thereby improves the chemical stability of the formed nanoparticles. The major advantages of these methods are that they do not require any specialized equipment, they have a solution-based processing, and large quantities of nanoparticles can be synthesized [64]. These metal nanocrystals exhibit resonance of electrons in the conducting band, also called plasmons, which cause optical absorption by these nanoparticles. This resonance of electrons depends on the metal, morphology, and size of the nanocrystals [1]. In addition to these noble metal nanoparticles biosensor systems, there has been an emerging role of magnetic nanoparticles as magnetic resonance imaging agents [1, 65]. In most cases, the research is being conducted on $Fe_3O_4$ or Fe/Pt nanoparticles [65]. The use of these nanocrystals for imaging offers specific advantages, including stability against photobleaching and a potential improvement with

multicolor experiments owing to the narrow spectral linewidth, the flexible emission characteristic of luminescent nanocrystals, and an improvement in the signal intensity in the case of magnetic resonance measurements. Therefore, many labeling experiments that are not possible with organic dyes may be performed with nanocrystals, such as multicolor labeling with a minimal set of filters. An example of this technique has recently been demonstrated for the visualization of the self-assembly of tubulin [66].

Another class of biosensors that has been recently developed is nanotransducers, which can transform the signal resulting from the interaction of the analyte with the biological element into another signal that can be more easily measured and quantified. Cantilever-based sensors that utilize micromechanically produced cantilever probes are the most recent examples of these nanotransducer systems. The biosensing interaction on the surface of the system bends a several hundreds of nanometers thick cantilever, which can be optically sensed by a laser. The sensitivity of this nanotransducer can be tuned down to single-molecule interaction analysis [1, 67, 68]. The nanotransducers involve the use of nanomaterials like metal oxide or luminescent nanocrystals for biosensing in array-type assays or *in vivo* monitoring, and have currently replaced organic dyes, radioactive or metal labels, and contrast agents. The conjugation between the biomolecule and the nanocrystal is critical in the regulation of the overall biological properties of the conjugate for every nanobiosystem.

## 4.3 Evaluation of Nanoparticle-Based Nanosensors

### 4.3.1 Structural Characterization of Nanoparticle-Based Biosensors

The structural characterizations of nanoparticle-based biosensors are performed by the following techniques.

#### 4.3.1.1 Scanning Electron Microscopy

The scanning electron microscope is capable of producing high-resolution images of a sample surface by scanning it with a high-energy beam of electrons in a raster scan pattern. Therefore, the scanning electron microscopy (SEM) technique allows evaluation of the physical appearance and surface characteristics of nanoparticle-based biosensors [69]. In SEM, an electron beam is thermionically emitted from an electron gun fitted with tungsten or lanthanum hexaboride ($LaB_6$) cathode filament. Alternatively, electrons can be emitted from field emission guns (FEG), which may be of the cold-cathode type using tungsten single-crystal emitters or the thermally assisted Schottky type using emitters of zirconium oxide. The electron beam, which typically has an energy ranging from a few hundred to 50 keV, is focused by one or two condenser lenses into a very fine spot about 0.4–5 nm in diameter. The beam then passes through the objective lens, where

pairs of scanning coils or pairs of deflector plates in the electron column deflect the beam either linearly or in a raster fashion over a rectangular area of the sample surface. As the primary electrons strike the sample surface, the electrons loose energy by repeated random scattering and absorption within a teardrop-shaped volume of the specimen known as the interaction volume extending from less than 100 nm to around 5 μm into the surface. Interactions in this region lead to the subsequent emission of electrons that are then detected to produce an image. X-rays are produced when electrons interact with the sample atoms that are detected by a scanning electron microscope equipped with energy dispersive X-ray (EDX) spectroscopy. The EDX system coupled with SEM enables the elemental analysis of the samples [70].

For SEM studies the samples have to be first converted into a dry powder, which is then mounted rigidly on a specimen holder called a specimen stub. For conventional SEM imaging, specimens must be electrically conductive, at least at the surface, and electrically grounded to prevent the accumulation of electrostatic charge at the surface. Nonconductive specimens should be coated with an ultrathin coating of conductive material either by low vacuum sputter coating or high vacuum evaporation. The currently used materials for coating are gold, Au/Pd alloy, platinum, osmium, tungsten, chromium, and graphite. The primary reason for coating is to prevent the accumulation of static electric charge on the specimen during electron irradiation. The other reason for coating is to increase signal and surface resolution, especially with samples of low atomic number.

#### 4.3.1.2 Transmission Electron Microscopy

Although the principle of transmission electron microscopy (TEM) is different from SEM, the same type of information, such as particle size and distribution [71], observation of particle shape, and morphology [72], of the nanoparticles can be obtained by TEM as with SEM. Transmission electron microscopes are capable of imaging at a significantly higher resolution than light microscopes, due to the small de Broglie wavelength of electrons, which enables them to examine fine detail – even as small as a single column of atoms. A transmission electron microscope is operated under high vacuum (in the order of $10^{-7}$ torr) to avoid scattering of electrons from the air molecules and arcing due to high voltage. Transmission electron microscopes are equipped with an emission source, which may be a tungsten filament or a $LaB_6$ source [73]. The electron gun is connected to a high voltage source (typically around 100–300 kV) to emit electrons either by thermionic or field electron emission into the vacuum. This electron beam is then illuminated on a thin sample placed on a copper grid and negatively stained with phosphotungstic acid or derivatives. The transmission electron microscope builds an image by way of differential contrast. Contrast formation in TEM depends greatly on the mode of operation. The most common mode of operation for a transmission electron microscope is the bright field imaging mode. In this mode electrons that pass through the sample go on to form the image while those that are stopped or deflected by dense atoms in the specimen are subtracted from the image. In this way a black and white image is formed [74].

For conventional TEM analysis the specimen has to be reasonably dried and thin to ensure electron transparency, and stable under the extreme conditions such as high vacuum or intense heat generated by the beam of electrons.

TEM is an excellent technique to determine surface characteristics of particles; however, it has many drawbacks such as being time-consuming, causes damage to the samples, particularly in the case of biological samples, and is difficult to carry out on a routine basis.

#### 4.3.1.3 Atomic Force Microscopy

Atomic force microscopy (AFM) is a form of very-high-resolution scanning probe microscopy that offers a capability of three-dimensional visualization and is mainly used for physical characterization of the electrode surface to gather useful information about fabrication of biosensing elements on the surface of electrodes [75, 76]. The atomic force microscope consists of a silicon or silicon nitride cantilever with a sharp tip (probe) at its end that is used to scan the specimen surface. The surface scanning is done either by direct-contact or near-contact mode. AFM can be performed in liquid or gas medium. In the case of dried particles, scanning can be performed in both ambient air and in controlled environments such as nitrogen or argon gas. The liquid dispersion of solid particles can be scanned by anchoring the dispersion to the substrate provided that the dispersant is not corrosive to the probe tip. Particles dispersed in a solid matrix can also be analyzed by topographical or material sensing scans of cross-sections of the composite material. AFM has many advantages over SEM, such as providing true three-dimensional images of a sample, no requirement of sample coating that would irreversibly change or damage the sample, and higher resolution than SEM. However, the main drawback of AFM compared to SEM is its small image size.

#### 4.3.1.4 X-Ray Diffraction

X-ray diffraction (XRD) is often used to obtain information about the crystal structural [70] and size [77] of nanoparticle-based samples. When a monochromatic X-ray ($\lambda$ = 1–100 Å) beam is focused on a powder crystal placed in a sample holder, the scattered X-rays from the regularly placed atoms interfere with each other to yield a strong diffraction signal in particular directions. The directions of the diffracted beams depend on the shape and unit cell dimensions of the crystalline lattice. The diffraction intensities depend on the atomic numbers of the constituent atoms and their geometrical relationship with respect to the lattice points. To produce a significant diffraction pattern, the wavelength of incident radiation should be similar to or less than the interatomic spacing in the lattice. The peak intensities in the diffraction pattern from a regular crystal lattice are determined by Bragg's equation [78]:

$$n\lambda = 2d\sin\theta \tag{4.1}$$

where $n$ is any integer referring to the order of reflection, $\lambda$ is the wavelength of the incident X-ray beam, $d$ is the distance between atomic layers in a crystal, and $\theta$ is the angle between the incident ray and scattering plane. Thus, $2d\sin\theta$ is the

path length difference between the incident beam and the beams reflected from two consecutive crystal planes. In order to produce a reinforced diffracted beam the path length should be an integer value of the λ of the incident X-ray beams. An X-ray diffractometer consists of an X-ray source, X-ray generator, diffractometer assembly, and X-ray data collection and analysis system. The XRD technique is used to differentiate between amorphous and crystalline materials. Crystalline materials produce many diffraction bands, while amorphous compounds display a more or less regular baseline. The mean particle size of submicron particles or crystallites is determined by XRD using Scherrer's equation:

$$d = \frac{0.9\lambda}{\beta \cos\theta} \tag{4.2}$$

where $d$ is the mean diameter of the nanoparticles, λ is the wavelength of X-ray radiation, β is the angular full width at half maximum of the XRD peak and θ is the Bragg angle [78].

#### 4.3.1.5 X-Ray Photoelectron Spectroscopy

X-ray photoelectron spectroscopy (XPS) is a quantitative surface analytical technique with a sampling depth of 2–5 nm [79] and it is well suited for the surface characterization of colloidal nanoparticles [80]. In XPS the sample is illuminated with a beam of soft X-rays in ultrahigh vacuum. The resulting kinetic energy and number of photoelectrons that escape from the top of the materials being analyzed are determined by a β-ray spectrometer. This energy spectrum allows us to determine the composition of the sample. XPS is very sensitive to chemical composition and the environment of the element in the samples. In XPS spectra, each element will give rise to a characteristic set of XPS peaks at the respective binding energies. The positions of the peaks in the spectrum allow us to identify the atomic composition of the sample surface while the intensity of the characteristic peaks is directly related to the amount of the element within the illuminated region [81]. Thus, the XPS technique provides a quantitative analysis of the surface composition.

#### 4.3.1.6 UV/Visible Spectroscopy

UV spectroscopy is routinely used to determine the degree of immobilization as well as condition of biosensing elements at the electrode surface [70, 82]. When a beam of electromagnetic radiation incidents on an object it can be absorbed, transmitted, scattered, reflected, or excite fluorescence. UV/visible spectroscopy is based on the absorption and transmission of radiation. Therefore, samples should be examined under conditions that reduce the other processes such as scattering and reflectance, and do not excite fluorescence. The basic components of a spectrophotometer are a light source, sample holder, diffraction grating or monochromator to separate the different wavelengths of light, and detector. A hydrogen or deuterium lamp for the UV region and a tungsten/halogen lamp for the visible region are used as light sources. A photodiode or charge-coupled device is typically used for detection.

The sample to be analyzed is either dissolved or dispersed in a suitable solvent and placed in the sample holder. The most commonly used solvents are water for water-soluble compounds and ethanol for lipid-soluble compounds. The polarity and pH of solvents can affect the absorption spectrum of organic compounds.

### 4.3.2 Functional Characterization of Nanoparticle-Based Biosensors

#### 4.3.2.1 Quartz Crystal Microbalance

The Quartz crystal microbalance (QCM) is a high-resolution, label-free mass sensing technique based upon the piezoelectric effect. In biosensor technology, the QCM is used for monitoring and characterization of (bio) film deposition, detection of specific antigens, biomolecule binding kinetics, cell adhesion, and DNA detection [83]. The QCM can be used under vacuum, in the gas phase, and also in liquid environments. The QCM works by sending an electrical signal through a gold-plated quartz crystal that causes vibration at some resonant frequency followed by measurement of the frequency of oscillation in the crystal. The QCM can measure the mass per unit area by measuring the changes in frequency of the quartz crystal resonator. The frequency of oscillation of the quartz crystal can be used to measure the changes of thickness of the crystal by keeping the other influencing variables constant. If a mass is deposited on the crystal that increases the thickness, the frequency of oscillation decreases from its initial value. Therefore, a QCM device can be used to measure the real-time changes in mass during a chemical or biochemical process and be employed for the characterization of piezoelectric-based biosensors. Sauerbrey's equation is employed to correlate between the changes of frequency and the mass change [84]:

$$\Delta F = S\Delta m = \frac{-2F^2}{Zp} \cdot \Delta m \tag{4.3}$$

where $\Delta F$ is the frequency shift (Hz), $\Delta m$ is the change of mass per unit area ($ng\,cm^{-2}$), $S$ is the mass sensitivity ($Hz\,ng^{-1}\,cm^{-2}$), $F$ is the resonant frequency (Hz), and $Zp$ is the acoustical impedance ($Hz\,ng\,cm^{-2}$).

The QCM can also be coupled with other surface analytical tools. Electrochemical-QCM used to determine the ratio of mass deposited at the electrode surface during an electrochemical reaction to the total charge passed through the electrode [85].

#### 4.3.2.2 Ellipsometry

Ellipsometry is a powerful reflection-based, label-free optical technique for the investigation of dielectric properties of thin films. It is often used for surface characterization [86] and can be used *in situ* at the solid–liquid interface to monitor kinetics of biochemical reaction happening on the biosensor surface [87]. It is generally used to characterize films having a thickness ranging from a few angstroms to several nanometers. It is a very accurate contactless and nondestructive technique. One of the major advantages of this technique is that sample analysis can be performed in an ambient air, liquid, or vacuum environment. Ellipsometry

deals with the measurement and interpretation of the state of polarized light reflected from the sample surface. When linearly polarized light is reflected from a thin layer of the boundary surface between two medium it is converted to elliptically polarized light. By measuring changes of the ellipsometric angles ($\Psi$, $\Delta$), the optical properties, thickness, morphology, or roughness of layers or films on the surface can be calculated and can be used to determine the amount of adsorbed protein on a surface with the details of the kinetics of layer formation [17]. Care should be taken during sample preparation so that the sample is composed of a small number of discrete, well-defined, optically homogeneous isotropic layers.

#### 4.3.2.3 Surface Plasmon Resonance

SPR is an optical technique that measures the small changes of refractive index near a surface of a sensor. The sensor is composed of a glass substrate coated with a thin film of conducting metal, most often a noble metal (gold, silver, or copper). Light passes through the substrate and is reflected off the gold surface. When the gold surface is irradiated by light of a certain wavelength at a specific angle (SPR angle), a portion of the light energy couples through the gold coating and creates a surface plasmon wave at the sample/gold surface interface. The SPR angle is very sensitive to changes in refractive index at the surface, and these changes are used to detect and monitor the association and dissociation of biomolecules.

In order to study binding interactions the ligand is immobilized onto the sensor surface and the analyte is injected in aqueous solution (sample buffer) through the flow cell, under continuous flow. Accumulation of mass at the sensor surface during a binding interaction results in an increase in the refractive index and therefore an increase in signal is observed. After the sample is replaced by buffer, mass will decrease at the surface, which is indicated by the decrease in the resonance unit response. By repeating this cycle at different concentrations of analyte, calculations can be made for the association and dissociation constants of the biomolecular interaction. Hence, the systematic characterization of the effects of affinity of the sensor specificity element for target analyte, the effect of analyte mass on signal size, general performance of the sensor system with respect to sensitivity and selectivity, and distribution of biospecificity elements on the sensor surface can be achieved by the application of SPR [88].

#### 4.3.2.4 Cyclic Voltammetry

Cyclic voltammetry is a type of electroanalytical technique to obtain information about the redox potential and electrochemical reaction rates of analyte solutions. Therefore, cyclic voltammetry is often used to characterize the performance of electrochemical biosensors. In cyclic voltammetry the voltage is switched between two values ($V_2$ and $V_1$) at a fixed rate until it reaches the set potential ($V_2$). After reaching the set potential ($V_2$), the scan is reversed and the voltage is switched back to $V_1$. The inversion of scanning can happen multiple times during a single experiment. The scan rate is a critical factor, since the duration of scan should provide sufficient time to allow the chemical reaction to be complete. Therefore, varied results are obtained by varying the scan rate [9]. In a cyclic voltammetry

experiment, the voltage is measured between the reference electrode and working electrode, and the current is measured between the working electrode and counter-electrode. The current is plotted versus the voltage to obtain a voltammogram, which is used to study the electrochemical properties of analyte in solution [89]. The shape of the voltammogram for a specific compound depends on many factors, such as scan rate, electrode surface, and catalyst concentration [17].

## 4.4 Applications of Nanoparticle-Based Biosensors

Nanoparticle-based biosensors have been investigated for diverse biosensing applications. Noble metal nanoparticles, especially gold nanoparticles (Au-NPs), are prominently used in these nanobiosensors due to their distinct optical properties, ease of fabrication, relatively low toxicity, and amenability to attachment of various functionalities [90]. Nanobiosensors based on use of Au-NPs have been employed for electrochemical detection of various analytes such as glucose [91–95], $H_2O_2$ [96–98], urea [99], amyloid-β [100], $NAD^+$ and NADH cofactors [101], DNA [102], dopamine and uric acid [103], immunoglobulins [104], oxygen [105], phenols [106, 107] and hormones [107], *Salmonella* species [108], carcinoembryonic antigen [109], as well as adhesion and viability of the tumor cells [110]. Gold nanostructure-based biosensors are also reported for optical detection of glucose [111, 112], adenosine and cocaine [113], prostate-specific antigen [114], DNA/nucleic acids [115, 116] and their hybridization [117], homocysteine and thiolactone [118], enzymatic cleavage of nucleic acids [119], and detection [120–123] and identification [122] of proteins and heavy metals, such as mercury [124] and lead [114].

SPR has been used for the detection of proteins [125], immunoglobulins [126], and *Salmonella typhimurium* [127] using Au-NP-based biosensors. Zayats *et al*. [128] have reported a Au/CdS nanoparticle-based biosensor for the detection of acetylcholine esterase inhibitors, while Nusz *et al*. [129] have demonstrated label-free detection of biomolecular binding using streptavidin as a model compound with gold nanorod-based biosensors. Au-NPs in combination with magnetic and silver nanoparticles have been used to fabricate biosensors to electrochemically detect thrombin [130] and luteolin [131], respectively. Other noble metal nanoparticle-based biosensors [132–137] have been reported for detection of various analytes, primarily via electrochemical detection.

Quantum dots made up of materials such as cadmium/technetium [138–140], selenium/zinc sulfide [141], and carboxyl-coated materials [142] are reported for their optical biosensing applications. Various other materials used in the fabrication of nanobiosensors include titanium dioxide [143–144], silica [145, 146], porous zinc oxide [147], magnetic/core–shell-type nanoparticles [148–150], Ni/Al-based nanoflakes [151], hexacyanoferrates [152] and oxides [153] of nickel, Prussian blue [154], colloidal clay [155], conducting polymers [156], cobalt oxide [157], polyelectrolyte nanocapsules [158], and copper [159] and its alloy with gold [160]. The choice of the material for the nanoparticles depends upon factors such as the

nature of analyte, the detection system and, importantly, the physicochemical, electrochemical, or optical properties of the material itself.

## 4.5 Conclusions

Nanoparticle-based biosensors offer a variety of features that are tunable for the detection of various analytes, by using diverse detection techniques. Advances in fields of material science and nanotechnology has led to the availability of exciting novel materials for the fabrication of sensitive and specific biosensors. However, constructing a nanoparticle-based biosensor essentially involves striking a balance between various complicated and often contrasting factors, including the choice of the nanoparticle material, targeted analyte, detection environment, desired detection method, biosensing reaction and its sensitivity/selectivity, and the operating environment. The general fabrication methods described in this chapter are some of the most widely employed methods for biosensors. The evaluation of the biosensors, especially the functional evaluation, is usually complicated and involves the use of more than one instrumental technique. Although there is no fixed set of techniques amenable to all materials, analytes, and detection techniques, awareness of the general principles described in this chapter can be important in the successful fabrication and evaluation of a nanoparticle-based biosensor.

## References


**1** Urban, G.A. (2009) *Meas. Sci. Technol.*, **20**, 012001.

**2** IUPAC (1997) *IUPAC Compendium of Chemical Terminology (The Gold Book)*, Blackwell Scientific, Oxford.

**3** Foster, L.E. (ed.) (2005) *Nanotechnology: Science, Innovation, and Opportunity*, Pearson Prentice Hall, Upper Saddle River, NJ.

**4** Pathak, P., Katiyar, V.K., and Giri, S. (2007) *J. Nanotechnol. Online*, **3**, 1–14.

**5** Cavalcanti, A., Shirinzadeh, B., Zhang, M., and Kretly, L.C. (2008) *Sensors*, **8**, 2932–2958.

**6** Asefa, T., Duncan, C.T., and Sharma, K.K. (2009) *Analyst*, **134**, 1980–1990.

**7** Clark, L.C.J. and Lyons, C. (1962) *Ann. NY Acad. Sci.*, **102**, 29–45.

**8** Wang, J. (2001) *Electroanalysis*, **13**, 983–988.

**9** Eggins, B.R. (ed.) (2002) *Chemical Sensors and Biosensors (Analytical Techniques in the Sciences)*, John Wiley & Sons, Ltd, Chichester.

**10** D'Orazio, P. (2003) *Clin. Chim. Acta*, **334**, 41–69.

**11** Schöning, M.J. and Poghossian, A. (2002) *Analyst*, **127**, 1137–1151.

**12** Chaubey, A. and Malhotra, B.D. (2002) *Biosens. Bioelectron.*, **17**, 441–456.

**13** Guiseppi-Elie, A. and Lingerfelt, L. (2005) *Immobilization of DNA on Chips I* (ed. C. Wittmann), Springer, Berlin, pp. 161–186.

**14** Thévenot, D.R., Toth, K., Durst, R.A., and Wilson, G.S. (2001) *Biosens. Bioelectron.*, **16**, 121–131.

**15** Santandreu, M., Alegret, S., and Fàbregas, E. (1999) *Anal. Chim. Acta*, **396**, 181–188.

**16** Bakker, E. and Pretsch, E. (2005) *Trends Anal. Chem.*, **24**, 199–207.

**17** Grieshaber, D., MacKenzie, R., Vörös, J., and Reimhult, E. (2008) *Sensors*, **8**, 1400–1458.

**18** Caras, S. and Janata, J. (1980) *Anal. Chem.*, **52**, 1935–1937.

**19** Lud, S.Q., Nikolaides, M.G., Haase, I., Fischer, M., and Bausch, A.R. (2006) *ChemPhysChem*, **7**, 379–384.

**20** Ngeontae, W., Janrungroatsakul, W., Maneewattanapinyo, P., Ekgasit, S., Aeungmaitrepirom, W., and Tuntulani, T. (2009) *Sens. Actuators B*, **137**, 320–326.

**21** Sukeerthi, S. and Contractor, A.Q. (1994) *Ind. J. Chem.*, **33A**, 565–571.

**22** Patolsky, F., Zheng, G., and Lieber, C.M. (2006) *Anal. Chem.*, **78**, 4260–4269.

**23** Städler, B., Solak, H.H., Frerker, S., Bonroy, K., Frederix, F., Vörös, J., and Grandin, H.M. (2007) *Nanotechnology*, **18**, 155306.

**24** Khadro, B., Namour, P., Bessueille, F., Leonard, D., and Jaffrezic-Renault, N. (2009) *J. Environ. Sci.*, **21**, 545–551.

**25** Marrakchi, M., Dzyadevych, S.V., Lagarde, F., Martelet, C., and Jaffrezic-Renault, N. (2008) *Mater. Sci. Eng. C*, **28**, 872–875.

**26** Yagiuda, K., Hemmi, A., Ito, S., Asano, Y., Fushinuki, Y., Chen, C., and Karube, I. (1996) *Biosens. Bioelectron.*, **11**, 703–707.

**27** Spink, C. and Wads, I. (1976) *Methods of Biochemical Analysis* (ed. D. Glick), John Wiley & Sons, Inc., Hoboken, NJ, pp. 1–159.

**28** Flygare, L. and Danielsson, B. (1988) *Ann. NY Acad. Sci.*, **542**, 485–496.

**29** Scheller, F., Siegbahn, N., Danielsson, B., and Mosbach, K. (1985) *Anal. Chem.*, **57**, 1740–1743.

**30** Narayanaswamy, R. and Wolfbeis, O.S. (eds) (2004) *Optical Sensors: Industrial, Environmental and Diagnostic Applications*, Springer, New York.

**31** Fan, X., White, I.M., Shopova, S.I., Zhu, H., Suter, J.D., and Sun, Y. (2008) *Anal. Chim. Acta*, **620**, 8–26.

**32** Passaro, V., Dell'Olio, F., Casamassima, B., and De Leonardis, F. (2007) *Sensors*, **7**, 508–536.

**33** Moerner, W.E. (2007) *Proc. Natl. Acad. Sci. USA*, **104**, 12596–12602.

**34** Velasco-Garcia, M. (2009) *Semin. Cell Dev. Biol.*, **20**, 27–33.

**35** Tan, W., Wang, K., and Drake, T.J. (2004) *Curr. Opin. Chem. Biol.*, **8**, 547–553.

**36** Mayo, C.S. and Hallock, R.B. (1989) *J. Immunol. Methods*, **120**, 105–114.

**37** Lan, Y., Wang, S., Yin, Y., Hoffmann, W.C., and Zheng, X. (2008) *J. Bionic Eng.*, **5**, 239–246.

**38** Skoog, D.A., Holler, F.J., and Crouch, S.R. (2006) *Principles of Instrumental Analysis*, Brooks Cole, Boston, MA.

**39** Luong, J.H.T. and Guilbault, G.G. (1999) *Biosensor Principles and Applications* (eds L.J. Blum and P.R. Coulet), Dekker, New York.

**40** Encarnação, J.M., Rosa, L., Rodrigues, R., Pedro, L., da Silva, F.A., Gonçalves, J., and Ferreira, G.N. (2007) *J. Biotechnol.*, **132**, 142–148.

**41** Teles, F. and Fonseca, L. (2008) *Mater. Sci. Eng. C*, **28**, 1530–1543.

**42** Cassidy, J.F., Doherty, A.P., and Vos, J.G. (1998) *Principles of Chemical and Biological Sensors* (ed. D. Diamond), John Wiley & Sons, Inc., New York, pp. 73–132.

**43** Gerard, M., Chaubey, A., and Malhotra, B.D. (2002) *Biosens. Bioelectron.*, **17**, 345–359.

**44** Yang, Y., Yang, M., Jiang, J., Shen, G., and Yu, R. (2005) *Chin. Chem. Lett.*, **16**, 951–954.

**45** Saxena, V. and Malhotra, B.D. (2003) *Curr. Appl. Phys.*, **3**, 293–305.

**46** Amine, A., Mohammadi, H., Bourais, I., and Palleschi, G. (2006) *Biosens. Bioelectron.*, **21**, 1405–1423.

**47** Guilbault, G.G. (1988) *Methods Enzymol.*, **137**, 14–29.

**48** Cosnier, S. (2000) *Appl. Biochem. Biotechnol.*, **89**, 127–138.

**49** Domschke, A., March, W.F., Kabilan, S., and Lowe, C. (2006) *Diabetes Technol. Ther.*, **8**, 89–93.

**50** Barlen, B., Mazumdar, S.D., and Keusgen, M. (2009) *Phys. Stat. Sol. A.*, **206**, 409–416.

**51** Lazcka, O., Campo, F.J.D., and Muñoz, F.X. (2007) *Biosens. Bioelectron.*, **22**, 1205–1217.

**52** Liedberg, B., Nylander, C., and Lundström, I. (1995) *Biosens. Bioelectron.*, **10**, i–ix.

**53** Koubová, V., Brynda, E., Karasová, L., Skvor, J., Homola, J., Dostálek, J., Tobiska, P., and Rosický, J. (2001) *Sens. Actuators B*, **74**, 100–105.

**54** Homola, J., Yee, S., and Myszka, D.G. (2002) *Optical Biosensors: Present & Future* (eds F.S. Ligler and C.R. Taitt), Elsevier, San Diego, CA, pp. 207–252.

**55** Subramanian, A.S. and Irudayaraj, J.M. (2006) *Trans. ASABE*, **49**, 1257–1262.

**56** Jyoung, J., Hong, S., Lee, W., and Choi, J. (2006) *Biosens. Bioelectron.*, **21**, 2315–2319.

**57** Subramanian, A., Irudayaraj, J., and Ryan, T. (2006) *Biosens. Bioelectron.*, **21**, 998–1006.

**58** Bokken, G.C.A.M., Corbee, R.J., van Knapen, F., and Bergwerff, A.A. (2003) *FEMS Microbiol. Lett.*, **222**, 75–82.

**59** Fratamico, P., Strobaugh, T., Medina, M., and Gehring, A. (1998) *Biotechnol. Tech.*, **12**, 571–576.

**60** Burbridge, D.J., Crampin, S., Viau, G., and Gordeev, S.N. (2008) *Nanotechnology*, **19**, 445302.

**61** Yu, Y., Chang, S., Lee, C., and Wang, C. (1997) *J. Phys. Chem. B*, **101**, 6661–6664.

**62** Jin, R., Cao, Y., Mirkin, C.A., Kelly, K.L., Schatz, G.C., and Zheng, J.G. (2001) *Science*, **294**, 1901–1903.

**63** Sun, Y. and Xia, Y. (2002) *Science*, **298**, 2176–2179.

**64** Tao, A.R., Habas, S., and Yang, P. (2008) *Small*, **4**, 310–325.

**65** Nitin, N., LaConte, L.E.W., Zurkiya, O., Hu, X., and Bao, G. (2004) *J. Biol. Inorg. Chem.*, **9**, 706–712.

**66** Riegler, J., Nick, P., Kielmann, U., and Nann, T. (2003) *J. Nanosci. Nanotechnol.*, **3**, 380–385.

**67** Zhang, J., Lang, H.P., Huber, F., Bietsch, A., Grange, W., Certa, U., McKendry, R., Güntherodt, H., Hegner, M., and Gerber, C. (2006) *Nat. Nanotechnol.*, **1**, 214–220.

**68** Huber, F., Hegner, M., Gerber, C., Güntherodt, H., and Lang, H.P. (2006) *Biosens. Bioelectron.*, **21**, 1599–1605.

**69** Wang, J., Wang, L., Di, J., and Tu, Y. (2009) *Talanta*, **77**, 1454–1459.

**70** Baby, T.T. and Ramaprabhu, S. (2010) *Talanta*, **80**, 2016–2022.

**71** Yang, L., Ren, X., Tang, F., and Zhang, L. (2009) *Biosens. Bioelectron.*, **25**, 889–895.

**72** Mohagheghpour, E., Rabiee, M., Moztarzadeh, F., Tahriri, M., Jafarbeglou, M., Bizari, D., and Eslami, H. (2009) *Mater. Sci. Eng. C*, **29**, 1842–1848.

**73** Egerton, R. (ed.) (2005) *Physical Principles of Electron Microscopy: An Introduction to TEM, SEM, and AEM*, Springer, New York.

**74** Goodhew, P.J., Humphreys, J., and Beanland, R. (eds) (2001) *Electron Microscopy and Analysis*, Taylor & Francis, New York.

**75** Yang, L. and Li, Y. (2005) *Biosens. Bioelectron.*, **20**, 1407–1416.

**76** Parra, A., Casero, E., Vázquez, L., Pariente, F., and Lorenzo, E. (2006) *Anal. Chim. Acta*, **555**, 308–315.

**77** Kaushik, A., Khan, R., Solanki, P.R., Pandey, P., Alam, J., Ahmad, S., and Malhotra, B.D. (2008) *Biosens. Bioelectron.*, **24**, 676–683.

**78** Cullity, B. and Stock, S. (2001) *Elements of X-Ray Diffraction*, Addison-Wesley, Reading, MA.

**79** Briggs, D. and Seah, M.P. (eds) (1996) *Practical Surface Analysis, Auger and X-Ray Photoelectron Spectroscopy*, John Wiley & Sons, Ltd, Chichester.

**80** Maye, M.M., Luo, J., Lin, Y., Engelhard, M.H., Hepel, M., and Zhong, C. (2003) *Langmuir*, **19**, 125–131.

**81** Hota, G., Idage, S., and Khilar, K.C. (2007) *Colloids Surf. A*, **293**, 5–12.

**82** Chen, Q., Ai, S., Zhu, X., Yin, H., Ma, Q., and Qiu, Y. (2009) *Biosens. Bioelectron.*, **24**, 2991–2996.

**83** Ferreira, G.N.M., da-Silva, A., and Tomé, B. (2009) *Trends Biotechnol.*, **27**, 689–697.

**84** Hauck, S., Drost, S., and Prohaska, E. (2002) *Protein–Protein Interactions: A Molecular Cloning Manual* (ed. E. Golemis), Cold Spring Harbor Laboratory Press, Cold Spring Harbor, NY, p. 273.

**85** Buttry, D.A. and Ward, M.D. (1992) *Chem. Rev.*, **92**, 1355–1379.

**86** Azzam, R. and Bashara, N. (1987) *Ellipsometry and Polarized Light*, North Holland, Amsterdam.

**87** Arwin, H. (2000) *Thin Solid Films*, **377–378**, 48–56.

**88** Furlong, C.E., Woodbury, R.G., Yee, S.S., Chinowsky, T.M., Carr, R., Elkind, J.L., Kukanskis, K.A., Bartholomew, D.U., and Melendez, J.L. (1996) *Chemical, Biochemical, and Environmental Fiber Sensors VIII* (ed. R.A. Lieberman), SPIE, Denver, CO, pp. 208–215.

**89** Bard, A.J. and Faulkner, L.R. (2000) *Electrochemical Methods: Fundamentals and Applications*, John Wiley & Sons, Inc., New York.

**90** Chen, Y., Preece, J.A., and Palmer, R.E. (2008) *Ann. NY Acad. Sci.*, **1130**, 201–206.

**91** Dondapati, S.K., Lozano-Sanchez, P., and Katakis, I. (2008) *Biosens. Bioelectron.*, **24**, 55–59.

**92** Qiu, J., Wang, R., Liang, R., and Xia, X. (2009) *Biosens. Bioelectron.*, **24**, 2920–2925.

**93** Zeng, X., Li, X., Xing, L., Liu, X., Luo, S., Wei, W., Kong, B., and Li, Y. (2009) *Biosens. Bioelectron.*, **24**, 2898–2903.

**94** Barbadillo, M., Casero, E., Petit-Domínguez, M.D., Vázquez, L., Pariente, F., and Lorenzo, E. (2009) *Talanta*, **80**, 797–802.

**95** Liu, S. and Ju, H. (2003) *Biosens. Bioelectron.*, **19**, 177–183.

**96** Chen, S., Yuan, R., Chai, Y., Zhang, L., Wang, N., and Li, X. (2007) *Biosens. Bioelectron.*, **22**, 1268–1274.

**97** Lin, J., Qu, W., and Zhang, S. (2007) *Anal. Biochem.*, **360**, 288–293.

**98** Luo, X., Xu, J., Zhang, Q., Yang, G., and Chen, H. (2005) *Biosens. Bioelectron.*, **21**, 190–196.

**99** Tiwari, A., Aryal, S., Pilla, S., and Gong, S. (2009) *Talanta*, **78**, 1401–1407.

**100** Chikae, M., Fukuda, T., Kerman, K., Idegami, K., Miura, Y., and Tamiya, E. (2008) *Bioelectrochemistry*, **74**, 118–123.

**101** Zayats, M., Pogorelova, S.P., Kharitonov, A.B., Lioubashevski, O., Katz, E., and Willner, I. (2003) *Chemistry*, **9**, 6108–6114.

**102** Ovádeková, R., Jantová, S., Letasiová, S., Stepánek, I., and Labuda, J. (2006) *Anal. Bioanal. Chem.*, **386**, 2055–2062.

**103** Huang, X., Li, Y., Wang, P., and Wang, L. (2008) *Anal. Sci.*, **24**, 1563–1568.

**104** Liu, G. and Lin, Y. (2005) *J. Nanosci. Nanotechnol.*, **5**, 1060–1065.

**105** Zhang, H. and Hu, N. (2007) *Biosens. Bioelectron.*, **23**, 393–399.

**106** Carralero, V., Mena, M.L., Gonzalez-Cortés, A., Yáñez-Sedeño, P., and Pingarrón, J.M. (2006) *Biosens. Bioelectron.*, **22**, 730–736.

**107** González-Cortés, A., Yáñez-Sedeño, P., and Pingarrón, J.M. (2009) *Methods Mol. Biol.*, **504**, 157–166.

**108** Huang, J., Hou, S., Fang, S., Yu, H., Lee, H., and Yang, C. (2008) *J. Ind. Microbiol. Biotechnol.*, **35**, 1377–1385.

**109** Wu, J., Tang, J., Dai, Z., Yan, F., Ju, H., and El Murr, N. (2006) *Biosens. Bioelectron.*, **22**, 102–108.

**110** Du, D., Liu, S., Chen, J., Ju, H., Lian, H., and Li, J. (2005) *Biomaterials*, **26**, 6487–6495.

**111** Lim, S.Y., Lee, J.S., and Park, C.B. (2009) *Biotechnol. Bioeng.*, **105**, 210–214.

**112** Bahshi, L., Freeman, R., Gill, R., and Willner, I. (2009) *Small*, **5**, 676–680.

**113** Liu, J. and Lu, Y. (2005) *Angew. Chem. Int. Ed.*, **45**, 90–94.

**114** Shaikh, K.A., Ryu, K.S., Goluch, E.D., Nam, J., Liu, J., Thaxton, C.S., Chiesl, T.N., Barron, A.E., Lu, Y., Mirkin, C.A., *et al.* (2005) *Proc. Natl. Acad. Sci. USA*, **102**, 9745–9750.

**115** Thaxton, C.S., Georganopoulou, D.G., and Mirkin, C.A. (2006) *Clin. Chim. Acta*, **363**, 120–126.

**116** Toubanaki, D.K., Christopoulos, T.K., Ioannou, P.C., and Flordellis, C.S. (2009) *Anal. Chem.*, **81**, 218–224.

**117** Du, B., Li, Z., and Liu, C. (2006) *Angew. Chem. Int. Ed.*, **45**, 8022–8025.

**118** Huang, C. and Tseng, W. (2008) *Anal. Chem.*, **80**, 6345–6350.

**119** Zhao, W., Lam, J.C.F., Chiuman, W., Brook, M.A., and Li, Y. (2008) *Small*, **4**, 810–816.

**120** Xie, F., Goldys, E., and Baker, M. (2007) *Biofactors*, **30**, 249–253.

**121** Wang, W., Chen, C., Qian, M., and Zhao, X.S. (2008) *Anal. Biochem.*, **373**, 213–219.

**122** You, C., Miranda, O.R., Gider, B., Ghosh, P.S., Kim, I., Erdogan, B., Krovi, S.A., Bunz, U.H.F., and Rotello, V.M. (2007) *Nat. Nanotechnol.*, **2**, 318–323.

**123** Jena, B.K. and Raj, C.R. (2008) *Biosens. Bioelectron.*, **23**, 1285–1290.

**124** Huang, C. and Chang, H. (2006) *Anal. Chem.*, **78**, 8332–8338.

**125** Zhu, S. and Fu, Y. (2009) *Biomed. Microdevices*, **11**, 579–583.

**126** Hsieh, B., Chang, Y., Ng, M., Liu, W., Lin, C., Wu, H., and Chou, C. (2007) *Anal. Chem.*, **79**, 3487–3493.

**127** Ko, S., Park, T.J., Kim, H., Kim, J., and Cho, Y. (2009) *Biosens. Bioelectron.*, **24**, 2592–2597.

**128** Zayats, M., Kharitonov, A.B., Pogorelova, S.P., Lioubashevski, O., Katz, E., and Willner, I. (2003) *J. Am. Chem. Soc.*, **125**, 16006–16014.

**129** Nusz, G.J., Marinakos, S.M., Curry, A.C., Dahlin, A., Höök, F., Wax, A., and Chilkoti, A. (2008) *Anal. Chem.*, **80**, 984–989.

**130** Zheng, J., Feng, W., Lin, L., Zhang, F., Cheng, G., He, P., and Fang, Y. (2007) *Biosens. Bioelectron.*, **23**, 341–347.

**131** Franzoi, A.C., Vieira, I.C., Dupont, J., Scheeren, C.W., and de Oliveira, L.F. (2009) *Analyst*, **134**, 2320–2328.

**132** Wang, X., Dong, P., Yun, W., Xu, Y., He, P., and Fang, Y. (2009) *Biosens. Bioelectron.*, **24**, 3288–3292.

**133** Lu, J., Do, I., Drzal, L.T., Worden, R.M., and Lee, I. (2008) *ACS Nano*, **2**, 1825–1832.

**134** Xiao, F., Zhao, F., Mei, D., Mo, Z., and Zeng, B. (2009) *Biosens. Bioelectron.*, **24**, 3481–3486.

**135** Yang, M., Yang, Y., Liu, Y., Shen, G., and Yu, R. (2006) *Biosens. Bioelectron.*, **21**, 1125–1131.

**136** Tsai, Y., and Chien, H. (2007) *J. Nanosci. Nanotechnol.*, **7**, 1611–1617.

**137** Li, M., Shang, Y., Gao, Y., Wang, G., and Fang, B. (2005) *Anal. Biochem.*, **341**, 52–57.

**138** Zhang, Q., Zhang, L., Liu, B., Lu, X., and Li, J. (2007) *Biosens. Bioelectron.*, **23**, 695–700.

**139** Liu, X. and Ju, H. (2008) *Anal. Chem.*, **80**, 5377–5382.

**140** Du, D., Chen, S., Song, D., Li, H., and Chen, X. (2008) *Biosens. Bioelectron.*, **24**, 475–479.

**141** Freeman, R., Gill, R., Shweky, I., Kotler, M., Banin, U., and Willner, I. (2009) *Angew. Chem. Int. Ed.*, **48**, 309–313.

**142** Chakraborty, S.K., Fitzpatrick, J.A.J., Phillippi, J.A., Andreko, S., Waggoner, A.S., Bruchez, M.P., and Ballou, B. (2007) *Nano Lett.*, **7**, 2618–2626.

**143** Kafi, A.K.M., Wu, G., and Chen, A. (2008) *Biosens. Bioelectron.*, **24**, 566–571.

**144** Wu, H., Cheng, T., and Tseng, W. (2007) *Langmuir*, **23**, 7880–7885.

**145** Qu, B., Chu, X., Shen, G., and Yu, R. (2008) *Talanta*, **76**, 785–790.

**146** Latterini, L. and Amelia, M. (2009) *Langmuir*, **25**, 4767–4773.

**147** Dai, Z., Shao, G., Hong, J., Bao, J., and Shen, J. (2009) *Biosens. Bioelectron.*, **24**, 1286–1291.

**148** Grancharov, S.G., Zeng, H., Sun, S., Wang, S.X., O'Brien, S., Murray, C.B., Kirtley, J.R., and Held, G.A. (2005) *J. Phys. Chem. B*, **109**, 13030–13035.

**149** Tang, L., Zeng, G., Liu, J., Xu, X., Zhang, Y., Shen, G., Li, Y., and Liu, C. (2008) *Anal. Bioanal. Chem.*, **391**, 679–685.

**150** Aryal, B.P., and Benson, D.E. (2006) *J. Am. Chem. Soc.*, **128**, 15986–15987.

**151** Ai, H., Huang, X., Zhu, Z., Liu, J., Chi, Q., Li, Y., Li, Z., and Ji, X. (2008) *Biosens. Bioelectron.*, **24**, 1054–1058.

**152** Yang, M., Yang, Y., Qu, F., Lu, Y., Shen, G., and Yu, R. (2006) *Anal. Chim. Acta*, **571**, 211–217.

**153** Salimi, A., Sharifi, E., Noorbakhsh, A., and Soltanian, S. (2007) *Biophys. Chem.*, **125**, 540–548.

**154** Li, L., Sheng, Q., Zheng, J., and Zhang, H. (2008) *Bioelectrochemistry*, **74**, 170–175.

**155** Shumyantseva, V.V., Ivanov, Y.D., Bistolas, N., Scheller, F.W., Archakov, A.I., and Wollenberger, U. (2004) *Anal. Chem.*, **76**, 6046–6052.

**156** Rahman, M.A., Kwon, N., Won, M., Choe, E.S., and Shim, Y. (2005) *Anal. Chem.*, **77**, 4854–4860.

**157** Salimi, A., Hallaj, R., and Soltanian, S. (2007) *Biophys. Chem.*, **130**, 122–131.

**158** Brown, J.Q. and McShane, M.J. (2003) *IEEE Eng. Med. Biol. Mag.*, **22**, 118–123.

**159** Luechinger, N.A., Loher, S., Athanassiou, E.K., Grass, R.N., and Stark, W.J. (2007) *Langmuir*, **23**, 3473–3477.

**160** Cai, H., Zhu, N., Jiang, Y., He, P., and Fang, Y. (2003) *Biosens. Bioelectron.*, **18**, 1311–1319.

# 5
# Enzyme-Based Biosensors: Synthesis and Applications

*Shunsheng Cao, Juanrong Chen, Xin Jin, Weiwei Wu, and Zhiyuan Zhao*

## 5.1
## Introduction

Nanoscience is exhibiting more and more significance in material science and technology development. This is, in turn, leading to great breakthroughs in physics, electronics, chemistry, and biology, and has driven many researchers to investigate and discuss the possibilities of applying nanotechnology to fabricate a variety of functional materials with electronic, magnetic, optical, or catalytic properties [1, 2]. Among them, biosensor materials have been a fast-growing research field over the past several decades due to their potential application in a various analytical tasks, such as medical diagnostics, food industry, water quality control, health safety, environmental monitoring, pharmaceutics, and bioassays [3–7]. As a result, various kinds of biosensor materials, including carbon nanotubes (CNTs) [8, 9], titanate nanotube (TNT) [10, 11], inorganic particles [4, 12], nanoporous spheres [13, 14], and polymer membranes [15, 16], have been prepared as enzyme carriers by using established strategies for enzyme immobilization.

What exactly is a biosensor? Most readers and researchers have a general idea of what a biosensor is or does, but they will be hard pushed to provide a precise definition. In its broadest sense, a biosensor is defined as an analytic device that uses specific biochemical reactions mediated by a biological recognition element (i.e., enzyme, cell, tissues, antibodies, DNA, etc.) immobilized on a signal transducer [17–20]. At one time, it would have been appropriate simply to answer that it is any sensor used in a biological system. The main analytical advantages of biosensors are that they are adaptable, portable, simple to use in relatively complex environments due to their rapid response, and show high sensitivity and intrinsic selectivity [9]. Therefore, sample treatment can be minimized, effectively avoiding any related processes and problems. The pioneering work on biosensors is undoubtedly ascribed to the efforts of Clark and Lyons due to their first report about a glucose sensor at a New York Academy of Sciences Symposium in 1962 [21], in which they showed that glucose in whole blood could be monitored by measuring the amount of oxygen consumed through the use of an amperometric

*Biosensor Nanomaterials*. Edited by Songjun Li, Jagdish Singh, and Ipsita A. Banerjee

ISBN: 978-3-527-32841-3

electrode; a commercial clinical analyzer was then introduced by Yellow Springs Instrument Company [4, 19, 22].

Currently, enzyme-based biosensors are a hot topic in research since essentially all chemical reactions in living systems are catalyzed by enzymes [16]. In the last decade, significant efforts have been made in the research, development, and commercialization of enzyme-based biosensors, and such biosensors now are extensively applied to the *in vivo* detection and quantification of numerous biologically relevant molecules, as shown in various publications, including Jones *et al*. [23], Xue *et al*. [24], Ramanathan *et al*. [25], and Yeung *et al*. [26]. In general, an ideal biosensor should effectively combine nature's sensitivity and specificity with the advantages of modern microelectronics. Therefore, an enzyme-based biosensor should, in principle, possess the following features: (i) specificity for target analytes, (ii) stability under normal storage conditions, (iii) reusability and high sensitivity, (iv) accuracy and reproducibility of the response, and (v) reduced cost [19]. Currently, from the practical and application point of view, only several enzyme targets, including glucose [9, 27, 28] (diagnosis and treatment of diabetes, food science, biotechnology), lactate [28, 29] (sports medicine, critical care, food science, biotechnology), urea [30, 31] (medical diagnostics, heavy metal monitor), and glutamate/glutamine [32, 33] (food science, biotechnology) have received special attention [22]. Those corresponding enzymes were widely coopted in biosensors. Among them, the glucose–glucose oxidase (GOx) system is, by far, the most widely employed as a model system, and thus continues to drive research toward better sensors due to its good stability, low cost, widespread knowledge about its unique properties, and numerous reports on its catalytic activity, particularly for the measurement of glucose in biological samples [22, 34, 35]. There are some general reviews on the fabrication, development, and application of amperometric biosensors, artificial based-enzyme biosensors, DNA biosensors, and so on [19, 20, 22, 36–38]. However, here, we focus primarily on the progress in the synthesis and applications of enzyme-based biosensors, especially emphasizing development that have occurred from 2000 to 2010. We attempt to look into all aspects of this field, from systematic synthetic approaches of enzyme immobilization to major applications of biosensors. Nevertheless, not every work can be discussed in detail; some subareas are beyond the scope of this chapter. We mainly address works related to important biosensor supports (CNTs, nanoparticles, and polymer membrane) for enzyme immobilization and their most demanding applications, such as environmental monitoring and medical diagnostics.

## 5.2
## Synthesis and Characterization of Biosensor Supports

It is universally accepted that enzymes are considered very useful in analytical chemistry because they can show high selectivity and sensitivity for a variety of assays. Recently, the direct electron transfer between redox proteins and electrode surfaces has attracted much interest [39]. In the absence of mediating small

molecules, however, the observation of well-defined electrochemical behavior of loaded flavoprotein oxidase systems such as GOx is rendered very difficult. As the flavin adenine dinucleotide group is embedded deep within the protein structure, this makes the transmission coefficient for direct electron transfer between the latter and a support electrode very small [40, 41]. Moreover, the free enzyme usually is not stable and cannot be easily reused. For example, most reports indicated that enzyme-based biosensors need a suitable support (solvent, gel, or solid) for optimizing the activity and stability of all the involved sensing elements in order to ensure that immobilized enzymes (or enzymes localized on those supports) could be used repeatedly enough times without severely losing their activity and sensitivity [34, 42–44]. On the other hand, the lifetime of an enzyme-based biosensor mainly depends on how long the biological activity of the loaded enzyme is retained, which in turn depends on the immobilization strategy for the enzyme. As a result, the immobilization of enzymes is a decisive way for constructing high-performance biosensors [45–48]. To date, a variety of approaches and strategies for enzyme immobilization have been proposed to immobilize mediators, including physical or chemical adsorption onto an electrode or a solid surface [49, 50], electropolymerization [51, 52], entrapment within a membrane, matrix, sol–gel, nanoporous polymer, or microcapsule [4, 52–54], cross-linking between molecules [55, 56], and covalent bonding to a surface [57–59], in which adsorption of enzyme from a solution onto a solid surface or an electrode can be carried out by either physical or chemical interactions, including van der Waals forces, electrostatic attractions, hydrophobic interactions, or hydrogen bonding [60, 61]. Nevertheless, there are several limitations concerning the immobilization of mediators on electrode surfaces via such adsorption because some soluble enzymes with a low molecular weight can easily diffuse away from the surface of supports into the bulk solution when the biosensor is used continuously, which would lead to significant signal loss, and greatly affect the sensitivity and lifetime of the biosensor [50]. Such challenges could be overcome by covalent linking or cross-linking strategies, as introduced by Zhang *et al*. [57], Kaneto *et al*. [59], and Lee *et al*. [55]. Unfortunately, these techniques might denature the enzyme or partially change the native structure so as to result in low sensitivity and short lifetime of biosensors. As a consequence, the immobilization method used for biomolecules will depend on a number of factors, but in general the method needs to be compatible with the biomolecules being immobilized, and must satisfy the following criteria if the biosensors are to be of practical and commercial use: (i) the biomolecules immobilized must retain high sensitivity and substantial biological activity; (ii) the loaded enzyme biosensor should have long-term stability and durability; and (iii) the biological material needs to have a high degree of specificity to a particular biological component [36]. These conditions must be fully considered for fabrication of an efficient sensing device. In addition, the immobilized enzyme biosensor also should be investigated with regard to whether the biosensor can effectively resist a wide variety of changes in pH, temperature, ionic strength, and chemical composition, while retaining its stability and activity. Here, several typical widely used biosensor supports have been selected as

examples to describe and discuss the process in fabricating enzyme-based biosensors.

## 5.2.1 Carbon Nanotubes

### 5.2.1.1 Characterization of Carbon Nanotubes

CNTs are considered as the result of folding grapheme layers into carbon cylinders. They can be divided in general into two distinct types of structures: single-walled carbon nanotubes (SWNTs) and multiwalled carbon nanotubes (MWNTs) [62, 63]. The SWNT is a single shell extending from end to end, produced by rolling up a single graphite sheet into a tube, and therefore tends to have a smaller diameter than MWNTs (about 1.3–2 nm in tube diameter), as shown in Figure 5.1 [62]. For comparison, the MWNT is composed of several concentric cylinders, each formed with rolled graphite sheets, with diameters normally varying from 10 to 50 nm. These multiple layers provide MWNTs with a stiffer structure, which in turn leads to less thermal vibration compared with SWNTs [64]. There are many approaches and strategies to fabricate CNTs, including chemical vapor deposition, electric arc, or laser adsorption methods [63, 65, 66]. Ever since CNTs were first discovered by Sumio Iijima [67], they have attracted much attention, and have led to many new technical developments and applications due to their unique spatial geometry (high surface area-to-volume ratio), high mechanical strength, remarkable electronic properties, and chemical structure stability [62, 63, 68, 69]. Therefore, CNTs can present metallic, semiconducting, and superconducting electron transport depending on their structure, possess a hollow core suitable for entrapping guest molecules, and have the largest elastic modulus of any known material [63, 70]. The unique properties of CNTs make them extremely attractive as a biosensor support, particularly as an amperometric biosensor support, and they have been introduced in a wide variety of fields, including chemical sensors [71], biosensors [9, 27], cell counters [72], and so on. To full understand and fabricate such unique nanomaterials in sensing applications, CNTs need to be properly functionalized and immobilized. It is the purpose of this section to summarize recent progress in the synthesis and application of CNTs for biosensors.

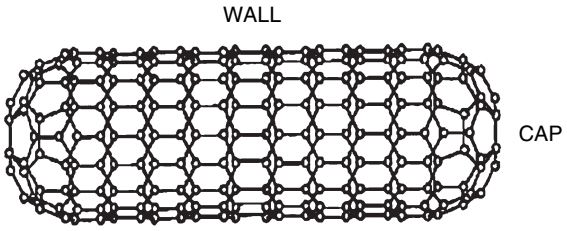


**Figure 5.1** General structure of a SWNT. (Reproduced with permission from [63].)

#### 5.2.1.2 Application of Carbon Nanotubes as Biosensor Supports

Since Crooks *et al.* [73] first attempted to use an individual CNT as an electrochemical probe by describing the fundamental electrochemical behavior of CNT electrodes, there has been considerable attention on the fabrication and development of such new nanomaterials consisting of CNTs and organic binders for electrochemical and material science applications due to their unique highly conductive electrical properties [27, 74]. The combination of polymers with CNTs and biorecognition elements forming a composite is of fast-growing importance due to its simplicity of construction and its ability to incorporate conducting materials into porous polymers in order to construct electrochemical biosensors [75]. As mentioned above, however, the CNTs need to be properly functionalized to take full advantage of fabricating such biosensors. For this, many approaches have been reported to modify CNTs by using nitric or sulfonic acid in order to introduce the chemically active functional groups, as shown in various publications, including Azamian *et al.* [76], Gooding *et al.* [77], Li *et al.* [78], Liu *et al.* [79], etc. Evidently, other new synthetic schemes and more rigid materials are needed to broaden the application and market of CNT-based electrochemical sensors. CNT (bio)composites with a binder such as Nafion [9, 80], Teflon [81], sol-gel [82], poly(methyl methacrylate) [83], redox hydrogel [84], poly(dimethyldiallylammonium chloride) [85], chitosan [86], and electropolymerized film [87] were prepared in order to improve the robustness of CNT electrodes and to facilitate immobilization of biocomponents. However, these methods indicate that enzymes and other biomolecules must receive careful treatment in order to retain their tertiary structure. In addition, when using such wet processes, it is hard to control the nanoscale fabrication with adequate precision [62]. Therefore, a more sophisticated process has been employed to exhibit the electrochemistry of enzyme bound on the ends of vertically aligned CNTs. Undoubtedly, such biosensor fabrication strategies are very complex and require highly skilled personnel for reproducible fabrication [27]. For this, Muguruma *et al.* undertook considerable efforts to propose and introduce an amperometric biosensor based on a plasma-polymerized thin film (PPF) comprised of highly branched and incompletely cross-linked aliphatic hydrocarbon backbone chains containing nitrogen atoms in the form of primary amine groups, in which the PPF is obtained in a glow discharge or plasma in the vapor phase [62, 88–91]. Munge *et al.* [92] demonstrated a new amplification method by using layer-by-layer assembly, which has been extensively employed to construct a variety of enzyme biosensors (glucose, DNA, etc.) [85, 93] owing to its simplicity and inherent precise control of film thickness, of enzyme labels on CNTs support for detecting DNA and proteins. Recently, Munge *et al.* [27] further fabricated a sensitive $H_2O_2$ sensor by using horseradish peroxidase (HRP) covalently attached to layered nonoriented MWNT-modified electrodes via the layer-by-layer method.

The application of CNTs has attracted much interest due to their excellent conductivity, including the improvement of electron transfer between the enzymes and the electrode surfaces, while providing a very good matrix for enzyme immobilization [94, 95]. In these devices, the biomacromolecules are loaded into the

CNT matrix of the composite forming a CNT-based amperometric biosensor with unique properties. For instance, Kim *et al.* [69] fabricated a small needle-type nanobisensor based on one MWNT on an etched tungsten tip and used it as an electrochemical biosensor to determine dopamine. Sánchez *et al.* [75] fabricated and characterized HRP/CNT/polysulfone thickfilm screen-printed electrodes for electrochemical sensing. Zou *et al.* [9] prepared a Pt/MWNT nanocomposite biosensor with high sensitivity, good reproducibility, long-term stability, and freedom from interference in a simple and robust way, in which platinum nanoparticles can be gown by electrodeposition onto MWNTs directly, with the average diameter of the nanoparticles being about 30–40 nm. Recent developments in conducting polymer composites based on CNTs applied to electrochemistry have opened a new range of possibilities for the construction of electrochemical biosensors, and will continue to optimize existing approaches and to drive new, facile procedures for the fabrication of electrochemical biosensors in this field [8, 96].

### 5.2.2
### Nanoparticles for Enzyme Immobilization

#### 5.2.2.1 General Consideration

It is well known that enzymes are versatile biocatalysts and are fast increasing applications in many fields due to their high specificity, selectivity, and efficiency [38, 97]. However, even when an enzyme is identified as being useful for a given field, the exciting possibility of using enzymes is subject to severe challenges due their sensitivity to organic solvents, limited availability, poor thermal stability, and high price, as well as by difficulties in recovery and recycling [38, 97, 98]. Enzymes loaded to supports can to a significant extent overcome such problems, and can be found in a wide variety of applications in biosensors, diagnostics, industrial biocatalysis, organic transformations, and biotechnology [38, 99]. Enzyme immobilization, however, often leads to a decrease in activity and stability. Although rapid progress has been made in this field, there are no specific, detailed guidelines available in various publications to fabricate and prepare improved biocatalysts for biosensor applications. A rational approach to prepare such biocatalysts is to eliminate or minimize the unfavorable interactions between the immobilized enzyme and the support, as demonstrated in Figure 5.2 [38]. The development of

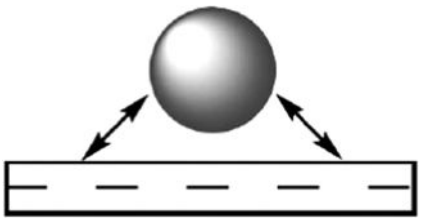

**Figure 5.2** Typical demonstration of enzyme–support interactions (Reproduced with permission from [38])

a general method, therefore, is necessary to evaluate and quantify their interactions in order to better control them.

#### 5.2.2.2 Application of Nanoparticles as Biosensor Supports

In the last several decades, the design and application of nanomaterials has been attracting considerable interest in the field of biotechnology and bioanalytical chemistry. Compared with other traditional supports, immobilization of enzymes on to nanoparticles offers several operational advantages. For example, nanoparticles can be finely dispersed in aqueous media, thus reducing mass transfer problems related to enzymes loaded on conventional bulk supports. In addition, they can also be easily recovered and reused by centrifugation (or by magnetic sedimentation in the case of magnetic nanoparticles) [12, 100, 101]. More importantly, they can be easily produced in a wide variety of sizes, morphologies, and compositions, and can be modified for immobilization systems by introducing a variety of established methods [4, 97]. Inorganic nanosized particles such as calcium carbonate [4] and some semiconductor nanoparticles (i.e., polystyrene) [12] are promising materials for biomolecule supports, and possess improved biocompatibility for proteins and/or facilitate rapid and enhanced electron transfer to the sensor surface [4].

Currently, several conducting polymers such as polypyrrole, poly(*N*-methyl pyrrole), polyindole, polyaniline (PANI), and polycarbazole have been widely used to load desired enzymes (GOx, urease, cholesterol oxidase) by using physical adsorption and entrapment strategies [28, 102, 103]. For this purpose, PANI is considered to be an attractive biosensor polymer because such electronic material exhibits two redox couples in the right potential range to facilitate an enzyme–polymer charge transfer. Therefore, PANI is one of the most widely used biosensor carriers due to its good environmental stability and the fact that its electrical properties can easily be tuned through dopant inclusion/exclusion principles, and it has found a variety of uses in biosensor technology, electrochromic devices, energy storage systems, and anticorrosion materials [104]. Doped PANI, however, is difficult, brittle, and insoluble in common organic solvents, making its large-scale processability difficult.The insolubility/infusibility of PANI is related to its rigid $\pi$–$\pi$ conjugation effect [104]. In addition, the monomer aniline is a carcinogen and also must be distilled prior to use [105]. As a result, its large-scale applicability has been challenged by its poor thermal stability and difficult processability [104, 105]. For these, considerable efforts have been undertaken to face up to the challenge in order to overcome PANI organic and inorganic insolubility problems. The introduction of substituents on the aromatic ring or imine nitrogen, copolymerization with aliphatic monomers, and preparation of PANI blends/composites with other functional polymers have produced more soluble PANI [106–108]. In general, PANI is produced readily from aqueous media by means of chemical and electrosynthetic routes. The chemical technique needs the oxidative polymerization of the requisite monomers in an acidic media by using strong oxidants in the presence or absence of templates [104, 109]. Unfortunately, acidic media is required for the construction of the most highly

conductive form of aniline, which does not lend itself to entrapment of protein for biosensing applications. Excitingly, the use of nanoparticles avails to overcome the processability issues associated with PANI because nanoparticles are readily dispersed in aqueous media, as illustrated by Zhang *et al.* [110], Wan *et al.* [111], and Smyth *et al.* [105]. Apart from processability, the ability of PANI to load and provide direct electrical communication between the enzyme and electrode in amperometric biosensors has been demonstrated, as reported by Morrin *et al.* [112], Kathleen *et al.* [113], and Iwuoha *et al.* [104]. Moreover, other particles are also widely used as supports for enzyme immobilization in biosensor applications. $CaCO_3$ is one of the nanoparticles and can be employed to entrap a wide range of enzymes by physical adsorption due to the large interfacial area in $CaCO_3$ aggregates [4]. For example, Peng *et al.* [114] immobilized lipase with $CaCO_3$ powder as a carrier for forming monoacylglycerol. Petrov *et al.* [115] reported the preparation of the protein-loaded $CaCO_3$ particles via adsorption while the encapsulated biomaterials retained their activity. Recently, Xue *et al.* [4] exploited a glucose amperometric biosensor based on the mild immobilization of GOx by using $CaCO_3$ as support. Polystyrene nanoparticles are another type of nanoparticle and are widely used in agglutination tests for the detection of a variety of biological analytes [12, 116, 117].

### 5.2.3 Polymer Membranes

Enzyme-based biosensors are fabricated to exhibit a wide analytical range, and good antifouling and antiinterference properties. Although numerous established strategies have been successfully employed to construct new nanocomposite biosensors, several limitations, such as time and cost, difficulty of large-scale production, and absence of universality, inevitably hinder the practical applications of such methods [15, 43]. Since Decher [118] pioneeringly introduced an alternative way to develop a new generation of nanocomposite biosensor based on the alternative deposition of oppositely charged species on the substrates by using the electrostatic layer-by-layer self-assembly technique, membranes designed layer-by-layer are expected to contribute in that sense due to their simplicity, economy, universality, and environmentally friendly properties [15, 119, 120]. In most cases, membranes are in the form of permselective planar films (organosilane, polyurethane, cellulose acetate, etc.) on which an enzyme is directly absorbed or absorbed via a lipid film [43, 121, 122]. In some cases, a closed geometry is preferred, such as polymer microcapsules [123], microtubules [124], or liposomes [125, 126], into which enzymes are entrapped. For example, Gerard *et al.* [28] prepared an enzyme-based biosensor by using PANI film as matrix for immobilization of GOx and lactate dehydrogenase enzymes. Timur *et al.* [16] developed a novel homocysteine biosensor based on a L-homocysteine desulfhydrase enzyme-immobilized eggshell membrane for homocysteine determinaiton. Faure *et al.* [43] also reported generating amperometric biosensors by a new enzyme immobiliza-

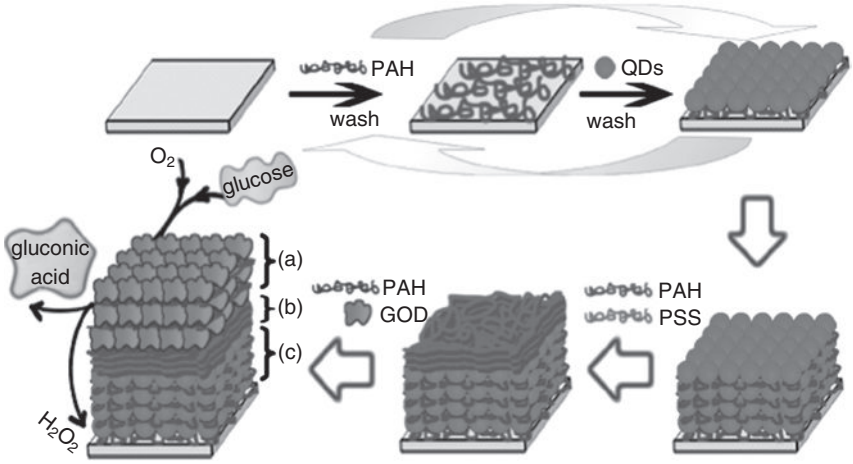


**Figure 5.3** Sensing assembly: (a) top three bilayers of PAH/GOD, (b) three bilayers of PAH/PSS, and (c) 12 bilayers of PAH/CdTe QDs. PAH = poly(allylamine) hydrochloride; GOD = GOx; PSS = poly(sodium 4-styrenesulfonate). Reproduced with permission from [15].)

tion process and investigated the analytical properties of polypyrrole biosensors made with free or encapsulated GOx. Recently, Tang *et al.* [15] fabricated a blood glucose sensor based on multilayer films of CdTe semiconductor quantum dots (QDs) and GOx by using the layer-by-layer assembly technique, as shown in Figure 5.3.

Biosensors based on lipid films have recently shown rapid developments in the design, analytical applications, and stabilization of such biosensors. This type of biosensor provides a generic method for the transduction of selective binding events into an analytical signal, and possesses advantages such as high sensitivity and fast response times. Additionally, lipid films are also excellent materials as host matrices for the maintenance of the activity and sensitivity of many biochemically selective species, such as enzymes, antibodies, and molecular receptors, as introduced by Drivelos *et al.* [127], Psaroudakis *et al.* [128], and Nikolelis *et al.* [129].

It should also be point out that it is hard for loaded biochemically active sensors to retain their native stability and activity, although a number of techniques (e.g., adsorption, covalent, entrapment, cross-linking) and supports (e.g., CNTs, nanoparticles, polymer membranes) have been widely used for the immobilization of enzymes. Therefore, there is still a demand and challenge for new immobilization methods and matrices to achieve improved enzymatic activity and stability. Apart from the previously mentioned matrices, other biosensor supports, such as nanostructured TNTs [10, 11], nanoporous particles [13, 130, 131], and metal-based materials [53, 132, 133] , have been extensively used as carriers for enzyme immobilization.

## 5.3 Application of Enzyme-Based Biosensors

### 5.3.1 Environmental Monitoring

Many toxic compounds such as organic pesticides, heavy metals, and other pollutants can be found in a wide range of environments, and result in problems with human health such as cancer, endocrine-disrupting activities, acute congestion, and degenerative changes in the nervous systems, as well as environmental problems [134]. Therefore, it is necessary to develop biosensor technologies for continuous monitoring in environmental and healthcare applications because it can provide on-site, real-time detection and quantification of beneficial and toxic compounds, such as at the laboratory bench, the field, or in containment facilities [135–138]. In general, such devices are made up of a biological sensing element connected to a transducer that converts the specific biorecognition event to an electrical signal [137]. Significant progress has been made in developing methods for the highly sensitive and selective determination of toxic compounds [136, 138]. Although these techniques have achieved great contributions toward environmental determination, each of such approaches presents some disadvantage that may limit its practical use, such as the poor stability and sensitivity of some biosensors. Therefore, several typical widely used toxic pollutants have been selected as examples to describe and discuss the process of fabricating enzyme-based biosensors for environmental monitoring.

#### 5.3.1.1 Phenolic Derivatives

Phenol is one of the most important and extensively used industrial chemicals. It is widely used in drugs, plastics, dyes, disinfectants, antioxidants, paper pulp, and pesticides, and directly released into the environment as waste [24, 59, 139]. Many reports have demonstrated the existence of phenols as pollutants of air, water, and soil. In nature, they are a class of polluting chemicals, and easily adsorbed by animals, microorganisms, and other living organisms including humans through the skin and mucous membranes [24]. In most cases, high amounts of phenols have been shown to have detrimental effects on animal health. Prolonged oral or subcutaneous exposure causes ecologically undesirable effects on the lungs, liver, kidney, and genitourinary tract in humans [59]. As a result, it is very important to monitor and control phenolic compounds due to their toxicity and persistency in the environment.

There is a fast-increasing and urgent demand for high-performance devices to monitor phenols in complex environments, foods, pharmaceuticals, and industrial matrices. The conventional strategies for phenol determination are chromatography and spectrometric analysis [140, 141]. These techniques, however, do not easily allow continuous on-site monitoring, and are expensive, time-consuming, need skilled operators, and sometimes suffer from complicated sample pretreatment steps [59, 142]. Thus, numerous endeavours have been made for the simple and

effective determination of phenolic compounds. The construction, application, and marketing of biosensors are promising due to many generally established advantages such as high selectivity and sensitivity, low cost of realization, sometimes good storage stability, potential for miniaturization and easy automation, and design of simple portable devices for fast screening purposes and in-field/on-site monitoring [142]. Over the last decade, biosensors for environmental phenol determination and control have become more prevalent in the literature [8, 143], as reported in a variety of publications, including carbon-paste biosensors [144], graphite composite electrodes [96], conducting polymer-modified electrodes [145], and silica sol–gel composite films [146], pH-sensitive field-effect transistors [142], and rigid conducting CNT/polymer-based composites [8]. Among biosensors, those based on the enzyme polyphenol oxidase (PPO) are very promising tools for detecting and controlling phenolic compounds, and until now the most sensitive phenolic biosensor has been fabricated via entrapment of PPO within attractive material, as reported by Shan *et al.* [136], Mousty *et al.* [147], and Han *et al.* [24]. In nature, PPO is a metalloenzyme that is made up of a binuclear copper active site and catalyzes, in the presence of dioxygen, the hydroxylation of monophenols to catechols (monooxygenase activity), which in turn are oxidized to *o*-quinone (catecholase activity) [24, 148]. The phenol biosensor transduction is therefore based on the amperometric detection of the enzymatically produced corresponding *o*-quinone [8, 149], in which the generated quinine species can be further electrochemically reduced to phenolic substances at low potential in the absence of mediators [8]. Electrochemical reduction of quinines, however, is incomplete since quinones are highly unstable in water and thus they easily polymerize to polyaromatic compounds [150]. More importantly, low operational stability, especially for detecting *o*-diphenols [151, 152], is also a main challenge due to the fact that the enzyme is lost in the surrounding environment (especially when physical methods are used for enzyme immobilization) or due to its inactivation by the radical species that appear during the biocatalytic oxidation [153]. As a result, there is an urgent need to optimize established approaches and develop new strategies to detect phenol derivatives with high selectivity and sensitivity.

#### 5.3.1.2 **Pesticides**

Many tons of pesticides, such as organophosphorus pesticides, atrazine, and carbamate, are used annually in agriculture and horticulture due to their pesticidal activity and low persistence in the environment [154, 155]. Although most such pesticides can be effectively degraded and removed by microbial degradation and photodegradation, as well as chemical hydrolysis, the presence of minute quantities of pesticides is a very considerable health hazard that produces serious symptoms, and eventually may lead to death because they interfere in the neuron pulse transmissions of numerous living organisms and may induce delayed neuropathy caused by inhibiting esterase enzymes due to their structurally similarity to the nerve gases soman and sarin [154, 156–158]. In addition, intermediate products generated by these degradation processes may exhibit more toxicity than the corresponding initial products, and may contaminate air, water, and soil over large

areas [155]. As a result, there is an urgent demand to develop rapid, selective, and sensitive tools for toxicity assessment and monitoring of environmental samples. Currently, a huge array of analytical methods for toxic agent detection are widely used, including spectrophotometry, chromatography, mass spectrometry, and various hyphenated techniques; however, their complex laboratory-based instrumentation techniques, the need for highly trained operators, and their time-consuming nature make such strategies unsuitable for field application [25, 60, 154–156]. Moreover, these instruments are rather expensive and hard to deploy *in situ* in the environment. Obviously, searching for sensitive, selective, simple, and rapid tools is an urgent requirement. Therefore, a number of enzyme-based biosensors have emerged in the past decades with rapid, high selectivity for on-site measurements of pesticides. These biosensors were quickly developed and extensively introduced for detecting a wide range of compounds in the environment, such as organophosphorous pesticides [60], organochlorine pesticides, and derivatives of carbamic acid insecticides [159], because such techniques in pesticide analysis require minimal sample pretreatment and can provide solutions for the above challenges [154, 156, 160, 161]. In addition, the biosensor usually is combined with a variety of transducers, such as amperometric [60, 160–162], potentiometric or conductometric electrodes [163, 164], and optical or mass-sensitive devices [154, 157, 165–167]. Among them, the electrochemical amperometric transducer came to be the principal choice due to its high sensitivity and has received great attention [60, 168]. Although biosensor systems based on enzyme inhibition through a quantitative measurement of the enzyme activity of an immobilized enzyme before and after exposure to a target analyte are very sensitive and have been extensively used in environmental monitoring, the enzyme–analyte system is carefully selected such that the analyte often may result in the inhibition of normal enzyme function [169]. In addition, inhibition biosensors often present some major limitations like tedious incubation procedures and multiple reaction steps, the permanent nature of the enzyme inhibition leading to irrecoverable after-to-use activity, and poor selectivity [25, 156, 169]. These drawbacks can be effectively overcome in catalytic-mode biosensors based on the organophosphorus hydrolase enzyme for organophosphorus pesticides, as shown by Rainina *et al.* [170], Chen-Goodspeed *et al.* [171], Mulchandani *et al.* [156], and Grimsley *et al.* [172].

Apart from the toxic compounds mentioned above, enzyme-based biosensors are also extensively used to monitor other some important pollutants, including nitroaromatic compounds [173, 174], heavy metals [31], and typical infectious agents [42, 134], and have achieved considerable success. However, poor stability of the biosensor and short lifetime, mainly caused by electrode fouling and enzyme inactivation and desorption from immobilization supports, are both very important limitations because such challenges will not only impede biosensor transport, but also increase per-measurement cost. As a result, it is envisioned that future research will, to a large extent, continue to be focused on optimizing existing approaches, developing new procedures to further improve the selectivity of detection, sensitivity response, and long-term stability of enzyme-based biosensors for simple and effective quantitative environmental estimation.

### 5.3.2 Medical Diagnostics

Many new diagnostic methods have been developed and reported for measuring biomolecules and their abundance with high sensitivity and high throughput [3, 175], enabling early disease detection and providing valuable insights into biology [176, 177]. Evidently, such technology platforms can effectively provide reliable, rapid, quantitative, low-cost, and multichannel identification of biomarkers [3, 177]. For example, early detection is very important for cancer and other pathologies because the early stages of disease are typically treated with the greatest probability of success [3]. Many of the conventional devices and techniques, including nuclear magnetic resonance [178], surface plasmon resonance [179] and mass spectrometry [180], however, requiring time-consuming purification of samples, may lack the ability for multiplexed measurements that are desirable in identifying complex diseases, or may be uncontrollable for easy point-of-care translation [3, 175]. In contrast, biosensors enable direct, sensitive, selective, and rapid analysis of biological and chemical species, and thus are widely used in many areas of healthcare and life sciences, ranging from uncovering and diagnosing disease to the discovery and screening of new drugs and biomolecules [20, 181, 182]. For example, in brain monitoring, L-glutamate is the most widespread excitatory neurotransmitter in the mammalian central nervous system, plays a important role in a broad range of brain functions, and has been implicated in a number of neurological disorders [33, 183]. Systems for monitoring glutamate in brain extracellular fluid (ECF) have been an area of intense interest in the analytical and neurobiological sciences in recent years. Therefore, the fabrication and development of devices for glutamate detection on-line has become a very vibrant research area due to the advantages of monitoring this amino acid in a number of complex matrixes, including food processing, cell cultures, tissue slices *ex vivo*, and intact brain *in vivo* [33, 184, 185]. In general, there have been two main methods for the detection and quantification of brain ECF glutamate concentrations: those using microdialysis perfusion followed by *ex situ* analysis [186] and those involving direct detection of glutamate in the ECF by using implanted amperometric biosensors [187, 188]. Such devices are more commonly based on the stereospecific oxidative deamination of glutamate, catalyzed by glutamate oxidase [33], in which signal transduction systems used in glutamate biosensors include optical technologies [189], and electrochemical oxidation of enzymatically produced $H_2O_2$ [190]. Clearly, the high spatial and temporal resolutions provided by electrochemical sensors are particularly appealing for investigations of the neurochemical correlates of behavior; the general process can be demonstrated in Figure 5.4 [187].

The reader interested in obtaining further information is referred to a detailed review of the relative advantages and disadvantages of two such approaches [191]. To date, a range of biosensor designs, based mainly on glutamate oxidase, have been introduced and described for direct monitoring of glutamate in brain ECF [32, 33]. The task of monitoring brain ECF glutamate, however, is significantly more challenging than glucose detection, mainly because the baseline ECF

$$\text{1-Glutamate} + H_2O + \text{GluOx/FAD} \rightarrow \alpha\text{-ketoglutarate} + NH_3 + \text{GluOx/FADH}_2$$

$$\text{GluOx/FADH}_2 + O_2 \rightarrow \text{GluOx/FAD} + H_2O_2$$

$$H_2O_2 \rightarrow O_2 + 2H^+ + 2e$$

**Figure 5.4** Basic skeleton of glutamate used by electrochemical oxidation. (Reproduced with permission from [33]).

concentration of glutamate appears to be 5 μM or below, although low values as high as 15 μM have also been suggested [192], compared to around 500 μM for ECF glucose [32, 193]. As a result, optimization of glutamate sensitivity is critical for physiological applications. In addition, although considerable efforts have been made for minimizing contamination of biosensor signals by endogenous electroactive species present in brain ECF [187], the challenge of interference by fluctuating levels of the cosubstate of the most commonly used enzyme in glutamate biosensors and other interferences (i.e., oxygen), glutamate oxidase, has not been investigated and addressed in detail. Another typical example is diabetes. It is well known that diabetes is among the most prevalent and costly diseases in the world, and its associated complications often result in disability and even death [194]. Therefore, diabetes control and complications require continuous monitoring of blood glucose levels. An easy-to-use, inexpensive, and reliable method is to fabricate and develop an implantable glucose sensor, based on coupling of GOx with an electrochemical system [22, 194, 195], in which quantitative analysis can be obtained by detecting the consumption of oxygen or the production of $H_2O_2$. As with monitoring brain ECF glutamate, such detection methods usually suffer a limitation because a number of potentially interfering factors (such as ascorbic acid, catechol, uric acid, and acetaminophen) are electroactive at the applied potential required for peroxide oxidation [194]. Therefore, improvement in selectivity and sensitivity during blood glucose measurement is a very promising prospect for designing glucose-based biosensors. Other examples, including those for Alzheimer's [196], cystic fibrosis [197], and other neurological and psychiatric disorders [25, 198, 199], have also been reported and developed for clinical analysis.

Enzyme-based diagnostic methods are preferred over other conventional strategies because of their selectivity, sensitivity, and greater accuracy. Although the immobilization of enzyme onto an insoluble support can effectively overcome challenges generated by the use of free enzymes, such as high cost and limited stability, the issue of biocompatibility should also be considered in constructing such enzyme-based biosensors, because the biological recognition molecules used in the biosensors, such as immobilized enzymes, antibodies, and DNAs, may lose their biological activities in biologically incompatible environments [10]. In addition, the nature of the support and the immobilization procedures considerably affect the behavior of enzyme-based biosensors (stability, sensitivity, and lifetime) because the biotransformation equilibrium of the substrate occurs at the support–solution interface [200]. As a result, attention should be paid to developing such

biocompatibility supports and to optimizing immobilization approaches in further works.

## 5.4 Conclusions

Although enzyme-based biosensors have been a fast increasing research field over the past several decades due to their potential application in analytical chemistry and biological sciences, such biosensors in many cases will be inevitable suffer some challenges mainly imposed by the nature of the enzyme, support, immobilization procedures, and so on. This chapter has summarized the synthesis and application of enzyme-based biosensors. As evidenced by the described and discussed literature, a basic understanding of the development of support and immobilization procedures has enabled the fabrication and preparation of various enzyme-based biosensors with high selectivity, sensitivity, and stability. However, the nature of the support immobilization steps should be understood and considered, to make full use of these strategies for the fabrication and application of such biosensors. This understanding will drive the processes to continue to evolve and provide more facile immobilization approaches. Accordingly, it is expected to find facile, new, and exciting immobilization methods and biocompatible supports for the fabrication and application of such enzyme-based biosensors.

## Acknowledgments

This paper was supported by the Advanced Professional Faculty Foundation of Jiangsu University (06jdg054). Clearly, the success of this work has largely depended on the creativity and devotion of many researchers whose names are listed in the references.

## References

1 Yu, T., Zhang, Y., You, C., Zhuang, J., Wang, B., Liu, B., Kang, Y., and Tang, Y. (2006) *Chem. Eur. J.*, **12**, 1137–1143.
2 Nam, J.M., Thaxton, C.S., and Mirkin, C.A. (2003) *Science*, **301**, 1884–1886.
3 Cheng, M.M., Cuda, G., Bunimovich, Y.L., Gaspari, M., Heath, J.R., Hill, H.D., Mirkin, C.A., Nijdam, A.J., Terracciano, R., Thundat, T., and Ferrari, M. (2006) *Curr. Opin. Chem. Biol.*, **10**, 11–19.
4 Shan, D., Zhu, M., Xue, H., and Cosnier, S. (2007) *Biosens. Bioelectron.*, **22**, 1612–1617.
5 Cosnier, S., Mousty, C., de Melo, J., Lepellec, A., Novoa, A., Polyak, B., and Marks, R.S. (2004) *Electroanalysis*, **16**, 2022–2029.
6 Reeves, T.E., Paliwal, S., Wales, M.E., Wild, J.R., and Simonian, A.L. (2009) *Langmuir*, **25**, 9615–9618.
7 Willner, I. and Katz, E. (2000) *Angew. Chem. Int. Ed.*, **112**, 1230–1269.

**8** Lopez, B.P. and Merkoci, A. (2009) *Analyst*, **134**, 60–64.
**9** Zou, Y., Xiang, C., Sun, L., and Xu, F. (2008) *Biosens. Bioelectron.*, **23**, 1010–1016.
**10** Dai, H., Chi, Y., Wu, X., Wang, Y., Wei, M., and Chen, G. (2010) *Biosens. Bioelectron.*, **25**, 1414–1419.
**11** Zhang, Y., Xiao, P., Zhou, X., Liu, D., Garcia, B.B., and Cao, G. (2009) *J. Mater. Chem.*, **19**, 948–953.
**12** Wong, L.S., Okrasa, K. and Micklefield, J. (2010) *Org. Biomol. Chem.*, **8**, 782–787.
**13** Vamvakaki, V. and Chaniotakis, N.A. (2007) *Biosens. Bioelectron.*, **22**, 2650–2655.
**14** Piao, Y., Lee, D., Kim, J., Kim, J., Hyeon, T., and Kim, H. (2009) *Analyst*, **134**, 926–932.
**15** Li, X., Zhou, Y., Zheng, Z., Yue, X., Dai, Z., Liu, S., and Tang, Z. (2009) *Langmuir*, **25**, 6580–6586.
**16** Alacam, S., Timur, S., and Telefoncu, A. (2007) *J. Mol. Catal. B*, **49**, 55–60.
**17** Xu, F., Zhen, G., Yu, F., Kuennemann, E., Textor, M., and Knoll, W. (2005) *J. Am. Chem. Soc.*, **127**, 13084–13085.
**18** Li, J., Wang, J., and Bachas, L.G. (2002) *Anal. Chem.*, **74**, 3336–3341.
**19** Vial, L. and Dumy, P. (2009) *New J. Chem.*, **33**, 939–946.
**20** Alaejos, M.S. and García Montelongo, F.J. (2004) *Chem. Rev.*, **104**, 3239–3265.
**21** Clark, L.C. and Lyons, C. (1962) *Ann. NY Acad. Sci.*, **102**, 29–45.
**22** Wilson, G.S. and Hu, Y. (2000) *Chem. Rev.*, **100**, 2693–2704.
**23** Jones, J.T., Myers, J.W., Ferrell, J.E., and Meyer, T. (2004) *Nat. Biotechnol.*, **22**, 306–312.
**24** Han, E., Shan, D., Xue, H., and Cosnier, S. (2007) *Biomacromolecules*, **8**, 971–975.
**25** Ramanathan, M. and Simonian, A.L. (2007) *Biosens. Bioelectron.*, **22**, 3001–3007.
**26** Yeung, T., Gilbert, G.E., Shi, J., Silvius, J., Kapus, A., and Grinstein, S. (2008) *Science*, **319**, 210–213.
**27** Munge, B.S., Dowd, R.S., Krause, C.E., and Millord, L.N. (2009) *Electroanalysis*, **21**, 2241–2248.
**28** Gerard, M. and Malhotra, B.D. (2005) *Curr. Appl. Phys.*, **5**, 174–177.
**29** Zayats, M., Willner, B., and Willner, I. (2008) *Electroanalysis*, **20**, 583–601.
**30** Pereira, C.M., Oliveira, J.M., Silva, R.M., and Silva, F. (2004) *Anal. Chem.*, **76**, 5547–5555.
**31** Michel, C., Ouerd, A., Battaglia-Brunet, F., Guigues, N., Grasa, J., Bruschi, M., and Ignatiadis, I. (2006) *Biosens. Bioelectron.*, **22**, 285–290.
**32** McMahon, C.P., Rocchitta, G., Kirwan, S.M., Killoran, S.J., Serra, P.A., Lowry, J.P., and O'Neill, R.D. (2007) *Biosens. Bioelectron.*, **22**, 1466–1473.
**33** McMahon, C.P., Rocchitta, G., Serra, P.A., Kirwan, S.M., Lowry, J.P., and O'Neill, R.D. (2006) *Anal. Chem.*, **78**, 2352–2359.
**34** Blanes, L., Mora, M.F., do Lago, C.L., Ayon, A., and Garca, C.D. (2007) *Electroanalysis*, **19**, 2451–2456.
**35** Alexander, P.W. and Rechnitz, G.A. (2000) *Electroanalysis*, **12**, 343–350.
**36** Collings, A.F. and Caruso, F. (1997) *Rep. Prog. Phys.*, **60**, 1397–1445.
**37** Chaniotakis, N.A. (2004) *Anal. Bioanal. Chem.*, **378**, 89–95.
**38** Mudhivarthi, V.K., Bhambhani, A., and Kumar, C.V. (2007) *Dalton. Trans.*, 5483–5497.
**39** Armstrong, F.A. (2005) *Curr. Opin. Chem. Biol.*, **9**, 110–117.
**40** Lyons, M.E.G. and Keeley, G.P. (2008) *Chem. Commun.*, 2529–2531.
**41** Willner, I. and Katz, E. (2000) *Angew. Chem. Int. Ed.*, **39**, 1180–1218.
**42** Achmann, S., Hämmerle, M., and Moos, R. (2008) *Electroanalysis*, **20**, 410–417.
**43** Olea, D., Viratelle, O., and Faure, C. (2008) *Biosens. Bioelectron.*, **23**, 788–794.
**44** Girelli, A.M. and Mattei, E. (2005) *J. Chromatogr. B*, **819**, 3–16.
**45** Li, B., Lan, D., and Zhang, Z. (2008) *Anal. Biochem.*, **374**, 64–70.
**46** Alivisatos, S.G.A., Ungar, F., and Abraham, G. (1964) *Nature*, **203**, 973–975.
**47** Gorton, L. and Dominguez, E. (2002) *Encyclopedia of Electrochemistry*, vol. 9 (eds A.J. Bard, M. Stratmann, and G.S. Wilson), Wiley-VCH Verlag GmbH, Weinheim, pp. 67–143.

**48** Potyrailo, R.A. (2006) *Angew. Chem. Int. Ed.*, **45**, 702.

**49** Zheng, H., Xue, H.G., Zhang, Y.F., and Shen, Z.Q. (2002) *Biosens. Bioelectron.*, **17**, 541–545.

**50** Chen, S., Yuan, R., Chai, Y., and Li, N. (2008) *Electroanalysis*, **20**, 418–425.

**51** Fu, Y., Zou, C., Xie, Q., Xu, X., Chen, C., Deng, W., and Yao, S. (2009) *J. Phys. Chem. B*, **113**, 1332–1340.

**52** Cosnier, S., Mousty, C., Gondran, C., and Lepellec, A. (2006) *Mater. Sci. Eng. C*, **26**, 442–447.

**53** Lin, J., Zhang, L., and Zhang, S. (2007) *Anal. Biochem.*, **370**, 180–185.

**54** Rubio-Retama, J., López-Cabarcos, E., and López-Ruiz, B. (2005) *Talanta*, **68**, 99–107.

**55** Lee, J., Na, H.B., Kim, B.C., Lee, J.H., Lee, B., Kwak, J.H., Hwang, Y., Park, J., Gu, M.B., Kim, J., Joo, J., Shin, C., Grate, J.W., Hyeon, T., and Kim, J. (2009) *J. Mater. Chem.*, **19**, 7864–7870.

**56** Xiao, Y., Ju, H.X., and Chen, H.Y. (2000) *Anal. Biochem.*, **278**, 22–28.

**57** Zhang, M.G. and Gorski, W. (2005) *J. Am. Chem. Soc.*, **127**, 2058–2059.

**58** Zhang, M.G. and Gorski, W. (2005) *Anal. Chem.*, **77**, 3960–3965.

**59** Kaneto, R.K. (2005) *Curr. Appl. Phys.*, **5**, 178–183.

**60** Hao, W.Z., Uge, P.Y., Xu, J.J., and Chen, H.Y. (2009) *Environ. Sci. Technol.*, **43**, 6724–6729.

**61** Zhao, W., Sun, S.X., Xu, J.J., Chen, H.Y., Cao, X.J., and Guan, X.H. (2008) *Anal. Chem.*, **80**, 3769–3776.

**62** Muguruma, H., Shibayama, Y., and Matsui, Y. (2008) *Biosens. Bioelectron.*, **23**, 827–832.

**63** Wang, J. (2005) *Electroanalysis*, **17**, 7–14.

**64** Nguyen, C.V., So, C., Stevens, R.M., Li, Y., Delziet, L., Sarrazin, P., and Meyyappan, M. (2004) *J. Phys. Chem. B*, **108**, 2816–2821.

**65** Journet, C., Maser, W.K., Bernier, P., Loiseau, A., Lamy de la Chapells, M., Lefrant, S., Deniard, P., Lee, R., and Fischer, J.E. (1997) *Nature*, **388**, 756–758.

**66** Thess, A., Lee, R., Nikolaev, P., Dai, H., Petit, P., Robert, J., Xu, C., Lee, Y.H., Kim, S.G., Rinzler, A.G., Colbert, D.T., Scuseria, G.E., Tomanek, D., Fischer, J.E., and Smalley, R.E. (1996) *Science*, **273**, 483–487.

**67** Iijima, S. (1991) *Nature*, **354**, 56–58.

**68** Ajayan, P.M. (1999) *Chem. Rev.*, **99**, 1787–1799.

**69** Boo, H., Jeong, R., Park, S., Kim, K.S., An, K.H., Lee, Y.H., Han, J.H., Kim, H.C., and Chung, T.D. (2006) *Anal. Chem.*, **78**, 617–620.

**70** Davis, J.J., Coleman, K.S., Azamian, B.R., Bagshaw, C.B., and Green, M.L.H. (2003) *Chem. Eur. J.*, **9**, 3732–3739.

**71** Collins, P.G., Bradley, K., Ishigami, M., and Zettl, A. (2000) *Science*, **287**, 1801–1804.

**72** Ito, T., Sun, L., Henriquez, R.R., and Crooks, R.M. (2004) *Acc. Chem. Res.*, **37**, 937–945.

**73** Campbell, J.K., Sun, L., and Crooks, R.M. (1999) *J. Am. Chem. Soc.*, **121**, 3779–3780.

**74** Tasis, D., Tagmatarchis, N., Bianco, A., and Prato, M. (2006) *Chem. Rev.*, **106**, 1105–1136.

**75** Sánchez, S., Pumera, M., Cabrujac, E., and Fábregas, E. (2007) *Analyst*, **132**, 142–147.

**76** Azamian, B.R., Davis, J.J., Colemann, K.S., Bagshaw, C.B., and Green, M.L.H. (2002) *J. Am. Chem. Soc.*, **124**, 12664–12665.

**77** Gooding, J.J., Wibowo, R., Liu, J., Yang, W., Losic, D., Orbons, S., Mearns, F.J., Shapter, J.G., and Hibbert, D.B. (2003) *J. Am. Chem. Soc.*, **125**, 9006–9007.

**78** Li, J., Wang, Y.B., Qiu, J.D., Sun, D.C., and Xia, X.H. (2005) *Anal. Bioanal. Chem.*, **383**, 918–922.

**79** Liu, J., Chou, A., Rahmat, W., Paddon-Row, M.N., and Gooding, J.J. (2005) *Electroanalysis*, **17**, 38–46.

**80** Lee, C.H., Wang, S.C., Yuan, C.J., Wen, M.F., and Chang, K.S. (2007) *Biosens. Bioelectron.*, **22**, 877–884.

**81** Wang, J. and Musameh, M. (2003) *Anal. Chem.*, **75**, 2075–2079.

**82** Kandimalla, V.B., Tripathi, V.S., and Ju, H. (2006) *Biomaterials*, **27**, 1167–1174.

**83** Rege, K., Raravikar, N.R., Kim, D.Y., Schadler, L.S., Ajayan, P.M., and Dordick, J.S. (2003) *Nano Lett.*, **3**, 829–832.

**84** Wang, Y., Joshi, P.P., Hobbs, K.L., Johnson, M.B., and Schmidtke, D.W. (2006) *Langmuir*, **22**, 9776–9783.

**85** Zhao, H. and Ju, H. (2006) *Anal. Biochem.*, **350**, 138–144.

**86** Rivas, G.A., Miscoria, S.A., Desbrieres, J., and Barrera, G.D. (2007) *Talanta*, **71**, 270–275.

**87** Tsai, Y.C., Li, S.C., and Liao, S.W. (2006) *Biosens. Bioelectron.*, **22**, 495–500.

**88** Muguruma, H., Hiratsuka, A., and Karube, I. (2000) *Anal. Chem.*, **72**, 2671–2675.

**89** Muguruma, H., Kase, Y., and Uehara, H. (2005) *Anal. Chem.*, **77**, 6557–6562.

**90** Muguruma, H. and Kase, Y. (2006) *Biosens. Bioelectron.*, **22**, 737–743.

**91** Muguruma, H., Kase, Y., Murata, N., and Matsumura, K. (2006) *J. Phys. Chem. B*, **110**, 26033–26039.

**92** Munge, B., Liu, G., Collin, G., and Wang, J. (2005) *Anal. Chem.*, **77**, 4662–4666.

**93** Liu, G. and Lin, Y. (2006) *Electrochem. Commun.*, **8**, 251–256.

**94** Merkoc, A. (2006) *Microchim. Acta*, **152**, 157–174.

**95** Pérez, B., Sola, J., Alegret, S., and Merkoçi, A. (2008) *Electroanalysis*, **20**, 603–610.

**96** Pérez, B., Pumera, M., Del Valle, M., Merkoçi, A., and Alegret, S. (2005) *J. Nanosci. Nanotechnol.*, **5**, 1694–1698.

**97** Cao, S. and Liu, B. (2009) *Macromol. Biosci.*, **9**, 361–368.

**98** Fessner, W.D. (1999) *Top. Curr. Chem.*, **200**, 266–267.

**99** Torchilin, V.P. (1991) *Progress in Clinical Biochemistry and Medicine: Immobilized Enzymes in Medicine*, vol. 11, Springer-Verlag, Berlin, p. 206.

**100** Herdt, A.R., Kim, B.S., and Taton, T.A. (2007) *Bioconjugate. Chem.*, **18**, 183–189.

**101** Scarberry, K.E., Dickerson, E.B., McDonald, J.F., and Zhang, Z.J. (2008) *J. Am. Chem. Soc.*, **130**, 10258–10262.

**102** Gerard, M., Chaubey, A., and Malhotra, B.D. (2002) *Biosens. Bioelectron.*, **17**, 345–359.

**103** Malhotra, B.D. and Chaubey, A. (2003) *Sens. Actuators B*, **91**, 117–127.

**104** Michira, I., Akinyeye, R., Somerset, V., Klink, M.J., Sekota, M., Al-Ahmed, A., Baker, P.G.L., and Iwuoha, E. (2007) *Macromol. Symp.*, **255**, 57–69.

**105** Morrin, A., Ngamna, O., Kill, A.J., Moulton, S.E., Smyth, M.R., and Wallace, G.G. (2005) *Electroanalysis*, **17**, 423–430.

**106** Gök, A., Sari, B., and Talu, M. (2004) *Synth. Met.*, **142**, 41–48.

**107** Han, M.G., Cho, S.K., Oh, S.G., and Im, S.S. (2002) *Synth. Met.*, **126**, 53–60.

**108** Zheng, W.Y., Levon, K., Laasko, J., and Osterholm, J.E. (1994) *Macromolecules*, **27**, 7754–7768.

**109** Malinauskas, A. (2001) *Polymer*, **42**, 3957–3972.

**110** Zhang, Z. and Wan, M. (2002) *Synth. Met.*, **128**, 83–89.

**111** Zhang, L. and Wan, M. (2002) *Nanotechnology*, **13**, 750–755.

**112** Morrin, A., Wilbeer, F., Ngamna, O., Moulton, S.E., Killard, A.J., Wallace, G.G., and Smyth, M.R. (2005) *Electrochem. Commun.*, **7**, 317–322.

**113** Kathleen, G., Killard, A.J., Hanson, C.J., Cafolla, A.A., and Smyth, M.R. (2006) *Talanta*, **68**, 1591–1600.

**114** Peng, L.F., Liu, X.X., and Yang, G.Y. (2001) *Chin. Surf. Deter. Cosmet.*, **5**, 13–16.

**115** Petrov, A.I., Volodkin, D.V., and Sukhorukov, G.B. (2005) *Biotechnol. Prog.*, **21**, 918–925.

**116** Wong, L.S., Thirlway, J., and Micklefield, J. (2008) *J. Am. Chem. Soc.*, **130**, 12456–12464.

**117** Gella, F.J., Serra, J., and Gener, J. (1991) *Pure. Appl. Chem.*, **63**, 1131–1134.

**118** Decher, G. (1997) *Science*, **277**, 1232–1237.

**119** Yu, A., Liang, Z., and Caruso, F. (2005) *Chem. Mater.*, **17**, 171–175.

**120** Podsiadlo, P., Kaushik, A.K., Arruda, E.M., Waas, A.M., Shim, B.S., Xu, J., Nandivada, H., Pumplin, B.G., Lahann, J., Ramamoorthy, A., and Kotov, N.A. (2007) *Science*, **318**, 80–83.

**121** Ohashi, E., Tamiya, E., and Karuke, I. (1990) *J. Membr. Sci.*, **49**, 95–102.

**122** Maines, A., Ashworth, D., and Vadgama, P. (1996) *Anal. Chim. Acta*, **333**, 223–231.

**123** Blandino, A., Macias, M., and Cantero, D. (2001) *Process Biochem.*, **36**, 601–606.

**124** Parthasarathy, R.V. and Martin, C.R. (1996) *J. Appl. Polym. Sci.*, **62**, 875–885.

**125** Yoshimoto, M.S., Fukunaga, W., Fournier, K., Walde, D., Kuboi, P., and Nakao, P.K. (2005) *Biotechnol. Bioeng.*, **90**, 231–238.

**126** Wang, S., Yoshimoto, M., Fukunaga, K., and Nakao, K. (2003) *Biotechnol. Bioeng.*, **83**, 444–453.

**127** Nikolelis, D.P., Drivelos, D.A., Simantiraki, M.G., and Koinis, S. (2004) *Anal. Chem.*, **76**, 2174–2180.

**128** Nikolelis, D.P., Psaroudakis, N., and Ferderigos, N. (2005) *Anal. Chem.*, **77**, 3217–3221.

**129** Nikolelis, D.P., Raftopoulou, G., Nikoleli, G., and Simantiraki, M. (2006) *Electroanalysis*, **18**, 2467–2474.

**130** Sotiropoulou, S., Vamvakaki, V., and Chaniotakis, N.A. (2005) *Biosens. Bioelectron.*, **20**, 1674–1679.

**131** Lee, D., Lee, J., Kim, J., Kim, J., Na, H.B., Kim, B., Shin, C., Kwak, J.H., Dohnalkova, A., Grate, J.W., Hyeon, T., and Kim, H. (2005) *Adv. Mater.*, **17**, 2828–2833.

**132** Jena, B.K. and Raj, C.R. (2006) *Anal. Chem.*, **78**, 6332–6339.

**133** Scodeller, P., Flexer, V., Szamocki, R., Calvo, E.J., Tognalli, N., Troiani, H., and Fainstein, A. (2008) *J. Am. Chem. Soc.*, **130**, 12690–12697.

**134** Kim, G., Shim, J., Kang, M., and Moon, S. (2008) *J. Environ. Monit.*, **10**, 632–637.

**135** Lee, W.E., Thompson, H.G., Hall, J.G., and Bader, D.E. (2000) *Biosens. Bioelectron.*, **14**, 795–804.

**136** Liu, J. and Lu, Y. (2003) *J. Am. Chem. Soc.*, **125**, 6642–6643.

**137** Shan, D., Cosnier, S., and Mousty, C. (2003) *Anal. Chem.*, **75**, 3872–3879.

**138** Kong, R., Zhang, X., Zhang, L., Jin, X., Huan, S., Shen, G., and Yu, R. (2009) *Chem. Commun.*, 5633–5635.

**139** Canofeni, S., Sario, S.D., Mela, J., and Pilloton, R. (1994) *Anal. Lett.*, **27**, 1659–1662.

**140** Poerschmann, J., Zhang, Z., Kopink, F.D., and Pawliszyn, E.T. (1997) *Anal. Chem.*, **69**, 597–600.

**141** Marko-Varga, G. (1993) *Environmental Analysis: Techniques, Applications and Quality Assurance* (ed. D. Barselo), Elsevier, Amsterdam, pp. 225–2271.

**142** Dzyadevych, S.V., Mai Anh, T., Soldatkin, A.P., Duc Chien, N., Jaffrezic-Renault, N., and Chovelon, J.-M. (2002) *Bioelectrochemistry*, **55**, 79– 81.

**143** Rogers, K.R. (1995) *Biosens. Bioelectron.*, **10**, 533–541.

**144** Merkoçi, A., Pumera, M., Llopis, X., Perez, B., Del Valle, M., and Alegret, S. (2005) *Trends Anal. Chem.*, **24**, 826–838.

**145** Adeyoju, O., Iwuoka, E.J., Smyth, M.R., and Leech, D. (1996) *Analyst*, **121**, 1885–1889.

**146** Li, J., Chia, L.S., Goh, N.K., and Tan, S.N. (1998) *Anal. Chim. Acta*, **362**, 203–211.

**147** Shan, D., Mousty, C., and Cosnier, S. (2004) *Anal. Chim.*, **76**, 178–183.

**148** Duckworth, H.W., and Coleman, J.E. (1970) *J. Biol. Chem.*, **245**, 1613–1625.

**149** Land, E.J., Ramsden, C.A., and Riley, P.A. (2003) *Acc. Chem. Res.*, **36**, 300–308.

**150** Horowitz, N.H., Fling, M., and Horn, G. (1970) *Methods in Enzymology*, Academic Press, New York, p. 120.

**151** Yaropolov, A.I., Kharybin, A.N., Emnéus, J., Marko-Varga, G., and Gorton, L. (1995) *Anal. Chim. Acta*, **308**, 137–144.

**152** Ortega, F., Domínguez, E., Burestedt, E., Emnéus, J., Gorton, L., and Marko-Varga, G. (1994) *J. Chromatogr.*, **A675**, 65–78.

**153** Nistor, C. and Emnéus, J. (1999) *Waste Manag.*, **19**, 147–170.

**154** Vidal, J.C., Bonel, L., and Castillo, J.R. (2008) *Electroanalysis*, **20**, 865–873.

**155** Dzyadevych, S.V., Soldatkin, A.P., Arkhypova, V.N., El'skaya, A.V., Chovelon, J., Georgiou, C.A., Martelet, C., and Jaffrezic-Renault, N. (2005) *Sens. Actuators B*, **105**, 81–87.

**156** Mulchandani, P. and Ashokmulchandani, W. (2001) *Environ. Sci. Technol.*, **35**, 2562–2565.

**157** Zourob, M., Ong, K.G., Zeng, K., Mouffouk, F., and Grimes, C.A. (2007) *Analyst*, **132**, 338–343.

**158** He, F.S. (2000) *Neurotoxicology*, **21**, 829–835.

**159** Cremisini, C., Sario, S.D., Mela, J., Pilloton, R., and Palleschi, G. (1995) *Anal. Chim. Acta*, **311**, 273–280.

**160** Amine, A., Mohammadi, H., Bourais, I., and Palleschi, G. (2006) *Biosens. Bioelectron.*, **21**, 1405–1423.

**161** Andreescu, S. and Marty, J.L. (2006) *Biomol. Eng.*, **23**, 1–15.

**162** Du, D., Huang, X., Cai, J., and Zhang, A.D. (2007) *Sensor. Actuators B*, **127**, 531–535.

**163** Anh, T.M., Dzyadevych, S.V., Prieur, N., Duc, C.N., Pham, T.D., Renault, N.J., and Chovelon, J.M. (2006) *Mater. Sci. Eng. C*, **26**, 453–456.

**164** Dondoi, M.P., Danet, A.F., Bucur, B., and Cheregi, M.C. (2005) *Rev. Chim.*, **56**, 327–330.

**165** Patel, P.D. (2002) *Trends Anal. Chem.*, **21**, 96–115.

**166** Pribyl, J., Hepel, M., Halasmek, J., and Skladal, P. (2003) *Sens. Actuators B*, **91**, 333–341.

**167** Mulchandani, A., Pan, S., and Chen, W. (1999) *Biotechnol. Prog.*, **15**, 130–134.

**168** Sole, S., Merkoci, A., and Alegret, S. (2003) *Crit. Rev. Anal. Chem.*, **33**, 89–96.

**169** Zhang, S., Zhao, H., and John, R. (2001) *Electroanalysis*, **13**, 1528–1534.

**170** Rainina, E.I., Efremenco, E.N., Varfolomeyev, S.D., Simonian, A.L., and Wild, J.R. (1996) *Biosens. Bioelectron.*, **11**, 991–1000.

**171** Chen-Goodspeed, M., Sogorb, M.A., Wu, F., Hong, S.-B., and Raushel, F.M. (2001) *Biochemistry*, **40**, 1325–1331.

**172** Grimsley, J.K., Calamini, B., Wild, J.R., and Mesecar, A.D. (2005) *Arch. Biochem. Biophys.*, **442**, 169–179.

**173** Gwenin, C.D., Kalaji, M., Williams, P.A., and Jones, R.M. (2007) *Biosens. Bioelectron.*, **22**, 2869–2875.

**174** Gwenin, C.D., Kalaji, M., Kay, C.M., Williams, P.A., and Novaes Tito, D. (2008) *Analyst*, **133**, 621–625.

**175** Lee, H., Sun, E., Ham, D., and Weissleder, R. (2008) *Nat. Med.*, **14**, 869–874.

**176** Wulfkuhle, J.D., Liotta, L.A., and Petricoin, E.F. (2003) *Nat. Rev. Cancer*, **3**, 267–275.

**177** Hood, L., Heath, J.R., Phelps, M.E., and Lin, B. (2004) *Science*, **306**, 640–643.

**178** Schroder, L., Lowery, T.J., Hilty, C., Wemmer, D.E., and Pines, A. (2006) *Science*, **314**, 446–449.

**179** Aslan K., Lakowicz J.R., and Geddes, C.D. (2005) *Curr. Opin. Chem. Biol.*, **9**, 538–544.

**180** Aebersold, R. and Mann, M. (2003) *Nature*, **422**, 198–207.

**181** Abu-Rabeah, K., Polyak, B., Ionescu, R.E., Cosnier, S., and Marks, R.S. (2005) *Biomacromolecules*, **6**, 3313–3318.

**182** Cosnier, S. (2003) *Anal. Bioanal. Chem.*, **377**, 507–520.

**183** Belsham, B.H. (2001) *Pharmacol. Clin. Exp.*, **16**, 139–146.

**184** O'Neill, R.D., Chang, S.C., Lowry, J.P., and McNeil, C.J. (2004) *Biosens. Bioelectron.*, **19**, 1521–1528.

**185** Qhobosheane, M., Wu, D.H., Gu, G.R., and Tan, W.H. (2004) *J. Neurosci. Methods*, **135**, 71–78.

**186** Hutchinson, P.J., O'Connell, M.T., Kirkpatrick, P.J., and Pickard, J.D. (2002) *Physiol. Meas.*, **23**, R75–109.

**187** McMahon, C.P. and O'Neill, R.D. (2005) *Anal. Chem.*, **77**, 1196–1199.

**188** Burmeister, J.J., Pomerleau, F., Palmer, M., Day, B.K., Huettl, P., and Gerhardt, G.A. (2002) *J. Neurosci. Methods*, **119**, 163–171.

**189** Marquette, C.A., Degiuli, A., and Blum, L.J. (2003) *Biosens. Bioelectron.*, **19**, 433–439.

**190** Burmeister, J.J. and Gerhardt, G.A. (2001) *Anal. Chem.*, **73**, 1037–1042.

**191** Khan, A.S. and Michael, A.C. (2003) *Trends Anal. Chem.*, **22**, 503–508.

**192** Kulagina N.V., Shankar L., and Michael, A.C. (1999) *Anal. Chem.*, **71**, 5093–5100.

**193** Chen, K.C. (2005) *J. Neurochem.*, **92**, 46–58.

**194** Pei, J., Tian, F., and Thundat, T. (2004) *Anal. Chem.*, **76**, 292–297.

**195** Karyakin, A.A., Kotel'nikova, E.A., Lukachova, L.V., Karyakina, E.E., and Wang, J. (2002) *Anal. Chem.*, **74**, 1597–1603.

**196** Lenigk, R., Lam, E., Lai, A., Wang, H., Han, Y., and Carlier, P. (2000) *Biosens. Bioelectron.*, **15**, 541–547.

**197** Feriotto, G., Corradini, R., Sforza, S., Bianchi, N., Mischiati, C., Marchelli, R.,

and Gambari, R. (2001) *Lab. Invest.*, **81**, 1415–1427.

**198** Stoica, L., Lander, A.L., Ruzgas, T., and Gorton, L. (2004) *Anal. Chem.*, **76**, 4690–4696.

**199** Cuccioloni, M., Mozzicafreddo, M., Barocci, S., Ciuti, F., Pecorelli, I., Eleuteri, A.M., Spina, M., Fioretti, E., and Angeletti, M. (2008) *Anal. Chem.*, **80**, 9250–9256.

**200** Hooda, V., Gahlaut, A., Kumar, H., and Pundir, C.S. (2009) *Sens. Actuators B,* **136**, 235–241.

**Keywords/Abstract**

Dear Author,

Keywords and abstracts will not be included in the print version of your chapter but only in the online version.

Please check and/or supply keywords. If you supplied an abstract with the manuscript, please check the typeset version.

If you did not provide an abstract, the section headings will be displayed instead of an abstract text in the online version.

**Keywords:**
enzyme-based biosensor, nanoparticles, matrix, environmental monitoring, medical diagnostics

**Abstract:**
There is growing interest in the construction and commercialization of enzyme-based biosensors due to their potential application in analytic chemistry and biological science. This chapter focuses primarily on considerable advances in the synthesis and applications of enzyme-based biosensors, especially emphasizing achievements that have occurred in the last 10 years, in order to help the reader to understand and construct various enzyme-based biosensors with high performance.

# 6
# Energy Harvesting for Biosensors Using Biofriendly Materials

*Radheshyam Rai*

## 6.1
## Introduction

### 6.1.1
### What is a Sensor?

A sensor is a device that measures physical and chemical properties, and converts them into a signal that can be measured by an observer or by an instrument. For example, a mercury-in-glass thermometer converts the measured temperature into expansion and contraction of a liquid that can be read on a calibrated glass tube. A thermocouple converts temperature to an output voltage that can be read by a voltmeter. Thus, we can define a sensor as a device that receives and responds to a signal and converts it into electrical (or magnetic) form. Alternatively, we can define sensor as a device that receives a signal and converts it into electrical form that can be further used for electronic devices. A transducer is also a sensor, but there are some minor differences between a sensor and a transducer. A transducer converts one form of energy into other form, whereas a sensor converts the received signal in electrical form only. A sensor's sensitivity indicates how much the sensor's output changes when the measured quantity changes.

Sensors are routinely used in everyday life, such as touch-sensitive elevator buttons lamps that dim or brighten by touching the base and gas sensors. There are also innumerable applications for sensors of which most people are never aware. Applications include cars, machines, aerospace, medicine, manufacturing, robotics, and so on.

Thus, sensors are important things for our life and it exists in all our surroundings or our daily life activity. By the use of sensors we can improve our life activity. But main problem is that sensors materials, are environmentally and body friendly?

*Biosensor Nanomaterials*. Edited by Songjun Li, Jagdish Singh, and Ipsita A. Banerjee

ISBN: 978-3-527-32841-3

### 6.1.2
### Why are We Moving Towards Biofriendly Materials?

The market for different sensors components is dominated by lead-based materials containing more than 60 wt% lead. Lead is a heavy metal and its toxicity is well known. Some of the symptoms of lead poisoning are headaches, constipation, nausea, anemia, and reduced fertility. Continuous uncontrolled exposure could cause more serious symptoms such as nerve, brain, or kidney damage. Some other compounds are based on bismuth and/or barium, which are also heavy metals with associated problems of toxicity. But due to its high-performance properties, lead has been extensively used in sensors, energy harvesting, actuators, memory display, and other electronic devices [1–3]. In view of the environmental viewpoint, the accumulation of lead compounds has developed into a worldwide social problem (e.g., the volatization of lead during firing processes and the final disposal of electronic parts including lead compounds). Thus, lead has recently been prohibited from many commercial applications and materials owing to concerns regarding its toxicity. However, in practice, it is considered to be impossible to collect all of the lead compounds from disposed electronic devices with the present technology. In electronic parts, it is just in the piezoelectric materials in which that concentration of lead is the highest. Therefore, this provides a strong impetus to develop the substitution of lead-free materials. Thus, we are going towards biofriendly materials for sensor device applications.

### 6.1.3
### Why are We Moving Towards Energy Harvesting?

For the electronic product and application, and its demand increases with the increasing demands for electronic devices. Hence, energy production is a very difficult task for modern civilization. Currently, research is focused on stable and cheap sources of electricity. For energy production, we are using all of the resources of nature. However, the problem is that some resources have limited options. Some sources (coal, atomic) affect the environment and health, causing a number of medical diseases (bronchitis, tuberculosis, loss of lung function, etc.). Using natural resources produces climate warming and may result in natural disasters. Thus, we are heading towards energy harvesting on a large scale. For this we are using solar energy, hydro energy, and other resources (e.g., piezoelectric energy harvesting).

## 6.2
## Energy Production and Consumption

Current trends in technology allow a decrease in size and power consumption of complex digital systems. This decrease in size and power gives rise to new concepts of computing and uses of electronics, with many small devices working collaboratively or at least with strong communication capabilities and medical applications.

Human movement, breathing, and blood pressure are sources of energy production (60–70 W). According to Swallow *et al.* [4], power is consumed during walking and a piezoelectric material in a shoe with a conversion efficiency of 12.5% could produce 8.4 W of power.

Solar energy is a very attractive source for powering sensor arrays and the technology has matured over the years. However, light intensity (cloudy versus sunny day) can reduce the efficiency of this system. One of the major challenges in the implementation of solar technology on the "energy-on-demand" platform has been the requirement for bulky electronics. The variation in the light intensity (cloudy vs. sunny day) can drop the efficiency.

Air flow and mechanical vibration are other attractive alternatives in locations where these are available. Mechanical energy can be converted into electrical energy using piezoelectric, electromagnetic, or electrostatic devices. Piezoelectric transducers are more suitable mechanical-to-electrical energy converters.

## 6.3 Classification of Energy-Harvesting Devices

The following classification can made for energy harvesting.

The first kind of energy is derived from the human body or human-made devices, and so it is fully dependent on human activity and the surrounding environment. We can produce different levels of energy as per specific requirements [5–8]. Energy-harvesting devices are available through body heat or body movement. In the case of kinetic Human energy, one may distinguish between those actions made specifically to generate energy and casual movements made during normal behavior [9] (Figures 6.1 and 6.2).

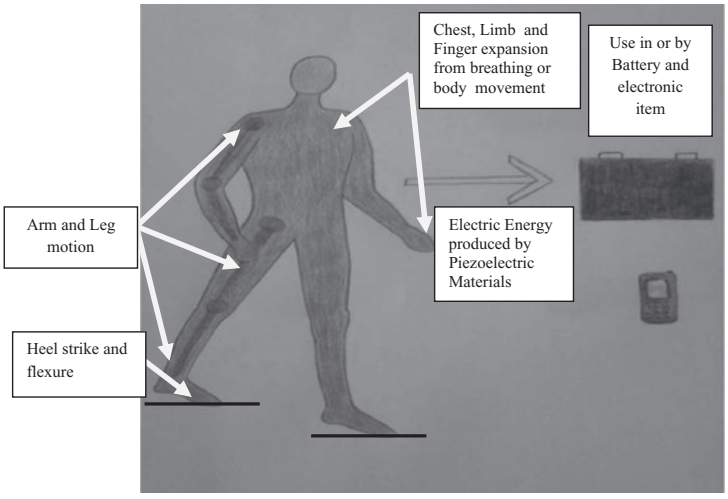


**Figure 6.1** Human body sections applicable for energy harvesting [9].

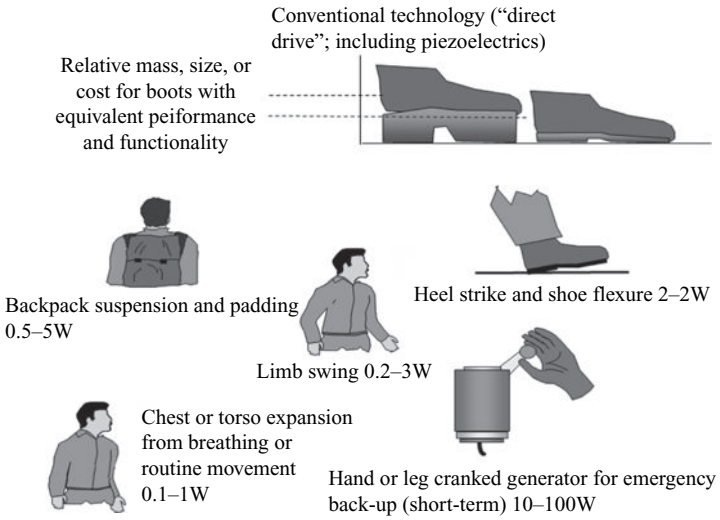


**Figure 6.2** Limitation of power generation by human movement [9].

**Table 6.1** Classification of energy-harvesting devices from different sources.

| **Human (kinetic, thermal)** | | | | **Nature (kinetic, thermal, radiation)** |
|---|---|---|---|---|
| **Human body** | **Vehicles** | **Structures** | **Industrial** | **Environment** |
| Breathing, blood pressure, exhalation, body heat | Aircraft, unmanned aerial vehicle, helicopter, automobiles, trains | Bridges, roads, tunnels, farm house structures | Motors, compressors, chillers, pumps, fans | Fossil fuels, nuclear power, solar power, wind power, etc. |
| Walking, arm motion, finger motion, jogging, swimming, eating, talking | Tires, tracks, peddles, brakes, shock absorbers, turbines | Control switch, heating, ventilating, and air conditioning systems, ducts, cleaners, etc. | Conveyors, cutting and dicing, vibrating machines | Ocean currents, acoustic waves |

Energy-harvesting devices can use human body vibration, other places of vibrating sources, or environmental energy sources like to solar energy, wind energy, and so on. All of these sources are affected by the external causes. Finally, the circuit also affects the production of energy by the devices.

Piezoelectric materials are the first prime factor affecting the performance of a generator. Commonly used piezoelectric materials are based on lead zirconate

titanate (PZT) ceramics, relaxor ferroelectrics, and polyvinylidene fluoride (PVDF). The primary factor in the selection of piezoelectric materials for energy-harvesting devices or sensor applications is the transduction rate.

In view of the environmental point, the accumulation of lead compounds has been developed into a social problem in the worlds; e.g. the volatization of lead during firing process and the final disposal of electronic parts including lead compounds. In practice it is impossible to collect all lead compounds from disposed electronic devices with the present technology. In electronic parts, it is just in piezoelectric materials that the concentration of lead is the highest and majority of those are PZT systems. Jacques and Pierre discovered the phenomenon of piezoelectricity in 1880. Piezoelectric materials produce an electric potential when stress is applied and also exhibit produce of stress and/or strain when an electric field is applied. PZT, PVDF, and so on, show piezoelectric properties. In terms of these materials, PVDF and PZT are very popular ceramics [4, 10].

Several kinds of non-lead-based materials have been reported: the $BaTiO_3$ (BT) system [11], the $Na_{0.5}K_{0.5}NbO_3$ (NKN) sodium potassium niobate system [11, 12], the $(BiNa)TiO_3$ system [13, 14], bismuth-layered structural ferroelectrics [15, 16], the langasite system [17], and $BiMeO_3$ (Me = Sc, Fe, In, etc.) [18, 19]. However, there are no suitable materials that could perfectly substitute PZT and this has been the stimulus for growing research on this subject. Among the oxide perovskite-structured ferroelectric materials, NKN has recently emerged as one of the most promising materials in radiofrequency and microwave applications due to its high dielectric tunability and low dielectric loss. NKN is a promising candidate material for ferroelectric random access memory devices, because it has high remnant polarization, low processing temperature, and fatigue-free characteristics. A large number of researchers are working on replacing PZT (either complete or partially) by some other ferroelectric and piezoelectric systems. Similar to PZT, NKN $(Na_{1-x}K_x)NbO_3$ is a combination of a ferroelectric ($KNbO_3$) and antiferroelectric ($NaNbO_3$) [20], which makes it a promising base material for lead-free piezoelectrics. Among all the non-lead ferroelectric materials, NKN systems have a similar Curie temperature and high electromechanical coupling constant compared with PZT. Even though lead-based materials have better properties than NKN-based materials, considering the fact of lead being not

**Table 6.2** Potential sources for energy harvesting.

| Activities | Available power (W) | Conversion efficiency (%) |
|---|---|---|
| Body heat | 116 | 3 |
| Breath | 1 | 40 |
| Blood pressure | 0.9 | 2 |
| Upper-limb motion | 24–60 | Few |
| Heel strike | 67 | 7–50 |
| Body waste | 1–5 | 50 |

environment friendly, research in NKN-based materials has gained a new importance. Moreover, a lot of desirable changes in the properties of ceramics are expected when prepared from nanosized powders. This gave us an insight to investigate NKN and doped NKN systems for their use in electronics. Here, we explore the development of a novel system suitable for both micro and macro electronic industries. Generally, these novel systems act as passive elements that simply conduct electricity between power sources (e.g., batteries) and various devices such as high-brightness light-emitting diodes in an integrated and flexible substrate. Even when the phrase "energy harvesting" has been used, the system is a simply a passive component that conducts electricity generated by solar cells or by thermoelectric generator chips (i.e., converts body heat to electricity). Perovskite piezoelectric ceramics are generally synthesized with constituent compounds in suitable stoichiometry. They are very sensitive and more effective at both lower and higher temperatures. After different types of doping, the properties may change with as per the requirements. Some piezoelectrics with a perovskite structure of a general formula $ABO_3$ (where A = mono- or divalent ions, B = tri-, tetra- or pentavalent ions) have been found to be very useful and interesting for different solid-state devices. These materials with a perovskite structure exhibit a simple cubic symmetry with no dipole moment. At temperatures below the Curie temperature each crystal has a tetragonal or rhombohedral symmetry, exhibiting ferroelectric–paraelectric phase transitions. The direction of polarization in a piezoelectric ceramic is random so the ceramic has no overall polarization. Thus, it requires the alignment of the entire domain in one direction. We align the domains in the ceramic by poling.

Recently, the lead-free ferroelectric $Na_{1-x}K_xNbO_3$ (NKN) has attracted interest as an electrically tunable material for piezoelectrics, optoelectronics, and so on. Lead-free NKN-based ceramics can be prepared on various substrates by the pulsed laser deposition method, using pure and doped targets and thermal treatments of crystallization under high-intensity excimer laser irradiation. The appropriate processing conditions will be determined with the aim of obtaining ceramics with ferroelectric responses comparable to those of the corresponding ceramics. A complete characterization of the materials will include the test of capacitance and piezoelectric/ferroelectric properties, trying to relate these properties with the processing conditions and to establish their use in real devices.

Here, we will focus on NKN, which is a solid solution of the antiferroelectric $NaNbO_3$ and the ferroelectric $KNbO_3$. The study on piezoelectric harvesting began in 1984, when a PVDF patch was used to obtain energy during inspiration of a human being [21]. However, the power generated was insufficient to power the desired electronics. This study was performed in the early stages of low-power electronics and the properties of the piezomaterial were not optimized. The energy taken from human walking being can reach 67 W and thus be used for harvesting [22]. The first use of piezoelectrics for harvesting energy from a human body was described in several papers [23, 24], which also reported that it can be improved by the piezoceramic material itself and the circuitry. A design study was conducted by Ramsey and Clark [25], who investigated the feasibility of using a piezoelectric

transducer for *in vivo* microelectromechanical system applications. Their research confirmed the possibility of bio-microelectromechanical systems powered from vibration energy existing in a human body. Some authors [26] studied the efficiency of commercial multilayer piezoelectric actuators for energy harvesting and showed that the frequency of vibration is a critical factor for efficiency. The design of a multilayer actuator has to be adjusted to a specific frequency range. Some papers [27–30] reported different types of piezoelectric materials for energy harvesting. The power densities for various environmental sources are available in literature [31–36]. Solar energy has the capability of providing power of higher magnitudes compared to other sources.

The solid solution of $KNbO_3$ and $NaNbO_3$ displays a good piezoelectric response, particularly for the morphotropic phase boundary composition $Na_{0.5}K_{0.5}NbO_3$ (NKN), with piezoelectric properties of $d_{33} = 80$ pC $N^{-1}$, $k_p = 36$–40%, $Q_m = 130$, and $\varepsilon_r = 290$, when prepared by ordinary sintering. We optimized NKN ceramic to be a promising candidate for piezoelectric transducer and tunable microwave components.

In these days the world is moving towards a technological way of living. More and more people are carrying portable electronic devices or more and more sensors are attached to remote locations. However, although the technology for portables has grown tremendously, battery and energy storage technology has not kept up. Piezoelectric materials are capable of converting mechanical excitations into electrical outputs and vice versa. Studies have shown that, in the case of ceramic/polymer composites, when the volume fraction exceeds a critical value, the effective piezoelectric coefficients of the composite become comparable to, or even larger than, the bulk ceramic material. Piezoelectric materials have been used extensively for energy harvesting, relying essentially on mechanical vibrations of structures to which they are attached.

The magnitude of the transduction is governed by the effective piezoelectric stress constant $d$ and the effective piezoelectric voltage constant $g$. The primary factor for the selection of a piezoelectric material for energy-harvesting devices or sensor applications is the transduction rate and figure of merit. Our research also explored the relationship between the mechanical quality factor, the coupling coefficient, and the transformation efficiency of mechanical to electrical energy in lead-free piezoelectric disks. We noted that high efficiency for piezoelectric conversion devices requires high-quality, electromechanical coupling factors, so we present a general approach to establishing the relationship between $Q$ and $k_2$ for device development.

A critical component of any energy-harvesting system is the electrical circuit that connects the piezoelectric element to the device to be powered. Optimized circuits for these specific types of application have been constructed and successfully tested. Two main functions were considered in energy-harvesting circuits: (i) to effectively transfer the electrical charge from the piezoelectric transducer into an effective storage mechanism such as a super-capacitor and (ii) to match the impedance of the generator to the external load. The commonly used converter circuit is called a buck converter and it operates in the discontinuous

current mode. Several other techniques are used in conjunction with the circuit for reducing the matching impedance such as the multilayer piezoelectric transducer structure and increasing the area aspect ratio (area/thickness).

A literature review shows that all previous efforts were mainly concentrated on lead-based devices and lead-based efficient piezoelectric materials. Thus, further progress is needed in lead-free devices and lead-free piezoelectric materials. NKN is an attractive candidate because of its large piezoelectric coefficient and high rare-earth solid solubility. It can be doped with rare-earth ions like neodymium, erbium, ytterbium, thulium, and praseodymium to incorporate laser-active properties. Of these ions, erbium has gained the most interest.

Finally, the scientific activity in energy harvesting is strongly motivated by possible applications in the power sector and energy conservation. In view of the above, it is highly relevant to try and find alternatives and/or replacements for conventional lead-based materials, and therefore several lead-free and low-lead systems have been suggested. NKN is one of the most important classes of non-lead ferroelectric compounds that have received significant attention from researchers in the last decade. The present proposal will begin with the synthesis of NKN compounds by the solid-state reaction method followed by detail structural and electrical characterizations.

As the miniaturization of electronic devices continues, desired characteristics and processing of the starting powders becomes a critical issue. For improved properties it is desired to have smaller (nanosized) particles (i.e., bigger surface area) of the starting NKN powder with low loss and conductivity with controlled particle morphology and dispersibility.

The sol–gel emulsion process has been successfully used for the synthesis of single- to multicomponent ceramic powders with controlled particle size. The proposed sol–gel emulsion process will be used to prepare NKN and different metal ion-incorporated nanosized NKN powders having a tailored size and shape. Various process parameters like surfactant and support solvent ratio, and the nature of the surfactant, are known to affect the powder size and morphology. This process has the potential to synthesize nanostructured powders with controlled chemical composition at low calcination temperatures.

For the development of energy-harvesting materials we carried out a detailed investigation of the above-mentioned physical/chemical routes for the synthesis of ultrafine NKN-based powders. The effect of the particle size and presence of different dopants in the NKN structure has to be critically investigated to achieve the desired electrical and electronics properties of the final product that can be a competitive alternative to lead-based materials.

## 6.4 Conclusions

This main objectives will be achieved by the choice of effective piezoelectric materials, the development of the devices, and testing the devices together with the

available electronics in real vibration conditions. Strain in piezoelectric material causes a charge separation. Thus, stress/strain on piezoelectric materials can develop an electric charge. As We know that in the direct piezoelectric effect the mechanical energy transforms to electrical energy. We can store this energy using a storage circuit. The mechanical stress can be in different forms and it depends on the source. There are three primary steps for this application: (i) to trap the mechanical stress from the source, (ii) to convert the stress into electrical energy, and (iii) processing and storing the electrical energy. During the transformation, some mechanical loss or electromechanical loss may present in the system because of a mismatch in mechanical impedance by the damping factor and reflection ratio, and also depending upon the magnitude of coupling factor. Thus, the frequency and amplitude of the mechanical stress play an important role in designing transducers or final-stage devices.

Thus, we will focus on these problem during materials synthesis and the development of energy-harvesting devices.

Materials prepared from non-lead-based materials (NKN, NKN-BT) provide commercial powder with high piezoelectric coefficients and minimum porosity. The following subtasks will be the focus of further research:

i) Identification of suitable powder, binder, and material for internal electrodes (gold, gold/palladium).
ii) Fabrication of piezoelectric multilayers by screen printing of metal electrodes and laminating the composite structure.
iii) Choosing proper annealing strategies to obtain dense samples without second phases.

The work will be concentrated on polishing, electroding, bonding of single crystals, and investigation of their piezoelectric performance. Both the geometrical dimensions and poling strategies will be varied to obtain high piezoelectric response and reliability.

## References


1 Uchino, K. (2000) *Ferroelectric Devices*, Marcel Decker, New York.
2 Yamashita, K., Katata, H., Okyama, M., Kato, G., Aayagi, S., and Suzuki, Y. (2002) *Sens. Actuators A*, **97**, 30.
3 Priya, S., Taneja, R., Mayers, R., and Islam, R. (2008) *Piezoelectric and Acoustic Materials for Transducer Applications* (ed. A. Safari and E.K. Akdogan), Springer, New York, p. 373.
4 Swallow, L.M., Luo, J.K., Siores, E., Patel, I., and Dodds, D. (2008) *Smart Mater. Struct.*, **17**, 025017.
5 Farmer, J.R. (2007) Thesis, Faculty of the Virginia Polytechnic Institute and State University, Mechanical Engineering, Blacksburg, VA.
6 Jia, D. and Liu Front, J. (2009) *Energy Power Eng. China*, **3**, 27–46.
7 Kim, S., Clark, W.W., and Wang, Q.M. (2003) *Proc. SPIE*, **5055**, 307.
8 Mateu, L. and Moll, F. *Proceedings of the SPIE Microtechnologies for the New Millenium*, **5837**, 359 (2005).
9 Wang, K. (2010) A new renewable energy. Generating power from EPAM (Electroactive Polymer Artificial Muscle);

folk.ntnu.no/keshengw/eit/ArtificialMuscle.ppt.
**10** Kawai, H. (1969) *Jpn. J. Appl. Phys.*, **8**, 975.
**11** Saito, Y., Takao, H., Tani, T., Kimura, T., Takatori, K., and Tani, T. (2003) *Ceramic Trans.*, **136**, 389.
**12** Ichiki, M., Zhang, L., Tanaka, M., and Maeda, R. (2004) *J. Eur. Ceramic Soc.*, **24**, 1693.
**13** Smolenski, G.A., Isupov, V.A., Agranovskaya, A.I., and Kainik, N.N. (1961) *Sov. Phys. Solid State*, **2**, 2651.
**14** Takenaka, T., Maruyama, K., and Sakata, K. (1991) *Jpn. J. Appl. Phys.*, **30**, 2236.
**15** Takenaka, T., Gotoh, T., Mutoh, S., and Sasaki, T. (1995) *Jpn. J. Appl. Phys.*, **34**, 5384.
**16** Hirose, M., Suzuki, T., Oka, H., Itakura, K., Miyaauchi, Y., and Tsukada, T. (1999) *Jpn. J. Appl. Phys.*, **38**, 5561.
**17** Shimamura, K., Takeda, H., Kohno, T., and Fukuda, T. (1996) *J. Crystal Growth*, **163**, 288.
**18** Eitel, R.E., Randall, C.A., Shrout, T.R., and Park, S.E. (2002) *Jpn. J. Appl. Phys.*, **41**, 2099.
**19** Zhang, S., Randall, C.A., and Shrout, T.R. (2003) *Appl. Phys. Lett.*, **83**, 3150.
**20** Wang, R., Xie, R., Sekiya T., and Shimojo, Y. (2004) *Mater. Res. Bull.*, **39**, 1709.
**21** Hausler, E. and Stein, E. (1984) *Ferroelectrics*, **60**, 277.
**22** Starner, T. (1996) *IBM Syst. J.*, **35**, 618.
**23** Kymissis, T., Kendall, C., Paradiso, J., and Gershenfeld, N. (1998) Proc. *IEEE Symp. on Wearable Computers*, Pittsburg, PA, pp. 132–139.
**24** Shlenk, N.S. (1998) Thesis, MIT, Cambridge, MA.
**25** Ramsey,M.J. Clark, W.W. *Proc. SPIE* 8th Annual Smart Materials and Structures Conference, Newport Beach, CA2001, **4332**, 429.
**26** Goldfarb, M. and Jones, L.D. (1996) *ASME J. Dyn. Syst. Control*, **121**, 566.
**27** Sodano, A.H., Magliula, E.A., Park, G., and Inman, D.J. (2002) Proc. 13th Int. Conf. on Adaptive Structures and Technologies, Potsdam, p. 132.
**28** Sodano, H.A., Park, G., Leo, D.J., and Inman, D.J. (2003) *Proc. SPIE*, **5050**, 101.
**29** Sodano, H.A., Park, G., and Inman, D.J. (2004) *Mech. Syst. Sign. Proc.*, **18**, 683.
**30** Sodano, A.H., Park, G., Leo, D.J., and Inman, D.J. (2004) *Proc. ASME*, **40**, 2.
**31** Roundy, S., Wright, P.K., and Rabaey, J.M. (2004) *Energy Scavenging for Wireless Sensor Networks*, Kluwer, Boston, MA.
**32** Calaway, E.H., Jr. (2004) *Wireless Sensor Networks*, Auerbach,, New York.
**33** Shenck, N. and Paradiso, J.A. (2001) *IEEE Micro*, **21**, 30.
**34** Meninger, S., Mur-Miranda, J.Q., Amirtharajah, R., Chandrakasan, A.P., and Lang, J.H. (2001) *IEEE Trans. VLSI Syst.*, **9**, 64.
**35** Roundy, S., Wright, P.K., and Rabaey, J. (2003) *Comput. Commun.*, **26**, 1131.
**36** Paradiso, J. and Starner, T. (2005) *IEEE Pervas. Comput.*, **4**, 18.

# 7
# Carbon Nanotubes: *In Vitro* and *In Vivo* Sensing and Imaging

*William Cheung and Huixin He*

## 7.1
## Introduction

Studying various cellular and molecular processes in living subjects is important to many facets of biomedical research. Nondestructive molecular imaging with high sensitivity, high spatial and temporal resolution, and high multiplex capability will speed up the development of methodologies for early diagnosis of various diseases. It also helps to develop more clinically relevant drugs and drug delivery systems due to the capability for *in situ and in vivo* evaluation of their therapeutic outcomes. Current noninvasive imaging techniques, such as positron emission tomography (PET), computed tomography, magnetic resonance imaging, and ultrasound cannot simultaneously meet all these needs. Bioluminescence and fluorescence strategies will continue to evolve rapidly for molecular imaging of living subjects, in particular for small-animal models.

Current methods used to label cells and subcellular components are generally based on organic fluorophores, such as fluorescein, rhodamine, cyanine, or Alexa Fluor families. However, most organic fluorophores experience photobleaching, which limits the ability for continuous mapping over long periods of observation. Furthermore, these organic fluorophores also quench when applied concurrently with hematoxylin and eosin–an important stain used by pathologists and other researchers for the evaluation of histological sections. Heller *et al.* [1] summarized the properties of an ideal robust cellular label, which should not (i) have untoward effects on nuclear or cell-membrane function, (ii) impact cellular viability during long-term studies, (iii) quench after cytochemical staining, and (iv) blink or photobleach under prolonged excitation.

Carbon nanotubes (CNTs) exhibit many unique intrinsic physical and chemical properties, specifically their small size, unique shape, and their remarkable optical properties, which may satisfy all these criteria for *in vitro* and *in vivo* molecular sensing and imaging. First, nanotubes can easily enter cells, and the potential *in vitro* and *in vivo* toxicity can be eliminated by careful modification of the CNT surface [2, 3]. Single-walled CNTs (SWNTs) absorb and emit strongly in the near-IR (NIR) region of the spectrum where biological tissues are highly transparent

*Biosensor Nanomaterials.* Edited by Songjun Li, Jagdish Singh, and Ipsita A. Banerjee

ISBN: 978-3-527-32841-3

and the background cellular autofluorescence is low [4, 5]. Compared with traditional fluorophores, SWNT fluorescence also demonstrates a large Stokes shift between the excitation and emission bands, which allows a range of excitation energies to be used [4]. Their NIR emission changes immediately in the presence of a target analyte without the need for additional sample processing, which is ideal for rapid, real-time identification of biological analytes *in vitro* and *in vivo* where it can be detected down to the single-molecule level. Furthermore, the NIR emission is much more stable than other common fluorophores such as organic dye molecules and semiconductor quantum dots (QDs), showing no evidence of blinking or photobleaching after prolonged exposure or excitation at high fluence [1]. Finally, the emission wavelength differs depending on the diameter and chirality of the SWNTs, which can be exploited to detect different biological analytes simultaneously. Therefore, selective detection of molecules associated with diseased cells and tissues by the use of nanotubes that can insert themselves into such areas of interest may possibly provide for a more sensitive and localized diagnostic approach. Consequently, great strides have been made in recent years with biolabeling, sensing, and imaging endeavors [6].

In addition, SWNTs have distinctive resonance-enhanced Raman signatures for Raman detection/imaging, with large scattering cross-sections for single tubes [1, 7–9]. Raman scattering spectra of SWNTs are simple, with strong, well-defined, and sharp Lorentzian peaks, and can be easily distinguished from the autofluorescence background of biological species. The full-width half-maximum (FWHM) of the G-band from SWNTs is smaller than 2 nm, allowing for high degrees of multiplicity for simultaneous imaging with many colors [10–12]. The nanotube Raman signals are very stable and no quenching or bleaching is observed even under extraordinarily high laser powers – a reflection of the stability of the SWNT $sp^2$ carbon lattice [1]. Compared to the NIR fluorescence of SWNTs, the NIR Raman scattering of SWNTs, especially the sharp and strong G-band intensity, is relatively insensitive to the diameter and bundling of nanotubes [7, 13]. It is also relatively insensitive to the type of noncovalent coatings and solution environment of the SWNTs, providing more benefits for robust sensing and imaging. In this chapter, we first provide a general introduction to the structure, properties, and broad applications of CNTs to give readers a general picture of the usefulness and versatility of CNTs. Then the unique optical properties, specifically the NIR absorption, NIR photoluminescence, and Raman scattering of CNTs, will be introduced and accompanied with the exploitation of these remarkable optical properties for *in vitro* and *in vivo* molecular sensing and imaging. The studies of CNT cellular internalization mechanism, *in vitro* cellular distribution, *in vivo* blood circulation, and long-term fate of the CNTs in animals will be also included.

## 7.2
## Carbon Nanotubes: Structure, Physical and Chemical Properties, and Applications

CNTs are well-ordered, all-carbon hollow graphitic nanomaterials with very high aspect ratios, lengths from several hundred nanometers to several micrometers,

and with diameters of 0.4–2 nm for SWNT and 2–100 nm for multiwalled CNTs (MWNTs). Conceptually, the structure of SWNTs can be viewed as "wrapping-up" a graphene sheet into a seamless hollow cylinder. (Graphene is a one-atom-thick planar sheet of $sp^2$-bonded carbon atoms that are densely packed in a honeycomb crystal lattice.) The structure of MWNTs can be pictured as several coaxially arranged SWNTs of different radii with an intertube separation close to the interplane separation in graphite (0.34–0.35 nm) (Scheme 7.1) [14].

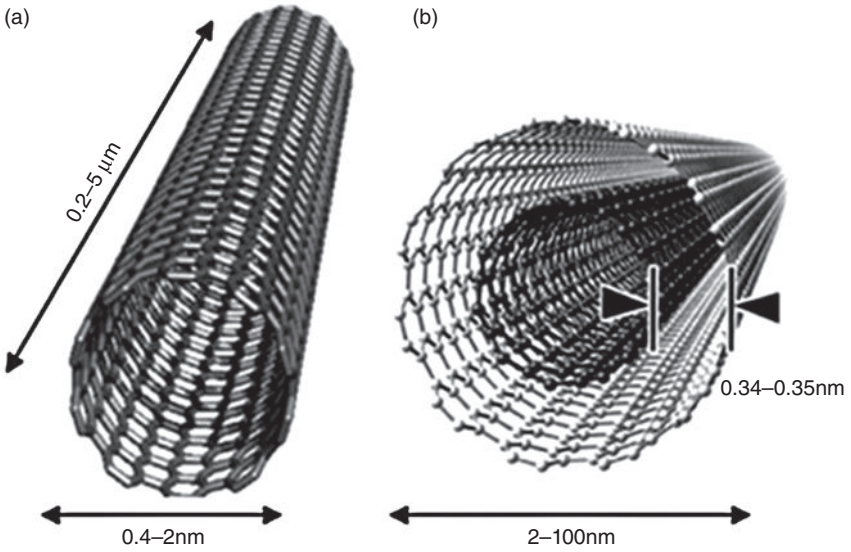


**Scheme 7.1** (A) SWNT. (B) Double-walled CNT.

There are an infinite number of ways of rolling a graphene sheet into a cylinder. The large variety of possible helical geometries, defining the tube chirality, provides a family of nanotubes with different diameters and chirality, which determines the physical and electronic properties of SWNTs [15]. The tubes are usually labeled in terms of the graphene lattice vectors by a pair of indices ($n$, $m$) called the chiral vector (Scheme 7.2). The integers $n$ and $m$ denote the number of unit vectors along two directions in the honeycomb crystal lattice of graphene [16]. This chiral vector is denoted as $C_h = na_1 + ma_2$, where $n$, $m$ are the chiral indices and $a_1$, $a_2$ are the lattice vectors. The indices $n$ and $m$ denote the number of unit vectors along two directions in the honeycomb crystal lattice of graphene [16]. The diameter of the nanotube is related to the chiral vector by:

$$d = \frac{c}{\pi} = \frac{A_c\sqrt{n^2 + nm + m^2}}{\pi}$$

where $A_c$ is the carbon–carbon distance between two neighboring atoms. The chiral angle ($\theta$), which determines the hexagonal network arrangement of the nanotube, thus the chirality, is given by:

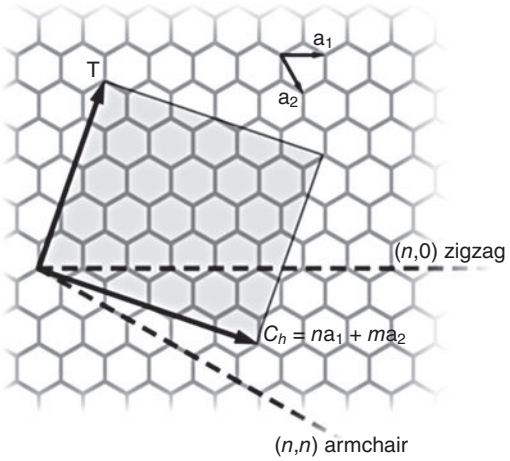


**Scheme 7.2** Unrolled honeycomb lattice of a CNT. The shaded region defines the unit cell for the nanotube.

$$\theta = \tan^{-1}\left(\frac{m\sqrt{3}}{m+2n}\right)$$

SWNTs are either semiconducting or metallic depending on the chiral vectors. It has been shown that for a given ($n$, $m$), the nanotube is metallic if $n = m$ or if $n - m$ is a multiple of 3, otherwise the nanotube is semiconducting [15–22]. By varying the nanotube diameter or chiral angle, nanotubes with various properties can be obtained. MWNTs are essentially metallic in nature due to intertube interactions [23].

CNTs display exceptional and unusual electrical, mechanical, and optical properties because of their one-dimensional structure. CNTs have excellent electronic properties: metallic nanotubes can carry an electrical current density of $4 \times 10^9$ A $cm^{-2}$, which is three orders of magnitude higher than a typical metal, such as copper or aluminum [24]. Individual semiconducting SWNTs are known to possess an extremely high carrier mobility of 10 000 $cm^2$ $Vs^{-1}$ at room temperature and can be operated at high frequencies (2.6 GHz). These values exceed those for all known semiconductors, such as silicon [25], which bodes well for application of nanotubes in high-speed transistors, single- and few-electron memories, and chemical/biochemical sensors [26, 27]. Moreover, they are flexible owing to their small diameter. SWNTs are therefore also an ideal candidate material for high-performance, high-power, flexible electronics [28, 29]. CNTs are also the strongest and stiffest materials yet discovered in terms of tensile strength and elastic modulus, respectively. The Young's modulus is over 1 TPa and is as stiff as diamond. The estimated tensile strength is 200 GPa [30]. The strength results from the covalent $sp^2$ bonds formed between the individual carbon atoms, and these properties are ideal for reinforced composites [31–34] and nanoelectromechanical systems [35]. Furthermore, the heat transmission capacity of individual CNTs at

room temperature has been shown to exceed 3000 W $m^{-1} K^{-1}$, which is greater than natural diamond, excellent for thermal management [36]. Equally important, both SWNTs and MWNTs are now produced in substantial quantities for a variety of commercial applications.

In recent years, efforts have also been devoted to exploring the potential biological applications of CNTs, motivated by their interesting size, shape, and structure, as well as attractive optical and electrical properties [6, 37]. First, the large surface area, the highly π-conjugated polyaromatic surface, and the flexible one-dimensional nanostructure of CNTs have been explored for efficient drug delivery. With all atoms exposed on the surface, SWNTs have an ultrahigh surface area (theoretically 1300 $m^2 g^{-1}$) that permits efficient loading of multiple molecules along the length of the nanotube sidewall. Supramolecular binding of aromatic molecules can be easily achieved by π–π stacking of those molecules onto the polyaromatic surface of nanotubes [38]. Moreover, the flexible one-dimensional nanotube may bend to facilitate multiple binding sites, therefore largely improving the binding affinity of nanotubes conjugated with targeting ligands [39].

The intrinsic optical and electrical properties of SWNTs can be utilized for multimodality imaging and therapy. Due to quantum confined effects, SWNTs behave as quasi-one-dimensional quantum wires with sharp densities of electronic states at the Van Hove singularities, which impart distinctive optical properties to SWNTs [40]. SWNTs are highly absorbing materials with strong optical absorption in the NIR range (800–1600 nm). These wavelengths include the tissue-transparent region of the electromagnetic spectrum (800–1400 nm), in which radiation passes through without significant scattering, absorption, heating, or damage to tissues. Therefore, SWNTs can be utilized for photothermal therapy [41–43] and photoacoustic imaging [44]. SWNTs can also be used to deliver therapeutic drugs with externally controlled release capabilities [42].

Semiconducting SWNTs with small band gaps on the order of 1 eV exhibit photoluminescence in the NIR range. The emission range of SWNTs is 800–2000 nm [5, 6, 45], which covers the biological tissue transparency window and is therefore suitable for biological imaging. SWNTs also have distinctive resonance-enhanced Raman signatures for Raman detection/imaging, with large scattering cross-sections for single tubes [1, 7]. The selective detection of diseased cells and tissues by the use of nanotubes that can insert themselves into such areas of interest may possibly provide for a more sensitive and localized diagnostic approach [43]. In summary, motivated by various properties of CNTs, research towards applying CNTs for biomedical applications has been progressing rapidly. Very recently, Liu *et al*. [39] gave a comprehensive review on this field and clarified that surface functionalization is critical to the behavior of CNTs in biological systems. Kostarelos *et al*. [46] summarized the promises, facts, and current challenges for CNTs in imaging and therapeutics. We have surveyed CNTs as unique vehicles and mediators for therapeutic DNA/small interfering RNA delivery [47]. Readers interested in this area should reference these works. In this chapter, we focus on the NIR absorption, emission, and Raman scattering properties of CNTs, and their application as unique NIR fluorescence and Raman tags for *in vitro* and *in vivo*

sensing and imaging. In the following sections, we first provide a detailed introduction of the optical properties, followed by the unique capabilities exhibited by CNTs in molecular detection and imaging both *in vitro* and *in vivo*. Finally, we summarize the major advantages, opportunities, and challenges ahead for clinical application of CNT for *in vitro* and *in vivo* imaging and sensing.

## 7.3
## Near-IR Absorption of Carbon Nanotubes

The high optical absorbance of CNTs in the 700- to 1100-nm NIR window originates from the electronic transitions between the first and second Van Hove singularities of the nanotubes [4, 5]. The electronic structure of SWNTs, including semiconducting versus metallic tubes, depends on their diameter and chirality [48]. At the Fermi energy level, the density of states is finite for metallic nanotubes and zero for semiconducting nanotubes (Scheme 7.3) [17–20, 22]. As the energy is increased, sharp peaks in the density of states, called Van Hove singularities, appear at specific energy levels. The optical absorption spectrum of a particular tube is dominated by a series of relatively sharp interband transitions, at energies denoted *E*11, *E*22, and so on, associated with these Van Hove singularities [49].

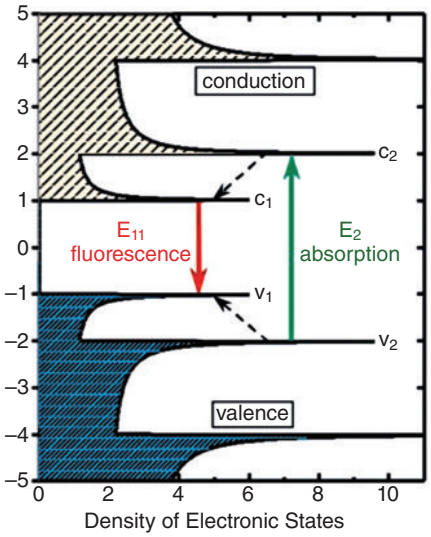


**Scheme 7.3** Schematic density of electronic states for a semiconducting SWNT. The sharp features of the DOS are attributed to Van Hove singularities. *E*11, *E*22, and *E*33 optical transitions correspond to photon absorption in the NIR, visible, and UV ranges, respectively. The solid arrows depict the optical excitation (green) and emission (red) transitions of interest; dashed arrows denote nonradiative relaxation of the electron (in the conduction band) and hole (in the valence band) before emission. (Reproduced from [4] with permission.)

The first Van Hove transitions of the direct band gap of semiconducting tubes, $E11$, is in the 800- to 1600-nm wavelength range and their second transitions, $E22$, is in the range of 550–900 nm. The highest energy Van Hove transitions are for the metallic tubes appearing between 400 and 600 nm [5]. For specific tubes, the wavelength at which the SWNTs have the highest absorption varies depending on the chirality of the tubes (Figure 7.1). The absorption peaks shifts to higher energy with decreasing nanotube diameters. SWNTs are normally produced as a mixture

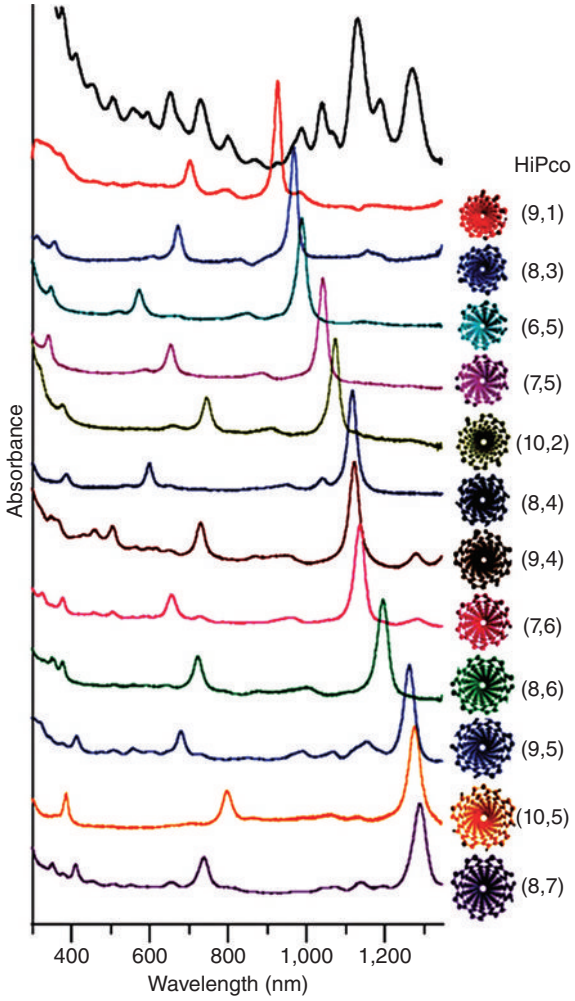


**Figure 7.1** UV/visible/NIR absorption spectra of 12 purified semiconducting SWNTs (ranked according to the measured $E11$ absorption wavelength) and the starting HiPCO mixture. The structure of each purified SWNT species (viewed along the tube axis) and its ($n$, $m$) notation are given at the right side of the corresponding spectrum. (Reproduced from [50] with permission.)

of metallic and semiconducting tubes with different diameters and chiralities, therefore the UV/visible/NIR spectrum normally shows multiple small peaks (the curve on top in Figure 7.1).

## 7.4
## Near-IR Photoluminescence of Single-Walled Carbon Nanotubes

During photoexcitation, light is directed onto a sample where electrons within the material are moved into permissible excited states. As the electrons return to their original ground state, energy is released and photoluminescence occurs. The energy released from this process is the difference in energy levels between the electron transition from the excited state and the original ground state. The two most common forms of photoluminescence are fluorescence, where the transitions are typically a fast process, and phosphorescence, where absorbed photons encounters the triplet state and experience a slow process of radiative transitions back to the singlet state. These processes can be summarized in a Jablonski diagram (Scheme 7.4).

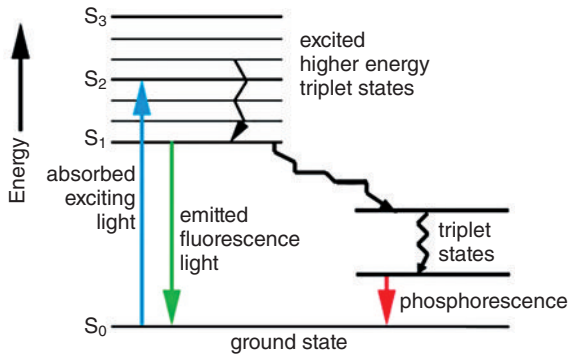


**Scheme 7.4** Jablonski diagram showing possible routes by which an excited molecule can return to its ground state.

When CNTs are excited, they display a bright, structured photoluminescence in the NIR region. As indicated in Scheme 7.3, CNTs that are excited with a photon energy of *E*22 is followed by fluorescence emission near *E*11, therefore the fluorescence emission from CNTs has a very large Stokes effect due to the large band gap difference between *E*11 and *E*22. The values of *E*11 and *E*22 will vary with different CNTs, therefore by studying the excitation and emission spectra one can rapidly determine the detailed composition of bulk SWNT samples, providing distributions in both tube diameter and chirality [4]. Figure 7.2 is an example of a photoluminescence spectrum of SWNT dispersed with sodium dodecylsulfate (SDS) micelles in $D_2O$ after pulsed laser excitation at 532 nm. Comparison with

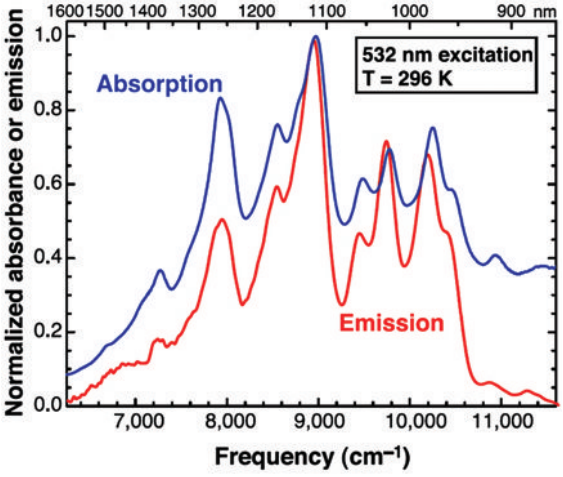


**Figure 7.2** Emission spectrum (red) of individual CNTs suspended in SDS micelles in $D_2O$ excited by 8-ns, 532-nm laser pulses, overlaid with the absorption spectrum (blue) of the sample in this region of first Van Hove band gap transitions. The detailed correspondence of absorption and emission features indicates that the emission is band gap photoluminescence from a variety of semiconducting nanotube structures. (Reproduced from [5] with permission.)

the overlaid absorption spectrum of the same sample reveals a striking correspondence. Each absorption component in the spectral region of the first Van Hove "band gap" transition of the semiconducting tubes, $E11$, is present in the emission spectrum [5].

Only the well-dispersed and isolated CNTs show bright emission. The photoluminescence intensity is dramatically reduced by aggregation of the isolated nanotubes or surface defects on the CNTs. It was assumed the presence of a metallic nanotube within a bundle will quench electronic excitation on an adjacent semiconducting tube, preventing its luminescence. The electronic band gap, which is the origin of the distinctive NIR photoluminescence, is sensitive to the local dielectric environment around the SWNT and defects on CNTs; therefore the NIR emission would also sensitively respond to local dielectric environment changes. However, the bright NIR emission does not photobleach even under high excitation powers, which is much more stable than organic fluorescent dyes and even QDs (Figure 7.3) [1]. These remarkable properties are the foundation for CNT-based NIR molecular sensing and imaging.

It is worth mentioning that the SWNT NIR fluorescent emission is mostly in the IR-A (1–1.4 μm) region, which is ideal for biological probes because of the inherently low autofluorescence in the NIR range (0.8–1.7 μm) [51]. In this region, radiation passes through without significant scattering, absorption, heating, or damage to tissue. Lim *et al.* predicted that NIR fluorophores with emission in the 1100- to 1400-nm range have higher tissue penetration than those near 800 nm by considering the wavelength-dependent scattering by tissues [52]. The large Stokes

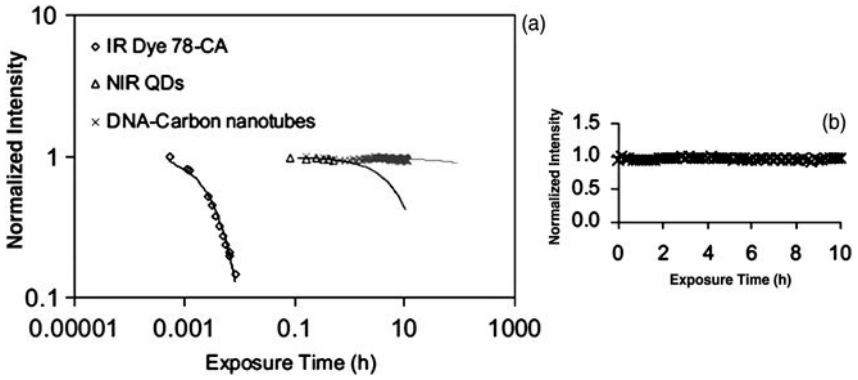


**Figure 7.3** (a) Photobleaching comparison for organic, QD, and SWNT fluorescence. The organic NIR dye 78-CA and NIR CdTe/CdSe QDs were excited at 600 mW $cm^{-2}$ fluence and CNTs were excited at $6.17 \times 106$ mW $cm^{-2}$. (b) CNTs show no bleaching over 10 h. (Reproduced from [1] with permission.)

shift between the excitation and emission bands allows excitation in the biological transparency window near 800 nm while further reducing the background effects of autofluorescence and scattering [52]. Nanotubes provide a unique way to probe this advantageous emission region, therefore allowing them to act as excellent NIR fluorescent tags for molecular sensing and imaging, in both *in vitro* and *in vivo* settings for various applications.

### 7.4.1 Study of Internalization Mechanism and *In Vitro*, *In Vivo*, and Long-Term Fate of Carbon Nanotubes

A clear understanding of the internalization mechanism and the intracellular properties of SWNTs is essential for the development of this nanomaterial as a drug delivery vector, as a NIR fluorescence or Raman tag, and as a drug itself to kill cancer cells and bacteria. Furthermore, it is also necessary to explore the behavior and fate of CNTs in mammals. Recently, SWNTs covalently linked with visible-wavelength fluorophores and radiotracers have been used for imaging SWNTs in cells [53, 54], and studying the biodistribution and blood clearance rates of CNTs [55, 56]. In these approaches, however, the chemical linkage between the tube and the dye must resist enzymatic cleavage, and one must be aware that chemical processing of SWNTs may dramatically change their biological fate [57]. In addition, photobleaching is another major limitation for real-time measurements when organic dyes and QDs are used. The photobleaching time constrains the observation window during tracking so that events occurring on the order of several hours must be observed through multiple and distinct tracking periods. In practice, this lack of continuity has prevented the complete and continuous mapping of the transport pathway of CNTs.

Taking advantage of the extremely stable NIR fluorescence properties of SWNTs, Cherukuri *et al.* [6] studied the internalization mechanism of mouse macrophage-like cells by imaging the intrinsic NIR fluorescence of SWNTs dispersed with Pluronic F108 surfactant. They found that the nanotube uptake at 27 °C was 40% of that at 37 °C. This finding differs sharply from the temperature-independent cell penetration by functionalized SWNTs reported by Pantarotto *et al.* [54], but it is consistent with the temperature dependence of macrophage phagocytosis [58], suggesting active ingestion of the nanotubes. Taking another step further, Cherukuri *et al.* [59] reported the use of the intrinsic NIR fluorescence to measure blood elimination kinetics of CNTs in rabbits and to identify the organs in which they concentrated. The nanotube concentration in the blood serum decreased exponentially with a half-life of 1.0–0.1 h. By performing NIR fluorescence microscopy on tissue specimens, significant concentrations of nanotubes were found only in the liver at 24 h after intravenous administration. The results were compared with those from a report by Singh *et al.* [56], in which they chemically functionalized CNTs and covalently linked a chelating radioactive tracer ($^{111}$In). In the report by Singh *et al.* intravenous administration of the functionalized SWNTs in mice led to efficient uptake and clearance by the kidneys, with much less accumulation in the liver and other organs. These different results were argued by the intrinsic NIR fluorescence of SWNTs allows unambiguous observation of unmodified nanotubes while the use of linked fluorophores or radioactive labels requires covalent derivatization and relies on *in vivo* stability of the linking structure for valid tracking.

Heller *et al.* applied both NIR fluorescence emission and Raman spectroscopy to study DNA-dispersed SWNT internalization mechanisms and SWNT intracellular distributions [1]. They found that upon addition to the cell media, DNA/SWNTs exhibited red-shifted fluorescence emission and a lower fluorescent/Raman tangential mode ratio relative to the starting material. The shift and relative decrease in fluorescence of nanotubes upon entering the cell is believed to be caused by environmental effects, including ion binding to the DNA backbone and a decrease in pH in the vicinity of the nanotube/DNA complex [60]. After 8 days in culture, nanotube spectra in 3T3 cells showed a marked decrease in the fluorescence relative to the Raman scattering, although the nanotubes continued to exhibit both types of emission and clearly showed that the SWNTs were localized in the perinuclear region of the fibroblasts. The perinuclear accumulation of DNA/SWNTs was confirmed by transmission electron microscopy. This finding suggested an endocytotic transport mechanism of DNA/SWNT complex into cytoplasm-bound vesicles without penetration of the DNA/SWNT complexes into the nuclear envelope.

Using the single particle tracking technique, Jin *et al.* [61] studied the endocytosis and exocytosis of SWNTs dispersed and functionalized with single-stranded DNA (DNA/SWNTs). Since SWNT emission undergoes no observable photobleaching and cells do not autofluorescence in the NIR region, they were able to completely map the pathway involved in cellular uptake for the first time by continuously tracking over 10 000 trajectories for up to 340 min. They found that the

rates of endocytosis and exocytosis of DNA/SWNTs are closely monitored and regulated by the cell itself, which is expected based upon the known mechanism for the recycling of membrane receptors [62]. The observed exocytosis shows that the DNA/SWNTs can be recycled back onto the membrane together with their receptors. Endocytosis rate is highest initially and the exocytosis rate is closely matched with a negligible temporal offset. Only recently it was found that gold nanoparticles of diameters from 14 to 100 nm undergo exocytosis following a linear relationship to size, with the larger particles less likely to be exocytosed [63]. This self-regulated mechanism and the lack of persistent accumulation of SWNT keeps the concentration below the cytotoxicity level, thus explaining why there is no apparent cytotoxicity observed for many nanoparticle systems even after chronic exposures [53, 54, 64]. The identification and mapping of the endocytosis, intracellular trafficking, and exocytosis have significant implications for the use of CNTs in biological systems.

UV/visible luminescence of functionalized CNTs in liquid phase has been reported [65]. Such luminescence seems to be an intrinsic property of CNTs and becomes pronounced following their functionalization [65]. Riggs *et al.* [66] have proposed that the visible luminescence of functionalized CNTs is due to the extended π-conjugated electronic structure of the carbon backbone and the trapping of excitation energy at various defect sites. The better the dispersion and functionalization of the CNTs, the more intense the luminescence emissions. This phenomenon has been exploited to evaluate dispersion and aggregation state of functionalized CNTs. It is also used to characterize the complexation between positively charged functionalized CNTs and plasmid DNA [67]. Recently, this intrinsic optical property of functionalized CNTs was used to systematically study the mechanism of cellular uptake and intracellular localizations of the functionalized CNTs [68].

### 7.4.2 *In Vitro* and *In Vivo* Molecular Detection and Imaging

Based on the properties of the SWNT NIR fluorescence, there are three main transduction mechanisms for molecular detection. The first approach is based on the intrinsic bright NIR fluorescence. The construction of the sensor is similar to the widely used immunoassay sandwich structure. The second approach is based on the fact that the band gap structure of SWNTs is sensitive to their local dielectric environment. The third sensing mechanism depends on the quenching capability of CNTs. In this approach, both metallic and semiconducting tubes can be used to construct a sensing complex. However, the first two approaches are limited to semiconducting tubes.

#### 7.4.2.1 Molecular Detection and Imaging Based on the Intrinsic Near-IR Fluorescence: Immunoassay

By direct measurement of SWNT fluorophore emission in immunoassay formats, Dai *et al.* [45] reported the use of semiconducting SWNTs as NIR fluorescent tags

for selective probing of cell surface receptors and cell imaging. The high specific detection was achieved by modifying the SWNT surface with specific antibodies and high-molecular-weight (5400 Da) poly(ethylene glycol) (PEG) to block nonspecific binding in serum environments. The PEG also increased the water solubility and biocompatibility of the SWNTs. In this work, a Rituxan antibody, which is specific for the mature B cell membrane receptor CD20, or a Herceptin antibody, specific for a receptor known as HER2/*neu* found on breast cancer cell membranes, were conjugated on the distal end of the PEG chain. The selective SWNT/antibody binding to cells was detected by imaging the intrinsic NIR photoluminescence of nanotubes. The NIR photoluminescence emission spectrum of a solution of SWNT/antibody conjugates under 785-nm laser excitation showed peaks in the 1000- to 1600-nm region (Figure 7.4). These peaks were due to photoluminescence of SWNTs in the high-pressure carbon monoxide (HiPCO)

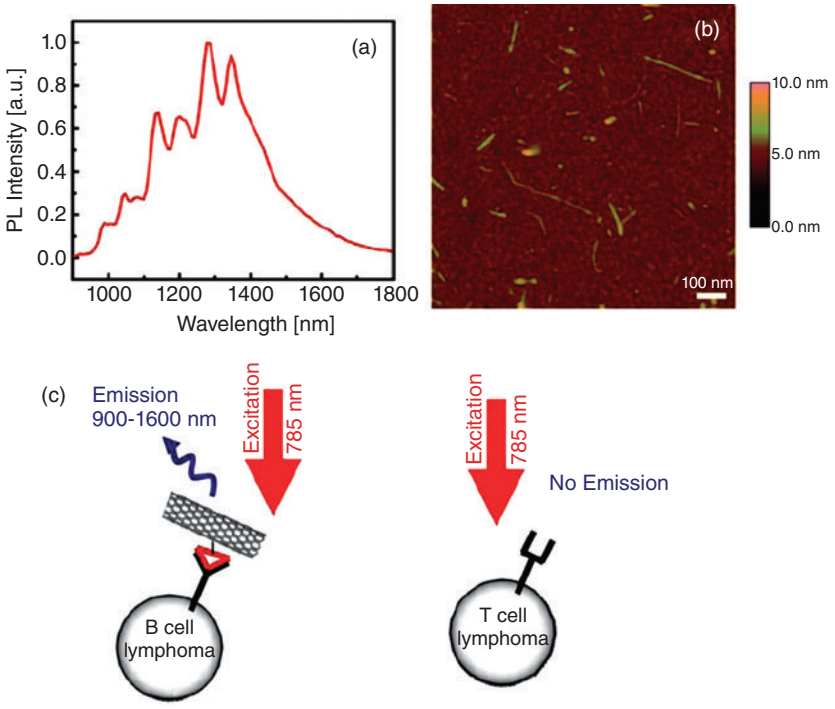


**Figure 7.4** (a) NIR photoluminescence (PL) spectrum of SWNT/Rituxan conjugate, showing typical SWNT emission peaks. (b) Atomic force microscopy image of the PEGylated SWNTs. The average SWNT length was around 83 nm. The average SWNT diameter was found to be 1.6 nm, which is consistent with HiPCO SWNTs (average diameter 0.7–1.1 nm) that have been well PEGylated. (c) Schematic of NIR photoluminescence detection of SWNT/Rituxan conjugate selectively bound to CD20 cell surface receptors on B-cell lymphoma (left). The conjugate is not recognized by T-cell lymphoma (right). (Reproduced from [45] with permission.)

materials with certain chiralities (i.e., the [10, 3], [19, 5], and [9, 7] SWNTs) in resonance with the 785-nm laser [4]. High sensitivity was achieved based on the strong NIR fluorescence of SWNTs and negligible background signals due to autofluorescence of cells in the NIR region. Therefore SWNT as NIR tags may allow for highly sensitive detection of low expression levels of cell surface proteins, which could be valuable in various biological and medical applications such as disease diagnosis and assessment of response to therapy at the cellular level. It is worth mentioning that highly hydrophilic and inert functionalization of SWNTs to afford no nonspecific binding in biological system is critical to develop SWNT NIR spectroscopic tags. This differs from the direction of developing SWNT as molecular transporters for intracellular delivery, for which nanotubes exhibiting high nonspecific binding to a wide range of cells are needed to facilitate cellular binding and subsequence internalization/uptake via endocytosis [3, 42]. This strategy of high-degree PEGylation followed by ligand or antibody conjugation can be used for selective binding to specific cells for *in vitro* and *in vivo* imaging and targeted delivery applications [38, 42, 55].

To further increase the imaging sensitivity, Dai *et al*. produced brighter and biocompatible SWNTs for *in vivo* imaging. They first debundled pristine SWNTs with nonbiocompatible surfactants in sodium cholate. It has been demonstrated that this dispersion approach can produce SWNTs suspension with much higher quantum yield (brighter) because a better isolation of the bundled SWNTs was achieved and the intrinsic conjugation structure of SWNTs was largely kept during sonication. To render the brighter SWNTs with biocompatibility for *in vivo* specific imaging, they then displaced the sodium chlorate with a phospholipid–PEG [69]. Compared to the SWNTs directly dispersed in phospholipid–PEG, the relative quantum yield of the resulting SWNT solutions increased more than one order of magnitude, while still maintaining the high biocompatibility – a characteristic of SWNTs functionalized by phospholipid–PEG. Importantly, a near-zero autofluorescence background was observed in the SWNT emission range (1100–1700 nm). Using these bright, low-background, and biocompatible SWNTs to perform whole-animal NIR photoluminescence imaging, they demonstrated that SWNT dosage was largely decreased (10 times) compared to that when using SWNTs directly suspended in phospholipid–PEG. These bright and biocompatible SWNTs also made possible high-resolution intravital tumor vessel imaging through thick skin in a live mouse.

#### 7.4.2.2 Near-IR Photoluminescence Transduction Based on Band Gap Modulation of Single-Walled Carbon Nanotubes

The electronic band gap that is the origin of the distinctive NIR photoluminescence is sensitive to the local dielectric environment around the SWNT, but remains stable to permanent photobleaching, and this property was exploited in chemical sensing [45, 70–73]. Strano *et al*. have pioneered this sensing mechanism for the use of SWNTs as fluorescent optical sensors for molecular detection within living cells and tissues. Adding divalent metal ions into DNA/SWNT solution induced a DNA secondary structure transition from an analogous B to Z confor-

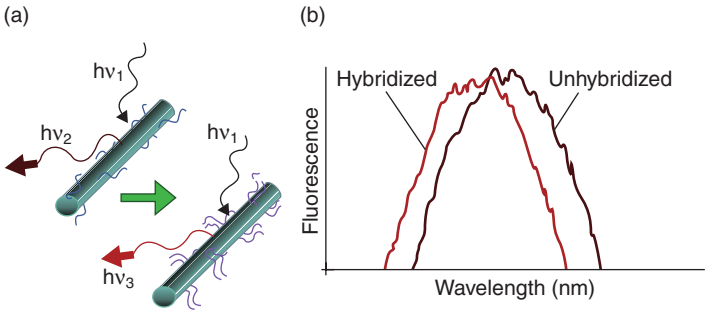


**Figure 7.5** (a) Schematic drawing for NIR fluorescent detection of DNA hybridization on the surface of solution suspended s SWNTs through a SWNT band gap fluorescence modulation. (b) Hybridization of a 24-mer oligonucleotide sequence with its complement produces a hypsochromic shift of 2 meV, with a detection sensitivity of 6 nM. (Reproduced from [72] with permission.)

mation on the tubes. This conformational change modulated the dielectric environment of the SWNTs and decreased their NIR emission energy up to 15 meV [72, 74] (Figure 7.5). This fluorescence signal change has been used to detect divalent metal cations that bind to DNA and stabilize the Z form of DNA. More importantly, the detection can be performed in blood and muscle tissues due to the intrinsic NIR photoluminescence of SWNTs. The team has also studied hybridization, and hybridization kinetics of DNA physically wrapped around SWNTs was also studied by detecting the unique SWNT NIR fluorescence and the optical modulation of the fluorescence upon DNA hybridization [73, 75]. These studies are important for developing DNA sensors which can be used *in vitro* and *in vivo*.

A NIR optical glucose sensor for real-time, constant monitoring of blood glucose concentrations was developed [71], which is very different from the previously reported CNT-based glucose sensors [76, 77]. In this sensor, SWNTs as NIR fluorophores were initially suspended in aqueous solution with a phenoxy-derivatized dextran, which is a polysaccharide that functions as a glucose analog. Adding concanavalin A (Con A) at pH 7.4 into this solution results in aggregation of the dextran–nanotube complexes because each Con A has four saccharide binding sites. The formation of the aggregation also in the same time decreased photoluminescence of the SWNT due to energy transfer effects. When glucose was introduced to the aggregated dextran–nanotube complex solution, due to the competitive binding between the glucose and dextran for Con A-binding sites, the SWNT aggregates dissociated and the SWNT photoluminescence recovered due to the dissolution. These results demonstrated the first solution-phase-affinity glucose sensor based on SWNT photoluminescence.

In a different approach, coadsorption of glucose oxidase and ferricyanide $[Fe(CN)_6^{3-}]$ on the surface of SWNTs was used to develop another NIR optical glucose sensor [70]. The enzyme has multiple functions, which include the

prevention of SWNTs from aggregating and also for catalyzing the reaction of glucose to glucono-1,5-lactone with a $H_2O_2$ coproduct. $[Fe(CN)_6^{3-}]$ can irreversibly adsorbs onto the SWNT surface and alter the electron density of the SWNT, and thus its NIR fluorescence. Partial reduction of the $[Fe(CN)_6^{3-}]$ on the SWNT surface due to the $H_2O_2$ at 37° C and pH 7.4 can reversibly couple the CNT NIR fluorescence to the glucose concentration. They integrated this sensor to a capillary device, which has the potential for implantation into thick tissue or whole-blood media for real-time monitoring of glucose fluctuation *in vivo*.

Nitric oxide (NO) is a ubiquitous messenger in the cardiovascular and nervous systems. However, it is difficult to detect directly *in vivo* with high spatial and temporal resolution, because of its large diffusivity and high reactivity with other radicals and metal-containing proteins in biological systems. The Strano group designed and developed SWNT- based sensors for *in vitro* and *in vivo* imaging of NO (Scheme 7.5) [78]. The SWNTs were wrapped and functionalized with

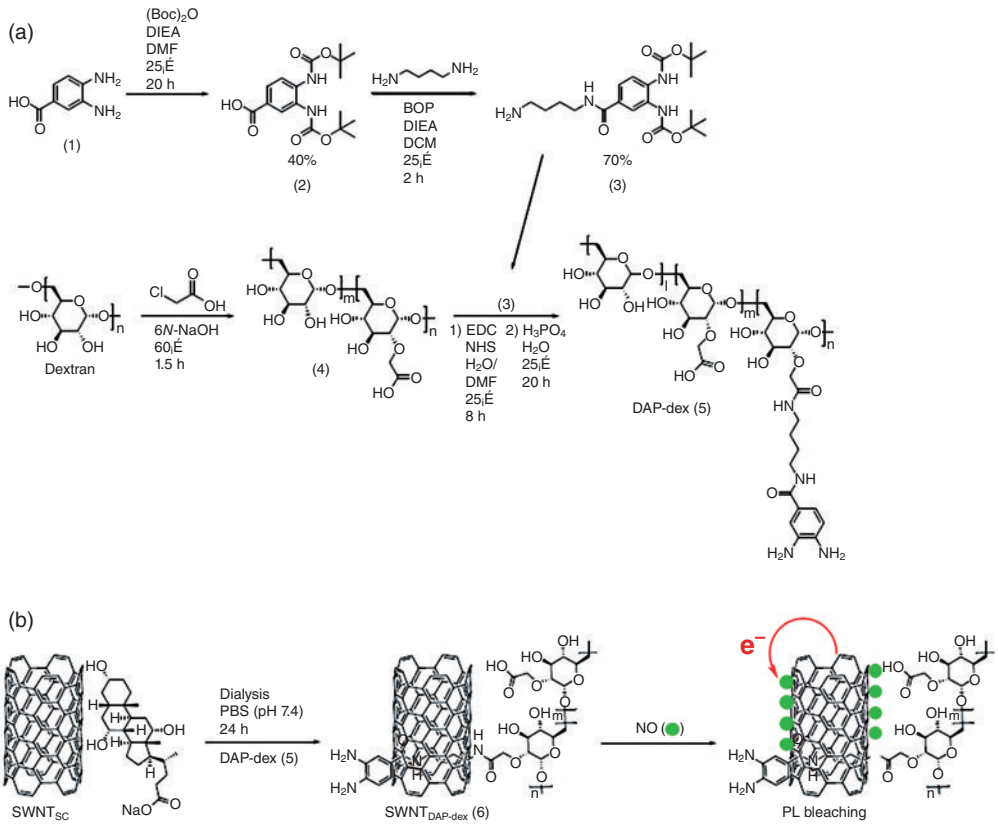


**Scheme 7.5** Schematic illustration for NO detection using SWNT/polymer hybrid. (a) Synthesis of DAP-dex. (b) Preparation of SWNT/DAP-dex hybrid via dialysis and mechanism for NIR fluorescence bleaching by NO. (Reproduced from [78] with permission.)

3,4-diaminophenyl functionalized dextran (DAP-dex), which confers the SWNTs with more electron density by the donation of lone-pair electrons from the amine groups. The detection of NO is based on the rapid bleaching in the NIR fluorescence of SWNT/DAP-dex by NO, but not by other reactive nitrogen and oxygen species. This bleaching is reversible and shown to be caused by electron transfer from the top of the valence band of the SWNT to the lowest unoccupied molecular orbital of NO. The resulting optical sensor is capable of real-time and spatially resolved detection of NO produced by stimulating NO synthase in macrophage cells. In this work, they also demonstrated the potential of the optical sensor for *in vivo* detection of NO in a mouse model.

In another work, they modified SWNTs with an enzyme, luciferase, for NIR fluorescent detection of ATP – a universal energy storage molecule in an organism [79]. In the luciferase-modified SWNTs, the ATP reacts at the luciferase enzyme in the presence of D-luciferin and $Mg^{2+}$, and produces oxyluciferin, which selectively quenches the NIR fluorescence, thus the ATP was detected (Scheme 7.6). The SWNT/luciferase sensor is very selective to ATP, but not to AMP, ADP, CTP, and GTP, and is also able to detect ATP temporally and spatially in living HeLa cells. This is the first SWNT-based optical sensor for the detection of ATP in living cells.

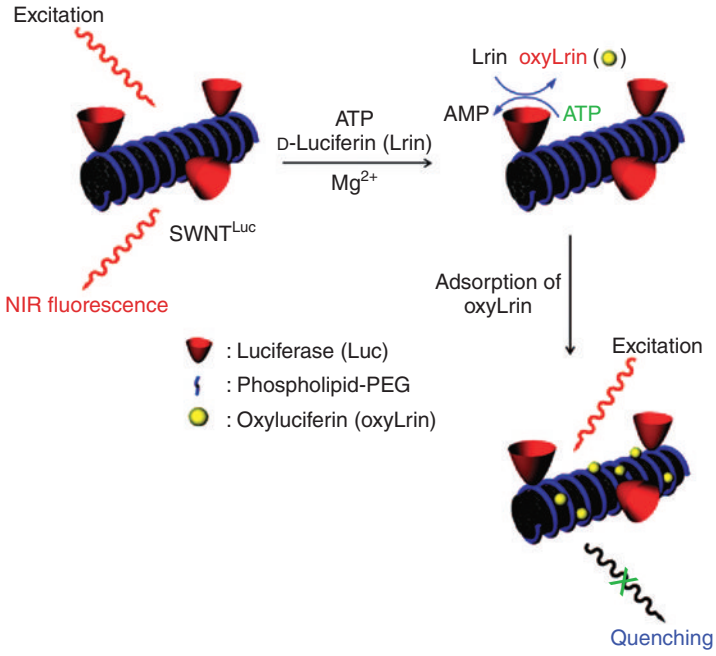


**Scheme 7.6** Schematic illustration of SWNT/luciferase sensor for ATP detection. (Reproduced from [79] with permission.)

Recent developments have extended the detection limit down to the single-molecule level by analyzing the stepwise quenching of excitons as molecules adsorb to the SWNT surface [80, 81]. Very recently, Strano's team developed an array of such single-molecule sensors for selectively imaging $H_2O_2$ in real-time and with spatial precision [82]. It can discriminate $H_2O_2$ signals generated at the membrane (near-field) from those originating from the cell interior (far-field) by mathematic data treatment. Using this sensor array, they successfully measured the signaling activity of epidermal growth factor receptor on single A431 cells and found that $H_2O_2$ generation is epidermal growth factor receptor-mediated; 2 nmol of $H_2O_2$ can be produced over a period of 50 min in A431 cells and all the $H_2O_2$ was produced on the cell membrane not inside the cells.

Remarkably, the single-molecule-level detection was recently extended for simultaneous detection of several species within living cells [83]. The principle for the development of the multimodal optical sensor is based on the different mechanisms that the electronic structure of SWNTs was modulated upon molecular adsorption. It also based on the fact that SWNTs with different chiralities respond differently for the same molecular species. Strano's team demonstrated the concept using a mixture of SWNTs with chiralities of (6, 5) and (7, 5). This mixture provides at least four modes that can be modulated to uniquely fingerprint agents by the degree to which they alter either the emission band intensity or wavelength. They validated this identification method *in vitro* by demonstrating the detection of six genotoxic analytes, including chemotherapeutic drugs and reactive oxygen species, which were spectroscopically differentiated into four distinct classes. The results from this work demonstrate that SWNTs can be used to develop a multiplexed, able free optical sensor. The specificity and versatility of detection suggest significant and numerous diagnostic and metrologic applications for this approach.

#### 7.4.2.3 Other Sensing and Imaging Mechanisms

In addition to quenching of the inherent SWNT band gap fluorescence for sensor applications, specific detection of biomolecules by quenching may also be realized by applying the CNT as both a scaffold for recognition ligands and as a quencher of molecule fluorophores. Tan *et al.* have presented major contributions for this sensing regime. An excellent example of their works is a novel "turn-on" DNA sensor [84]. A novel oligonucleotide/SWNT complex was constructed by self-assembly. The key component of this complex is the hairpin-structured fluorescent oligonucleotide that allows the SWNT to function as both a "nanoscaffold" for the oligonucleotide and a "nanoquencher" of the fluorophore conjugated on the oligonucleotide molecule (Scheme 7.7). Competitive binding of the target DNA with the oligonucleotide/SWNT complex results in the release of the fluorophore from the CNT surface, resulting in a dramatic fluorescence increase. In contrast to the common loop-and-stem configuration of molecular beacons, this novel oligonucleotide/SWNT complex needs only one fluorophore label, yet the emission can be measured with little or no background interference. They claimed that this property can greatly improve the signal-to-background ratio compared with

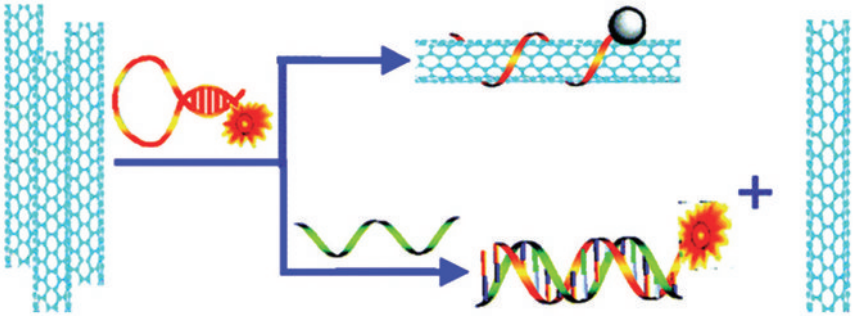

**Scheme 7.7** Schematic illustration of SWNT quenching-based DNA sensor. (Reproduced from [84] with permission.)

those for conventional molecular beacons, while the DNA-binding specificity is still maintained. Additionally, this new class of beacon affords improved thermal stability and is general to a wide variety of fluorophores [85, 86]. This CNT complex represents a new class of universal fluorescence quenchers that are substantially different from organic quenchers, and should therefore have many applications in molecular engineering and biosensor development.

## 7.5
## Raman Scattering of Carbon Nanotubes

Raman spectroscopy is one of the most widely used spectroscopic techniques for analyzing electronic, structural, vibrational, and rotational modes in a system. When light interacts with a molecule, the electron orbits of the molecule are perturbed periodically with the same frequency as the electric field of the incident wave. This causes an oscillating induced dipole moment where charge separation within the molecule occurs, thus resulting in scattered light. Most of the light that is scattered is at the same frequency as the incident light – a process known as elastic scattering or Rayleigh scattering. However, some scattering results in emitted light with different frequencies, known as inelastic scattering. Raman scattering is an example of inelastic scattering where the scattered photons have a frequency that is different from the frequency of the incident photons. Scattered photons with higher frequencies compared with the incident photons are known as anti-Stokes Raman scattering and scattered photons with lower frequencies compared with the incident photons are known as Stokes Raman scattering. In a Raman spectrum, the change in frequencies between the excited and ground states are observed in the form of Stokes scattering.

Raman scattering normally produces small intensities of Stokes- and anti-Stokes-scattered light from a molecule that exhibits anisotropic polarizability. CNTs, however, produce strong, resonance-enhanced Raman bands at 150–300, 1590–1600, and around 2600 $cm^{-1}$, which are far away from the excitation wavelength

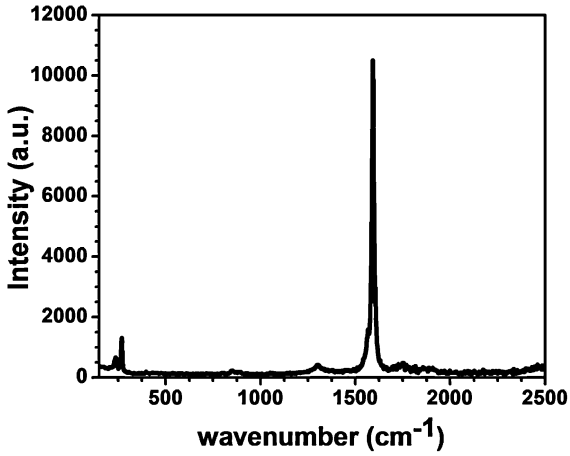


**Figure 7.6** Typical Raman spectrum of SWNTs.

(Figure 7.6). The bands at 150–300 $cm^{-1}$, called the radial breathing mode (RBM) vibration, is an out-of-plane phonon mode where the carbon atoms move in the radial direction. The RBM is a unique phonon mode of SWNTs, which is a direct indication of a CNT sample containing SWNTs. The RBM frequency is inversely proportional to the CNT diameter [87]. This phonon mode is normally used to determine and characterize the chirality of SWNTs [17–22]. Although it is possible to use the RBM signal to map the SWNT distribution within a biological sample, it is difficult to get a detailed image due to the relatively low intensity of the signal. The G-band originates from the tangential stretching motion of the carbon atoms in the nanotubes [18]. Due to the high intensity of this peak, which is normally located at 1590–1600 $cm^{-1}$, it is widely used for detection of SWNTs within cells and living animals with high sensitivity. Different from the NIR fluorescence, which was only emitted by semiconducting SWNTs, intense Raman scattering was demonstrated on both metallic and semiconducting SWNTs. The scattering exhibits resonance enhancement when incident light coincides with an optical transition of the nanotube, the Raman cross-sections can reach $5.7 \times 10^{-21}$ $cm^2 sr^{-1}$ $molecule^{-1}$ for a 1-μm nanotube excited at 785 nm, which is the highest known cross-section for single molecules. Due to the high Raman scattering cross-section of SWNTs and resonance enhancement at NIR absorption transitions, Raman scattering of nanotubes is easily detectable and unmistakable. Furthermore, it does not blink or quench and will not diminish under prolonged excitations. Although the RBM behaves similar to NIR fluorescence of SWNTs, and is sensitive to bundling of nanotubes and dielectric coating on the surface of nanotubes, the intensity of the G-band is relatively insensitive to the diameter and bundling of nanotubes [7, 13]. It is also relatively insensitive to the type of noncovalent coatings and solution environment of SWNTs, which is in contrast with the NIR fluorescence of SWNTs.

### 7.5.1 Molecule Sensing and Imaging Based on Carbon Nanotube Raman Scattering

To avoid the issues plaguing SWNT photoluminescence-based detection, Dai's group utilized the intense Raman scattering cross-section of SWNTs in an immunoassay format [10]. The surface modification methodology was similar to the fluorescence-based sandwich assays [88–90]. Combined with surface-enhanced Raman, by depositing a layer of gold on the CNTs, the detection sensitivity was extended to 1 fM – a three-order-of-magnitude improvement over most reports of fluorescence-based detection. Very recently, we constructed a anti-HER2 IgY/SWNT complex by chemically conjugating anti-HER2 IgY onto the surface of microwaved functionalized SWNTs [43]. The resulted complex was shown to successfully detect and destroy HER2-expressing breast cancer cells *in vitro*. Raman spectroscopy was used to detect the specific binding of the IgY antibody moiety from the complex to the HER2 receptor on the cancer cells. We demonstrated that single cancer cells can be detected and selectively eradicated while leaving the nearby normal cells unharmed. The major difference from previous reports is that internalization by cancer cells is not required in order to achieve the selective photothermal ablation, thus offering the advantage of being more easily extended to other cancer types.

Multicolor multiplexed molecular imaging and cellular detection is desired in order to simultaneously map out different species. Ideally, multicolor imaging of various molecular targets can be achieved with a single excitation, while both excitation and emissions in the narrow NIR range. Multicolor fluorescence imaging has been reported using different fluorescent dyes or QDs with excitations/emissions in the visible to NIR range (400–900 nm). However, the fluorescence peaks from fluorescent dyes or QDs are normally broad with FWHM as large as 50–100 nm; therefore the imaging multiplicity is limited due to their spectral overlay [91–93]. In addition, even though autofluorescence of a biological sample is low in the NIR region, it still exists and varies between different organs [51], so reliable fluorescence-based imaging still needs complex algorithms to differentiate the background [92]. In high contrast, SWNTs have a single, narrow Raman G-band peak with FWHM < 2 nm, allowing for high degrees of multiplicity. The multicolor Raman imaging was achieved by using SWNTs with different isotope compositions, which displayed well-shifted Raman G-band peaks, and served as different colors for Raman imaging. Cancer cells with specific receptors are selectively tagged with three different "color" SWNTs to realize multiplexed simultaneously imaging (Figure 7.7) [11]. Recently, multiplexed five-color molecular imaging of cancer cells and tumor tissues has been performed in the NIR region. Near-zero interfering background of imaging is achieved due to the sharp Raman peaks unique to nanotubes over the low, smooth autofluorescence background of biological species [12].

It is worth mentioning that the various SWNT Raman colors can easily be excited with a single light source. Although previous work has shown that Raman tags based on molecules and metal nanoparticle complexes can be used

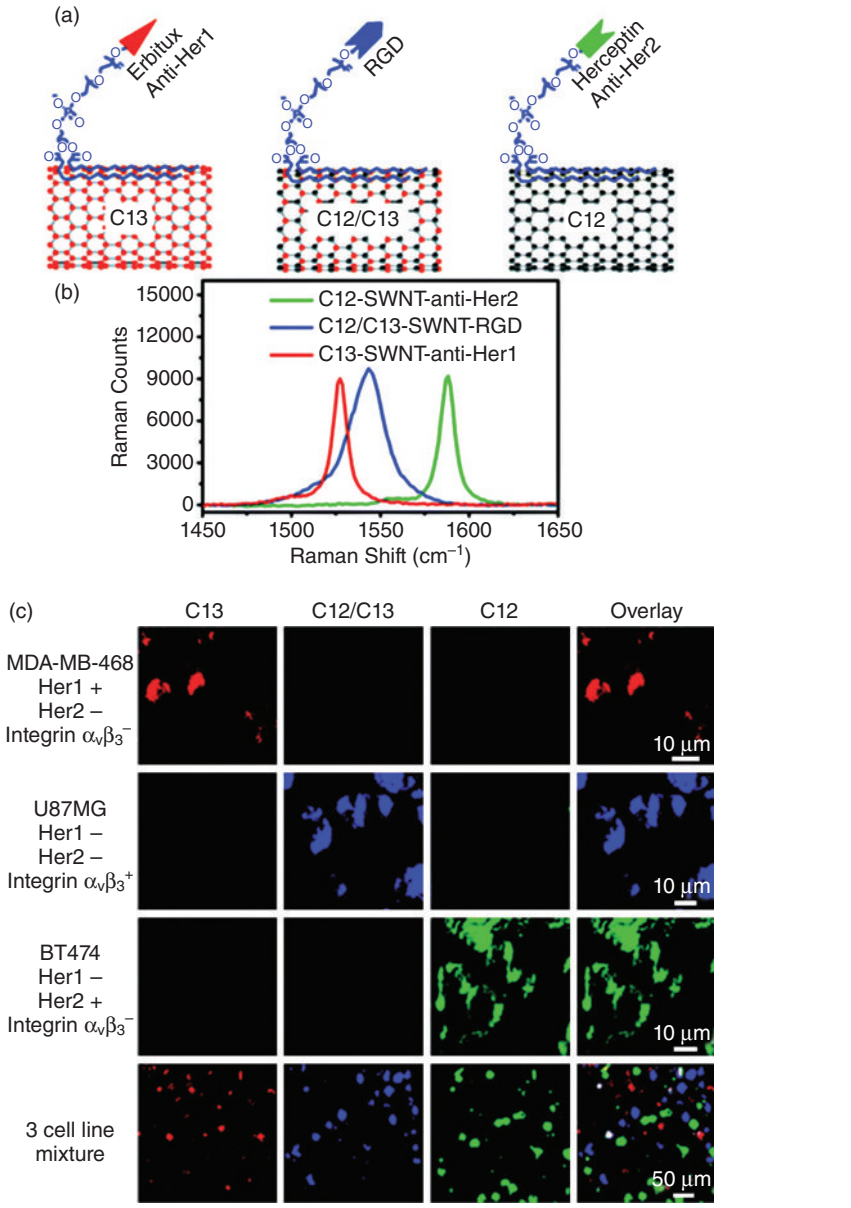


**Figure 7.7** (a) Schematic drawing showing SWNTs with three different isotope compositions conjugated with different targeting ligands. (b) Solution-phase Raman spectra of the three SWNT conjugates under a 785-nm laser excitation. (c) Deconvoluted confocal Raman spectroscopy images of three different cell lines after incubation with a mixture of the three-color SWNTs (top three rows, red, blue, and green colors are Raman intensities of C12, C12/C13, and C13 SWNTs, respectively). In the bottom row, a mixture of three cell lines was incubated with the three-color SWNT mixture. (Reproduced from [11] with permission.)

for multiplexed imaging with many colors [94, 95], nanotube Raman tags are advantageous over common Raman dye molecules. As mentioned earlier, the nanotube Raman signals are very stable and no quenching or bleaching was found under a wide range of imaging conditions [1]. Furthermore, the simple Raman spectrum of SWNTs and the large sharp G peak in the spectrum enables us to easily distinguish SWNT Raman signals from the low and slowly changing autofluorescence background. Thus, a "background-free" optical imaging can be easily achieved with high imaging and detection sensitivities. However, taking a Raman spectrum requires a longer time than a fluorescence spectrum, which may limit the Raman imaging approach for practical applications. Recently, a novel nonlinear Raman measurement technique [96] has been reported that may potentially reduce acquisition time, bringing hopes for practical application of the multiplexed SWNT Raman labels.

### 7.5.2
### Study of Internalization, *In Vitro* Cellular and *In Vivo* Tissue Biodistribution, and Long-Term Fate

Taking advantage of the intrinsic Raman signatures of SWNT, which does not decay over time while being relatively insensitive to the environment of SWNTs, Dai *et al.* [3] studied the ability of SWNTs to uptake into human T cells and primary cells as a function of chain length and terminal groups of PEG on SWNTs. They found that hydrophobic interaction is the most important driving force for the SWNT internalization. With longer PEG chain, the surface of SWNTs becomes more hydrophilic and more difficult to internalize into cells.

Recently, they also studied *in vivo* blood circulation and long-term (3 months) fate of CNTs intravenously injected into mice [97]. *Ex vivo* Raman microspectroscopy was used to track them for a long period of time with high fidelity, without the concern of labels falling off or decay over time. They found that the surface chemistry of nanotubes is critical to their *in vivo* behavior. Longer PEG chains, especially those with branched structures enabled low uptake in the reticuloendothelial system (RES). The SWNT blood circulation was up to 1 day, which is by far the longest circulation time that has been reached for nanomaterials. In around 2 months, the SWNTs were almost completely cleared out from the main organs (Figure 7.8) and no toxic side-effect of SWNTs was observed, which warrants safe *in vivo* biomedical applications in the very near future. Furthermore, using Raman spectroscopy, SWNTs were detected in the intestine, feces, kidney, and bladder of mice, indicating that the excretion and clearance of SWNTs from mice may be via biliary and renal pathways (Figure 7.9).

In another work, Dai *et al.* [55] linked an RGD peptide to a PEG-functionalized SWNT to study *in vivo* the accumulation of SWNTs in mice bearing tumors that express $\alpha_v\beta_3$ on their surfaces. *In vivo* PET and *ex situ* Raman microscopy demonstrated that SWNT accumulation in tumor can reach around 13% ID $g^{-1}$ over long periods (24 h), which is the best achieved for a nanomaterial (Figure 7.10). The unique one-dimensional shape and flexible structure of SWNTs enables

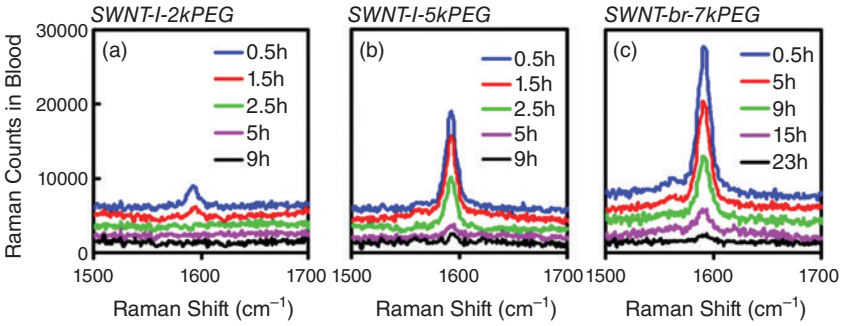


**Figure 7.8** Raman spectra of blood samples drawn from BALB/c mice at various time points after injection with SWNT/l-2kPEG (a) SWNT/l-5kPEG (b), and SWNT/br-7kPEG (c) solutions, respectively. (Reproduced from [98] with permission.)

polyvalency effect and enhances tumor binding affinity. The one-dimensional shape may also facilitate SWNTs leaking out from blood microvessels to reach cancer cells in the tumor through vascular and interstitial barriers [99].

In a similar context, Zavaleta *et al.* [98] used Raman spectroscopy to evaluate tumor targeting and localization of RGD-functionalized SWNTs introduced intravenously in mice. The results revealed increased accumulation of RGD/SWNTs in tumors as opposed to the case if SWNTs alone were introduced to the mice. RGD nanotubes accumulate in the tumor slightly over time in contrast to plain nanotubes where the concentration decreases dramatically after 20 min postinjection (Figure 7.11a). Furthermore, *in vivo* and *ex vivo* experiments show that the G-band is prominent for mice that received RGD-conjugated nanotubes and no G-band is visible for mice that received nontargeted plain nanotubes (Figure 7.11b).

Taking advantage of their large surface area, small size, and the unique needle-shaped structures, many studies have also focused on using SWNTs as targeted drug delivery vehicles [43, 100, 101]. Recently, Dai *et al.* constructed a water soluble SWNT/paclitaxel (PTX) complex by conjugating PTX, a widely used cancer chemotherapy drug, to branched PEG chains on SWNTs via a cleavable ester bond [102]. They found that SWNT/PTX had a much higher efficacy in suppressing tumor growth than clinical taxol in a murine 4 T1 breast cancer model. Compared to Taxol and PEGylated PTX, the SWNT/PTX complex led to higher tumor uptake of PTX and higher ratios of tumor to normal organ PTX uptake, which is highly desired for higher treatment efficacy and lower side-effects. Pharmacokinetics and biodistribution of SWNTs with and without PTX conjugation were studied by the intrinsic Raman scattering property of SWNTs without relying on radiolabels or fluorescent labels [55, 59, 103]. They found that the SWNT/PTX has much shorter blood circulation half-lives (around 1.1 h) compared to the PEGylated SWNTs without PTX attachments (3.3 h) (Figure 7.12). It seems that the high hydrophobicity of PTX reduces the hydrophilicity and biological inertness of the branched

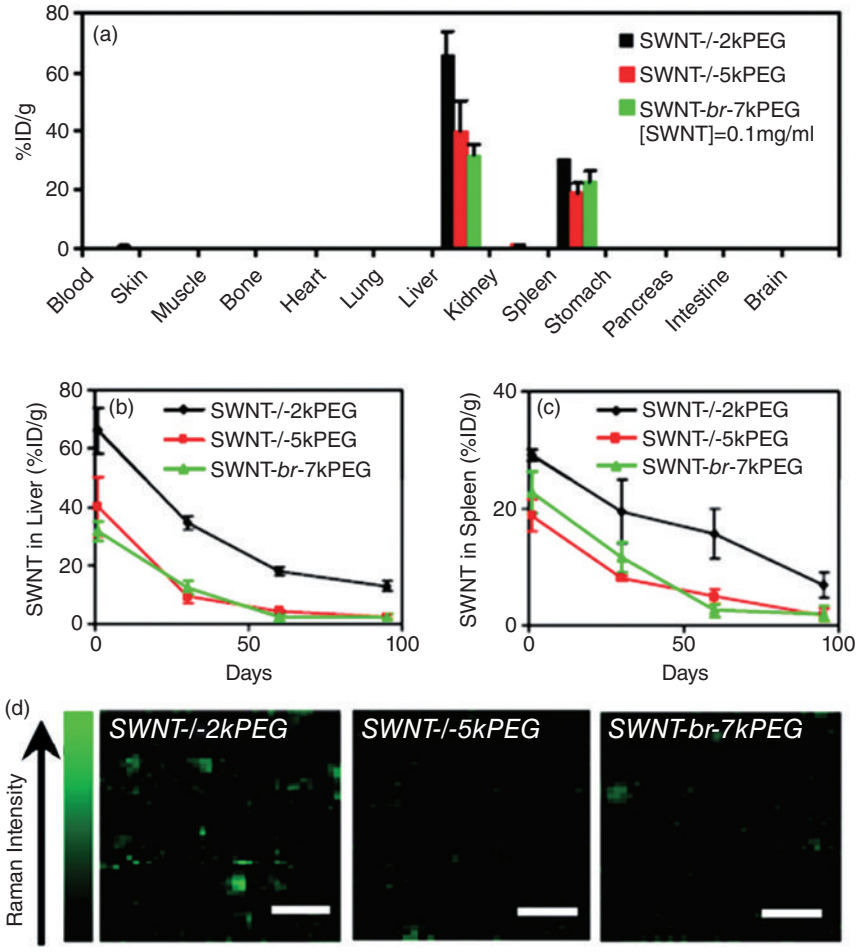


**Figure 7.9** SWNTs in mice tissues probed by *ex vivo* Raman spectroscopy after injection into mice. (a) Biodistribution of SWNT/l-2kPEG, SWNT/l-5kPEG, and SWNT/l-7kPEG, respectively, measured by Raman spectroscopy. (b and c) Evolution of the concentrations of SWNTs retained in the liver and spleen of mice over a period of 3 months. (d) Raman mapping images of liver slices from mice treated with (left) SWNT/l-2kPEG, (center) SWNT/l-5kPEG, and (right) SWNT/l-7kPEG at 3 months postinjection. (Reproduced from [97] with permission.)

PEG-functionalized SWNTs. The increased hydrophobicity results in more nonspecific protein adsorption on the nanotube conjugates, which accelerated the uptake by macrophages in RES organs. Nevertheless, this is the first successful report to use CNTs as drug delivery vehicles that achieved dramatic *in vivo* tumor treatment efficacy with mice.

Recently, Keren *et al.* [94] developing a new Raman spectroscopy instrumentation that extended the Raman imaging capability from *ex vivo* to whole-body deep

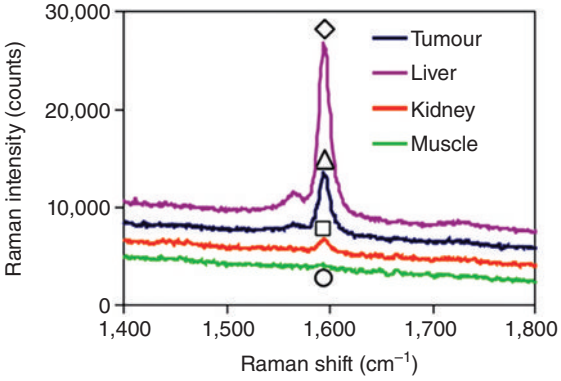


**Figure 7.10** Raman spectra in the G-band region of SWNTs recorded on lyophilized tumor and tissue powder samples suspended in surfactant solutions. (Reproduced from [55] with permission.)

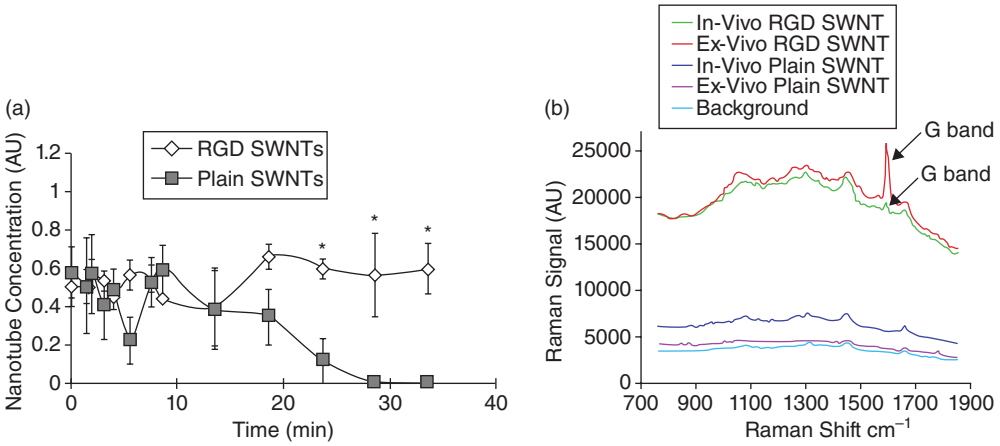


**Figure 7.11** (a) Pharmacokinetics of RGD/SWNTs ($n = 3$) and plain nontargeted SWNTs ($n = 3$) in the tumor of nude mice over time. (b) Raman spectrum acquired from *in vivo* (red) and *ex vivo* (green) tumors at 72 h from mice that received RGD nanotubes, and *in vivo* (blue) and *ex vivo* (purple) tumors from mice that received nontargeted nanotubes. (Reproduced from [98] with permission.)

tissue *in vivo* imaging of small living animals (Figure 7.13). This development can lead to faster image acquisition times, the potential to estimate signal depth, and, eventually, tomographic imaging. More promisingly, multiplexed multicolor Raman imaging of live cells with SWNTs was recently demonstrated [11, 12]. This new, highly sensitive, and noninvasive Raman instrumentation along with SWNTs' strong and multicolored Raman signal holds significant potential for biomedical imagining in living subjects.

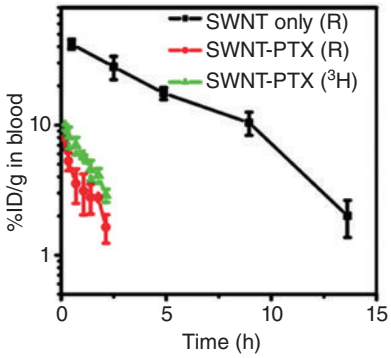


**Figure 7.12** Blood circulation data of SWNT with (red curve) and without PTX conjugation (black curve) measured by Raman detection of SWNTs in blood samples. Blood circulation data for SWNT/[$^3$H]PTX (green curve) were also obtained by scintillation counting of $^3$H radioactivity in blood. (Reproduced from [102] with permission.)

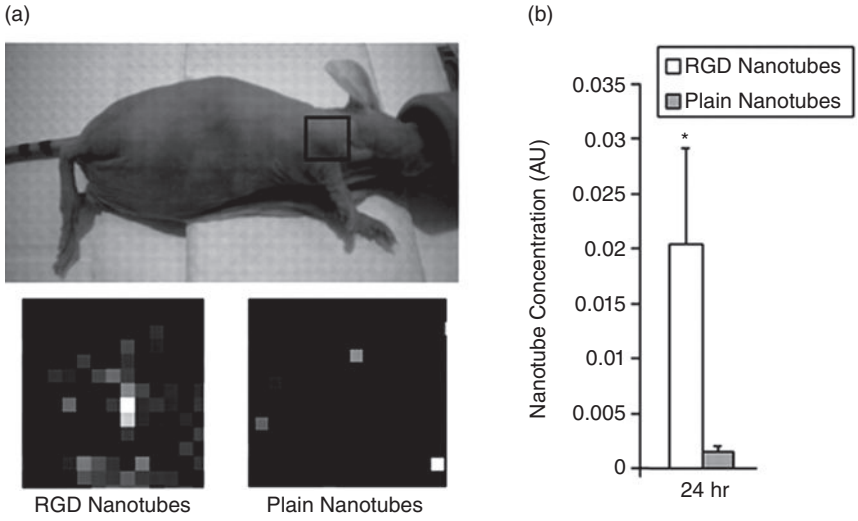


**Figure 7.13** (a) Digital photograph of a mouse depicting tumor area (black square) and corresponding Raman images acquired 24 h after SWNT injection by raster scan with 750-μm steps. Notice the accumulation of RGD/SWNTs in the tumor area as opposed to the plain nontargeted SWNTs that show little to no accumulation in the tumor area. (b) Raman spectral analysis of RGD/SWNTs and plain nontargeted nanotubes within the tumor at 24 h after SWNT injection. The graphed data show a significant increase ($^*P < 0.05$) in Raman signal in mice ($n = 3$ per group) injected with RGD/SWNTs as opposed to mice injected with plain nanotubes, thus indicating accumulation of RGD/SWNT at the tumor site. (Reproduced from [94] with permission.)

SWNTs are generally insoluble in aqueous solutions [104, 105]; however, surface functionalization can improve their solubility, biocompatibility, and thus processability [104]. Many different molecules with various functional groups can be attached to SWNT side walls, such as DNA [106, 107], polymers [108], and amino acids and peptides [109–111], for various applications. Covalent attachment of functional groups to SWNT side walls affects its electronic structure. Therefore, changes in the Raman spectrum are expected. Many have shown that covalent functionalizations of SWNT have led to a decrease in absolute Raman intensity [112–114]. Attachment of functional groups onto the SWNT side walls breaks the translational symmetry of the SWNTs and introduces defects with an irregular distribution of $sp^3$ carbon sites. Since the RBM mode is a symmetric radial phonon mode, a break in its symmetry would cause a decrease in its intensity on the Raman spectrum. Therefore, the RBM experiences a more pronounced change compared with the tangential modes [115–118]. The in-plane carbon–carbon vibrations would also be altered from introducing defect sites on the SWNT surface, thus G-band Raman intensity was also decreased. Furthermore, an additional band is usually seen in the Raman spectrum of functionalized SWNTs at around 1300 $cm^{-1}$. This peak, known as the D-band, is induced by defects on the SWNT. For a more comprehensive review of SWNT functionalization effects on the Raman spectrum, readers are referred to [2, 22, 119].

To further enhance the Raman signal intensity, besides using noncovalent functionalization of SWNT to preserve the SWNT electronic structure, thus retaining its intense Raman signals [43, 120, 121], surface-enhanced Raman scattering (SERS) was also proposed to further enhance the detection sensitivity. Since resonance Raman requires resonance between the excitation photons with the electronic transition over the band gap of the SWNTs, only the tubes' resonance with the excited laser wavelength can be detected and contribute to the Raman signals for molecular detection. The majority of the SWNTs in a sample cannot be detected using one excitation laser of fixed wavelength or even several wavelengths. After decoration of a layer of gold nanoparticles on the SWNT surface using an electroless deposition method, Li *et al.* demonstrated that all the SWNTs in a sample can be observed, including those nonresonant ones [122]. By depositing a layer of gold on CNTs by an evaporation method, Dai *et al.* also demonstrated that the Raman scattering intensity of SWNTs increased 60-fold [10]. They also demonstrated that the limit of protein detection was extended to the femtomolar level or below by coupling the intense resonance enhancement of one-dimensional SWNT Raman tags with SERS. Although this work focused on antibody–antigen interactions, the application of SWNT Raman tags can be extended for probing other protein–protein interactions and nucleic acid hybridization. Application of background-free, surface-enhanced, multicolor SWNT Raman labels may eventually enable simultaneous detection of multiple analytes in complex fluids, with 1 fM sensitivity in a multiplexed, arrayed fashion.

## 7.6 Conclusions and Outlook

Due to their unique shapes and remarkable optical properties, including their strong NIR absorption, stable, bright, and tunable NIR fluorescence, and their simple and sharp Raman scattering effects, CNTs show great potential for *in vitro* and *in vivo* molecular detection and imaging. However, several problems remain to be solved for future practical applications. As described in Section 7.1, conceptually, a single-walled CNT is a hollow cylinder formed by rolling up a graphene sheet made up of hexagonally bonded $sp^2$ carbon atoms. The direction and magnitude of a roll-up vector, denoted by chiral indexes (*n, m*), prescribe the chirality and diameter of the resulting tube. These geometric parameters in turn determine the electronic band structures of the tube, which serve as the foundation of the fascinating electronic and optical properties of the nanotubes. Recent studies demonstrated that the length of CNTs also impacts on the electronic structures, and therefore their NIR photoluminescence and Raman scattering [123, 124]. Furthermore, size also impacts CNT cell internalization and exocytosis, and biodistribution *in vivo* [125]. Tremendous progress has been made in CNT synthesis. However, most of the current synthesis technology normally produces a mixture of metallic and semiconductor tubes, with one-third of metallic tubes, which are known to be nonfluorescent. Furthermore, the existence of the metallic tubes could also quench the fluorescence emitted from the semiconducting ones, which further lowers the detection sensitivity. Physically separating different CNT structures through a room temperature solution-phase process into different electronic types and further into species with a specific chirality has drawn considerable attention over the past years. Tremendous progress has been made; however, large-scale production of the sorted SWNTs with single chirality and controlled lengths is still challenging [50, 126, 127]. Interested readers can consult several reviews papers and the cited reference articles in these review papers [127–129]. Since both NIR fluorescence and Raman imaging capabilities of CNTs are sensitively dependent on tube structures, the sensitivity can be largely improved by using well-sorted and length-controlled tubes.

Undoubtedly, CNTs may bring revolutionary strategies for molecular sensing and imaging both *in vitro* and *in vivo*, which may reveal untouchable fundamental biological issues and solve some current untreatable diseases. However, their potential toxic effects have become an issue of strong concern for the environment and for health. Such biomedical applications will not be realized if there is no proper assessment of the potential hazards of CNTs to humans and other biological systems. Tremendous amounts of work have been published on the toxicity of CNTs. However, the published data are inconsistent and widely disputed [55, 56, 59, 97, 130–140]. There is broad agreement that the large diversity of toxicity results in the literature stems from the application of tubes with a wide range distribution of tube diameters, lengths, and chiralities produced by the current synthesis methods. It is also due to tubes with different functionalization, the

degree of functionalization, and the method used for functionalization. Definite discrimination of toxicity of CNTs will continue to be impossible without implementation of precise measurements, complete characterization, and the use of well-defined materials. The other reason may be due to the different protocols, cell lines, and animal models used in evaluating the toxicity and long-term fate of the tubes. Standard experimental protocols (including but not limited to animal models, cell assays, quantification, and characterization methodologies) should be established so that studies may be compared across laboratories. We should be cautious when applying traditional toxicology assays to the safety assessment of nanoscale materials such as CNTs. Finally, further careful long-term studies of the absorption, deposition, metabolism and excretion of CNTs in animals are urgently needed. After all these problems solved, we can possible establish Good Manufacturing Practice procedures for clinical use and for large-scale production of drugs by the pharmaceutical industry.

## Acknowledgments

This material is based upon work supported by the National Science Foundation under grants CHE-0750201 and CBET-0933966. H.H. also acknowledges the Trustees Research Fellowship Program at Rutgers, State University of New Jersey.

## References

**1** Heller, D.A., Baik, S., Eurell, T.E., and Strano, M.S. (2005) *Adv. Mater.*, **17**, 2793–2799.
**2** Liu, Z., Tabakman, S.M., Chen, Z., and Dai, H.J. (2009) *Nat. Protoc.*, **4**, 1372–1382.
**3** Liu, Z., Winters, M., Holodniy, M., and Dai, H.J. (2007) *Angew. Chem. Int. Ed.*, **46**, 2023–2027.
**4** Bachilo, S.M., *et al.* (2002) *Science*, **298**, 2361–2366.
**5** O'Connell, M.J., *et al.* (2002) *Science*, **297**, 593–596.
**6** Cherukuri, P., Litovsky, S.H., and Weisman, R.B. (2004) *J. Am. Chem. Soc.*, **126**, 15638–15639.
**7** Rao, A.M., *et al.* (1997) *Science*, **275**, 187–191.
**8** Yao, Y.G., *et al.* (2007) *Nat. Mater.*, **6**, 283–286.
**9** Zhang, Y.Y., *et al.* (2007) *J. Phys. Chem. C*, **11**, 1983–1987.
**10** Chen, Z., *et al.* (2008) *Nat. Biotechnol.*, **26**, 1285–1292.
**11** Liu, Z., *et al.* (2008) *J. Am. Chem. Soc.*, **130**, 13540–13541.
**12** Liu, Z., *et al.* (2010) *Nano Res.*, **3**, 222–233.
**13** Peters, M.J., McNeil, L.E., Lu, J.P., and Kahn, D. (2000) *Phys. Rev. B*, **61**, 5939–5944.
**14** Harris, P.J.F. (1999) *Carbon Nanotubes and Related Structures*, Cambridge University Press, Cambridge.
**15** Charlier, J.-C., Blase, X., and Roche, S. (2007) *Rev. Mod. Phys.*, **79**, 677–732.
**16** Wilder, J.W.G., Venema, L.C., Rinzler, A.G., Smalley, R.E., and Dekker, C. (1997) *Nature*, **391**, 59–62.
**17** Dresselhaus, M.S., Dresselhaus, G., Jorio, A., Souza Filho, A.G., and Saito, R. (2002) *Carbon*, **40**, 2043–2061.
**18** Dresselhaus, M.S., Dresselhaus, G., Saito, R., and Jorio, A. (2005) *Phys. Rep.*, **409**, 47–99.
**19** Dresselhaus, M.S., Dresselhaus, G., Saito, R., and Jorio, A. (2008) Raman spectroscopy of carbon nanotubes, in

*Carbon Nanotubes: Quantum Cylinders of Graphene* (ed. S. Saito and A. Zettl), Contemporary Concepts of Condensed Matter Science, Elsevier,, Amsterdam, pp. 83–108.
**20** Dresselhaus, M.S. and Eklund, P.C. (2000) *Adv. Phys.*, **49**,, 705–814.
**21** Saito, R., Takeya, T., Kimura, T., Dresselhaus, G., and Dresselhaus, M.S. (1997) *Phys. Rev. B*, **57**, 4145–4153.
**22** Thomsen, C. and Reich, S. (2007) Raman scattering in carbon nanotubes, in *Light Scattering in Solids IX* (eds M. Cardona and R. Merlin), Springer, Berlin, pp. 108–232.
**23** Hatton, R.A., Miller, A.J., and Silva, S.R.P. (2008) *J. Mater. Chem.*, **18**, 1183–1192.
**24** Dai, H.J., *et al.* (2006) *NANO: Brief Rep. Rev.*, **17**, 1–13.
**25** Zhou, X., Park, J.-Y., Huang, S., Liu, J., and McEuen, P.L. (2005) *Phys. Rev. Lett.*, **95**, 146805.
**26** Durkop, T., Getty, S.A., Cobas, E., and Fuhrer, M.S. (2004) *Nano Lett.*, **4**, 35–39.
**27** Li, S., Yu, Z., Yen, S.-F., Tang, W.C., and Burke, P.J. (2004) *Nano Lett.*, **4**, 753–756.
**28** Hong, S. and Myung, S. (2007) *Nat. Nanotechnol.*, **2**, 207–208.
**29** Kang, S.J., *et al.* (2007) *Nat. Nanotechnol.*, **2**, 230–236.
**30** Kis, A. and Zettl, A. (2008) *Phil. Trans. R. Soc. A*, **366**, 1591–1611.
**31** Cheung, W., *et al.* (2009) *J. Mater. Chem.*, **19**, 6465–6480.
**32** Ma, Y., *et al.* (2008) *ACS Nano*, **2**, 1197–1204.
**33** Nijuguna, J., Pielichowski, K., and Alcock, J.R. (2007) *Adv. Eng. Mater.*, **9**, 835–847.
**34** Prashantha, K., Soulestin, J., Lacrampe, M.F., and Krawczak, P. (2009) *Polym. Polym. Compos.*, **17**, 205–245.
**35** Lassagne, B., Tarakanov, Y., Kinaret, J., Garcia-Sanchez, D., and Bachtold, A. (2009) *Science*, **325**, 1107–1110.
**36** Kim, P., Shi, L., Majumdar, A., and McEuen, P.L. (2001) *Phys. Rev. Lett.*, **87**, 215502.
**37** Chen, R.J., *et al.* (2003) *Proc. Natl. Acad. Sci. USA*, **100**, 4984–4989.
**38** Liu, Z., Sun, X., Nakayama-Ratchford, N., and Dai, H.J. (2007) *ACS Nano*, **1**, 50–56.
**39** Liu, Z., Tabakman, S., Welsher, K., and Dai, H.J. (2009) *Nano Res.*, **2**, 85–120.
**40** Tans, S.J., *et al.* (1997) *Nature*, **386**, 474–477.
**41** Chakravarty, P., *et al.* (2008) *Proc. Natl. Acad. Sci. USA*, **105**, 8697–8702.
**42** Kam, N.W.S., O'Connell, M., Wisdom, J.A., and Dai, H. (2005) *Proc. Natl. Acad. Sci. USA*, **102**, 116000–111605.
**43** Xiao, Y., *et al.* (2009) *BMC Cancer*, **9**, 351–361.
**44** de la Zerda, A., *et al.* (2008) *Nat. Nanotechnol.*, **3**, 557–562.
**45** Welsher, K., Liu, Z., Daranciang, D., and Dai, H.J. (2008) *Nano Lett.*, **8**, 586–590.
**46** Kostarelos, K.B., Bianco, A., and Prato, M. (2009) *Nat. Nanotechnol.*, **4**, 627–633.
**47** Cheung, W., Pontoriero, F., Taratula, O., Chen, A.M., and He, H.X. (2010) *Adv. Drug Deliv. Rev.* **62**, 633–649.
**48** Saito, S., Dresselhaus, G., and Dresselhaus, M.S. (1998) *Physical Properties of Carbon Nanotubes*, Imperial College Press, London.
**49** Saito, S., Dresselhaus, G., and Dresselhaus, M.S. (2000) *Phys. Rev. B.*, **61**, 2981.
**50** Tu, X.M., Manohar, S., Jagota, A., and Zheng, M. (2009) *Nature*, **460**, 250–253.
**51** Aubin, J.E. (1979) *J. Histochem. Cytochem.*, **27**, 36–43.
**52** Lim, Y.T. (2003) *Mol. Imag.*, **2**, 50–64.
**53** Kam, N.W.S., Jessop, T.C., Wender, P.A., and Dai, H. (2004) *J. Am. Chem. Soc.*, **126**, 6850–6851.
**54** Pantarotto, D., Briand, J.-P., Prato, M., and Bianco, A. (2004) *Chem. Commun.*, **1**, 16–17.
**55** Liu, Z., *et al.* (2007) *Nat. Nanotechnol.*, **2**, 47–52.
**56** Singh, R., *et al.* (2006) *Proc. Natl. Acad. Sci. USA*, **103**, 3357–3362.
**57** Gupta, A.K. and Curtis, A.S.G. (2004) *Biomaterials*, **25**, 3029–3040.
**58** Matsui, H., Ito, T., and Ohnishi, S.-I. (1983) *J. Cell Sci.*, **59**, 133–143.
**59** Cherukuri, P., Gannon, C.J., and Leeuw, T.K. (2006) *Proc. Natl. Acad. Sci. USA*, **103**, 18882–18886.

**60** Strano, M.S., *et al.* (2003) *J. Phys. Chem. B*, **107**, 6979–6985.
**61** Jin, H., Heller, D.A., and Strano, M.S. (2008) *Nano Lett.*, **8**, 1577–1585.
**62** Tzafriri, A.R., Wu, D., and Edelman, E.R. (2004) *J. Theor. Biol.*, **229**, 127–138.
**63** Chithrani, B.D. and Chan, W.C.W. (2007) *Nano Lett.*, **7**, 1542–1550.
**64** Pantarotto, D., *et al.* (2004) *Angew. Chem.*, **116**, 5354–5358.
**65** Sun, Y.P., *et al.* (2002) *Chem. Phys. Lett.*, **351**, 349.
**66** Riggs, Z.X., Guo, D.-S., Carroll, D.L., and Sun, Y.P. (2000) *J. Am. Chem. Soc.*, **122**, 5879.
**67** Lacerda, L., *et al.* (2006) *Adv. Funct. Mater.*, **16**, 1839–1846.
**68** Kostarelos, K., *et al.* (2007) *Nat. Nanotechnol.*, **2**, 108–113.
**69** Welsher, K., *et al.* (2009) *Nat. Nanotechnol.*, **4**, 773–780.
**70** Barone, P.W., Baik, S., Heller, D.A., and Strano, M.S. (2005) *Nat. Mater.*, **4**, 86–92.
**71** Barone, P.W. and Strano, M.S. (2006) *Angew. Chem. Int. Ed.*, **45**, 8138–8141.
**72** Heller, D.A., *et al.* (2006) *Science*, **311**, 508–511.
**73** Jeng, E.S., Moll, A.E., Roy, A.C., Gastala, J.B., and Strano, M.S. (2006) *Nano Lett.*, **6**, 371–375.
**74** Jin, H., *et al.* (2007) *Macromolecules*, **40**, 6731–6739.
**75** Jeng, E.S., Barone, P.W., Nelson, J.D., and Strano, M.S. (2007) *Small*, **3**, 1602–1609.
**76** Besteman, K., Lee, J.-O., Wiertz, F.G.M., Heering, H.A., and Dekker, C. (2003) *Nano Lett.*, **3**, 727–730.
**77** Lin, Y.H., Lu, F., Tu, Y., and Ren, B.Y. (2004) *Nano Lett.*, **4**, 191–195.
**78** Kim, J.H., *et al.* (2009) *Nat. Chem.*, **1**, 473–481.
**79** Kim, J.H., *et al.* (2010) *Angew. Chem. Int. Ed.*, **49**, 1456–1459.
**80** Cognet, L., *et al.* (2007) *Science*, **316**, 1465–1468.
**81** Jin, H., Heller, D.A., Kim, J.H., and Strano, M.S. (2008) *Nano Lett.*, **8**, 4299–4304.
**82** Jin, H., *et al.* (2010) *Nat. Nanotechnol.*, **5**, 302–U381.
**83** Heller, D.A., *et al.* (2009) *Nat. Nanotechnol.*, **4**, 114–120.
**84** Yang, R.H., *et al.* (2008) *J. Am. Chem. Soc.*, **130**, 8351–8358.
**85** Yang, R.H., *et al.* (2008) *Anal. Chem.*, **80**, 7408–7413.
**86** Zhu, Z., *et al.* (2010) *Anal. Bioanal. Chem.*, **396**, 73–83.
**87** Zhang, Y., Zhang, J., Son, H., Kong, J., and Liu, Z.F. (2005) *J. Am. Chem. Soc.*, **127**, 17156–17157.
**88** MacBeath, G. and Schreiber, S.L. (2000) *Science*, **289**, 1760–1763.
**89** Bailey, R.C., Kwong, G.A., Radu, C.G., Witte, O.N., and Heath, J.R. (2007) *J. Am. Chem. Soc.*, 129, 1959–1967.
**90** Robinson, W.H.e.a. (2002) *Nat. Med.*, **8**, 295–301.
**91** Alivisatos, A.P., Gu, W.W., and Larabell, C. (2005) *Annu. Rev. Biomed. Eng.*, **7**, 55–76.
**92** Xing, Ye.a. (2007) *Nat. Protoc.*, **2**, 1152–1165.
**93** Fountaine, T.J., Wincovitch, S.M., Geho, D.H., and Pittaluga, S. (2006) *Mod. Pathol.*, **19**, 1181–1191.
**94** Keren, S., Zavaleta, C., Cheng, Z., de la Zerda, A., and Gambhir, S.S. (2008) *Proc. Natl. Acad. Sci. USA*, **105**, 5844–5849.
**95** Cao, Y.W.C., Jin, R.C., and Mirkin, C.A. (2002) *Science*, **297**, 1536–1540.
**96** Freudiger, C.W, *et al.* (2008) *Science*, **322**, 1857–1861.
**97** Liu, Z., *et al.* (2008) *Proc. Natl. Acad. Sci. USA*, **105**, 1410–1415.
**98** Zavaleta, C., *et al.* (2008) *Nano Lett.*, **8**, 2800–2805.
**99** Jain, R.K. (1990) *Cancer Metast. Rev.*, **9**, 253–266.
**100** Wu, W., *et al.* (2005) *Angew. Chem. Int. Ed.*, **44**, 6358–6362.
**101** Zhang, X., Meng, L., Lu, Q., Fei, Z., and Dyson, P.J. (2009) *Biomaterials*, **30**, 6041–6047.
**102** Liu, Z., *et al.* (2008) *Cancer Res.*, **68**, 6652–6659.
**103** McDevitt, M.R., *et al.* (2007) *J. Nucl. Med.*, **48**, 1180–1189.
**104** Bianco, A., Kostarelos, K., Partidos, C.D., and Prato, M. (2004) *Chem. Commun.*, **5**, 571–577.
**105** Dai, H. (2002) *Acc. Chem. Res.*, **35**, 1035–1044.

**106** Zheng, M., *et al.* (2003) *Nat. Mater.*, 338–342.
**107** Zheng, M., *et al.* (2003) *Science*, 1545–1548.
**108** Andrews, R. and Weisenberger, M.C. (2004) *Curr. Opin. Solid State Mater. Sci.*, 31–37.
**109** Georgakilas, V., *et al.* (2002) *Chem. Commun.*, **24**, 3050.
**110** Pantarotto, D., *et al.* (2003) *J. Am. Chem. Soc.*, **125**, 6160.
**111** Wang, S., *et al.* (2003) *Nat. Mater.*, **2**, 196–200.
**112** Bahr, J.L., *et al.* (2001) *J. Am. Chem. Soc.*, **123**, 6536–6542.
**113** Dyke, C.A. and Tour, J.M. (2003) *J. Am. Chem. Soc.*, **125**, 1156–1157.
**114** Georgakilas, V., *et al.* (2002) *J. Am. Chem. Soc.*, **124**, 14318–14319.
**115** Banerjee, S. and Wong, S.S. (2002) *J. Phys. Chem. B*, **106**, 12144–12151.
**116** Buffa, F., Hu, H., and Resasco, D.E. (2005) *Macromolecules*, **38**, 8258–8263.
**117** Wang, Y., Iqbal, Z., and Mitra, S. (2006) *J. Am. Chem. Soc.*, **128**, 95–99.
**118** Zhang, M., Yudasaka, M., and Iijima, S. (2004) *J. Phys. Chem. B*, **108**, 149–153.
**119** Graupner, R. (2007) *J. Raman Spectrosc.*, **38**, 673–683.
**120** Karachevtsev, V.A., *et al.* (2005) Noncovalent functionalization of single-walled carbon nanotubes for biological application: raman and NIR absorption spectroscopy, in *Spectroscopy of Emerging Materials*, vol. 165 (eds E.C. Faulques, D.L. Perry, and A.V. Yeremenko), Springer, Berlin, pp. 139–150.
**121** Yang, W., Thordarson, P., Gooding, J.J., Ringer, S.P., and Braet, F. (2007) *Nanotechnology*, **18**, 412001.
**122** Chu, H.B., *et al.* (2009) *J. Am. Chem. Soc.*, **131**, 14310–14316.
**123** Chou, S.G., *et al.* (2007) *Appl. Phys. Lett.*, **90**, 131–109.
**124** Rajan, A., Strano, M.S., Heller, D.A., Hertel, T., and Schulten, K. (2008) *J. Phys. Chem. B*, **112**, 6211–6213.
**125** Jin, H., Heller, D.A., Sharma, R., and Strano, M.S. (2009) *ACS Nano*, **3**, 149–158.
**126** Heller, D.A., *et al.* (2004) *J. Am. Chem. Soc.*, **126**, 14567–14573.
**127** Tu, X. and Zheng, M. (2008) *Nano Res.*, **1**, 185–194.
**128** Hersam, M.C. (2008) *Nat. Nanotechnol.*, **3**, 387–394.
**129** Weisman, R.B. (2003) *Nat. Mater.*, **2**, 569–570.
**130** Carreor-Sanchez, J.C., *et al.* (2006) *Nano Lett.*, **6**, 1609.
**131** Dumortier, H., *et al.* (2006) *Nano Lett.*, **6**, 1522–1528.
**132** Jia, G., *et al.* (2005) *Environ. Sci. Technol.*, **39**, 1378.
**133** Kagan, V.E., *et al.* (2006) *Toxicol. Lett.*, **165**, 88–100.
**134** Lam, C.-W., James, J.T., McCluskey, R., Arepali, S., and Hunter, R.L. (2006) *Crit. Rev. Toxicol.*, **36**, 189.
**135** Magrez, A., *et al.* (2006) *Nano Lett.*, **6**, 1522.
**136** Sayes, C.M., *et al.* (2006) *Toxicol. Lett.*, **161**, 135–142.
**137** Smart, S.K., Cassady, A.I., Lu, G.Q., and Martin, D.J. (2006) *Carbon*, **44**, 1034–1047.
**138** Warheit, D.B. (2006) *Carbon*, **44**, 1064.
**139** Warheit, D.B., *et al.* (2003) *Toxicol. Sci.*, **77**, 117.
**140** Worle-Knirsch, J.M., Pulskamp, K., and Krup, H.F. (2006) *Nano Lett.*, **6**, 1261–1268.

# 8
# Lipid Nanoparticle-Mediated Detection of Proteins

*Erin K. Nyren-Erickson, Ryne C. Hendrickson, and Sanku Mallik*

## 8.1
## Introduction to Liposomes

Among various lipid nanoparticles, liposomes have been used extensively in the detection of proteins. Liposomes are spherical, self-closed lipid bilayer structures that enclose an aqueous core. Similar structurally to the bilayer of the cell membrane, liposomes are composed of lipid amphiphiles (molecules having hydrophilic head groups and hydrophobic lipid tails), primarily those with two hydrophobic tails such as glycerophospholipids, glyceroglycolipids, sphingophospholipids, and sphingoglycolipids, and they may or may not also contain cholesterol for added membrane stability. Although single-tailed lipids are usually not structurally important to the liposomes, they are often added as part of the lipid bilayer to impart some specific quality, such as fluorescence (through the incorporation of lipid-conjugated fluorescent dyes) or antigen recognition (through incorporation of lipid-conjugated antibodies) [1–3].

Use of liposomes in research applications has a number of advantages. Liposomes have the unique benefit of containing both hydrophobic and hydrophilic sections, and therefore may encapsulate a wide variety of cargos, carrying the hydrophobic within the lipid bilayer, and the hydrophilic within the internal core. In addition, liposomes are compatible with both *in vivo* and *in vitro* environments, and may therefore be incorporated into numerous biological, pharmacological, and molecular biology applications. Notwithstanding incorporation of antibodies or other functional groups that may be costly to obtain, liposomes are also generally produced without great cost. Finally, liposomes are able to simultaneously carry reactive moieties and store functional reagents (such as enzymes or chemiluminescent substrates), which can be released by using an external trigger. Consequently, liposomes have found a variety of applications in biophysics, chemistry, pharmacology, and medicine, as well as having cosmetic, diagnostic, and agricultural applications [1–3]. Our particular interest is with their application in the detection of protein antigens, enzymes, and viruses.

The importance of liposomes in the detection of proteins and viruses is 2-fold: they may be used as diagnostic tools, enabling us to visualize the presence of an

*Biosensor Nanomaterials*. Edited by Songjun Li, Jagdish Singh, and Ipsita A. Banerjee

ISBN: 978-3-527-32841-3

enzyme or antigen, and they may be used therapeutically for delivering drugs to the site of interest [4–9]. These properties may be controlled or enhanced by proper selection of the structural lipids, conjugated head groups, and encapsulated materials, each of which is represented by a wide variety of possibilities. For the remainder of this chapter, we will divide our focus into two broad categories of liposomes: saturated and polymerized vesicles.

## 8.2
## Saturated Liposomes

Saturated liposomes are those prepared from amphiphilic lipids having either saturated hydrophobic tails (e.g., disteroylphosphatidylcoline) or tails containing 1–3 double bonds (e.g., dioleylphosphatidylserine). When incorporated into a membrane these lipids do not react covalently with one another and their movement within the membrane is not strongly restricted (i.e., the membrane retains its semifluidic properties). Liposomes with these properties have several advantages: they are relatively easy to prepare and store; they may be induced to fuse, either with other liposomes or with cells [1, 9]; and they may be engineered to decompose under certain circumstances, such as after fusing with the cellular endosome [6, 7, 10], after reaching a certain temperature [8], or when coming into contact with a specific enzyme [4, 5]. They do, however, have the disadvantage of being rather unstable and may leak their contents under conditions of imbalanced osmolality.

There are many detection applications for which saturated liposomes have been used. This section will focus on their uses in antigen detection (both human and bacterial), viral detection, and enzyme detection.

### 8.2.1
### Detection of Antigens

In general, the detection of antigens involving liposomes may be divided into four broad categories: enzyme-linked immunosorbent assay (ELISA)-like assays, agglutination assays, compliment-dependent assays, and liposomes for radiology and other biosensing applications.

By far the most thoroughly explored application of liposomes for the detection of antigens are the ELISA-like assays, which utilize liposomes with surface-conjugated antibodies (“immunoliposomes”) to replace the more traditionally used polyclonal antibodies conjugated to an enzyme substrate. The conjugation of antibodies to the surface of liposomes usually involves preparing the liposomes, including any encapsulated compound, and then conducting synthetic reactions to activate the polar head groups, followed by conjugation to the C-terminus of the antibody heavy chain. These liposomes typically encapsulate either a chemiluminescent or fluorescent dye marker, or an enzyme. They are then added to a testing surface, typically a polystyrene microtiter plate, which has the antigen of interest

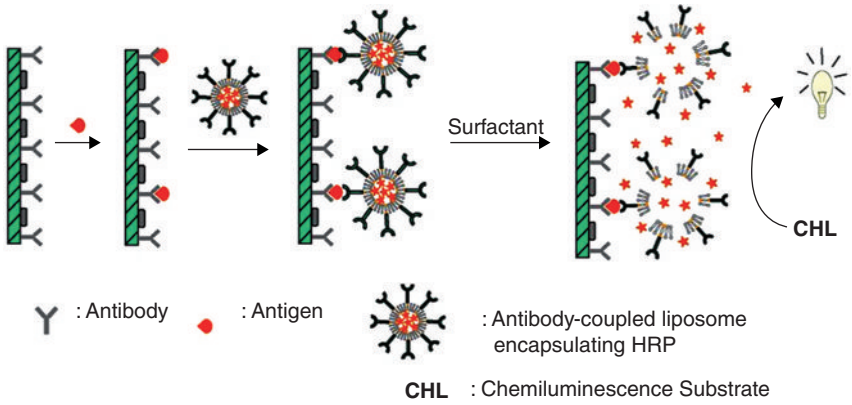


**Figure 8.1** Scheme for liposomal detection of PSA. (Used with permission from [11].)

immobilized on its surface. Zheng *et al.* [11] have reported the use of horseradish peroxidase (HRP) encapsulating liposomes for the detection of prostate-specific antigen (PSA) (Figure 8.1).

Monoclonal PSA140 antibodies were fixed in microtiter plate wells and the PSA sample solution added. The PSA was bound by the immobilized antibodies. The solution of liposomes was then added and the mouse anti-PSA antibodies conjugated to the liposomal surface then also bind the PSA. These bound liposomes were then lysed with a surfactant and the HRP molecules released detected by reaction with a chemiluminescent HRP substrate. They report detection of PSA concentrations of 0.74 pg $ml^{-1}$ to 0.74 μg $ml^{-1}$. Viswanathan *et al.* [12] report a similar assay for the detection of carcinoembryonic antigen, with detection limits of 1 pg $ml^{-1}$, and Ho *et al.* [13] have developed a liposome-based immunostrip for detection of *Salmonella*, which positively detects as few as 1680 cells.

In a slight variation on this theme, Edwards and March [14] have reported an assay for the cholera toxin B (CTB) by producing $GM_1$-functionalized liposomes. $GM_1$ is a ganglioside that binds to the pentameric CTB and therefore it functions in much the same way as would an antibody. In a further twist on this theme, Larsson *et al.* [15] have also developed a detection assay for CTB by using a lipid bilayer containing 5% nitrilotriacetic acid (NTA). The NTA serves to capture a histidine-tagged single-chained antibody fragment against cholera toxin. This antibody fragment then replaces the immobilized antibody in the final assay (Figure 8.2).

Other techniques have been developed for detecting the presence of antibodies against a particular antigen in patient serum. Thanyani *et al.* [16] have prepared liposomes containing mycolic acid (60–90 carbon branched α-alkyl, β-hydroxy fatty acids present in the outer layer of mycobacterium cell walls) in the lipid membrane and used these liposomes to detect antibodies against *Mycobacterium tuberculosis* in patients with human immunodeficiency virus (HIV) coinfections. By immobilizing the liposomes to the surface of a sample cuvette and adding dilutions of

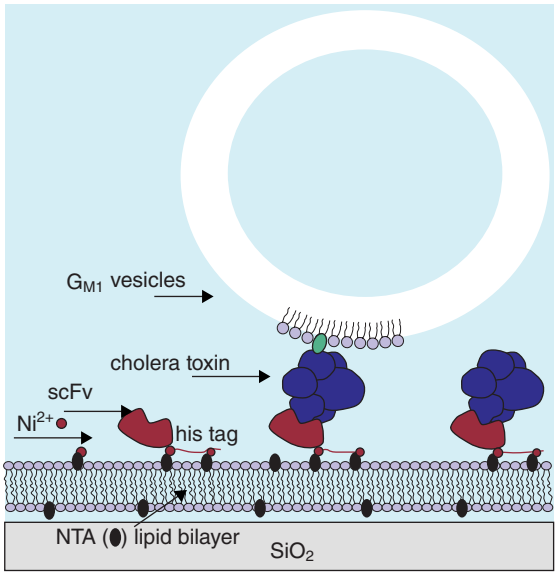


**Figure 8.2** Cartoon illustration the immobilization strategy: NTA-containing lipid vesicles, $Ni^{2+}$, single-chain Fv fragment, cholera toxin, and $GM_1$-containing vesicles. Not drawn to scale. (Used with permission from [15].)

serum from patients with tuberculosis (TB) infections, they were able to monitor the binding of antibodies to the immobilized liposomes using the IAsys biosensing system. This system can quantify the binding of analytes by detecting changes in the refractive index (the change in refractive index value is proportional to the change in accumulated mass). The assay was found to be 81.8% accurate overall, combining results from four different groups ($TB^+HIV^-$, $TB^+HIV^-$, $TB^-HIV^+$, and $TB^-HIV^-$).

Other variations of ELISA-like assays using immunoliposomes have also been demonstrated. Edwards and Baeummner [17] report the amplification of signal by employing two sets of liposomes. The first liposome is directed against the antigen of interest and encapsulates a fluorescein-tagged DNA oligonucleotide. These are lysed upon binding to the antigen and the oligonucleotides hybridize with a complimentary oligonucleotide in a second microtiter plate. A second liposome preparation that encapsulates a fluorescent dye and is tagged with antifluorescein antibodies is then added to the second plate, and these bound liposomes are lysed with surfactant. The resulting fluorescent signal is proportional to the original analyte concentration. (Figure 8.3) This assay reportedly yields a detection limit of 4.1 ng $ml^{-1}$, with an upper limit of 5 µg $ml^{-1}$.

Agglutination assays utilize dye-encapsulating immunoliposomes tagged with antibodies against an antigen or cocktail of antigens. When added to a solution containing the antigen of interest, these antigens may be bound by the antibodies

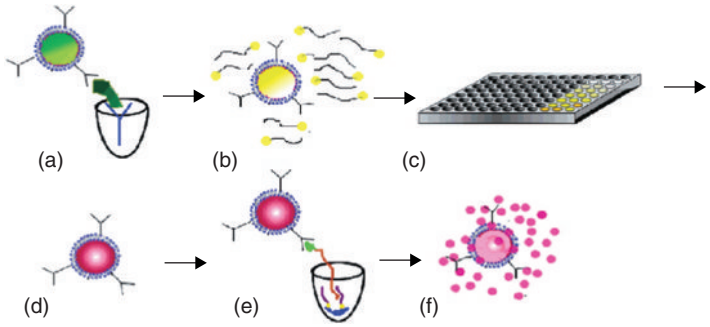


**Figure 8.3** Schematic of assay. (A) Antibody-tagged DNA-encapsulating (primary) liposomes participate in a sandwich immunoassay for the protective antigen from *B. anthracis*. (B) Bound liposomes are lysed with surfactant to release the encapsulated fluorescein-labeled probe, which then (C) hybridizes with the complementary sequence immobilized in a second microtiter plate. (D) Antifluorescein-tagged sulforhodamine B-encapsulating (secondary) liposomes bind to (E), fluorescein label on hybridized probe, and then (F) bound secondary liposomes are lysed with surfactant to yield a fluorescence signal proportional to the original analyte concentration. (Used with permission from [17].)

on multiple liposomes, causing the liposomes to form visible aggregates. The result is a qualitative assay that is rapid and easily interpreted. Such an assay was developed by Tiwari *et al.* against TB [18]. They immunized two young rabbits against a cocktail of glycolipid antigens form *M. tuberculosis* and purified the resulting polyclonal antibodies. After formation of liposomes containing Sudan black as a dye marker and the addition of *N*-hydroxysuccinamide to promote coupling efficiency, the polyclonal antibodies were added and incubated with the liposomes for 16 h at 4 °C. They were then dialyzed against distilled water and centrifuged. The recovered liposomes were tested against tissue biopsy (from pulmonary TB patients) or cerebrospinal fluid samples (from patients with TB meningitis) from 1360 patients with confirmed cases of *M. tuberculosis* infection. Reported final specificity of the assay was 100% against patients with confirmed TB infections and 98.3% overall for normal healthy patients (resulting from some false-positive results). Figure 8.4 below shows the overall reaction scheme. A similar assay has been designed by Petkova *et al.* for the diagnosis of trichinellosis [19].

Liposomes may also be used to detect antibodies against a particular infection. Lasic [1] reports an assay for syphilis in which the interaction of antibodies present in the blood of the infected individual are allowed to react with liposomes containing the antigen cardiolipin, resulting in agglutination.

Compliment-dependent assays utilize liposomes containing an antigen of interest as part of their lipid membrane, and are subsequently added to a mixture of antiserum for the antigen of interest and a sample that potentially contains the antigen of interest. Contact of the liposomes with the antiserum causes leakage of the encapsulated dye. In this assay, the presence of antigen in the sample will

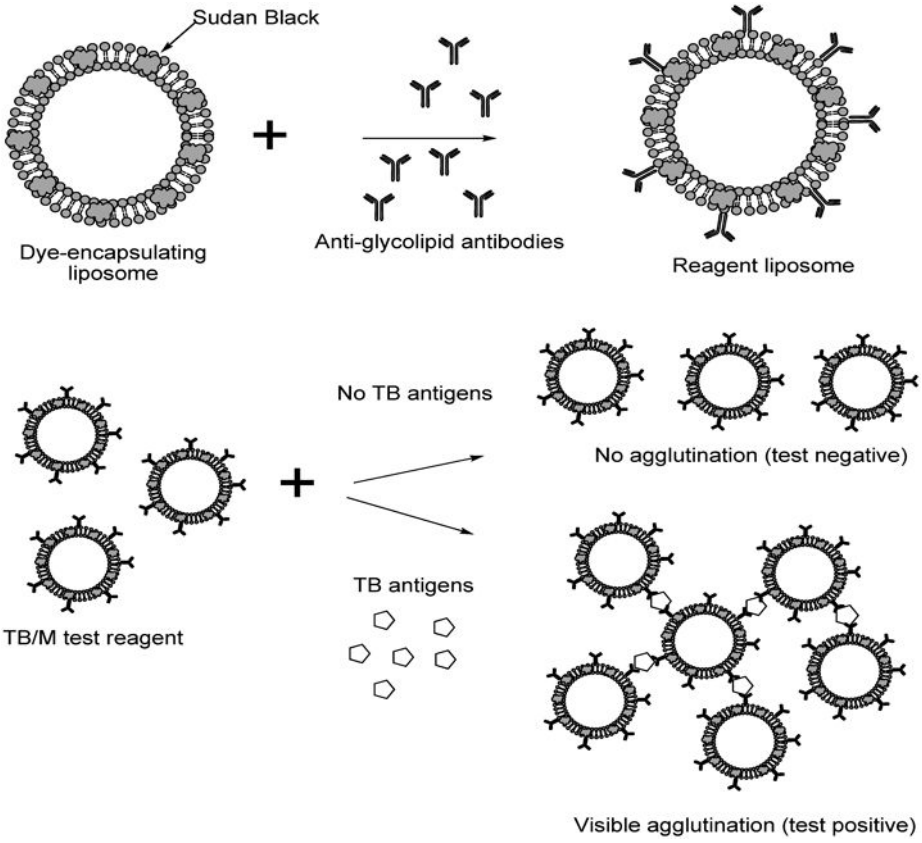


**Figure 8.4** Reaction scheme for agglutination test for TB. (Used with permission from [18].)

reduce the detectable level of dye marker by a level proportional to the amount of antigen present in the sample [20]. Skopinskaya *et al*. [21] prepared liposomes for compliment-dependent detection of *Vibrio cholera* cells. The liposomes were sensitized with *V. cholera* lipopolysaccharide and encapsulated calcein as a fluorescent marker dye. To determine presence of antigen, the maximum fluorescence emission intensity was first determined by incubating the liposomes in the presence of antiserum against *V. cholera* without the presence of any other intervening sample. This value was then taken as 100%. To conduct the assay, the antiserum was incubated with the sample of interest for 60 min, followed by addition of the liposome preparation. The threshold of detection for this assay ranged from 100 ng $ml^{-1}$ to 1.1 μg $ml^{-1}$.

Liposomes can also serve as contrast agents in radiological applications, as well as other biosensing applications [1]. These liposomes are typically immunoliposomes and either encapsulate gadolinium (for magnetic resonance imaging applications) [22] or a dye or contain entrapped air (for ultrasound applications) [23,

24]. Smith *et al.* [23] describe the production of liposomes containing entrapped air as a contrast agent by reconstituting a thin film of selected lipids and cholesterol using air-saturated deionized water. These liposomes were stable in the bloodstream during continuous B-mode imaging, but could be fragmented using Doppler pulses, demonstrating their potential as both diagnostic tools and drug delivery vehicles.

Krivanek *et al.* [24] have also produced immunoliposomes for use as ultrasound contrast agents. Using aerobically grown *Bacillus coagulans* cultures, they recrystallized the bacterial cell surface layers (S-layers) on the surface of liposomes, and immobilized human IgG against the *B. coagulans* antigens on the liposome outer surface. Using rabbit and swine antihuman IgG as "antigens," they were subsequently able to monitor the changes in ultrasound velocity, $[u]$, as a function of antigen–antibody interactions. At 25 °C, the interaction of rabbit and swine antihuman IgG resulted in the significant reduction of $[u]$ due to changes in membrane hydration.

### 8.2.2
### Detection of Viruses

The use of liposomes in viral detection can be classified into two groups: (i) ELISA-like, similar to those discussed in Section 8.2.1, and (ii) through the use of a DNA capture probe in a test strip format.

An ELISA-like procedure using immunoliposomes for detection of influenza virus which uses electrogenerated chemiluminescence (ECL) is reported by Egashira *et al.* [25]. They have prepared liposomes that encapsulate the ruthenium complex, bis(2,2′-bipyridine)[4,4′-bis(4aminobutyl)-2,2′-bipyridine] ruthenium perchlorate (Figure 8.5), a chemiluminescent compound, and are also tagged with antihemagglutinin monoclonal antibodies.

The antigen (hemagglutinin from the influenza virus) was immobilized onto gold electrodes formed on a glass plate. To this, they added the immunoliposomes and allowed the apparatus to stand at room temperature for 30 min. After 30 min the electrode was washed with buffer to remove unbound liposomes and then

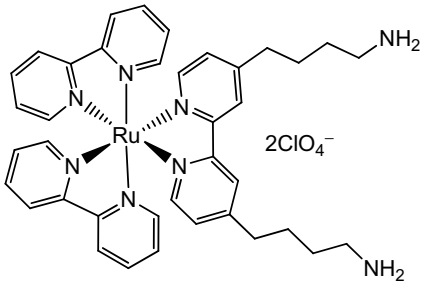


**Figure 8.5** Ruthenium complex used in chemiluminescent detection of influenza virus [25].

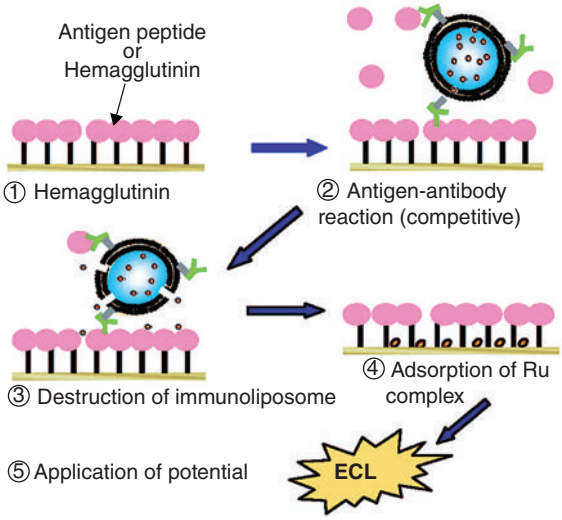


**Figure 8.6** Detection procedure for viral antigenic peptide or hemagglutinin: (1) immobilization of hemagglutinin (or antigen peptide) on a gold electrode; (2) binding of immunoliposomes with hemagglutinin onto the gold electrode through competitive antigen–antibody reaction; (3) destruction of immunoliposome by addition of ethanol; (4) adsorption of Ru(II) complex by heating at 60 °C for 10 min; (5) ECL measurement on application of potential. (Used with permission from [25].)

dried. The adherent liposomes were then destroyed with organic solvent and the electrode heated to 60 °C for 10 min to allow the ruthenium complex to adhere to the surface of the gold electrode. Buffer was then added to the electrode and a potential applied (1.3 V) in order to generate ECL (Figure 8.6). The lower limit of detection reported for this system was 500 ng $ml^{-1}$ of antigen.

Many of the viral detections incorporating liposomes have been developed as fast, qualitative assays to identify an infected individual. These assays frequently use viral RNA, amplified by polymerase chain reaction (PCR), to hybridize between a DNA probe present on a membrane and another DNA probe present on the dye-encapsulating liposomes. Such is the case with an assay developed by Baeumner *et al.* [26] for detection of Dengue virus: liposomes were prepared that encapsulate the dye sulforhodamine B and were tagged with a generic DNA probe conserved in all serotypes of Dengue virus. A serotype-specific probe was then immobilized on a membrane strip (the immobilized probe may also be a generic probe, like the one tagged on the liposomes). The Dengue RNA was amplified by PCR. The liposomes, Dengue RNA, and a hybridization buffer were then spotted on the membrane, followed by applying a running buffer to one end of the membrane strip. Results were analyzed using a reflectometer or evaluated visually (positive tests produced a pink spot where the liposomes and RNA were spotted). Their optimized assays were tested with virus samples containing 100–1000 PFU $ml^{-1}$, with results correlating well with ECL detection. Advantages of this assay are

portability and ease of use, as well as economy (the assays reportedly cost less than US$1 each). Similar assays have also been reported by Zaytseva *et al.* [27] (also for Dengue virus) and Tai *et al.* [28] (for detection of astrovirus).

### 8.2.3
### Detection of Enzymes

In this section, we refer only to procedures and assays that seek to quantify the presence of an enzyme of interest in a sample. There are many assays in the literature that utilize enzymes [29–33], but relatively few aim to quantify the presence of the enzymes. The most notable example is described by Banerjee *et al.* [34]. In this work, liposomes were formed which encapsulate HRP, and contained in the lipid bilayer the substrate for matrix metalloprotease-9 (MMP-9)—a metastatic cancer-associated enzyme. The reaction media contained an excess of chromogenic HRP substrate. When exposed to the enzyme of interest, the lipid membrane becomes unstable due to cleavage of the substrate, bringing HRP in contact with its chromogenic substrate. The absorbance of the oxidized product is proportional to the quantity of MMP-9 in the original sample. This technique offers many advantages over the more commonly used ELISA, examples of which are reduced assay time and elimination of expensive antibodies, without the sacrifice of sensitivity.

## 8.3
## Polymerized Liposomes

This section discusses the uses of polymerizable liposomes in the detection of viruses, antigens, and proteins. O'Brien *et al.* [35], Ringsdorf *et al.* [36], Regen *et al.* [37], and Plachetta [38] have conducted pioneering work in the preparation and uses of polymerizable liposomes. Various polymerizable groups, such as diacetylene [35], methacryloyl [35], styryl [39], dienoyl [39], and vinyl pyrrolidone [40], have all been used to prepare the polymerizable liposomes (Figure 8.7).

These groups can be incorporated in the fatty acid tails or in the polar head groups [39] (Figure 8.8) and can be polymerized thermally or photochemically [41].

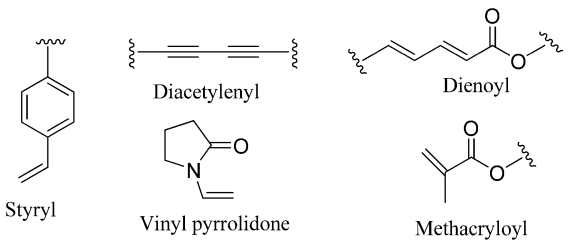


**Figure 8.7** Some of polymerizable groups used in the preparation of liposomes.

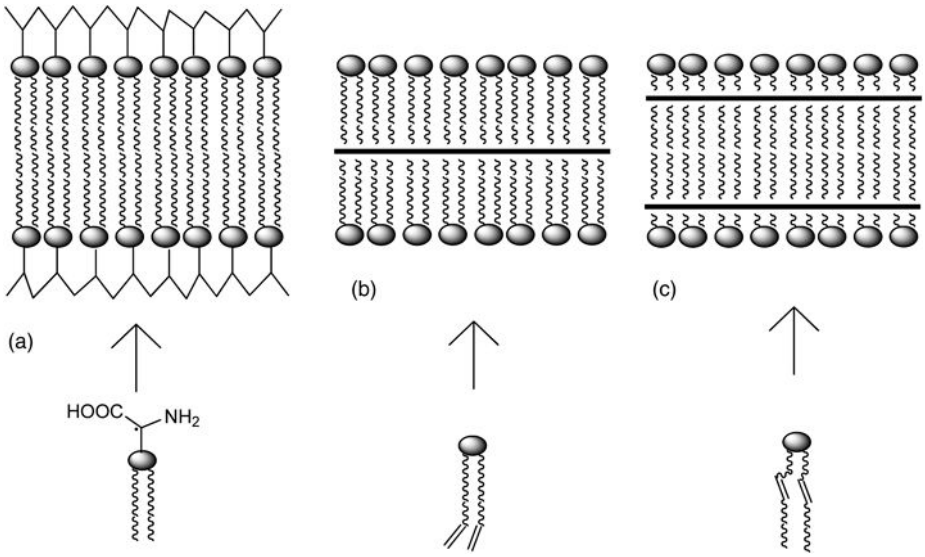


**Figure 8.8** Cut-out sections of liposome bilayer shown with locations of polymerizable groups: (A) within the polar head, (B) at the end of fatty acid tails, and (C) in the fatty acid tails. (Adapted from D. D. Lasic [1].)

Polymerization increases the stability of liposomes resulting in maintaining the shape for a longer time compared to saturated liposomes [42]. Okada *et al.* [41] have reported polymerized liposomes to be stable and nonaggregating for more than 1 year. Polymerization can occur in one or both of the lipid monolayers of the liposomes [1]. Polymerization of dialkyne lipids leads to two-dimensional polymerization, forming a spherical polymer or liposomes cross-linked in the lipid layers [1]. In contrast, polymerization of diene lipids can proceed in one dimension and the resultant polymerized liposomes may contain different polymerized domains [1]. Jelinek and Kolusheva [43] incorporated natural lipids such as phosphatidylcholine into the matrix of polymerized liposomes, especially for biosensing applications. The majority of the reports use polydiacetylene as the polymerizable group incorporated into the liposomes and the chromatic transitions are used to detect the target molecules.

### 8.3.1 Detection of Viruses

Charych *et al.* [44] designed polydiacetylene-polymerized liposomes that changes color in the presence of the influenza virus. The polymerizable 10,12-pentacosadiynoic acid was covalently attached to a sialic acid group that serves as the recognition element for the virus. The liposomes were photopolymerized using UV light (254 nm). When a solution of virus was added to the liposomes, the blue color

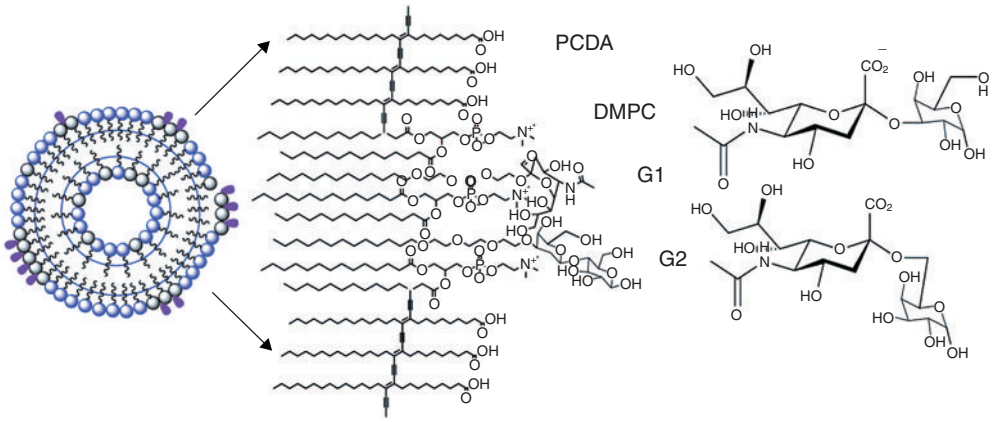


**Figure 8.9** Polydiacetylene liposomes with salic acid (G1) and lactose (G2) ligands on the outside of the liposome. PCDA = 10,12-pentacosadiynoic acid; DMPC = phosphatidylcholine. (Used with permission from [45].)

changed to a pink or orange. This chromatic transition is caused by irreversible structural changes in the ene–yne back bone of the polymerized liposomes upon the binding of the virus to sialic acid [44].

Deng *et al.* [45] have also used a similar strategy using polydiacetylene liposomes to detect the avian influenza virus H5N1. The polymerizable 10,12-pentacosadiynoic acid was used as the major component of the liposomes. Saturated lipids containing salic acid (G1), a lactose receptor (G2), and phosphatidylcholine were incorporated into the liposomes (Figure 8.9). Upon addition of the virus, the liposomes changed from a blue to red color. The head groups G1 and G2 resulted in a synergistic enhancement of the binding affinity of the viruses to the polymerized liposomes. This biosensor displayed higher sensitivity and faster response times compared to the previously reported assays.

### 8.3.2
### Detection of Antigens

Pan and Charych. [46] have used polymerizable liposomes (containing ganglioside $GM_1$ and 5,7-docosadiynoic acid) for the detection of the cholera toxin. The liposomes were then polymerized using a UV lamp (254 nm) for 60 min. Filtered cholera toxin was then added to the liposomes resulting in a blue to pinkish-orange color. The absorbance changes were also measured to quantify the colorimetric transition (percent change in the absorbance at 620 nm relative to the total absorbance at 620 and 490 nm [46]). Cholera toxin consists of A and B subunits. It was observed that the B subunit binds to the surface of the $GM_1$-incorporated liposomes. The detection of cholera toxin has also been accomplished using saturated liposomes as described in Section 8.2.1 [25].

Jelinek *et al*. [47] designed polymerized liposomes to detect antimicrobial membrane peptides. These cationic peptides consist of 12–35 amino acids and display broad-spectrum antimicrobial activity [48]. The liposomes consisted of dimiristoyl-*sn*-glycero-3-phosphocholine and 10,12-tricosdiynoic acid in a 4:6 molar ratio, respectively. The liposomes were photopolymerized at 254 nm, resulting in the conjugated ene–yne backbone and blue color [49]. The authors tested a number of peptide analogs along with melittin, mamagainin, and alamethicin against the liposomes. All of the added peptides rapidly produced different color changes. Melittin and its analogs displayed hues of red or orange color. One melittin analog even generated a violet color. This change in color is a result of differential interactions of the different amino acids in peptides with the polymerized liposomes.

Ma *et al*. [50] have prepared polymerized liposomes for the detection of *Escherichia coli*. The liposomes consisted of tricosa-2,4-diynoic acid and dioctadecyl glycerol ether-β-glucosides. The dioctadecyl glycerol ether-β-glucosides acted as the receptor for the bacteria and, as before, the color of the liposomes changed from blue to red upon the binding of bacteria to the polymerized liposomes.

Ma and Cheng [51] reported creating polydiacetylene liposomes for the detection of cytolytic pore-forming toxin streptolysin O (SLO). This toxin destroys the cell membranes of immune cells that are capable of eliciting a host response to an invading organism [52]. The liposomes consisted of glycine-terminated diacetylene monomer, 1,2-bis(10,12-tricosadiynoyl)-*sn*-glycero-3-phosphocholine, and cholesterol, and were photopolymerized (Figure 8.10). With the addition 2.5 nM of SLO toxin, the color of the polymerized liposomes changed from blue to red; increasing the concentration of SLO toxin led to a darker shade of red. Quantitative analysis was performed by monitoring the shift in absorbance maxima (from 649 to 545 nm) upon the addition of the SLO toxin.

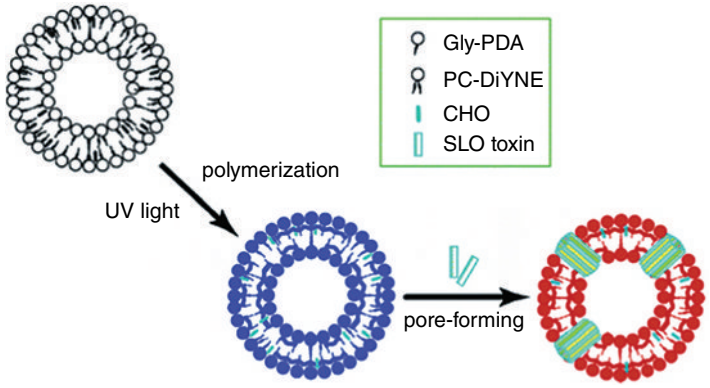


**Figure 8.10** Schematic representation of liposomes containing glycine-terminated diacetylene monomer (Gly-PDA), 1,2-bis(10,12-tricosadiynoyl)-*sn*-glycero-3-phosphocholine (PC-DIYNE), and cholesteryl (CHO) undergoing polymerization by UV light. SLO toxin permeates membrane causing color of PDA liposomes. (Used with permission from [51].)

### 8.3.3
### Detection of Proteins

Ferguson *et al.* [53] have developed a series assays for protein binding using polymerized liposomes incorporating phosphatidylinositol polyphosphates, 1,2-bis(10,12-tricosadiynoyl-*sn*-glycero-3-phosphatidylcholine, 1,2-bis(10,12-tricosadiynoyl-*sn*-glycero-3-phosphatidylethanolamine, and biotin-phosphatidylethanolamine. The liposome overlay assay (Figure 8.11) consisted of spotting the protein solution on a piece of nitrocellulose membrane and allowing it to dry. The membrane was then blocked for 2 h using a solution of phosphate-buffered saline and bovine serum albumin. The membrane was incubated with the polymerized liposomes and then treated with streptavidin–HRP conjugate. The binding of the protein to the liposomes was detected by chemiluminescence of the oxidized HRP substrate. A concentration of 0.21 pmol of protein was detected using the overlay assay.

Mallik *et al.* [54] have developed a luminescence-based detection method for human carbonic anhydrase, serum albumin, γ-globulins, and thermolysin. Polymerized liposomes were prepared incorporating polymerizable lipids chelated to $Eu^{3+}$ ions (EDTA-$Eu^{3+}$) as the head groups. The first coordination sphere of $Eu^{3+}$ ions can interact with water molecules in an aqueous solution. The weak vibronic coupling of the O–H oscillators with vibrational states of the europium ions leads to quenching of the luminescence from the lanthanide ions. When a protein binds to the $Eu^{3+}$ ions, it displaces the O–H oscillators resulting in the dequenching of the excited state. The intensity of the time-gated emission ($\lambda_{ex} = 320\,nm$, $\lambda_{em} = 545\,nm$, delay = 150 μs) increases linearly with the concentration of the added proteins. The excited state lifetime of the $Eu^{3+}$ ions was found to depend on the nature of the protein and can be used as a method to identify the protein analyte.

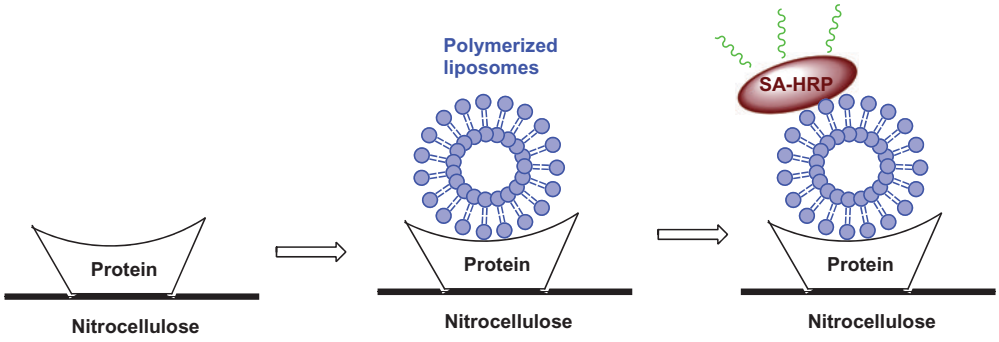


**Figure 8.11** Schematic illustration of the liposome overlay assay. SA = streptavidin. (Adapted with permission from [53].)

## 8.4 Conclusions

Both saturated and polymerized liposomes have been extensively used for the detection of proteins in solution, on the surface of viruses, and on cell membranes of bacteria. Usually, small molecules or antibodies are used for strong and selective binding to the target protein. Due to inherent structural differences, the signal transduction schemes from these two types of liposomes are different. For saturated liposomes, a reporter dye is encapsulated in the aqueous interior. The lipid bilayer is destabilized either due to binding of the target protein or by the addition of a destabilizing agent following binding. The enhancement of emission intensity of the dye molecules is monitored to detect the protein. When oligonucleotides or enzymes are encapsulated, the signal can be amplified by PCR or by using excess of suitable substrates in the assay buffer. For polymerized liposomes, binding of the analyte proteins leads to structural perturbations of the ene–yne backbones. In the assays, the resulting chromatic transitions are monitored as a function of the target protein. Luminescence properties of lanthanide ions incorporated on the surface of polymerized liposomes have been used for time-gated detection. Enzyme-linked assays using added enzymes have been implemented to detect proteins employing the polymerized liposomes. Very low limits of detection (nanograms per milliliter or less) have been achieved employing the amplified detection strategies.

## References


1 Lasic, D.D. (1993) *Liposomes: From Physics to Applications*, Elsevier, Amsterdam.
2 Gregoriadis, G. (ed.) (1992) *Liposome Technology*, vol. I, CRC Press, Boca Raton, FL.
3 Gregoriadis, G. (ed.) (1992) *Liposome Technology*, vol. III, CRC Press, Boca Raton, FL.
4 Banerjee, J., Hanson, A., Gadam, B., Elegbede, A., Tobwala, S., Ganguly, B., Wagh, A., Muhonen, W., Law, B., Shabb, J., Srivastava, D.K., and Mallik, S. (2009) *Bioconjug. Chem.*, **20**, 1332.
5 Elegbede, A., Banerjee, J., Hanson, A., Tobwala, S., Ganguly, B., Wang, R., Lu, X., Srivastava, D.K., and Mallik, S. (2008) *J. Am. Chem. Soc.*, **130**, 10633.
6 Sasaki, K., Kogure, K., Chaki, S., Nakamura, Y., Moriguchi, R., Hamada, H., Danev, R., Nagayama, K., Futaki, S., and Harashima, H. (2008) *Anal. Bioanal. Chem.*, **391**, 2717.
7 Kawano, K., Onose, E., Hattori, Y., and Maitani, Y. (2008) *Mol. Pharm.*, **6**, 98.
8 Kullberg, M., Mann, K., and Owens, J. (2009) *J. Drug Target.*, **17**, 98.
9 Mora, M., Sagrista, M.L., Trombetta, D., Bonina, F., De Pasquale, A., and Saija, A. (2002) *Pharm. Res.*, **19**, 1430.
10 Simard, P. and Leroux, J.C. (2009) *Int. J. Pharm.*, **381**, 86.
11 Zheng, Y., Chen, H., Liu, X.P., Jiang, J.H., Luo, Y., Shen, G.L., and Yu, R.Q. (2008) *Talanta*, **77**, 809.
12 Viswanathan, S., Rani, C., Anand, A.V., and Ho, J.A. (2009) *Biosens. Bioelectron.*, **24**, 1984.
13 Ho, J.A., Zeng, S.C., Tseng, W.H., Lin, Y.J., and Chen, C. (2008) *Anal. Bioanal. Chem.*, **391**, 479.
14 Edwards, K. and March, J. (2007) *Anal. Biochem.*, **368**, 39.
15 Larsson, C., Bramfeldt, H., Wingren, C., Borrebaeck, C., and Hook, F. (2005) *Anal. Biochem.*, **345**, 72.

**16** Thanyani, S., Roberts, V., Siko, D.G.R., Vrey, P., and Verschoor, J. (2008) *J. Immunol. Methods*, **332**, 61.

**17** Edwards, K. and Baeumner, A. (2007) *Anal. Chem.*, **79**, 1806.

**18** Tiwari, R.P., Garg, S.K., Bharmal, R.N., Kartikeyan, S., and Bisen, P.S. (2007) *Int. J. Tuberc. Lung Dis.*, **11**, 1143.

**19** Petkova, S., Gabev, E., Mihov, L., Komandarev, S., Kurdova, R., Vutova, K., Boeva, V., and Astrukova, N. (2004) *Exp. Pathol. Parasitol.*, **7**, 45.

**20** Alving, C., Shichijo, S., Mattsby-Baltzer, I., Richards, R., and Wassef, N. (1992) Preparation and use of liposomes in immunological studies, in *Liposome Technology*, vol. III (ed. G. Gregoriadis), CRC Press, Boca Raton, FL, p. 317.

**21** Skopinskaya, S.N., Yarkov, S.P., and Chramov, E.N. (2005) *Appl. Biochem. Microbiol.*, **41**, 199.

**22** Hengerer, A. and Grimm, J. (2006) *Biomed. Imaging Interv. J.*, **2**, 1.

**23** Smith, D., Porter, T., Martinez, J., Huang, S., MacDonald, R., McPherson, D., and Holland, C. (2007) *Ultrasound Med. Biol.*, **33**, 797.

**24** Krivanek, R., Rybar, P., Kupcu, S., Sleytr, U.B., and Hianik, T. (2002) *Bioelectrochemistry*, **55**, 57.

**25** Egashira, N., Morita, S., Hifmi, E., Mitoma, Y., and Uda, T. (2008) *Anal. Chem.*, **80**, 4020.

**26** Baeumner, A., Schlesinger, N., Slutzki, N., Romano, J., Lee, E.M., and Montagna, R. (2002) *Anal. Chem.*, **74**, 1442.

**27** Zaytseva, N., Montagna, R., Lee, E.M., and Baeumner, A. (2004) *Anal. Bioanal. Chem.*, **380**, 46.

**28** Tai, J., Ewert, M., Belliot, G., Glass, R., and Monroe, S. (2003) *J. Virol. Methods*, **110**, 119.

**29** Azagarsamy, M., Sokkalingam, P., and Thayumanavan, S. (2009) *J. Am. Chem. Soc.*, **131**, 14184.

**30** Vamvakaki, V., Fournier, D., and Chaniotakis, N. (2005) *Biosens. Bioelectron.*, **21**, 384.

**31** Scire, A., Tanfani, F., Saccucci, F., Bertoli, E., and Principato, G. (2000) *Proteins Struct. Funct. Genet.*, **41**, 33.

**32** Kamidate, T., Maruya, M., Tani, H., and Ishida, A. (2009) *Anal. Sci.*, **25**, 1163.

**33** Hwang, S.Y., Kumada, Y., Seong, G.H., Choo, J., Katoh, S., and Lee, E.K. (2007) *Anal. Bioanal. Chem.*, **389**, 2251.

**34** Banerjee, J., Hanson, A.J., Nyren-Erickson, E., Muhonen, W.W., Shabb, J.B., Srivastava, D.K., and Mallik, S. (2010) *J. Chem. Soc. Chem. Commun.*, **46**, 3209.

**35** O'Brein, D.F., Klingbiel, R.T., Specht, D.P., and Tyminski, P.N. (2006) *Macromolecules*, **446**, 282.

**36** Ringsdorf, H., Schlarb, B., and Venzmer, J. (1988) *Angew. Chem. Int. Ed. Engl.*, **27**, 113.

**37** Regen, S.L., Czech, B., and Singh, A. (1980) *J. Am. Chem. Soc.*, **102**, 6638.

**38** Plachetta, C. and Schulz, R.C. (1982) *Makromol. Chem. Rapid Commun.*, **3**, 815.

**39** O'Brien, D.F., Benedicto, B.A., Bennett, D.E., Lamparski, H.G., Lee, Y.S., Srisiri, W., and Sisson, T.M. (1998) *Acc. Chem. Res*, **31**, 861.

**40** Sivakumar, P.A. and Rao, K.P. (2002) *Biomed. Microdevices*, **4**, 197.

**41** Okada, S., Peng, S., Spevak, W., and Charych, D. (1998) *Acc. Chem. Res*, **32**, 229.

**42** Jeong, J.M., Chung, Y.C., and Hwang, J.H. (2002) *J. Biotechnol.*, **94**, 255.

**43** Jelinek, R. and Kolusheva, S. (2001) *Biotechnol. Adv.*, **19**, 109.

**44** Reichert, A., Nagy, J.O., Spevak, W., and Charych, D. (1995) *J. Am. Chem. Soc.*, **117**, 829.

**45** Deng, J., Sheng, Z., Zhou, K., Duan, M., Yu, C., and Jiang, L. (2009) *Bioconjug. Chem.*, **20**, 533.

**46** Pan, J.J. and Charych, D. (1997) *Langmuir*, **13**, 1365.

**47** Kolusheva, S., Boyer, L., and Jelinek, R. (2000 *Nat. Biotechnol.*, **18**, 225.

**48** Hancock, R.E.W. (1999) *Drugs*, **57**, 469.

**49** Tanaka, H., Gomez, M.A., Tonelli, A.E., and Thakur, M. (1989) *Macromolecules*, **22**, 1208.

**50** Ma, Z., Li, J., Liu, M., Cao, J., Zou, Z., Tu, J., and Jiang, L. (1998) *J. Am. Chem. Soc.*, **120**, 12678.

**51** Ma, G. and Cheng, Q. (2005) *Langmuir*, **21**, 6123.

**52** Alouf, E.J. and Palmer, W.M. (1999) *The Comprehensive Sourcebook of Bacterial*

*Protein Toxins*, 2nd edn, Academic Press, London.

**53** Ferguson, C.G., James, R.D., Bigman, C.S., Shepard, D.A., Abdiche, Y., Katsamba, P.S., Myszka, D.G., and Prestwich, G.D. (2005) *Bioconjug. Chem.*, **16**, 1475.

**54** Santos, M., Nadi, S., Goicoechea, H.C., Haldar, M.K., Campiglia, A.D., and Mallik, S. (2007) *Anal. Biochem.*, **361**, 109.

# 9
# Nanomaterials for Optical Imaging

*Anil V. Wagh, Ruchi Malik, and Benedict Law*

## 9.1
## Introduction

Optical imaging has become an indispensable tool for medical diagnosis. The basic principle of optical imaging relies on the interaction of photons with an exogenous fluorophore to create visual information through light emission. Compared with other imaging modalities, it offers several advantages including high sensitivity, low cost, minimal cell damage, and use of nonionizing radiation [1]. However, due to the presence of endogenous chromophores [2], image resolution can be affected by autofluorescence generated from the tissue. This can be minimized by employing a near-IR (NIR) light source (650–900 nm). Within this NIR window, the major tissue components such as hemoglobin and water have minimal absorptions, allowing light to propagate deeper (more than 1 cm) into the tissues [3, 4].

Indocyanine green (ICG) was the first NIR fluorophore approved by the US Food and Drug Administration (FDA) for diagnostic applications including hepatic function tests [5, 6], cardiac physiology tests [7], and ophthalmic angiography [8, 9]. Since then, various organic and inorganic fluorophores such as Cy5.5, Cy7, NIR-664, CyTE-777, and tris(2,2′-bipyridyl)dicholororuthenium(II) hexahydrate have also been developed (Figure 9.1). Organic fluorophores generally suffer from photobleaching [10], aggregation on storage [11], photo and thermal degradation [12], and their potential to bind to serum proteins [13]. To improve their pharmacokinetic properties (such as specific tissue accumulation), fluorophores can be conjugated to specific ligands such as antibodies [14, 15] or peptides [16] for active targeting.

According to the US National Nanotechnology Initiative (www.nano.gov), nanotechnology is the understanding and control of matter at dimensions between approximately 1 and 100 nm. Materials within this nanometer size range play a distinct role inside our body. For example, ultrasmall nanoparticles (3–5 nm) are eliminated predominantly by the kidney, while larger nanoparticles (above 10–20 nm) are captured in the liver [17, 18]. In certain disease conditions such as cancer, due to the hypervasculature and the lack of effective lymphatic drainage

*Biosensor Nanomaterials*. Edited by Songjun Li, Jagdish Singh, and Ipsita A. Banerjee

ISBN: 978-3-527-32841-3

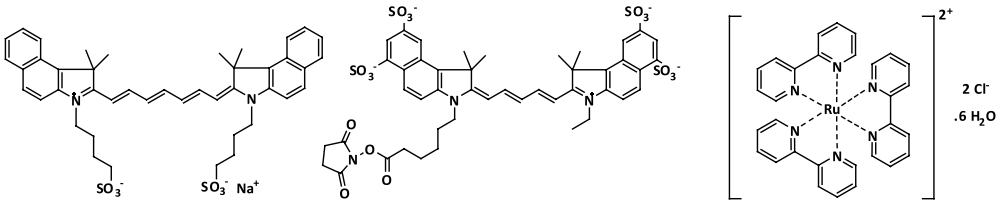


**Figure 9.1** Examples of organic and inorganic fluorophores developed for optical imaging.

at the tumor sites, nanoparticles (20–150 nm) tend to accumulate in the tissues via an enhanced permeability and retention (EPR) effect [19]. Efficient tumor delivery can be achieved by incorporating therapeutic and imaging agents into these inherent carriers [20]. Other diseases such as atherosclerosis [21, 22] and rheumatoid arthritis [23] are also the targets of nanoparticles (via the EPR effect). Some nanomaterials have been modified with target ligands such as antibodies [24], peptides [25], small molecules [26], and aptamers [27] for targeted delivery [28]. Also, when multiple ligands are covalently attached to the nanoparticles, their affinities can be increased by multivalency [29].

## 9.2 Doped Nanoparticles

As described above, organic fluorophores are often susceptible to photobleaching and rapid blood clearance [30, 31]. To prevent photodegradation, organic fluorophores can be doped into or onto the nanoparticles [32]. By controlling the loading density, the quantum yields of the organic fluorophores (i.e., the fluorescence signals) can also be enhanced to create ultrasensitive nanoparticles for imaging [33, 34].

### 9.2.1 Doped Nanoparticles for *In Vivo* Imaging

Silica ($SiO_2$) nanoparticles have been studied extensively for drug delivery. They are inert, photostable, and optically transparent [35, 36]. Fluorophores or drug molecules can be simply incorporated into the $SiO_2$ nanoparticles via ionic interaction [37], entrapment [38, 39], or covalent conjugation [40, 41]. Jeon *et al.* developed rhodamine B isothiocyanate (RITC)-doped $SiO_2$ nanoparticles to image sentinel lymph nodes [42]. *In vivo* study indicated that the RITC-$SiO_2$ nanoparticles tended to accumulate in the axillary and brachial lymph nodes within 5 min (Figure 9.2). In another study, He *et al.* designed a theranostic $SiO_2$ nanoparticle for imaging and photodynamic therapy [43]. Methylene blue, a phenothiazinium photosensitizer,

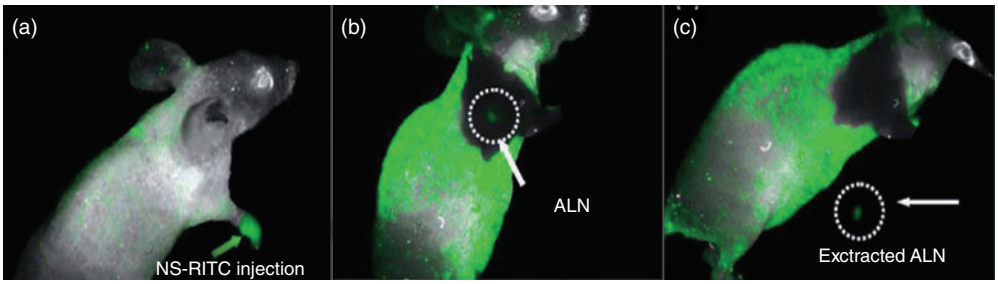


**Figure 9.2** *In vivo* sentinel node imaging. Fluorescence images of mice at 5 min after injecting RITC-$SiO_2$ nanoparticles (NS-RITC) into the right footpad on the fore leg. (a) Fluorescence image of mice with intact skin. (b) Image of the same mouse when the surrounding skin was removed. (c) The axillary lymph node (ALN) was extracted prior to image acquisition. (Reprinted with permission from [42], © 2009 Academy of Molecular Imaging.)

was encapsulated into the phosphonated-terminated $SiO_2$ matrix. The author demonstrated that $SiO_2$ nanoparticles can help direct a laser source to the area of interest for the purposes of photodynamic therapy [43].

The use of $SiO_2$ nanoparticles for *in vivo* imaging can be limited by their low solubility and their potential to possibly trigger local inflammation through the formation of reactive oxygen species and free radicals [4, 44]. Nanoparticles derived from biodegradable polymers are relatively nontoxic and retain the biodegradable of the original polymers [45, 46]. Yang *et al.* had succeeded in synthesizing core-cross-linked polymeric micelles (CCPMs) derived from an amine-terminated amphiphilic block copolymer for imaging [47]. Fluorescence emissions from Cy7-entrapped CCPMs were found to be 77% brighter than the free fluorophore. After intravenous injection, optical imaging revealed a gradual increase in tumor uptake (up to 120 h), suggesting that CCPMs are potential drug carriers. Despite their excellent safety profile, most biodegradable polymers are prone to leakage in blood circulation [48].

Calcium phosphosilicate nanoparticles (CPNPs) are another type of nanoparticle that has recently been proposed for drug delivery [49–51]. Compared with other nanomaterials, CPNPs are nontoxic and relatively easy to synthesize. They are insoluble in physiological pH, but are completely dissociate at pH < 6.5 facilitating the release of the encapsulated molecules [51]. Altinoglu *et al.* reported the first ICG-doped CPNPs for tumor imaging [49]. Fluorescence emissions from ICG-doped CPNPs were found to be significantly brighter (above 200%) than the free ICG. The nanoparticles were also less susceptible to photobleaching. Targeting ICG-doped CPNPs has also been used for imaging breast and pancreatic cancer [52]. These particles were covalently modified with targeting ligands such as anti-CD71 or gastrin peptide and had demonstrated enhanced tumor accumulation versus the nontargeted control vehicles [52].

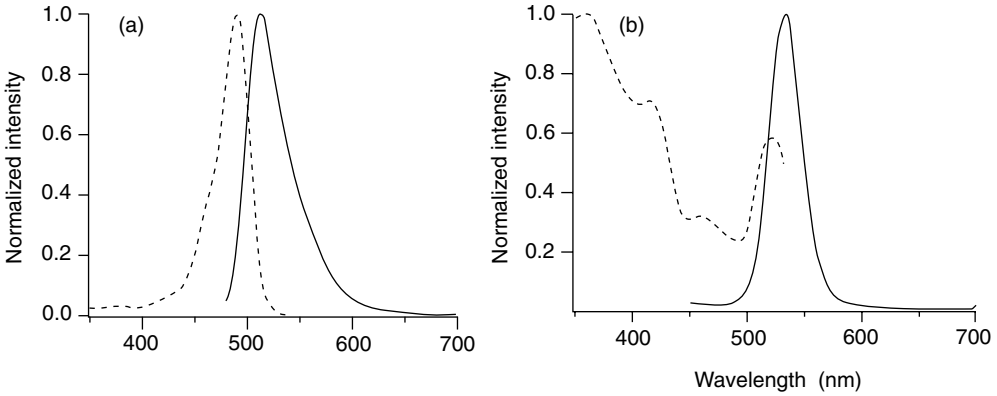


**Figure 9.3** Comparison of absorption (dashed curve) and fluorescence (solid curve) spectra of (a) fluorescein and (b) a typical water-soluble QDs. The excitation wavelength was 476 and 355 nm for fluorescein and QDs, respectively. (Reprinted with permission from [54], © 1998 AAAS.)

### 9.2.2 Quantum Dots

As described above, some nanoparticles are intrinsically fluorescent. Quantum dots (QDs) are synthetic semiconductor crystals that are composed of group II–VI (e.g., CdSe, CdTe, CdS, and ZnSe), group III–V (e.g., InP and InAs), or group IV–VI (e.g., PbSe and PbTe) elements of the periodic table and are defined as particles having physical dimensions smaller than an exciton Bohr radius [53]. The quantum confinement effects in QDs give rise to their unique optical properties. QDs have broad excitation profiles, but narrow and symmetric fluorescence spectra (Figure 9.3). Single QDs normally appear 10–20 times brighter than any conventional organic dye [10, 53–61] and are more photostable [10, 55]. By alternating the particle sizes or chemical compositions, individual QDs can be fabricated (fine-tuned) to have discrete emission maxima (a range of 400 to 2000 nm), which can be used for the multiplexed imaging of proteins, genes, and small-molecule libraries [62, 63].

QDs are hydrophobic in nature and are therefore incompatible with biological systems. To make water-soluble QDs, their surfaces must be tailored with coatings [64], which can be achieved by chemical exchange [54, 55] or hydrophobic-hydrophobic interaction [10, 57]. Surface coatings can also provide additional organic functional moieties such as COOH, $NH_2$, or SH for bioconjugation. Small molecules [54] or biomolecules including oligonucleotides [17, 65–67], antibodies [58, 68, 69], peptides [56], and proteins [70] can be attached onto the QD surfaces for diagnostic and therapeutic purposes.

When used for *in vivo* studies, QDs can be controversial [71] since the metallic constituents such as cadmium or selenium are toxic to many cells [72, 73]. It has been proposed that group III–V QDs (e.g., InP) are less toxic than group II–VI QDs (e.g., CdSe) [74] and are thus more suitable for biomedical applications.

Studies have shown that the cytotoxicity of QDs is correlated with the liberation of free $Cd^{2+}$ ions [75]. The mechanism of cell damage has been attributed to free radical formation or possible interaction with certain intracellular organelles such as mitochondria [76]. On the other hand, QDs were found to be stable in the embryos of the carnivorous frog *Xenopus* [57]. When injected into rodents, QDs were found to predominantly accumulate (within a range of days to months) in the livers, spleens, and kidneys [56, 77, 78]. Their biodistributions may vary with the coatings and actual sizes [56, 57]. Coating the QDs with poly(ethylene glycol) (PEG) can prevent their nonselective accumulation in the reticuloendothelial tissues [56]. Studies have shown that QDs coated with four different polymers (poly(acrylic acid), mPEG-750, mPEG-5000, and COOH-PEG-3400) gave rise to different circulating half-lives (varying from 12 to 70 min) [79]. Another study has demonstrated that QDs with diameters less than 10 nm were predominantly eliminated through the kidneys within 4 h postinjection [80]. Although many animal studies have suggested that QDs do not cause toxicity *in vivo*, their metabolism is still not fully understood.

### 9.2.3
### Application of Quantum Dots for *In Vivo* Imaging

QDs have been used for sensing, cell and tissue labeling [54], cell trafficking study [81, 82], and multiplex imaging [62, 63]. There are some excellent reviews published in these areas [64, 83–85]. For *in vivo* application, Akerman *et al.* reported the first injected QDs for targeting tumor vasculature [56]. Kim *et al.* used NIR type II QDs for sentinel lymph node mapping [86]. To minimize nonspecific deposition, QDs are generally modified with multiple targeting ligands. Gao *et al.* reported the first QDs for simultaneous targeting and real-time imaging of tumors [87]. The QDs were attached with tumor-targeting antibodies (J591) to prostate-specific membrane antigen, and were delivered to C5-2 tumor xenografts through both passive and active targeting mechanisms (Figure 9.4). Other examples of targeting QDs used for whole-animal imaging are illustrated in Table 9.1.

As described earlier, one of the major obstacles for optical imaging is the strong autofluorescence generated from endogenous chromophores. Recently, So *et al.* developed a new type of self-illuminating QDs that are fluorescent without an external illumination source [98]. These bioluminescent QDs were designed to couple with the bioluminescence resonance energy transfer donor luciferase. Upon binding to coelenterazine substrates, the bioluminescence energy produced from luminescent reactions can be transferred to the QD acceptors, resulting in fluorescence emission (Figure 9.5). Background fluorescence can be completely avoided by using bioluminescent QDs for *in vivo* imaging [98].

### 9.2.4
### Gold Nanoparticles

Gold preparations have been used for many years to treat diseases such as smallpox, various skin disorders, syphilis, and arthritis. Recently, gold nanoparticles

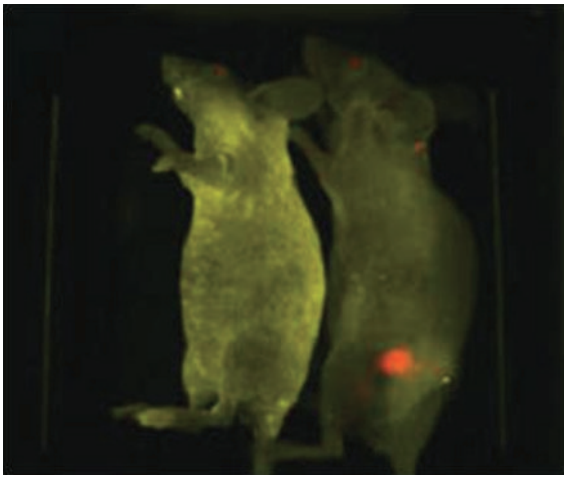

**Figure 9.4** Fluorescence imaging indicates a prostate tumor growing in a live mouse (right). Same amount of QDs also injected into a healthy mouse that has no tumor (left) as the control. (Reprinted with permission from [87], © 2004 Nature Publishing Group.)

**Table 9.1** Examples of QD conjugates used for *in vivo* imaging.

| Conjugate | Targeting ligand | Target | Disease |
|---|---|---|---|
| Peptide | RGD [88] | $\alpha_v\beta_3$ | Cancer |
| Antibody | Trastuzumab [89] | HER2 receptor | Cancer |
| | Anti-AFP [90] | α-Fetoprotein | Cancer |
| | Anti-PAR1 [91] | Proteinase activated receptor receptor | Cancer |
| | Anti-ICAM-1/ VCAM-1 [92] | Cell adhesion molecule | Diabetes |
| | Anti-CD45 [92] | Leukocyte | Uveitis |
| | Anti-CCR3 [93] | CCR3 receptor | Choroidal neovascularization |
| Protein | EGF [94] | Epidermal growth factor receptor | Cancer |
| | VEGF [95] | Vascular endothelial growth factor receptor | Cancer |
| | Lectin [96] | Blood–brain barrier | CNS related diseases |
| Small molecule | DPA-Zn [97] | Anionic phospholipids | Bacterial infection |

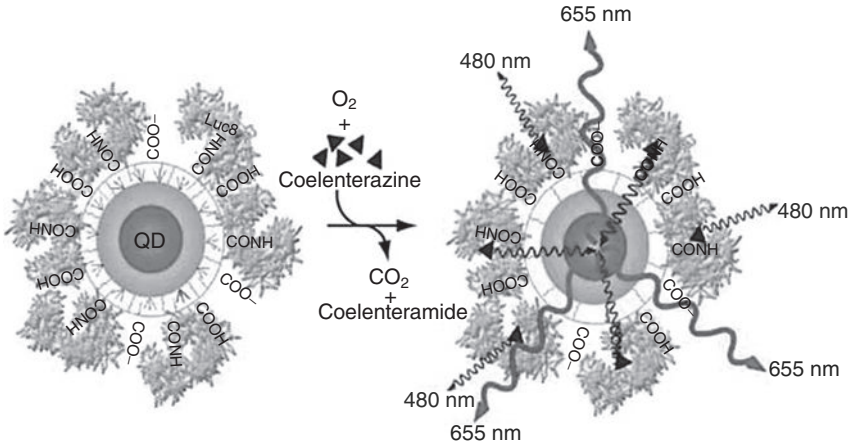


**Figure 9.5** Schematic presentation of QDs covalently conjugated with luciferases (Luc8). (Reprinted with permission from [98], © 2006 Nature Publishing Group.)

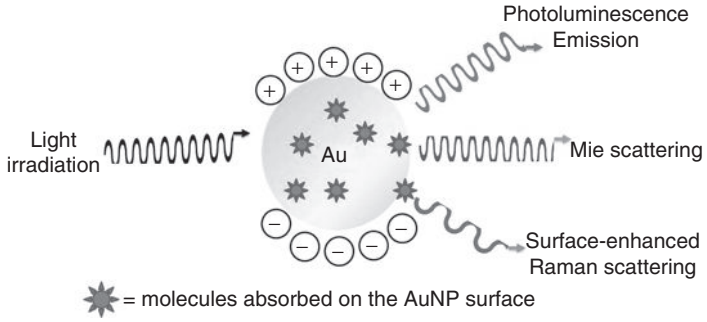


**Figure 9.6** Enhanced photophysical properties of Au-NPs. The irradiated light absorbed through the SPR effect [105] at particular frequency, which can be further scattered (by Mie [106] and Raman [107] scatterings) and/or re-emitted as photoluminescence [108].

(Au-NPs) have drawn a lot of attention for biomedical imaging purposes. Compared with other nanoparticles, gold is more flexible to synthesize [99–104]. Its photophysical properties can be altered or enhanced (Figure 9.6), as described by the surface plasmon resonance (SPR) [105]. When Au-NPs interact with light, the free electrons of the particle surface undergo a collective coherent oscillation with respect to the positive metallic lattice [105, 109]. This oscillation can subsequently be decayed radioactively by light scattering or nonradioactively by converting the light energy into heat.

Another unique property of Au-NPs is the fact that their absorbance (i.e., SPR frequency) can be fine-tuned by changing the size, shape, composition, or environment. For example, gold nanospheres with a broad size range (9–99 nm) have

resonances in the 520- to 580-nm region (Figure 9.7a) [110]. The SPR tunability of gold nanospheres is, however, limited (below 600 nm) as a result of the electromagnetic retardation effects in larger nanoparticles. Two approaches are known for tuning the Au-NPs wavelengths within the NIR windows for biological imaging. Changing the shape of Au-NPs from spheres to rods can create a SPR band at the longer wavelengths (Figure 9.7b). This additional band corresponds to the plasmon oscillation along the long axis [113]. Both the intensity and the red-shift of the SPR band have shown increases with the nanorod aspect ratio. The second approach

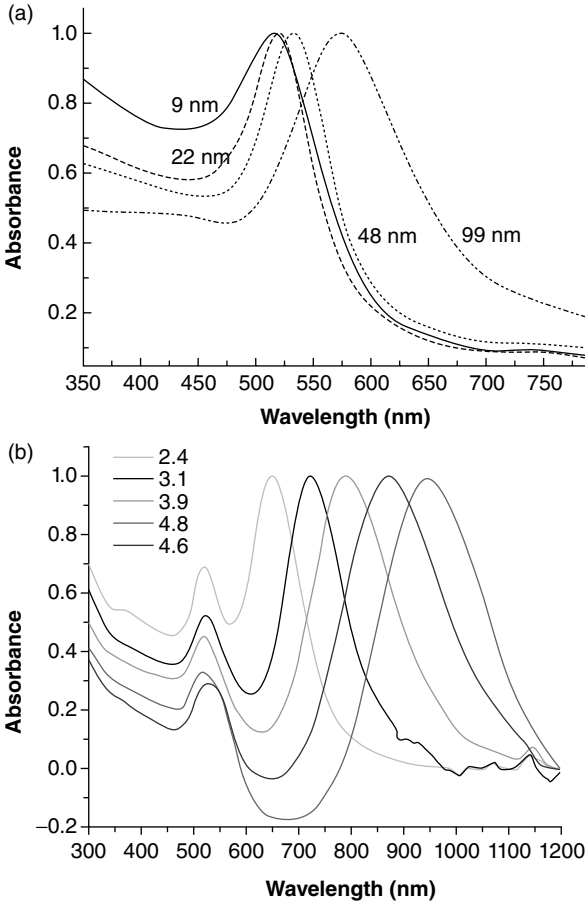


**Figure 9.7** Size and shape tunability of the SPR of gold nanostructures. (a) Absorbance spectra of spherical Au-NPs of different sizes. (Reprinted with permission from [110], © 1999 ACS). (b) The SPR frequency can be fine-tuned by synthetically controlling the aspect ratio of gold nanorods. (Reprinted with permission from [111], © 2006 ACS.) (c) By changing the thickness ($t$) relative to the core size (80 nm), gold nanoshells with different SPR can be synthesized. (Reprinted with permission from [112], © 2006 ACS.)

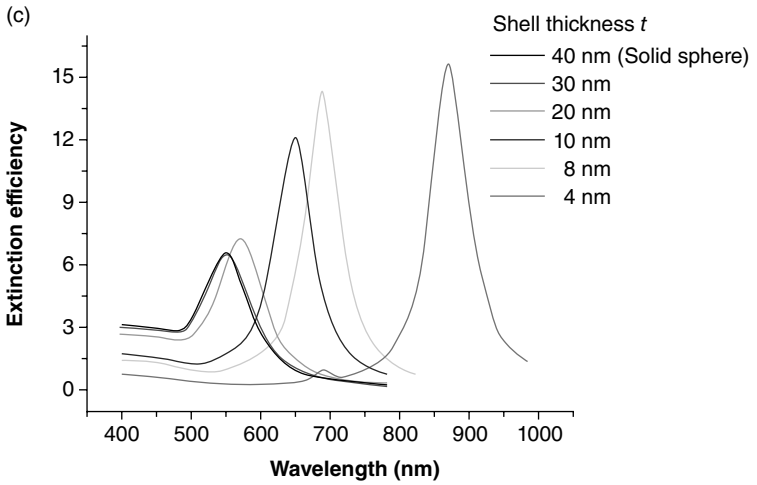


**Figure 9.7** (*Continued*)

is by designing a dielectric core–gold shell nanostructure (gold nanoshell). For example, a $SiO_2$ core can be coated with a thin layer (a few nanometers) of gold [114], in which the SPR can be fine-tuned by decreasing the thickness of the gold layer (Figure 9.7c). Other similar NIR nanostructures using polystyrene [115] and sulfide [116] as the core have also been reported.

#### 9.2.4.1 Application of Gold Nanoparticles in Fluorescence Imaging

Au-NPs are relatively nontoxic and compatible with cells [117]. The enhanced SPR effect of Au-NPs can become useful for biomedical imaging. For *in vivo* application, since Au-NPs have relatively weaker fluorescence emissions than QDs, they are seldom used alone as an optical contrast agent in fluorescence imaging. Organic fluorophores are normally attached to the Au-NP surfaces; the fluorescence emissions can be either quenched or enhanced, depending on the distance between the two counterparts [118, 119]. This unique property has been exploited to design a smart Au-NPs probe for detecting matrix metalloproteinase (MMP) activity *in vivo* [120]. By stabilizing a Cy5.5-conjugated MMP peptide substrate onto the Au-NPs, the molecular excitation energy of Cy5.5 was efficiently quenched by surface-energy transfer and possibly by static quenching and fluorescence resonance energy transfer [117, 121]. In the presence of MMP, the enzyme was able to digest the peptide substrate, release the Cy5.5-conjugated fragments, and subsequently initiated a dequenching process (i.e., fluorescent amplification) (Figure 9.8a). The probe was injected into the SCC7 squamous cell carcinoma xenografts for investigating the local MMP-2 activity [120]. Using a similar concept, an gold nanoprobe was also designed to report reactive oxygen species/hyaluronidase activity in rheumatoid arthritis (Figure 9.8b) [122].

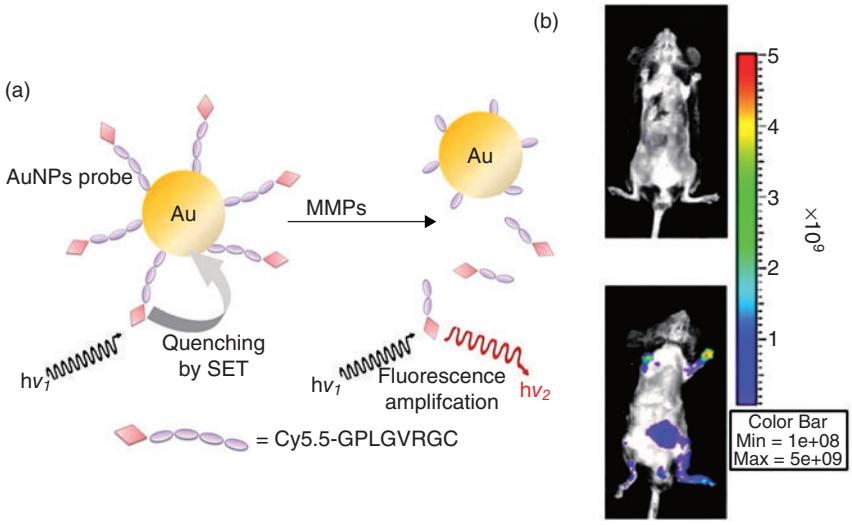


**Figure 9.8** The design of a gold nanoprobe for fluorescence imaging. (a) Schematic presentation of MMP-sensitive Au-NP probe for imaging MMP activities. SET = surface energy transfer. (b) Another gold nanoprobe was designed by immobilizing HilyteFluor647 dye-labeled hyaluronic acid onto the surface for imaging reactive oxygen species/ hyaluronidase activity. The probe (10 pmol) was administrated to a normal (top) and rheumatoid arthritis mouse model (bottom) by tail vein injection. The NIR fluorescence signals appeared in the inflamed limbs. (Reprinted with permission from [122], © 2008 Elsevier.)

**Table 9.2** Examples of Au-NPs used for photoacoustic imaging.

| Technique | Nanoplatform | Target/disease |
|---|---|---|
| Photoacoustic tomography | Nanocage [124] | Cerebral cortex |
| | Hallow nanosphere [125] | Brain vasculature |
| | Nanorod [126] | Sentinel lymph node mapping |
| | GNT [127] | Circulating tumor cell |

### 9.2.4.2 Application of Gold Nanoparticles in Photoacoustic Imaging

Photoacoustic tomography (PAT) is a noninvasive imaging technique that combines optical radiation and high ultrasonic detection in a single modality [123]. It was not until recently that Au-NPs were applied as the contrast agents for PAT (Table 9.2). The basic principle of PAT is that light absorbed by Au-NPs can be converted into heat, leading to transient variations in temperature and resulting in generation of acoustic signals [128]. Wang *et al.* reported the first Au-NPs for imaging the vasculature of a rat brain [129]. The optical absorption of a gold nanocage in the cerebral cortex can be enhanced by up to 81% [124]. Au-NPs have also been used for sentinel lymph nodes mapping [126, 130].

Recently, Galanzha *et al.* designed golden carbon nanotubes (GNTs) as contrast agents for simultaneous magnetic capturing (enrichment) as well as for photoacoustic detection of circulating tumor cells (CTCs) *in vivo* [127]. In this study, a cocktail of urokinase plasminogen activator (uPA)-conjugated ferric oxide nanoparticles and folic acid-conjugated GNTs was injected intravenously into a breast cancer xenograft mouse model with overexpressing uPA receptors and folate receptors. The two distinct circulating nanoparticles were proposed to simultaneously bind to their corresponding receptors on the CTCs. By attaching a magnet to the top of the mouse's ear vein, CTCs originating from the primary tumor sites were captured (enriched) by iron oxide nanoparticles, followed by detection of the photoacoustic signals generated by the cell-bound GNTs where the laser beam was located (Figure 9.9).

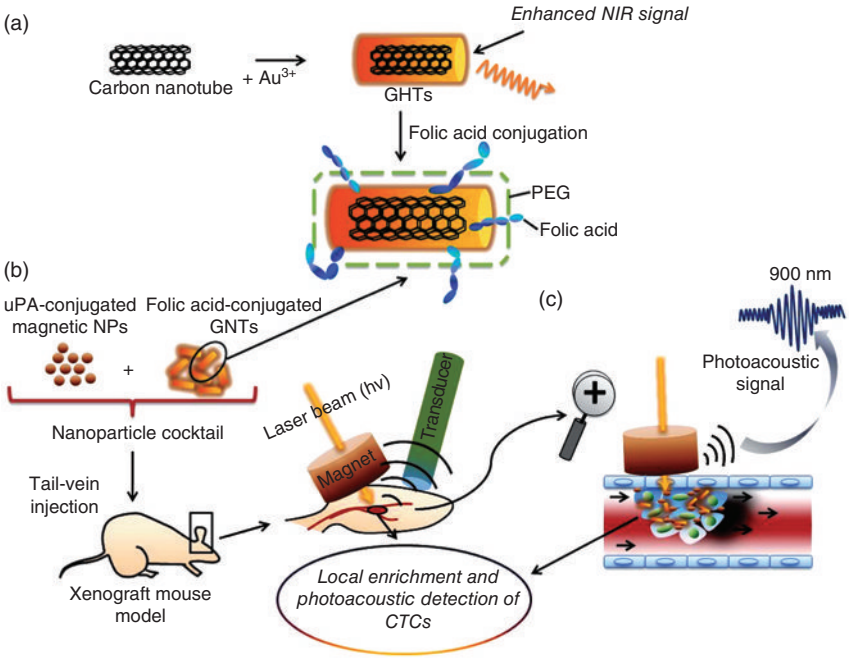


**Figure 9.9** *In vivo* magnetic enrichment and multiplex photoacoustic detection of CTCs. (a) Synthesis of folic acid-conjugated GNTs. GNTs were synthesized by depositing a thin layer of gold on SWNTs [131], followed by their functionalization with PEG and folic acid. (b) A cocktail of folic acid-conjugated GNTs and uPA-conjugated ferric oxide NPs was injected in tumor-bearing mice. After tail-vein injection, an external magnet was placed on top of the mouse's ear blood vessel to capture the CTCs, which caused a local enrichment of the CTCs. A laser beam was then delivered through a hole in the magnet using a fiber-based delivery system. The resulting photoacoustic signals generated by the cell-bound GNTs can be detected by a transducer. (c) Schematic representation showing the capture of CTCs and the generation of photoacoustic signals from CTC-bound GNTs inside a 70-μm vein of the mouse ear.

**Table 9.3** Various examples of liposomes as imaging carriers.

| Type of targeting | Mechanism of uptake and release | Targeting disease | Optical reporter | References |
|---|---|---|---|---|
| Passive targeting | Phagocytosis | Edema | DY-678 | [139] |
| | EPR and triggered release | Skin cancer | Carboxyfluorescein | [140] |
| | EPR and triggered release | Breast cancer | SIDA | [141] |
| Active targeting | Receptor-mediated endocytosis | Lung cancer | Cy5.5 | [142] |
| | Receptor-mediated endocytosis | Lung cancer | Cy5.5 | [143] |
| | Receptor-mediated endocytosis | Arthritis | Cy5.5 | [144] |

### 9.2.5 Lipid-Based Nanoparticles

Liposomes were first used as a model for studying biological membrane properties [132]. They are self-assembled lipid nanoparticles composed of lecithin and phospholipids [133], which have been widely used as drug carriers for over two decades. Some liposomal formulations have also been approved by the FDA [134]. Doxil, for example, is the first stealth liposome marketed for the treatment of Kaposi's sarcoma [135] and ovarian carcinoma [136]. The advantage of liposomes is that they are nontoxic and biocompatible. By controlling the sizes and the number of lipid layers during synthesis [134], substantial amounts of drug molecules/fluorophores can be either encapsulated inside or incorporated on the outside of the liposomes for drug delivery [137, 138] and imaging (Table 9.3). Without surface modifications, liposomes are cleared rapidly from the blood [145]. They can also interact with other lipoproteins [134], thus making them relatively unstable *in vivo*. To increase the plasma residence time, hydrophilic molecules such as PEG [146–150], and poly(*N*-(2-hydroxypropyl)methacrylamide) [151] can be integrated onto the particle surfaces for *in vivo* applications. Recently, a synthetic liposome "polymersome" was developed for *in vivo* imaging [152]. The polymersome was formed through cooperative self-assembly of amphiphilic diblock copolymers and conjugated multi(porphyrin)-based NIR fluorophores. They are considered more rigid than their natural counterparts.

#### 9.2.5.1 Liposomes as Imaging Carriers

Content release from conventional liposomes normally relies on passive diffusion. To enhance the drug release kinetics, triggered release preparations can be

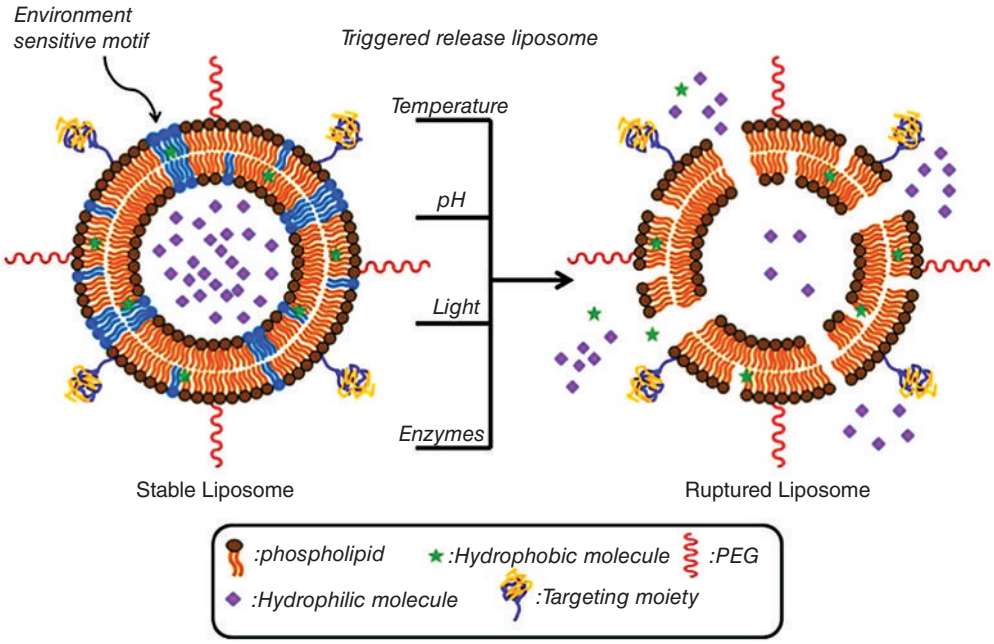


**Figure 9.10** Schematic presentation of the design of various triggered release liposomal preparations.

designed by simply incorporating environmentally sensitive motifs in the membrane bilayers. Drug release can be triggered by either exogenous or endogenous stimuli such as pH [153, 154], enzymes [155, 156], temperature [157], and light [158, 159]. Upon activation, these liposomes may undergo structural changes, subsequent loss of membrane integrity, and release (leakage) of the encapsulated contents (Figure 9.10).

This triggered release mechanism has been explored to develop smart probes for optical imaging, since a substantial amount of organic/inorganic fluorophores can be encapsulated inside a liposome to cause significant fluorescence self-quenching. Upon activation by external stimuli, the released fluorophores will contribute to fluorescence amplification (dequenching). This creates a high signal-to-background ratio at the local area for optical imaging. An early example of this effect is the temperature-sensitive liposome that can be triggered by microwaves or argon lasers to release carboxyfluorescein in the eye [160, 161]. Paoli *et al.* reported using a similar approach for monitoring drug release [162]. Another study also demonstrated that D-luciferin can be encapsulated inside a temperature-sensitive liposome for bioluminescence imaging of Met-1-*luc* tumors (Figure 9.11). Pharmacokinetic study has suggested that the liposomal D-luciferin is more stable (longer half-life) than the substrate alone [163].

Another advantage of liposomes is the fact that different molecules can be encapsulated inside the aqueous compartment, entrapped within the lipid bilayers,

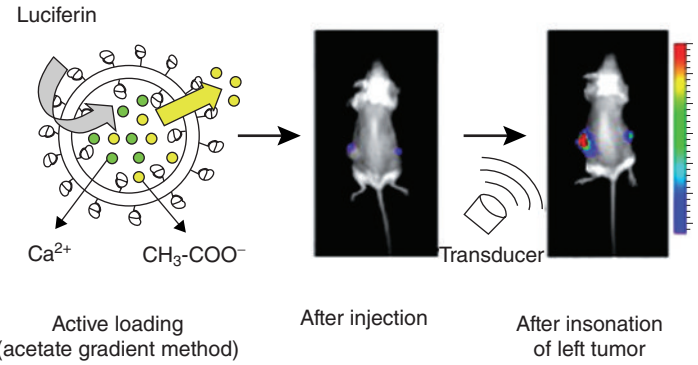


**Figure 9.11** *In vivo* bioluminescence imaging of Met-1-*luc* tumor-bearing mice using temperature-sensitive liposomes. The mice were administered (intratumoral injection) with temperature-sensitive liposome (left tumor) and free luciferin (right tumor). The liposomes were stable at body temperature, but can be triggered to release the encapsulated D-luciferin by insonation (39 °C for 1 min), as shown by the enhanced bioluminescence signal. (Reprinted with permission from [163], © 2010 Elsevier.)

or conjugated/absorbed onto the particle surfaces, thus making it feasible to design multimodality probes for imaging. For example, Shan *et al.* developed a liposome-based bimodal imaging probe for detecting solid tumors [164]. The probe was designed with a magnetic resonance imaging (MRI) contrast agent (gadopentetate dimeglumine) encapsulated inside the liposome. Multiple NIR-labeled transferring proteins were further linked to the particle surface for targeted delivery. This liposome can image the anatomical structure, as well as the heterogeneous pattern within the tumors by both MRI and optical imaging [164]. Recently, Feng *et al.* developed a bifunctional immunoliposome by conjugating a thiolated fusion protein of ZZ (Fc-affinity domain) and *Gaussia* luciferase for antibody binding and imaging [165]. Additionally, 8-hydroxypyrene-1,3,6-trisulfonic acid trisodium salt (HPTS) dye was chosen as a model drug for encapsulation. Bioluminescence imaging demonstrated that the liposomes were effectively delivered to the U87 ΔEGFR xenografts (Figure 9.12). High fluorescence signals from the encapsulated HPTS were observed on the frozen tumor sections, suggesting that this approach can be used for monitoring drug delivery [165].

#### 9.2.5.2 **Biomolecules**

Antribodies, proteins, and virsues are biomolecules that have physical dimensions within the nanmether size ranges. Compared with other synthetic nanoparticles, they are nonimmunogenic (with the exception of bacteriophage) and nontoxic, and are commonly used as the inherent carriers for drug molecules and imaging agents. Organic or inorganic fluorophores can be simply covalently or noncovalently attached to the biomolecules for imaging. For example, albumin is a natural protein carrier for hydrophobic molecules such as vitamins, hormones, and other

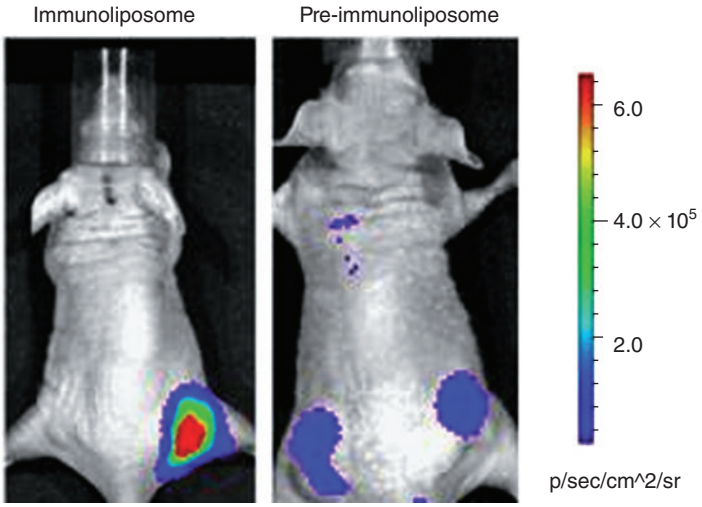


**Figure 9.12** Bioluminescence imaging in living nude mice implanted with U87 ΔEGFR xenografts. Animal injected intravenously with bifunctional immunoliposomes (left panel) and control liposomes that were not conjugated with targeting antibody (right panel). The mice were imaged at 4 h after injection with coelenterazine substrate at the tumor sites. The same amount of coelenterazine was injected to the site without tumor as the control background. (Reprinted with permission from [165], © 2010 Elsevier.)

plasma constituents. It can enhance the delivery of NIR fluorophore (via noncovalent binding) to the tumor sites (via passive targeting) for imaging cancers [166]. Alternatively, Aida *et al.* has covalently conjugated rhodamine green to galactosylated albumin for targeted imaging of the peritoneal cavities of SHIN3-xenografted mice [167]. Other peptide and protein scaffolds, such as "affibodies" and "nanobodies," are currently under development for molecular imaging [168].

Monoclonal antibodies are able to specifically recognize their epitopes with high avidity. To demonstrate the specificity of FDA-approved antibodies as imaging carriers, Barrett *et al.* injected a cocktail of Cy5.5-labeled cetuximab (anti-HER1) and Cy7-labeled trastuzumab (anti-HER2) into nude mice bearing multiple tumors. The antibodies were able to simultaneously differentiate between two types of tumors (A431 and 3T3/HER2$^+$) expressing distinct endothelial growth factor receptor expressions [169]. In another study, Hasan *et al.* employed a dye-conjugated antibody to monitor the changes of vascular endothelial growth factor expression in tumors after photodynamic therapy [170]. Recently, Hilderbrand *et al.* used a targeted M13 bacteriophage as the imaging platform [171]. By coupling multiple copies (hundreds) of pH-sensitive HCyC-646 and pH-insensitive Cy7 dyes onto the surface of the bacteriophage, it is possible to ratio-image the pH changes through optically diffuse tissue.

## 9.3 Conclusions and Outlook

We have discussed some unique characteristics of various nanoparticles. Examples were chosen to highlight their applications in optical imaging. It is to be noted there are many other nanoparticles that were not discussed, including but not limited to nanofibers [172], carbon nanotubes [173], superparamagnetic iron oxide crystals [174], dendrimers [175], and carbohydrate–ceramic nanoparticles, which have also been engineered as therapeutic or diagnostic cargos. Some of the concepts described in this chapter can also be applied to other imaging modalities. For example, radioactive liposomes have been developed for single-photon emission computed tomography and positron emission tomography imaging [176]. Others, such as superparamagnetic nanoparticles, were designed particular for MRI [177]. The bottom line is that there is no nanoparticle that is considered to be superior to the others for imaging. They each have their own unique qualities. Nanoparticles should be chosen according to the type of information one desires to obtain. This requires a profound understanding of disease molecular pathologies, their heterogeneities versus normal health states, and the intrinsic properties of the nanoparticle.

### Acknowledgments

This research was supported in part by North Dakota EPSCoR Program (FAR0014970) to B.L.

### References


1 Bremer, C., Ntziachristos, V., and Weissleder, R. (2003) *Eur. Radiol.*, **13**, 231.
2 Bornhop, D.J., Contag, C.H., Licha, K., and Murphy, C.J. (2001) *J. Biomed. Opt.*, **6**, 106.
3 Ntziachristos, V., Bremer, C., and Weissleder, R. (2003) *Eur. Radiol.*, **13**, 195.
4 Altinoglu, E.I. and Adair, J.H. (2010) *Wiley Interdiscip. Rev. Nanomed. Nanobiotechnol.*, **2**, 461.
5 Watanabe, Y. and Kumon, K. (1999) *J. Cardiothorac. Vasc. Anesth.*, **13**, 299.
6 Janssen, M.W., Druckrey-Fiskaaen, K.T., Omidi, L., Sliwinski, G., Thiele, C., Donaubauer, B., Polze, N., Kaisers, U.X., Thiery, J., Wittekind, C., Hauss, J.P., and Schon, M.R. (2009) *J. Hepatobiliary Pancreat. Surg.*, **17**, 180.
7 Schad, H., Brechtelsbauer, H., and Kramer, K. (1977) *Pflugers Arch.*, **370**, 139.
8 Schutt, F., Fischer, J., Kopitz, J., and Holz, F.G. (2002) *Clin. Experiment. Ophthalmol.*, **30**, 110.
9 Herbort, C.P., LeHoang, P., and Guex-Crosier, Y. (1998) *Ophthalmology*, **105**, 432.
10 Wu, X., Liu, H., Liu, J., Haley, K.N., Treadway, J.A., Larson, J.P., Ge, N., Peale, F., and Bruchez, M.P. (2003) *Nat. Biotechnol.*, **21**, 41.
11 Kirchherr, A.K., Briel, A., and Mader, K. (2009) *Mol. Pharm.*, **6**, 480.
12 Saxena, V., Sadoqi, M., and Shao, J. (2003) *J. Pharm. Sci.*, **92**, 2090.

**13** Faybik, P. and Hetz, H. (2006) *Transplant. Proc.*, **38**, 801.

**14** Falati, S., Gross, P., Merrill-Skoloff, G., Furie, B.C., and Furie, B. (2002) *Nat. Med.*, **8**, 1175.

**15** Hsu, E.R., Gillenwater, A.M., Hasan, M.Q., Williams, M.D., El-Naggar, A.K., and Richards-Kortum, R.R. (2006) *Int. J. Cancer*, **118**, 3062.

**16** Ke, S., Wen, X., Gurfinkel, M., Charnsangavej, C., Wallace, S., Sevick-Muraca, E.M., and Li, C. (2003) *Cancer Res.*, **63**, 7870.

**17** Pathak, S., Choi, S.K., Arnheim, N., and Thompson, M.E. (2001) *J. Am. Chem. Soc.*, **123**, 4103.

**18** Soo Choi, H., Liu, W., Misra, P., Tanaka, E., Zimmer, J.P., Itty Ipe, B., Bawendi, M.G., and Frangioni, J.V. (2007) *Nat. Biotechnol.*, **25**, 1165.

**19** Maeda, H., Fang, J., Inutsuka, T., and Kitamoto, Y. (2003) *Int. Immunopharmacol.*, **3**, 319.

**20** Reddy, L.H. (2005) *J. Pharm. Pharmacol.*, **57**, 1231.

**21** Moulton, K.S., Olsen, B.R., Sonn, S., Fukai, N., Zurakowski, D., and Zeng, X. (2004) *Circulation*, **110**, 1330.

**22** Meding, J., Urich, M., Licha, K., Reinhardt, M., Misselwitz, B., Fayad, Z.A., and Weinmann, H.J. (2007) *Contrast Media Mol. Imaging*, **2**, 120.

**23** Levick, J.R. (1981) *Arthritis Rheum.*, **24**, 1550.

**24** Mamot, C., Drummond, D.C., Noble, C.O., Kallab, V., Guo, Z., Hong, K., Kirpotin, D.B., and Park, J.W. (2005) *Cancer Res.*, **65**, 11631.

**25** Srinivasan, R., Marchant, R.E., and Gupta, A.S. (2010) *J. Biomed. Mater. Res. A*, **93**, 104.

**26** Kukowska-Latallo, J.F., Candido, K.A., Cao, Z., Nigavekar, S.S., Majoros, I.J., Thomas, T.P., Balogh, L.P., Khan, M.K., and Baker, J.R., Jr. (2005) *Cancer Res.*, **65**, 5317.

**27** Farokhzad, O.C., Cheng, J., Teply, B.A., Sherifi, I., Jon, S., Kantoff, P.W., Richie, J.P., and Langer, R. (2006) *Proc. Natl. Acad. Sci. USA*, **103**, 6315.

**28** Gu, F.X., Karnik, R., Wang, A.Z., Alexis, F., Levy-Nissenbaum, E., Hong, S., Langer, R.S., and Farokhzad, O.C. (2007) *Nano Today*, **2**, 14.

**29** Badjic, J.D., Nelson, A., Cantrill, S.J., Turnbull, W.B., and Stoddart, J.F. (2005) *Acc. Chem. Res.*, **38**, 723.

**30** Sharma, P., Brown, S., Walter, G., Santra, S., and Moudgil, B. (2006) *Adv. Colloid Interface Sci.*, **123–126**, 471.

**31** Resch-Genger, U., Grabolle, M., Cavaliere-Jaricot, S., Nitschke, R., and Nann, T. (2008) *Nat. Methods*, **5**, 763.

**32** Muddana, H.S., Morgan, T.T., Adair, J.H., and Butler, P.J. (2009) *Nano Lett.*, **9**, 1559.

**33** Lian, W., Litherland, S.A., Badrane, H., Tan, W., Wu, D., Baker, H.V., Gulig, P.A., Lim, D.V., and Jin, S. (2004) *Anal. Biochem.*, **334**, 135.

**34** Bringley, J.F., Penner, T.L., Wang, R., Harder, J.F., Harrison, W.J., and Buonemani, L. (2008) *J. Colloid Interface Sci.*, **320**, 132.

**35** Knopp, D., Tang, D., and Niessner, R. (2009) *Anal. Chim. Acta*, **647**, 14.

**36** Yan, J.L., Estevez, M.C., Smith, J.E., Wang, K.M., He, X.X., Wang, L., and Tan, W.H. (2007) *Nano Today*, **2**, 44.

**37** Sivakumar, S., Diamente, P.R., and Veggel, F.C.J.M.v. (2006) *Chem. Eur. J.*, **12**, 5878.

**38** Jain, T.K., Roy, I., De, T.K., and Maitra, A. (1998) *J. Am. Chem. Soc.*, **120**, 11092.

**39** Tsagkogeorgas, F., Ochsenkühn-Petropoulou, M., Niessner, R., and Knopp, D. (2006) *Anal. Chim. Acta*, **573–574**, 133.

**40** An, Y., Chen, M., Xue, Q., and Liu, W. (2007) *J. Colloid Interface Sci.*, **311**, 507.

**41** Kumar, R., Roy, I., Ohulchanskyy, T.Y., Goswami, L.N., Bonoiu, A.C., Bergey, E.J., Tramposch, K.M., Maitra, A., and Prasad, P.N. (2008) *ACS Nano*, **2**, 449.

**42** Jeon, Y.H., Kim, Y.H., Choi, K., Piao, J.Y., Quan, B., Lee, Y.S., Jeong, J.M., Chung, J.K., Lee, D.S., Lee, M.C., Lee, J., Chung, D.S., and Kang, K.W. (2010) *Mol. Imaging Biol.*, **12**, 155.

**43** He, X., Wu, X., Wang, K., Shi, B., and Hai, L. (2009) *Biomaterials*, **30**, 5601.

**44** Fubini, B. and Hubbard, A. (2003) *Free Radic. Biol. Med.*, **34**, 1507.

**45** Pridgen, E.M., Langer, R., and Farokhzad, O.C. (2007) *Nanomedicine,* **2**, 669.

**46** Lu, J.M., Wang, X., Marin-Muller, C., Wang, H., Lin, P.H., Yao, Q., and

Chen, C. (2009) *Expert Rev. Mol. Diagn.*, **9**, 325.
**47** Yang, Z., Zheng, S., Harrison, W.J., Harder, J., Wen, X., Gelovani, J.G., Qiao, A., and Li, C. (2007) *Biomacromolecules*, **8**, 3422.
**48** Saxena, V., Sadoqi, M., and Shao, J. (2004) *J. Photochem. Photobiol. B*, **74**, 29.
**49** Altinoglu, E.I., Russin, T.J., Kaiser, J.M., Barth, B.M., Eklund, P.C., Kester, M., and Adair, J.H. (2008) *ACS Nano*, **2**, 2075.
**50** Kester, M., Heakal, Y., Fox, T., Sharma, A., Robertson, G.P., Morgan, T.T., Altinoglu, E.I., Tabakovic, A., Parette, M.R., Rouse, S.M., Ruiz-Velasco, V., and Adair, J.H. (2008) *Nano Lett.*, **8**, 4116.
**51** Morgan, T.T., Muddana, H.S., Altinoglu, E.I., Rouse, S.M., Tabakovic, A., Tabouillot, T., Russin, T.J., Shanmugavelandy, S.S., Butler, P.J., Eklund, P.C., Yun, J.K., Kester, M., and Adair, J.H. (2008) *Nano Lett.*, **8**, 4108.
**52** Barth, B.M., Sharma, R., Altinoğlu, E.I., Morgan, T.T., Shanmugavelandy, S.S., Kaiser, J.M., McGovern, C., Matters, G.L., Smith, J.P., Kester, M., and Adair, J.H. (2010) *ACS Nano*, **4**, 1279.
**53** Chan, W.C., Maxwell, D.J., Gao, X., Bailey, R.E., Han, M., and Nie, S. (2002) *Curr. Opin. Biotechnol.*, **13**, 40.
**54** Bruchez, M., Jr., Moronne, M., Gin, P., Weiss, S., and Alivisatos, A.P. (1998) *Science*, **281**, 2013.
**55** Chan, W.C. and Nie, S. (1998) *Science*, **281**, 2016.
**56** Akerman, M.E., Chan, W.C., Laakkonen, P., Bhatia, S.N., and Ruoslahti, E. (2002) *Proc. Natl. Acad. Sci. USA*, **99**, 12617.
**57** Dubertret, B., Skourides, P., Norris, D.J., Noireaux, V., Brivanlou, A.H., and Libchaber, A. (2002) *Science*, **298**, 1759.
**58** Jaiswal, J.K., Mattoussi, H., Mauro, J.M., and Simon, S.M. (2003) *Nat. Biotechnol.*, **21**, 47.
**59** Larson, D.R., Zipfel, W.R., Williams, R.M., Clark, S.W., Bruchez, M.P., Wise, F.W., and Webb, W.W. (2003) *Science*, **300**, 1434.
**60** Ishii, D., Kinbara, K., Ishida, Y., Ishii, N., Okochi, M., Yohda, M., and Aida, T. (2003) *Nature*, **423**, 628.
**61** Medintz, I.L., Clapp, A.R., Mattoussi, H., Goldman, E.R., Fisher, B., and Mauro, J.M. (2003) *Nat. Mater.*, **2**, 630.
**62** Han, M., Gao, X., Su, J.Z., and Nie, S. (2001) *Nat. Biotechnol.*, **19**, 631.
**63** Gao, X. and Nie, S. (2004) *Anal. Chem.*, **76**, 2406.
**64** Jamieson, T., Bakhshi, R., Petrova, D., Pocock, R., Imani, M., and Seifalian, A.M. (2007) *Biomaterials*, **28**, 4717.
**65** Gerion, D., Parak, W.J., Williams, S.C., Zanchet, D., Micheel, C.M., and Alivisatos, A.P. (2002) *J. Am. Chem. Soc.*, **124**, 7070.
**66** Schroedter, A. and Weller, H. (2002) *Angew. Chem. Int. Ed.*, **41**, 3218.
**67** Pellegrino, T., Parak, W.J., Boudreau, R., Le Gros, M.A., Gerion, D., Alivisatos, A.P., and Larabell, C.A. (2003) *Differentiation*, **71**, 542.
**68** Sukhanova, A., Venteo, L., Devy, J., Artemyev, M., Oleinikov, V., Pluot, M., and Nabiev, I. (2002) *Lab. Invest.*, **82**, 1259.
**69** Goldman, E.R., Anderson, G.P., Tran, P.T., Mattoussi, H., Charles, P.T., and Mauro, J.M. (2002) *Anal. Chem.*, **74**, 841.
**70** Kloepfer, J.A., Mielke, R.E., Wong, M.S., Nealson, K.H., Stucky, G., and Nadeau, J.L. (2003) *Appl. Environ. Microbiol.*, **69**, 4205.
**71** Hardman, R. (2006) *Environ. Health Perspect.*, **114**, 165.
**72** Shen, H.M., Yang, C.F., and Ong, C.N. (1999) *Int. J. Cancer*, **81**, 820.
**73** Kondoh, M., Araragi, S., Sato, K., Higashimoto, M., Takiguchi, M., and Sato, M. (2002) *Toxicology*, **170**, 111.
**74** Bharali, D.J., Lucey, D.W., Jayakumar, H., Pudavar, H.E., and Prasad, P.N. (2005) *J. Am. Chem. Soc.*, **127**, 11364.
**75** Derfus, A.M., Chan, W.C.W., and Bhatia, S.N. (2004) *Nano Lett.*, **4**, 11.
**76** Medintz, I.L., Uyeda, H.T., Goldman, E.R., and Mattoussi, H. (2005) *Nat. Mater.*, **4**, 435.
**77** Yang, R.S., Chang, L.W., Wu, J.P., Tsai, M.H., Wang, H.J., Kuo, Y.C., Yeh, T.K., Yang, C.S., and Lin, P. (2007) *Environ. Health Perspect.*, **115**, 1339.
**78** Hauck, T.S., Anderson, R.E., Fischer, H.C., Newbigging, S., and Chan, W.C. (2009) *Small*, **6**, 138.

**79** Ballou, B., Lagerholm, B.C., Ernst, L.A., Bruchez, M.P., and Waggoner, A.S. (2004) *Bioconjug. Chem.*, **15**, 79.

**80** Choi, H.S., Liu, W., Liu, F., Nasr, K., Misra, P., Bawendi, M.G., and Frangioni, J.V. (2009) *Nat. Nanotechnol.*, **5**, 42.

**81** Stroh, M., Zimmer, J.P., Duda, D.G., Levchenko, T.S., Cohen, K.S., Brown, E.B., Scadden, D.T., Torchilin, V.P., Bawendi, M.G., Fukumura, D., and Jain, R.K. (2005) *Nat. Med.*, **11**, 678.

**82** Voura, E.B., Jaiswal, J.K., Mattoussi, H., and Simon, S.M. (2004) *Nat. Med.*, **10**, 993.

**83** Alivisatos, A.P., Gu, W., and Larabell, C. (2005) *Annu. Rev. Biomed. Eng.*, **7**, 55.

**84** Michalet, X., Pinaud, F.F., Bentolila, L.A., Tsay, J.M., Doose, S., Li, J.J., Sundaresan, G., Wu, A.M., Gambhir, S.S., and Weiss, S. (2005) *Science*, **307**, 538.

**85** Biju, V., Mundayoor, S., Omkumar, R.V., Anas, A., and Ishikawa, M. (2010) *Biotechnol. Adv.*, **28**, 199.

**86** Kim, S., Lim, Y.T., Soltesz, E.G., De Grand, A.M., Lee, J., Nakayama, A., Parker, J.A., Mihaljevic, T., Laurence, R.G., Dor, D.M., Cohn, L.H., Bawendi, M.G., and Frangioni, J.V. (2004) *Nat. Biotechnol.*, **22**, 93.

**87** Gao, X., Cui, Y., Levenson, R.M., Chung, L.W., and Nie, S. (2004) *Nat. Biotechnol.*, **22**, 969.

**88** Cai, W., Shin, D.W., Chen, K., Gheysens, O., Cao, Q., Wang, S.X., Gambhir, S.S., and Chen, X. (2006) *Nano Lett.*, **6**, 669.

**89** Tada, H., Higuchi, H., Wanatabe, T.M., and Ohuchi, N. (2007) *Cancer Res.*, **67**, 1138.

**90** Chen, L.D., Liu, J., Yu, X.F., He, M., Pei, X.F., Tang, Z.Y., Wang, Q.Q., Pang, D.W., and Li, Y. (2008) *Biomaterials*, **29**, 4170.

**91** Gonda, K., Watanabe, T.M., Ohuchi, N., and Higuchi, H. (2010) *J. Biol. Chem.*, **285**, 2750.

**92** Jayagopal, A., Russ, P.K., and Haselton, F.R. (2007) *Bioconjug. Chem.*, **18**, 1424.

**93** Takeda, A., Baffi, J.Z., Kleinman, M.E., Cho, W.G., Nozaki, M., Yamada, K., Kaneko, H., Albuquerque, R.J., Dridi, S., Saito, K., Raisler, B.J., Budd, S.J., Geisen, P., Munitz, A., Ambati, B.K., Green, M.G., Ishibashi, T., Wright, J.D., Humbles, A.A., Gerard, C.J., Ogura, Y., Pan, Y., Smith, J.R., Grisanti, S., Hartnett, M.E., Rothenberg, M.E., and Ambati, J. (2009) *Nature*, **460**, 225.

**94** Diagaradjane, P., Orenstein-Cardona, J.M., Colon-Casasnovas, N.E., Deorukhkar, A., Shentu, S., Kuno, N., Schwartz, D.L., Gelovani, J.G., and Krishnan, S. (2008) *Clin. Cancer Res.*, **14**, 731.

**95** Chen, K., Li, Z.B., Wang, H., Cai, W., and Chen, X. (2008) *Eur. J. Nucl. Med. Mol. Imaging*, **35**, 2235.

**96** Gao, X., Chen, J., Wu, B., Chen, H., and Jiang, X. (2008) *Bioconjug. Chem.*, **19**, 2189.

**97** Leevy, W.M., Lambert, T.N., Johnson, J.R., Morris, J., and Smith, B.D. (2008) *Chem. Commun.*, 2331.

**98** So, M.K., Xu, C., Loening, A.M., Gambhir, S.S., and Rao, J. (2006) *Nat. Biotechnol.*, **24**, 339.

**99** Jennings, T. and Strouse, G. (2007) *Adv. Exp. Med. Biol.*, **620**, 34.

**100** Huang, X., Jain, P.K., El-Sayed, I.H., and El-Sayed, M.A. (2007) *Nanomedicine*, **2**, 681.

**101** Radwan, S.H. and Azzazy, H.M. (2009) *Expert Rev. Mol. Diagn.*, **9**, 511.

**102** Boisselier, E. and Astruc, D. (2009) *Chem. Soc. Rev.*, **38**, 1759.

**103** Wilson, R. (2008) *Chem. Soc. Rev.*, **37**, 2028.

**104** Tong, L., Wei, Q., Wei, A., and Cheng, J.X. (2009) *Photochem. Photobiol.*, **85**, 21.

**105** Link, S. and El-Sayed, M.A. (2003) *Annu. Rev. Phys. Chem.*, **54**, 331.

**106** Yguerabide, J. and Yguerabide, E.E. (1998) *Anal. Biochem.*, **262**, 157.

**107** Campion, A. and Kambhampati, P. (1998) *Chem. Soc. Rev.*, **27**, 241.

**108** Boyd, G.T., Yu, Z.H., and Shen, Y.R. (1986) *Phys. Rev. B*, **33**, 7923.

**109** Jain, P.K., Lee, K.S., El-Sayed, I.H., and El-Sayed, M.A. (2006) *J. Phys. Chem. B*, **110**, 7238.

**110** Link, S., and El-Sayed, M.A. (1999) *J. Phys. Chem. B*, **103**, 4212.

**111** Huang, X., El-Sayed, I.H., Qian, W., and El-Sayed, M.A. (2006) *J. Am. Chem. Soc.*, **128**, 2115.

**112** Jain, P.K. and El-Sayed, M.A. (2007) *Nano Lett.*, **7**, 2854.

**113** Murphy, C.J., Sau, T.K., Gole, A.M., Orendorff, C.J., Gao, J., Gou, L., Hunyadi, S.E., and Li, T. (2005) *J. Phys. Chem. B*, **109**, 13857.

**114** Prodan, E., Radloff, C., Halas, N.J., and Nordlander, P. (2003) *Science*, **302**, 419.

**115** Shi, W., Sahoo, Y., Swihart, M.T., and Prasad, P.N. (2005) *Langmuir*, **21**, 1610.

**116** Zhou, H.S., Honma, I.I., Komiyama, H., and Haus, J.W. (1994) *Phys. Rev. B*, **50**, 12052.

**117** Connor, E.E., Mwamuka, J., Gole, A., Murphy, C.J., and Wyatt, M.D. (2005) *Small*, **1**, 325.

**118** Thomas, K.G. and Kamat, P.V. (2003) *Acc. Chem. Res.*, **36**, 888.

**119** Lakowicz, J.R., Geddes, C.D., Gryczynski, I., Malicka, J., Gryczynski, Z., Aslan, K., Lukomska, J., Matveeva, E., Zhang, J., Badugu, R., and Huang, J. (2004) *J. Fluoresc.*, **14**, 425.

**120** Lee, S., Cha, E.J., Park, K., Lee, S.Y., Hong, J.K., Sun, I.C., Kim, S.Y., Choi, K., Kwon, I.C., Kim, K., and Ahn, C.H. (2008) *Angew. Chem. Int. Ed.*, **47**, 2804.

**121** Dubertret, B., Calame, M., and Libchaber, A.J. (2001) *Nat. Biotechnol.*, **19**, 365.

**122** Lee, H., Lee, K., Kim, I.K., and Park, T.G. (2008) *Biomaterials*, **29**, 4709.

**123** Wang, L.V. (2008) *Med. Phys.*, **35**, 5758.

**124** Yang, X., Skrabalak, S.E., Li, Z.-Y., Xia, Y., and Wang, L.V. (2007) *Nano Lett.*, **7**, 3798.

**125** Lu, W., Huang, Q., Ku, G., Wen, X., Zhou, M., Guzatov, D., Brecht, P., Su, R., Oraevsky, A., Wang, L.V., and Li, C. (2010) *Biomaterials*, **31**, 2617.

**126** Song, K.H., Kim, C., Maslov, K., and Wang, L.V. (2009) *Eur. J. Radiol.*, **70**, 227.

**127** Galanzha, E.I., Shashkov, E.V., Kelly, T., Kim, J.W., Yang, L., and Zharov, V.P. (2009) *Nat. Nanotechnol.*, **4**, 855.

**128** Copland, J.A., Eghtedari, M., Popov, V.L., Kotov, N., Mamedova, N., Motamedi, M., and Oraevsky, A.A. (2004) *Mol. Imaging Biol.*, **6**, 341.

**129** Wang, Y., Xie, X., Wang, X., Ku, G., Gill, K.L., O'N eal P.O., Stoica G., and Wang, L.V. (2004) *Nano Lett.*, **4**, 1689.

**130** Song, K.H., Kim, C., Cobley, C.M., Xia, Y., and Wang, L.V. (2009) *Nano Lett.*, **9**, 183.

**131** Kim, J.W., Galanzha, E.I., Shashkov, E.V., Moon, H.M., and Zharov, V.P. (2009) *Nat. Nanotechnol.*, **4**, 688.

**132** Bangham, A.D., Standish, M.M., and Weissmann, G. (1965) *J. Mol. Biol.*, **13**, 253.

**133** Lasic, D.D. (1998) *Trends Biotechnol.*, **16**, 307.

**134** Immordino, M.L., Dosio, F., and Cattel, L. (2006) *Int. J. Nanomedicine*, **1**, 297.

**135** Krown, S.E., Northfelt, D.W., Osoba, D., and Stewart, J.S. (2004) *Semin. Oncol.*, **31**, 36.

**136** Rose, P.G. (2005) *Oncologist*, **10**, 205.

**137** Mayer, L.D. and Onge, G.S. (1995) *Anal. Biochem.*, **232**, 149.

**138** Rahman, A., Treat, J., Roh, J.K., Potkul, L.A., Alvord, W.G., Forst, D., and Woolley, P.V. (1990) *J. Clin. Oncol.*, **8**, 1093.

**139** Deissler, V., Ruger, R., Frank, W., Fahr, A., Kaiser, W.A., and Hilger, I. (2008) *Small*, **4**, 1240.

**140** Molina, M.A., Codony-Servat, J., Albanell, J., Rojo, F., Arribas, J., and Baselga, J. (2001) *Cancer Res.*, **61**, 4744.

**141** Qin, S., Seo, J.W., Zhang, H., Qi, J., Curry, F.R., and Ferrara, K.W. (2010) *Mol. Pharm.*, **7**, 12.

**142** Song, S., Liu, D., Peng, J., Deng, H., Guo, Y., Xu, L.X., Miller, A.D., and Xu, Y. (2009) *FASEB J.*, **23**, 1396.

**143** Saad, M., Garbuzenko, O.B., Ber, E., Chandna, P., Khandare, J.J., Pozharov, V.P., and Minko, T. (2008) *J. Control. Release*, **130**, 107.

**144** Hirai, M., Minematsu, H., Kondo, N., Oie, K., Igarashi, K., and Yamazaki, N. (2007) *Biochem. Biophys. Res. Commun.*, **353**, 553.

**145** Scherphof, G.L., Dijkstra, J., Spanjer, H.H., Derksen, J.T., and Roerdink, F.H. (1985) *Ann. NY Acad. Sci.*, **446**, 368.

**146** Allen, T.M., Hansen, C., Martin, F., Redemann, C., and Yau-Young, A. (1991) *Biochim. Biophys. Acta*, **1066**, 29.

**147** Needham, D., McIntosh, T.J., and Lasic, D.D. (1992) *Biochim. Biophys. Acta*, **1108**, 40.

**148** Woodle, M.C. (1995) *Adv. Drug Deliv. Rev.*, **16**, 249.

**149** Woodle, M.C., and Lasic, D.D. (1992) *Biochim. Biophys. Acta*, **1113**, 171.

**150** Woodle, M.C., Newman, M.S., and Cohen, J.A. (1994) *J. Drug Target.*, **2**, 397.

**151** Whiteman, K.R., Subr, V., Ulbrich, K., and Torchilin, V.P. (2001) *J. Liposome Res.*, **11**, 153.

**152** Ghoroghchian, P.P., Frail, P.R., Susumu, K., Blessington, D., Brannan, A.K., Bates, F.S., Chance, B., Hammer, D.A., and Therien, M.J. (2005) *Proc. Natl. Acad. Sci. USA*, **102**, 2922.

**153** Begu, S., Mordon, S., Desmettre, T., and Devoisselle, J.M. (2005) *J. Biomed. Opt.*, **10**, 024008.

**154** Simard, P. and Leroux, J.C. (2009) *Int. J. Pharm.*, **381**, 86.

**155** Pak, C.C., Ali, S., Janoff, A.S., and Meers, P. (1998) *Biochim. Biophys. Acta*, **1372**, 13.

**156** Sarkar, N., Banerjee, J., Hanson, A.J., Elegbede, A.I., Rosendahl, T., Krueger, A.B., Banerjee, A.L., Tobwala, S., Wang, R., Lu, X., Mallik, S., and Srivastava, D.K. (2008) *Bioconjug. Chem.*, **19**, 57.

**157** Peller, M., Schwerdt, A., Hossann, M., Reinl, H.M., Wang, T., Sourbron, S., Ogris, M., and Lindner, L.H. (2008) *Invest. Radiol.*, **43**, 877.

**158** Bondurant, B. and O'Brien, D.F. (1998) *J. Am. Chem. Soc.*, **120**, 13541.

**159** Mueller, A., Bondurant, B., and O'Brien, D.F. (2000) *Macromolecules*, **33**, 4799.

**160** Khoobehi, B., Peyman, G.A., McTurnan, W.G., Niesman, M.R., and Magin, R.L. (1988) *Ophthalmology*, **95**, 950.

**161** Zeimer, R.C., Khoobehi, B., Niesman, M.R., and Magin, R.L. (1988) *Invest. Ophthalmol. Vis. Sci.*, **29**, 1179.

**162** Paoli, E.E., Kruse, D.E., Seo, J.W., Zhang, H., Kheirolomoom, A., Watson, K.D., Chiu, P., Stahlberg, H., and Ferrara, K.W. (2010) *J. Control. Release*, **143**, 14.

**163** Kheirolomoom, A., Kruse, D.E., Qin, S., Watson, K.E., Lai, C.Y., Young, L.J., Cardiff, R.D., and Ferrara, K.W. (2010) *J. Control. Release*, **141**, 128.

**164** Shan, L., Wang, S., Sridhar, R., Bhujwalla, Z.M., and Wang, P.C. (2007) *Mol. Imaging*, **6**, 85.

**165** Feng, B., Tomizawa, K., Michiue, H., Han, X.J., Miyatake, S.I., and Matsui, H. (2010) *Biomaterials*, **31**, 4139.

**166** Montet, X., Rajopadhye, M., and Weissleder, R. (2006) *Chem. Med. Chem.*, **1**, 66.

**167** Regino, C.A., Ogawa, M., Alford, R., Wong, K.J., Kosaka, N., Williams, M., Feild, B.J., Takahashi, M., Choyke, P.L., and Kobayashi, H. (2010) *J. Med. Chem.*, **53**, 1579.

**168** Miao, Z., Levi, J., and Cheng, Z. (2010) *Amino Acids*.

**169** Barrett, T., Koyama, Y., Hama, Y., Ravizzini, G., Shin, I.S., Jang, B.S., Paik, C.H., Urano, Y., Choyke, P.L., and Kobayashi, H. (2007) *Clin. Cancer Res.*, **13**, 6639.

**170** Chang, S.K., Rizvi, I., Solban, N., and Hasan, T. (2008) *Clin. Cancer Res.*, **14**, 4146.

**171** Hilderbrand, S.A., Kelly, K.A., Niedre, M., and Weissleder, R. (2008) *Bioconjug. Chem.*, **19**, 1635.

**172** Silva, G.A., Czeisler, C., Niece, K.L., Beniash, E., Harrington, D.A., Kessler, J.A., and Stupp, S.I. (2004) *Science*, **303**, 1352.

**173** Klumpp, C., Kostarelos, K., Prato, M., and Bianco, A. (2006) *Biochim. Biophys. Acta*, **1758**, 404.

**174** Jaffer, F.A. and Weissleder, R. (2004) *Circ. Res.*, **94**, 433.

**175** Morgan, M.T., Carnahan, M.A., Immoos, C.E., Ribeiro, A.A., Finkelstein, S., Lee, S.J., and Grinstaff, M.W. (2003) *J. Am. Chem. Soc.*, **125**, 15485.

**176** Phillips, W.T., Goins, B.A., and Bao, A. (2009) *Wiley Interdiscip. Rev. Nanomed. Nanobiotechnol.*, **1**, 69.

**177** Gossuin, Y., Gillis, P., Hocq, A., Vuong, Q.L., and Roch, A. (2009) *Wiley Interdiscip. Rev. Nanomed. Nanobiotechnol.*, **1**, 299.

# 10
# Semiconductor Quantum Dots for Electrochemical Biosensors

*Chunyan Wang, Bernard Knudsen, and Xueji Zhang*

## 10.1
## Introduction

Quantum dots (QDs) or semiconductor nanoparticles are colloidal nanocrystalline semiconductors made of group II–VI or III–V elements. With diameters of between 1 and 100 nm, QDs demonstrate interesting optical and electronic properties. The unique photophysical properties of QDs, such as high fluorescence, quantum yield stability against photobleaching, and size-controlled luminescence properties, enable them to be utilized as optical labels for bioanalysis [1]. The photoexcitation of semiconductor QDs can result in the transfer of an electron from the valence band to the conduction band, thus yielding an electron hole pair. When the photoexcited QDs were confined to electrode surfaces, the cathodic photocurrent could be formed by the ejection of the conduction band electrons to an electron acceptor in the electrolyte solution, followed by the supply of electrons from the electrode to neutralize the valence-bound holes. By comparison, the anodic photocurrent can be yielded by transferring the conduction band electrons to the electrode with the transfer of electrons from an electron donor in the solution [2]. These photoelectrochemical properties of QDs can be used for developing light-to-electrical energy conversion systems. The optical and electrophotochemical applications of QDs for bioanalysis were reviewed by Zayats and Willner [2].

It is known that the surfaces of QDs can be chemically modified by a functional capping monolayer, which allows a tethering of the biomacromolecules for bioanalysis applications [3]. When biomacromolecules are immobilized on the surface of QDs, the semiconductor QDs also can promote direct electron transfer between the biomolecules and electrode surface, and improve the performance of the biosensor. Recently, QDs were incorporated with redox proteins by covalent bonding or electrostatic interaction to realize the direct electrochemistry of the biosensor. Electrochemical immunosensors or immunoassays for DNA and proteins have developed dramatically over the past two decades because of their high sensitivity, inherent simplicity, low cost, and miniaturization. Nanomaterials-based electrochemical immunoassays and immunosensors have attracted considerable interest, since they can enhance the sensitivity via the signal amplification. Of the various

*Biosensor Nanomaterials*. Edited by Songjun Li, Jagdish Singh, and Ipsita A. Banerjee

ISBN: 978-3-527-32841-3

nanomaterials, semiconductor crystal QDs are particularly attractive in view of the attractive stripping behavior and simultaneous determination of multiple targets. The present chapter summarizes some recent research activities directed at the utilization of semiconductor QDs for electrochemical biosensors to determine glucose, $H_2O_2$, ascorbic acid, or inhibitors. The progress in the use of QDs as labels for the electrochemical determination of proteins and DNA is also summarized.

## 10.2
## Attachment of Biomolecules to Quantum Dots

For QD-based biosensors, biomolecules are generally immobilized on QDs by two approaches: noncovalent attachment and covalent binding. For noncovalent attachment, physical adsorption and entrapment are generally used. On the one hand, QDs can be simply mixed with proteins to make a protein–QD-modified electrode. On the other hand, QDs can be stabilized with thioglycolic acid (TGA) or 3-mercaptopropionic acid to form an anionic surface [4, 5]. These stabilized QDs can form strong electrostatic interaction with proteins by the anionic groups on the QDs and cationic groups on the proteins. However, the biosensor based on this approach may suffer from stability or durability issues. To overcome these problems, some cross-linker agents (e.g., 1-ethyl-3-(3-dimethylaminopropyl) carbodiimide hydrochloride/*N*-hydroxysuccinimide) or Schiff bases are usually used for covalent binding [6]. The activity of the immobilized biomolecules may be affected due to steric hindrance by covalent binding.

## 10.3
## Quantum Dot-Based Redox Proteins Biosensor

Semiconductor QDs incorporated with redox proteins for electrochemical biosensors to determine glucose, $H_2O_2$, ascorbic acid, or inhibitors are discussed in this section. The linear ranges and detection limits of various QD-modified electrodes are listed in Table 10.1.

### 10.3.1
### Glucose Oxidase–Quantum Dot-Based Glucose Biosensor

Two different QD-modified glucose oxidase (GOx) electrodes (GOx/CdS/PGE (plane graphite disk electrode) and Nafion–CNT (carbon nanotube)–CdTe–GOx/GC (glassy carbon)) were developed to determine glucose by Huang *et al.* [7] and Liu *et al.* [8], respectively. The GOx/CdS/PGE electrode was prepared by casting the mixture of CdS nanoparticles and GOx solution at a 1 : 1 ratio onto a pyrolytic edge PGE. A cyclic voltammogram of using a GOx/CdS/PGE electrode in 0.1 M phosphate-buffered saline (PBS) solution at pH 6.0 shows a pair of well-defined and reproducible peaks, as shown in Figure 10.1(A). In contrast, CdS/PGE or a bare

**Table 10.1** List of QD-based redox protein biosensors.

| Redox protein | Analyte | Electrode | Linear range (μM) | Detection limit (μM) | Reference |
|---|---|---|---|---|---|
| Glucose oxidase | Glucose | GOx/GS/PGE | 0.5–11.1 | 50 | [7] |
| | | Nafion–CNT–CdTe–GOx/GC | –700[a)] | | [8] |
| Hemoglobin | $H_2O_2$ | Hb–CdTe–$CaCO_3$@ polyelectrolyte/GC | 5–45 | 2.5 | [5] |
| | | Nafion/Hb–CdS/GP | 0.5–300 | 0.06 | [9] |
| | | Nafion/Hb–CdTe/GC | 5–45 | 0.84 | [10] |
| Myoglobin | $H_2O_2$ | Mb–QD–MCF/GC | 2.5–60 | 0.7 | [4] |
| Laccase | Ascorbic acid | Lc/CdTe/Cys/Au | 10–140 | 1.4 | [11] |
| Acetylcholinesterase | Monocrotophos | AChE–CdTe–GNP–CM/GC | 0.001–1.0<br>2–15 | 0.0003 | [6] |

a) Not indicated in the reference.

PGE electrode is electrochemically silent. Therefore, the redox peaks are attributed to the redox reactions of GOx. CdS nanoparticles play an important role in improving GOx adsorption and facilitating electron exchange between GOx and PGE.

The Nafion–CNT–CdTe–GOx electrode was developed by casting the mixture of CNT/Nafion suspension, TGA-capped CdTe QDs, and GOx solution onto a GC electrode. From the cyclic voltammogram, no redox peaks were observed at the Nafion–CdTe/GC electrode (Figure 10.1B, curve a) and the redox peaks at the Nafion–GOx/GC electrode (Figure 10.1B, curve b) were very small. In contrast, there was a pair of well-defined and quasi-reversible redox peaks at the Nafion–CdTe–GOx/GC electrode (Figure 10.1B, curve c). The anodic peak potential and the cathodic peak potential of curve c in Figure 10.1B were, respectively, –0.359 and –0.385 V with a small peak potential separation ($\Delta E_p$ = 26 mV), revealing a fast electron transfer process. All of these results indicate that the direct electron transfer of GOx was achieved through the incorporation of QDs.

Figure 10.1C shows the cyclic voltammograms of three different modified electrodes: Nafion–CdTe–GOx/GC, Nafion–CNT–GOx/GC, and Nafion–CNT–CdTe–GOx/GC in 0.05 M PBS at pH 6.0 with $N_2$-saturated at a scan rate of 50 mV $s^{-1}$. All there three electrodes showed the direct electrochemistry of GOx. However, the

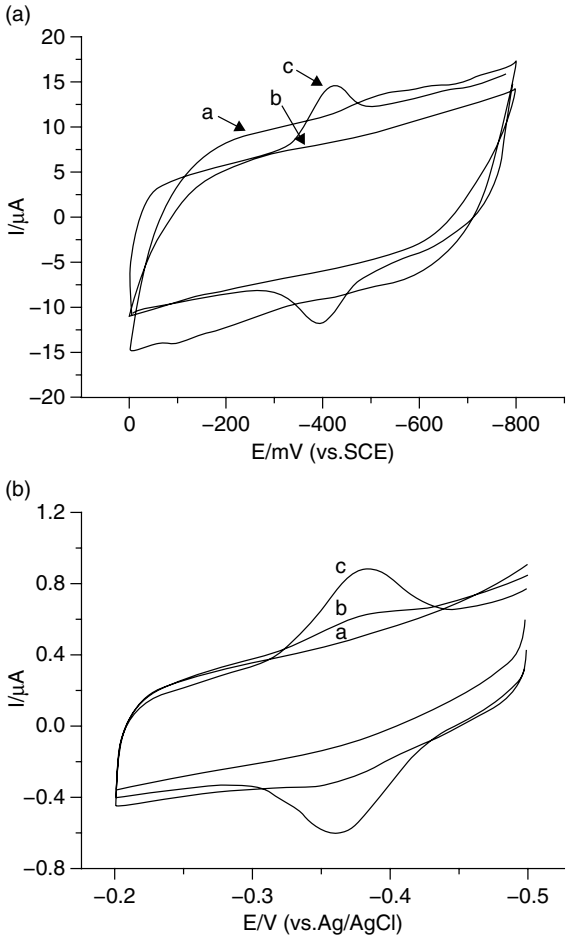


**Figure 10.1** (A) Cyclic voltammograms of bare PGE (a), CdS/PGE (b), and GOx/CdS/PGE (c) in a purged phosphate buffer solution at pH 6.0. Scan rate: 200 mV $s^{-1}$. (Reprinted with permission from [7], © 2005 Elsevier.) (B) Cyclic voltammograms of (a) Nafion–CdTe/GC, (b) Nafion–GOx/GC, and (c) Nafion–CdTe–GOx/GC electrodes in 0.05 M PBS at pH 6.0 with $N_2$-saturated at a scan rate of 50 mV $s^{-1}$. (Reprinted with permission from [8], © 2007 Elsevier.) (C) Cyclic voltammograms of (a) Nafion–CdTe–GOx/GC, (b) Nafion–CNT–GOx/GC, and (c) Nafion–CNT–CdTe–GOx/GC electrodes in 0.05 M PBS at pH 6.0 with $N_2$-saturated at a scan rate of 50 mV $s^{-1}$. (Reprinted with permission from [8], © 2007 Elsevier.)

performance of the Nafion–CNT–CdTe–GOx (Figure 10.1C, curve c)-modified electrode was much better than of Nafion–CdTe–GOx/GC (Figure 10.1C, curve a) and Nafion–CNT–GOx/GC (Figure 10.1C, curve b). Furthermore, the current of the Nafion–CNT–CdTe–GOx/GC electrode was larger than the sum current of the Nafion–CNT–GOx/GC and the Nafion–CdTe–GOx/GC electrode, which indicates the presence of synergistic effects in Nafion–CNT–CdTe–GOx films.

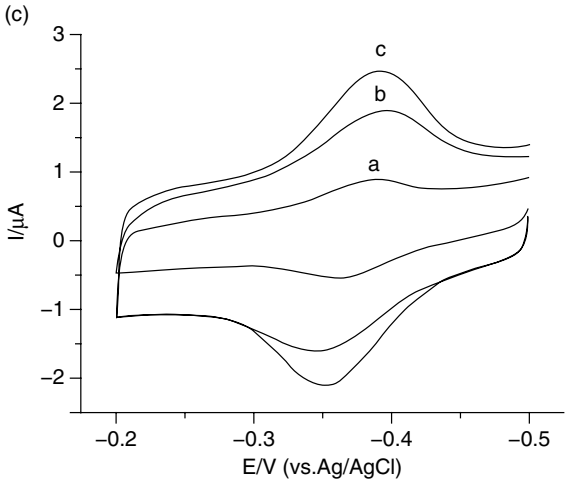


**Figure 10.1** (*Continued*)

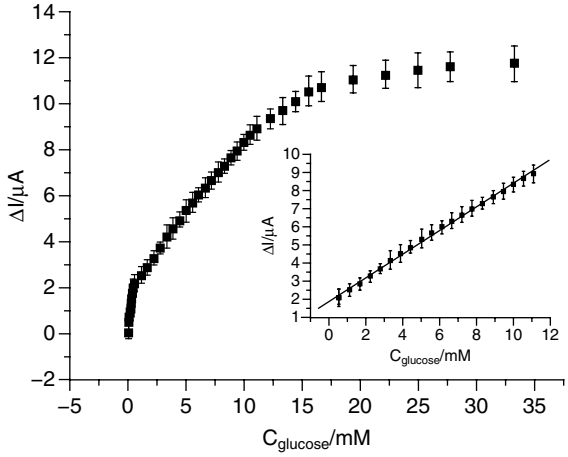


**Figure 10.2** Relationship between the decreased current of the reduction peak of a GOx/CdS-modified electrode and the concentration of glucose (inset is the linear plot) in PBS at pH 6.0. Scan rate: 200 m $Vs^{-1}$. (Reprinted with permission from [7], © 2005 Elsevier.)

The GOx/CdS/PGE electrode was used to determine the glucose concentration by the decrease of the reduction current. This mediator-free glucose sensor shows linear glucose concentration ranging from 0.5 to 11.1 mM ($r^2 = 0.998$) as shown in Figure 10.2, with a sensitivity of 7.0 μA $M^{-1}$, which is much higher than that of 1.22 μA $M^{-1}$ on a mediator polyelectrolyte glucose sensor [12], and 3 μA $M^{-1}$ on Prussian blue and a polyaniline-modified glucose sensor [13].

The performance of Nafion–CNT–CdTe–GOx/GC toward glucose sensing was improved compared to the GC electrode modified by CdTe QDs or CNTs alone. The decreased reduction peak current of Nafion–CNT–CdTe–GOx/GC demonstrates the linearity with the concentration of glucose up to 0.7 mM with the calculated sensitivity (1.018 μA $mM^{-1}$).

### 10.3.2
### Hemoglobin–Quantum Dot-Based $H_2O_2$ Biosensor

Three Nafion film-covered, hemoglobin (Hb)-immobilized, QD-modified $H_2O_2$ electrodes have been manufactured by different QDs or matrices. To make the Nafion/Hb–CdS/GP (graphite electrode) electrode, first, Hb was immobilized to QDs by physically mixing the $Cd(NO_3)_2$ with Hb and adding $Na_2S$ aqueous solution as shown in Figure 10.3 [9]. The QD-modified Hb solution was cast onto the graphite electrode, followed by a Nafion film coating to hold the Hb–QD film to the electrode.

Figure 10.4 shows the cyclic voltammograms of the Nafion/Hb–CdS/GP electrode in pH 7.0 buffer, which exhibits reversible redox peaks (Figure 10.4, curve b). However, no redox peak is observed for the Nafion/CdS/GP electrode and the Nafion/Hb/GP electrode in the same potential range (Figure 10.4, curves a and c). This indicates that Hb could exchange electrons directly with the GP electrode when it was modified with CdS.

Cyclic voltammograms of the Nafion/CdS–Hb/GP electrode in pH 7.0 PBS containing $H_2O_2$ are shown in Figure 10.5(A). Upon addition of 5 μM $H_2O_2$ to the electrochemical cell, the reduction peak current increases and the oxidation peak

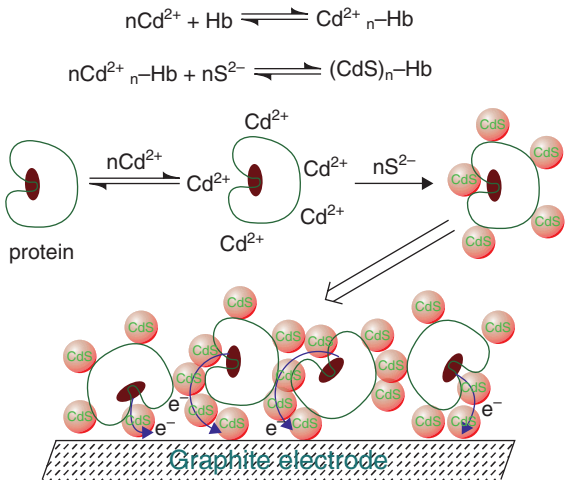


**Figure 10.3** Preparation process of the CdS–Hb/graphite electrode. (Reprinted with permission from [9], © 2007 Springer.)

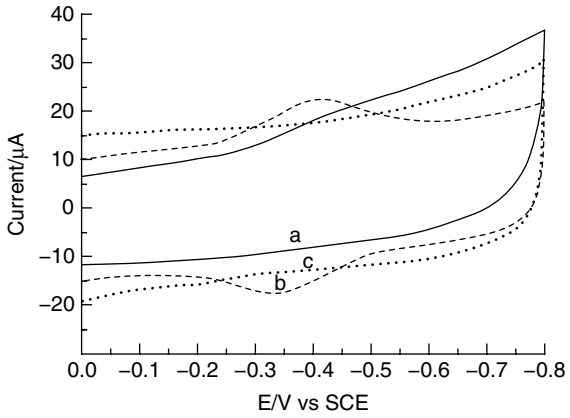


**Figure 10.4** Cyclic voltammograms of (a) Nafion/Hb/GP, (b) Nafion/CdS–Hb/GP and (c) Nafion/CdS/GP electrodes in 0.1 M PBS. Scan rate: 300 mV $s^{-1}$. (Reprinted with permission from [9], © 2007 Springer.)

current decreases, indicating a typical electrocatalytic reduction process of $H_2O_2$. The current response and the concentration of $H_2O_2$ have a linear relationship in the concentration range from $5 \times 10^{-7}$ to $3 \times 10^{-4}$ M. The sensitivity of the biosensor is 1.9 μA $\mu M^{-1}$, which is much higher than that of $H_2O_2$ sensors of Hb immobilized on a carbon paste electrode by a sol–gel film [14] or of Hb immobilized on zirconium dioxide nanoparticles [15].

The second kind of Hb-immobilized, QD-modified electrode was prepared by dropping the mixture of 3-mercaptopropionic acid-capped CdTe nanoparticles and Hb on the GC electrode [10]. Finally, the electrode was covered by Nafion film to hold Hb–CdTe on the electrode. The obtained Nafion/Hb–CdTe/GC electrode shows a pair of well-defined quasi-reversible redox peaks in cyclic voltammograms. However, Nafion/CdTe/GC and Nafion/Hb/GC electrodes have no peaks on cyclic voltammograms. These results also showed that Hb could exchange electrons with the GC electrode in the presence of CdTe. The Nafion/Hb–CdTe/GC electrode was used to determine $H_2O_2$ in PBS solution. The results showed that the catalytic current increased with the successive addition of $H_2O_2$. The current was linear with the $H_2O_2$ concentration from $5.0 \times 10^{-6}$ to $4.5 \times 10^{-5}$ M.

The third kind of $H_2O_2$ biosensor, based on the Hb-immobilized on CdTe–$CaCO_3$@polyelectrolyte three-dimensional architecture, was prepared by a stepwise layer-by-layer method shown in Figure 10.6 [5]. First, polyelectrolyte layers poly(sodium 4-styrenesulfonate)/poly(allylamine hydrochloride) (PSS/PAH) were assembled onto the $CaCO_3$ microsphere, which acts as an effective host for the loading of CdTe QDs due to its channel-like structure and the strong electrostatic interaction between the cationic groups (-$NH^{3+}$) of the PAH and the negatively charged carboxy (-$COO^-$) groups on the surface of CdTe QDs. The positively

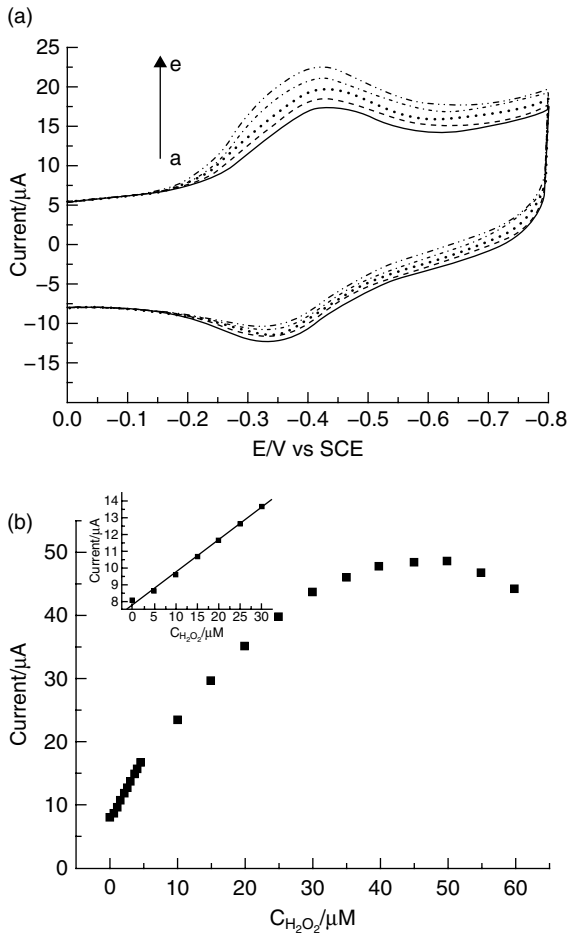


**Figure 10.5** (A) Cyclic voltammograms of Nafion/CdS–Hb/GP in 0.1 M PBS at pH 7.0 containing (a) 0, (b) 5, (c) 10, (d) 15, and (e) 20 μM $H_2O_2$. (B) Amperometric responses of Nafion/CdS–Hb/GP for successive addition of $H_2O_2$ in 0.1 M PBS at pH 7.0. Inset: catalytic peak current versus the concentration of $H_2O_2$. (Reprinted with permission from [9], © 2007 Springer.)

charged Hb (p*I* 6.8) at pH 6.0 in PBS was easily assembled onto the CdTe–$CaCO_3$@polyelectrolyte spheres. The bioconjugates are stable at neutral pH due to the strong interactions between the amino group of the protein and the carboxylic group of the CdTe QD surface. Finally, poly(vinyl alcohol) (PVA) film was coated on the outside of the hybrid material to hold it to the electrode.

Figure 10.7 shows the cyclic voltammograms of modified electrodes in 0.1 M PBS (pH 7.0) solution at 200 mV $s^{-1}$. CdTe–$CaCO_3$@polyelectrolyte/PVA and Hb–CdTe–MPS@PAH/PVA-modified electrodes exhibit no redox peaks in the poten-

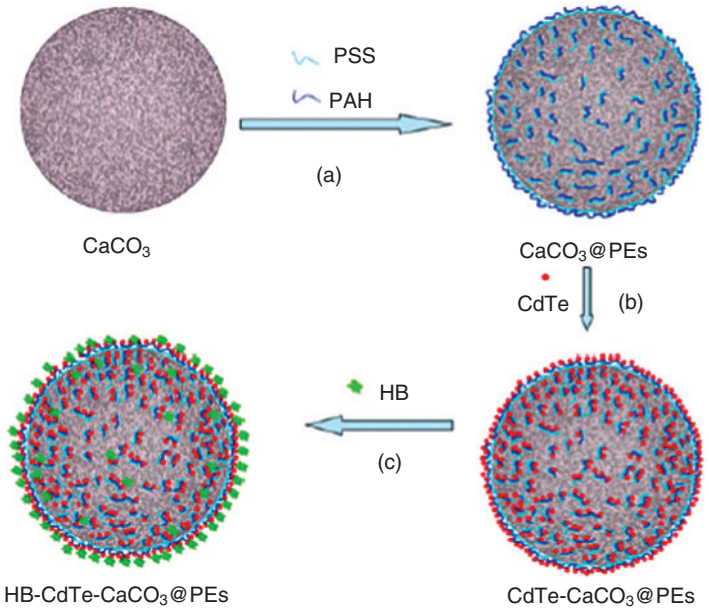


**Figure 10.6** Schematic illustration of the fabrication process of the Hb–CdTe–$CaCO_3$@polyelectrolyte three-dimensional architecture. (a) $CaCO_3$ microspheres were first coated with polyelectrolyte (PE) layers to produce $CaCO_3$@polyelectrolyte microspheres. (b) The polyelectrolyte-protected spheres were then used for the loading of CdTe QDs to fabricate the CdTe–$CaCO_3$@ polyelectrolyte hybrid material. (c) In the final step, the hybrid material was used for the loading of Hb. Protein was incorporated with QDs by electrostatic interactions. (Reprinted with permission from [5], © 2008 Wiley.)

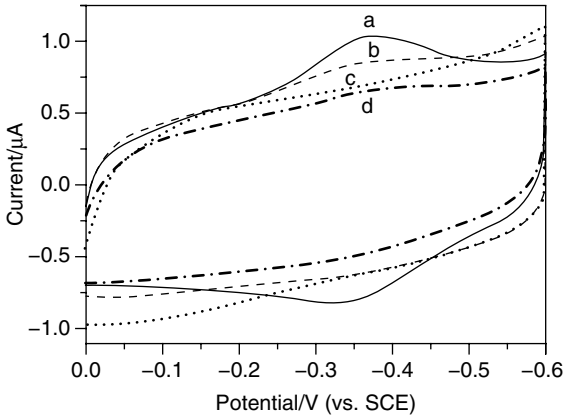


**Figure 10.7** Cyclic voltammograms of (a) Hb–CdTe–$CaCO_3$@polyelectrolyte/PVA, (b) Hb–$CaCO_3$@ polyelectrolyte/PVA, (c) CdTe–$CaCO_3$@polyelectrolyte/PVA, and (d) HB–CdTe–MPS@PAH/PVA-modified GC electrodes in 0.1 M PBS at pH 7.0. Scan rate: 200 mV $s^{-1}$. The mechanism of the direct electron transfer process. (Reprinted with permission from [5], © 2008 Wiley.)

tial window, indicating electroinactivity. Hb–$CaCO_3$@polyelectrolyte/PVA-modified electrodes exhibit one reduction peak that corresponds to the irreversible reduction of Hb. Only the Hb–CdTe–$CaCO_3$@polyelectrolyte electrode shows a pair of stable redox peaks.

Cai *et al.* suggested two different possible electron transfer modes for electron transfer among the electrode, QDs, and Hb [5]. When the electron transferred from the electrode to the CdTe QDs and then to the Hb as shown in Figure 10.8, the direct electrochemistry phenomenon between the Hb and the modified electrode was achieved. During this process the CdTe QDs assisted the direct electrochemistry by acting as electronic wires or nanoelectrodes between the electrode and the redox center of the protein [16]. The other possible mode is that the electron first transferred among the CdTe QDs and then reached the redox center of the protein (Figure 10.8). The electrocatalytic activity of Hb of the Hb–CdTe–$CaCO_3$@polyelectrolyte/PVA-modified electrode was investigated by the electrocatalytic reduction of $H_2O_2$ by cyclic voltammetry. From Figure 10.9, it can be seen that the reduction peak at about –0.37 V was enhanced (curves b–m) when the concentration of $H_2O_2$ increased. The current was linear with the concentration of $H_2O_2$ from around $5 \times 10^{-6}$ to $-4.5 \times 10^{-5}$ M with the detection limit $2.5 \times 10^{-6}$ M based on a signal-to-noise ratio of 3.

### 10.3.3
### Myoglobin–Quantum Dot-Based $H_2O_2$ Biosensor

Zhang *et al.* reported the Mb (myoglobin)–QD–MCF (mesopore cellular foam) silicate-modified electrode for $H_2O_2$ [4]. First, the TGA-modified CdTe QDs were incorporated into functionalized amino groups (MCFs), based on the strongly electrostatic interactions. Second, positively charged Mb (p*I* 7.0) at pH 6.5 assembled easily into a cavity of QD–MCF by electrostatic interaction. Figure 10.10 exhibits the process of fabricating Mb–QD–MCF hybrid material. The Mb–

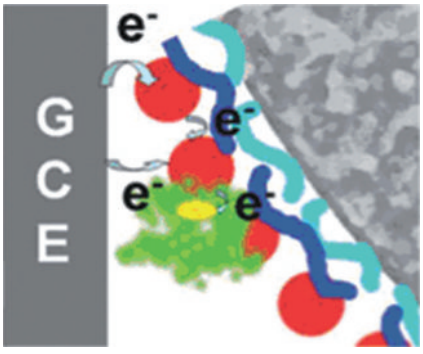


**Figure 10.8** Two possible electron transfer modes: directly and indirectly between one QD to the protein redox center. (Reprinted with permission from [5], © 2008 Wiley.)

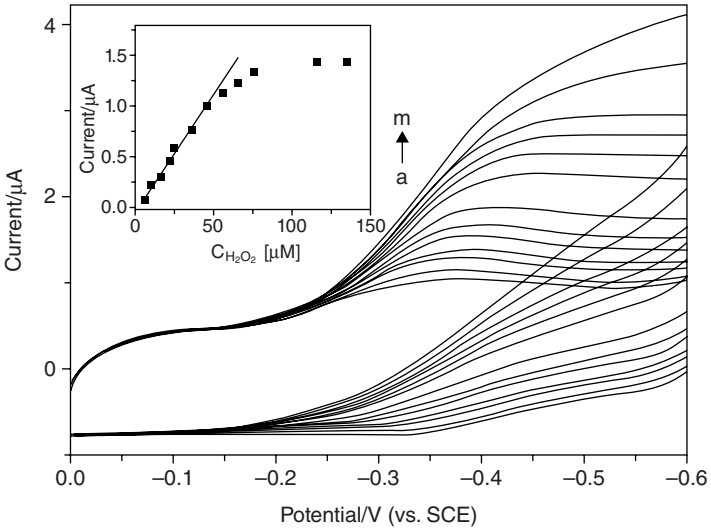


**Figure 10.9** Cyclic voltammograms of HB–CdTe–CaCO3@polyelectrolyte/PVA-modified GC electrodes in 0.1 M PBS at pH 7.0 in the presence of: (a) 0, (b) 5, (c) 10, (d) 15, (e) 20, (f) 25, (g) 35, (h) 45, (i) 55, (j) 65, (k) 75, (l) 135, and (m) 205 mM $H_2O_2$. Scan rate: 200 mV $s^{-1}$. The insert shows the calibration curve. (Reprinted with permission from [5], © 2008 Wiley.)

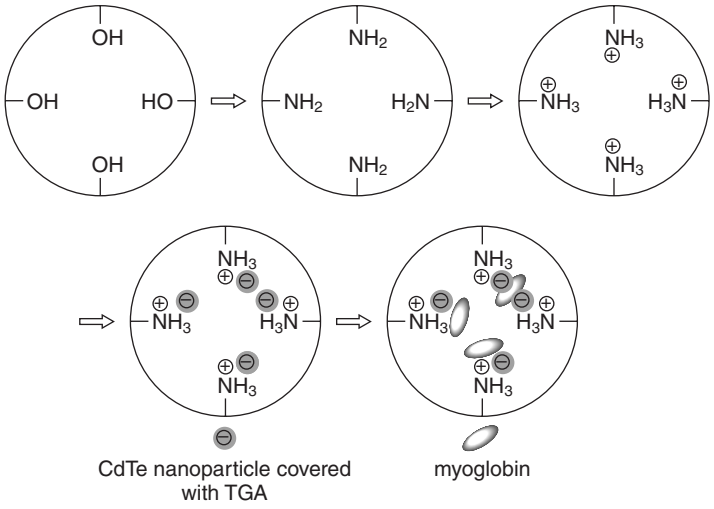


**Figure 10.10** Process of fabricating Mb–QD–MCF hybrid material. (Reprinted with permission from [4], © 2007 Elsevier.)

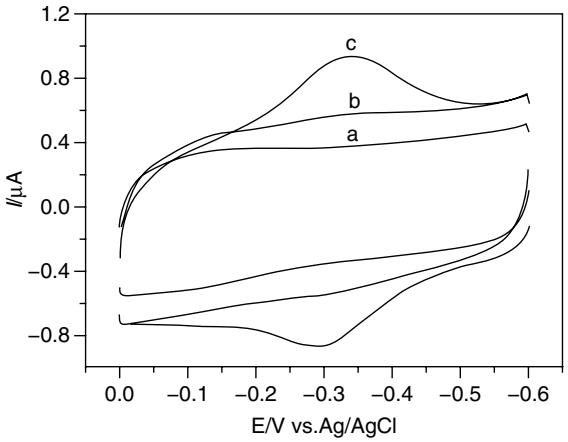


**Figure 10.11** Cyclic voltammograms of MCF/GC (a), Mb–MCF/GC (b), and Mb–QD–MCF/GC (c) electrodes in 0.1 M PBS solution at pH 7.0. Scan rate: 200 mV $s^{-1}$ (Reprinted with permission from [4], © 2007 Elsevier.)

QD–MCF suspension was cast onto the GC electrode with PVA solution for encapsulation.

Figure 10.11 displays the typical cyclic voltammograms for MCF/GC (a), Mb–MCF/GC (b) and Mb–QD–MCF/GC (c) electrodes in 0.1 M PBS at pH 7.0. There was no redox peaks at the MCF/GC electrode, indicating that MCFs were not electroactive in the potential range. The cyclic voltammogram of Mb–MCF/GC (Figure 10.11, curve b) showed relatively small but quasi-reversible redox peaks, which indicated the weak direct electron transfer between the immobilized Mb and the electrode. In contrast, on the Mb–QD–MCF/GC electrode remarkably large redox peaks were observed, which indicated the greatly enhanced direct electron transfer between the Mb and electrode after the protein immobilized in the QD–MCF matrix.

When $H_2O_2$ was added to a pH 7.0 PBS solution, an obvious increase of the reduction peak current at about –0.346 V was observed on the Mb–QD–MCF/GC electrode, accompanied by the decrease of the oxidation peak current shown in Figure 10.12(A). Figure 10.12(B) shows the calibration curves of the currents versus concentrations of $H_2O_2$ for Mb–QD–MCF/GC and Mb–MCF/GC electrodes. It demonstrates that under the same concentration of $H_2O_2$, the current obtained at the Mb–QD–MCF/GC electrode was much larger than that at the Mb–MCF/GC electrode. The linear range of the Mb–QD–MCF/GC and Mb–MCF/GC electrode is 2.5–60 and 5.0–35 μM, respectively. The sensitivities of the Mb–QD–MCF/GC and Mb–MCF/GC electrodes were calculated to be 9.0 and 6.9 mA $cm^{-2}$ $M^{-1}$. According to the linear range and sensitivity, it can be concluded that the Mb–QD–MCF/GC electrode behaved better in terms of electrocatalytic performance to $H_2O_2$ than the Mb–MCF/GC electrode.

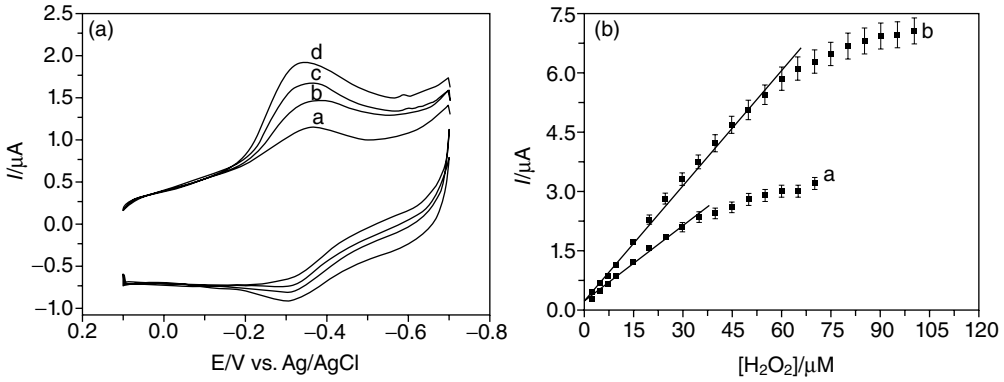


**Figure 10.12** (A) Cyclic voltammograms of Mb–QD–MCF/GC electrode in 0.1 M PBS solution at pH 7.0 with (a) 0, (b) 2.5, (c) 5.0, and (d) 7.5 μM $H_2O_2$. Scan rate: 200 mV $s^{-1}$. (B) Plots of the electrocatalytic current (*I*) versus $H_2O_2$ concentration for Mb–MCF/GC (a) and Mb–QD–MCF/GC (b) electrodes in 0.1 M PBS at pH 7.0. (Reprinted with permission from [4], © 2007 Elsevier.)

### 10.3.4
### Laccase–Quantum Dot-Based Ascorbic Acid Biosensor

An ascorbic acid (AA) biosensor based on laccase (Lc) immobilized on a gold electrode, which was modified with a cysteine (Cys) self-assembled monolayer and coated with mercaptopropionic acid-functionalized QDs, was developed by Wang *et al.* [11]

Cyclic voltammetry was carried out in Britton–Robinson (BR) buffer solution (pH 4.5). As shown in Figure 10.13, compared with a bare gold electrode (Figure 10.13, curve a) and a Cys/Au electrode (Figure 10.13, curve b), a pair of weak and irreversible peaks could be seen on the Lc/Cys/Au electrode (Figure 10.13, curve d). However, a pair of well-defined quasi-reversible peaks appeared on the Lc/CdTe/Cys/Au electrode after CdTe was introduced into this system (Figure 10.13, curve e). Since there were no redox peaks on the CdTe/Cys/Au electrode (Figure 10.13, curve c), the redox peaks on curve e were due to Lc and enhanced by CdTe QDs.

The modified electrode was used to determine AA in the 10–140 μM concentration range, with a linear response curve and a detection limit of 1.4 μM. These results demonstrated that immobilizing Lc on the Cys self-assembled monolayer and CdTe nanoparticle comodified electrode not only achieves direct electronic transfer of Lc, but also maintains Lc activity.

### 10.3.5
### Acetylcholinesterase–Quantum Dot-Based Inhibitor Biosensor

An enzyme biosensor, an acetylcholinesterase (AChE) biosensor based on a CdTe QD/GNP (gold nanoparticle)-modified chitosan microsphere (CM) interface,

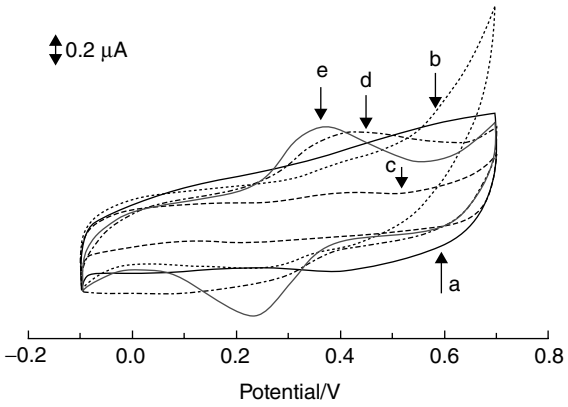


**Figure 10.13** Cyclic voltammograms of (a) bare gold, (b) Cys/Au, (c) CdTe/Cys/Au, (d) Lc/Cys/Au, and (e) Lc/CdTe/Cys/Au electrodes in BR buffer at pH 4.5. Scan rate: 100 mV $s^{-1}$. (Reprinted with permission from [11], © 2007 Springer.)

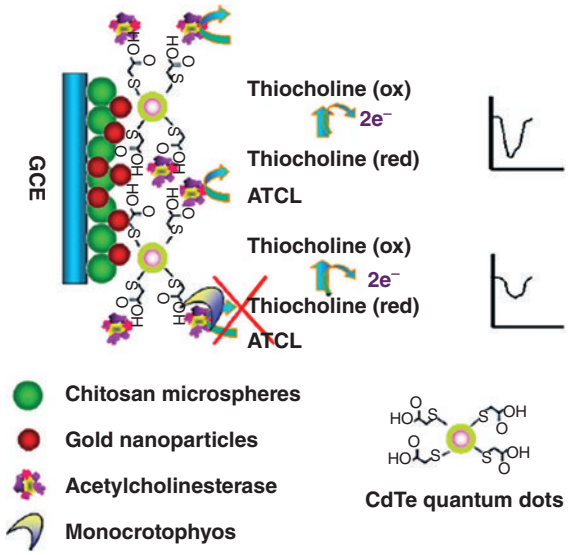


**Figure 10.14** Schematic diagram for biosensor fabrication and determination of monocrotophos. (Reprinted with permission from [6], © 2008 Elsevier.)

was developed for the amperometric determination of the inhibitor organophosphate pesticide as shown in Figure 10.14 [6]. The GC electrode was activated and covered by CMs. The CM-covered GC electrode was assembled with carboxyl group-functionalized CdTe QDs, which were bound to AChE through covalent binding of Schiff base. Figure 10.15 demonstrates the cyclic voltammetric behaviors of acetylthiocholine chloride (ATCl) at AChE–CdTe–CM/GC, AChE–GNP–CM/

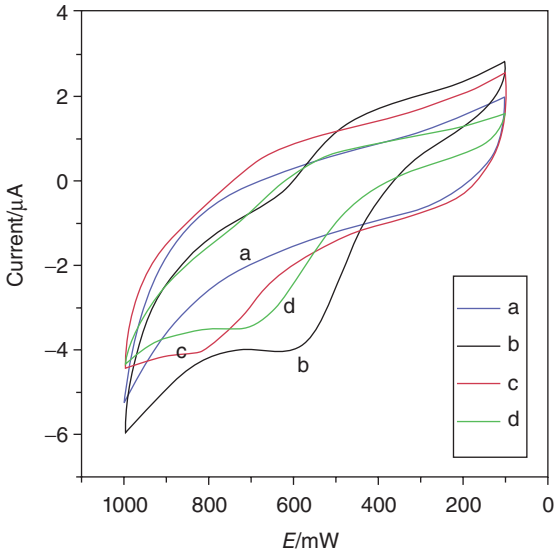


**Figure 10.15** Cyclic voltammograms of (a) AChE–CdTe–GNP–CM/GC, (b) AChE–CdTe–CM/GC, and (c) AChE–GNP–CM/GC electrodes in pH 7.0 PBS containing 1.0 mM ATCl. (Reprinted/adapted with permission from [6], © 2008 Elsevier.)

GC, and AChE–GNP–CM/GC electrodes. Compared to the oxidation peak on the AChE–CdTe–GNP–CM/GC electrode (curve d), the oxidation peak at 826 mV on the AChE–CdTe–CM/GC electrode (curve e) and 689 mV on the AChE–GNP–CM/GC electrode (curve f) shifted positively and the peak currents were much lower. This suggested that the CdTe QDs can promote the electron transfer of enzyme. However, their conductive properties and catalytic behavior are not as good as GNPs. GNPs were more efficient in facilitating electron transfer between the enzyme and the electrode surface. The combination of GNPs and CdTe QDs further improved the electronic transport, which may be due to the synergistic effects in CdTe–GNP film. The sensor was also used to detect the inhibition of monocrotophos, which is involved in the irreversible inhibition on AChE. The inhibition of monocrotophos was proportional to its concentration in two ranges, from 1 to 1000 ng ml$^{-1}$ and from 2 to 15 μg ml$^{-1}$ with a detection limit of 0.3 ng ml$^{-1}$ [6].

## 10.4 Quantum Dot-Based Electrochemical Biosensors of Proteins and DNA

QDs as the label for the electrochemical detection of DNA and protein have been reported by Wang *et al.* since 2002 [17–19]. The detection system is based on the stripping voltammetric detection of dissolved nanoparticles. For example, CdS nanoparticles conjugated with DNA were used for the detection of DNA hybridization [17]. Figure 10.16 demonstrates the steps of the determining protocol.

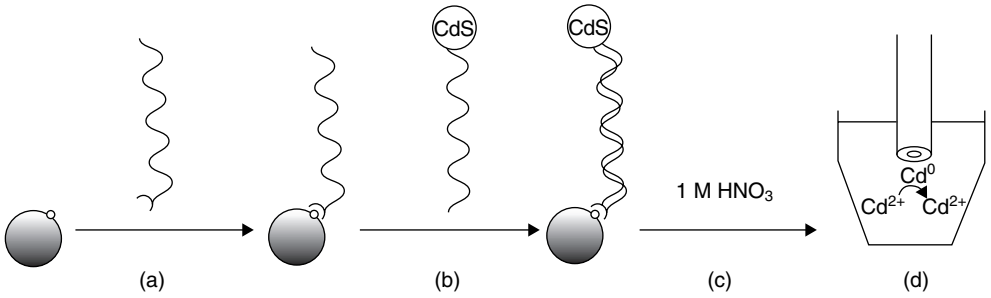


**Figure 10.16** Schematic representation of the analytical protocol: (a) binding of the target to the magnetic beads; (b) hybridization with the CdS-labeled probe; (c) dissolution of CdS tag; (d) potentiometric stripping detection at a mercury film electrode. (Reprinted with permission from [17], © 2002 Elsevier.)

After hybridization with the target modified magnetic beads, CdS was dissolved by 1 M nitric acid to form $Cd^{2+,}$ which was electrochemically reduced to Cd(0) and deposited on the surface of the electrode. The electrical signal for the DNA analysis was proportional to the cadmium signals of oxidizing metal Cd(0) to $Cd^{2+}$. The magnetic separation with magnetic particles effectively discriminated non-hybridized CdS nanoparticles, which can amplify the sensitivity of the electrochemical stripping method. In addition, with magnetic separation, the dissolution step can be eliminated and similar solid-state electrochemical detection can be achieved with CdS-based DNA assemblies. The DNA-linked CdS nanoparticles and magnetic particles can be magnetically anchored onto the film electrode to facilitate the anodic dissolution of the cadmium. The stripping peak obtained by the solid-state phase is similar to that by the solution phase, which reflects the efficiency of the solid-state detection (Figure 10.17).

Further amplification of the sensitivity of the DNA electrochemical detection can be achieved by catalytic precipitation of cadmium to produce larger particles or using CNT-loaded CdS tags. A large enhancement (greater than 12-fold) of the cadmium hybridization signal is observed by using a cadmium catalytic precipitation step. It is reported that the 20 ng ml$^{-1}$ detection limit can be estimated [17]. Compared with the conventional CdS nanoparticle-based procedures, the CNT-based protocol exhibits a substantially (40 times) larger cadmium signal for the significantly (50-fold) lower detection concentration. Furthermore, 500-fold lowering of the detection limit compared to 20 ng ml$^{-1}$ is observed with a CNT carrier [20]. Recently, the direct electrochemical detection of a drop solution of a CdS/DNA sandwich in connection with magnetic microparticles has been reported [21]. The detection method is simple, and uses a lower sample volume based on screen-printed electrodes as working electrodes and a hand-held potentiostatic device as a measuring system.

Simultaneous detection of multiple DNA, based on various semiconductor nanoparticle compositions, has also been developed by Wang's group [18, 22].

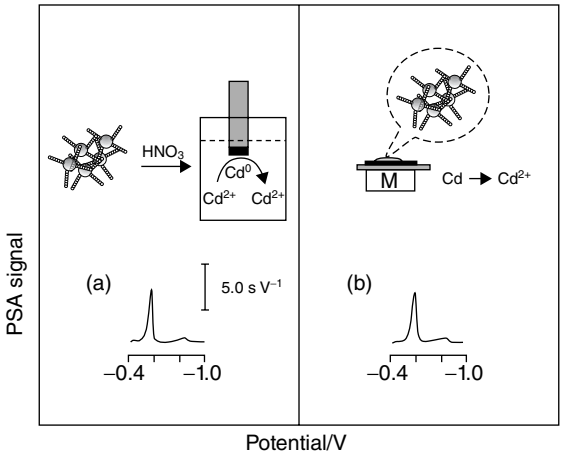


**Figure 10.17** Stripping potentiograms for 1 mg $l^{-1}$ target, following (a) acid dissolution and electrodeposition, and in connection (b) with magnetic "collection" and solid-state detection. (Reprinted with permission from [17], © 2002 Elsevier.)

The multitarget electrical DNA detection system based on different nanoparticles is shown in Figure 10.18 [18]. One magnetic particle was modified with three different DNA probes and subsequently hybridized with complementary DNA targets. The particles were then hybridized with three semiconductor nanoparticle (ZnS, CdS, PbS)-labeled DNA probes. The stripping voltammogram of these three semiconductor nanoparticles yields well-resolved and nonoverlapping peaks, which allowed simultaneously analysis of three different kinds of DNA. This method was further developed with four different magnetic beads for coding single-nucleotide polymorphisms using four different encoding QDs (ZnS, CdS, PbS, CuS) [23]. This procedure provides a distinct electronic fingerprint for each mutation and captures it via base-pairing different QD–mononucleotide conjugates.

The strategy of QDs as labels for the determination of protein is similar to DNA. Figure 10.19 gives an example of a CdS QD-based electrochemical immunoassay system for protein. The magnetic beads conjugated with primary interleukin (IL)-1α first capture IL-1α antigen. QD-linked secondary anti-IL-1α antibody is attached to the magnetic bead surface through the antibody–antigen immunocomplex. After the magnetic separation of the excess reagents, the captured QDs are dissolved with 1 M HCl to release cadmium ions. The electrochemical collection and stripping analysis of cadmium provides the electrochemical readout of the proteins. This QD-based electrochemical immunoassay shows high linearity over the range of 0.5–50 ng $ml^{-1}$ and a detection limit of 0.3 ng $ml^{-1}$ [19]. Liu *et al.* further developed a disposable electrochemical immunosensor diagnosis device based on QD labels and an immunochromatographic strip (Figure 10.20) [24]. The sandwich immunoreaction occurred on the immunochromatographic

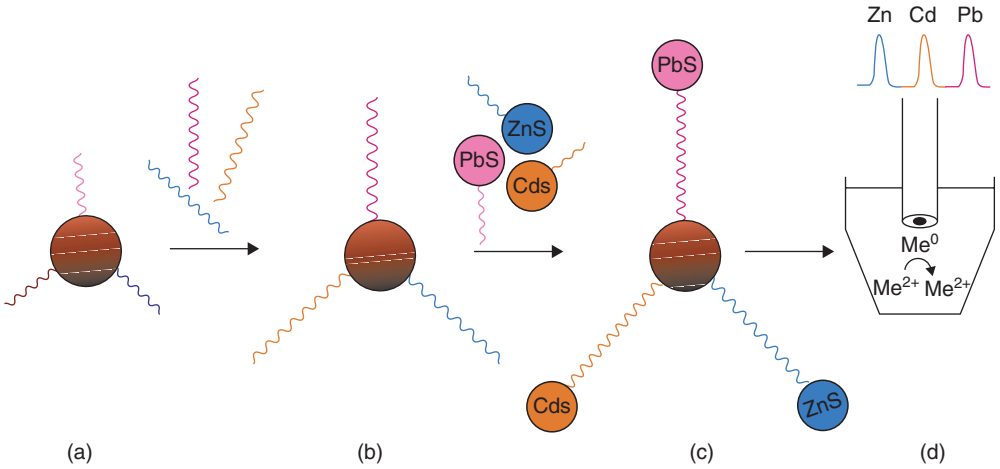


**Figure 10.18** Multitarget electrical DNA detection protocol based on different inorganic colloid nanocrystal tracers. (a) Introduction of probe-modified magnetic beads. (b) Hybridization with the DNA targets. (c) Second hybridization with the QD-labeled probes. (d) Dissolution of QDs and electrochemical detection. (Reprinted with permission from [18], © 2003American Chemical Society.)

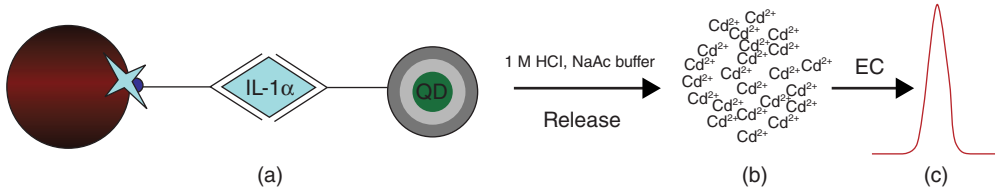


**Figure 10.19** Scheme of QD-based electrochemical immunoassay of IL-1a. (a) Magnetic bead-based sandwich immunoassay, (b) cadmium released with 1 M HCl, and (c) square-wave voltammetry measurement of the released cadmium ions. EC = electrochemical collection. (Reprinted with permission from [19], © 2007 Elsevier.)

strip, and the captured QD labels were dissolved and determined by highly sensitive stripping voltammetric measurement with a disposable screen-printed electrode. The optimized device shows a highly linear voltammetric response over the range of 0.1–10 ng ml$^{-1}$ IgG and an estimated detection limit of 30 pg ml$^{-1}$. The device has been successfully applied for the detection of prostate-specific antigen in human serum samples with a detection limit of 20 pg ml$^{-1}$. Recently, Wang's group reported the QD barcode made by the reverse micelle synthesis method for the electrochemical determination of a cancer marker (carcinoembryonic antigen (CEA)) [22]. The electrochemical stripping response of the dissolved CdS/PbS barcode shows a linear range for the logarithmic concentration of CEA from 0.01 to 80 ng ml$^{-1}$, with an estimated detection limit of 3.3 pg ml$^{-1}$.

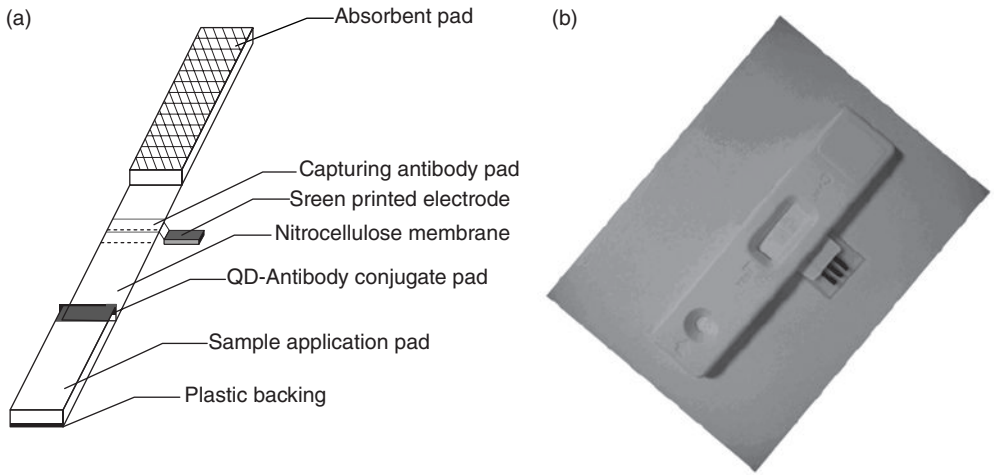


**Figure 10.20** (a) Schematic illustration of disposable electrochemical immunosensor diagnosis device. (b) photograph of disposable electrochemical immunosensor diagnosis device. (Reprinted with permission from [24], © 2007 American Chemical Society.)

This result implies that electrochemical QD barcodes could be a powerful tool in biodetection.

The analogous strategy of simultaneous analysis of different DNA was extended to the parallel analysis of different proteins by their specific aptamers [25]. Two different thiolated aptamers binding with the corresponding QD-tagged proteins were immobilized on the gold surface (Figure 10.21a). When the protein samples were added, analytes competitively displaced the respective QD-labeled proteins associated with the surface (Figure 10.21b). Electrochemical stripping detection of the remaining QDs on the gold surface enables the quantitative detection of the two proteins (Figure 10.21c).

## 10.5 Conclusions

This chapter has highlighted recent progress in the development of electrochemical biosensors based on QDs and their typical applications. QDs not only achieve direct electron transfer between the redox protein and electrodes, but also maintain the bioactivity of redox proteins, thereby improving the sensitivity and linear range of detection. QDs as the labels for detection of proteins and DNA can amplify the electrochemical detection, and the use of different QDs enables the parallel analysis of different targets. Electrochemical biosensors based on QDs show great promise for the fabrication of the third generation of mediator-free biosensors.

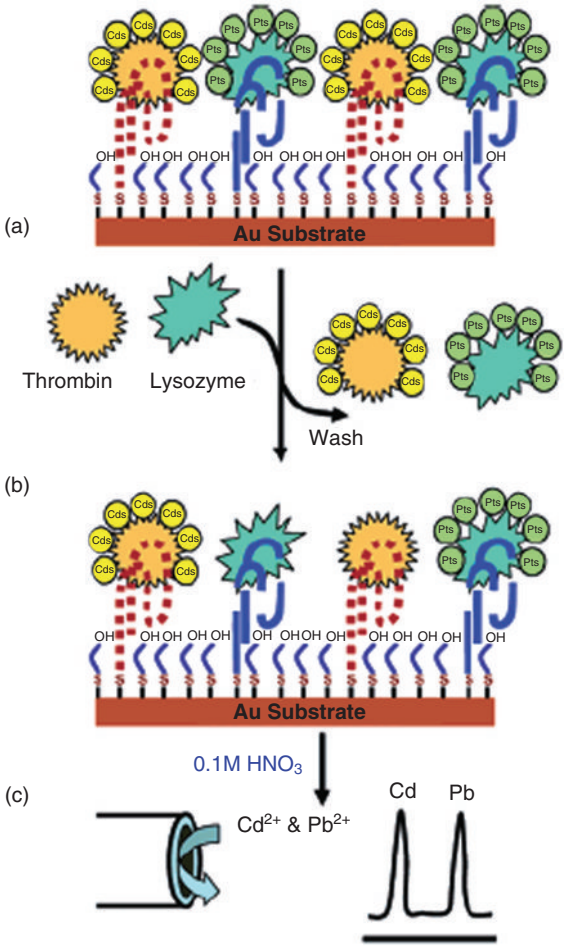


**Figure 10.21** (a) Mixed monolayer of thiolated aptamers on the gold substrate with the bound protein–QD conjugates. (b) Sample addition and displacement of the tagged proteins. (c) Dissolution of the remaining captured nanocrystals followed by their electrochemical stripping detection at a coated GC electrode. (Reprinted with permission from [25], © 2006 American Chemical Society.)

## References


1 Voura, E.B., Jaiswal, J.K., Mattoussi, H., and Simon, S.M. (2004) *Nat. Med.*, **10**, 993; Klostranec, J.M., and Chan, W.C.W. (2006) *Adv. Mater.*, **18**, 1953.

2 Zayats, M. and Willner, I. (2008) *Adv. Biochem. Eng./Biotechnol.*, **109**, 255.

3 Medintz, I.L., Uyeda, H.T., Goldman, E.R., and Mattoussi, H. (2005) *Nat. Mater.*, **4**, 435.

4 Zhang, Q., Zhang, L., Bin, L., Lu, X.B., and Li, J.H. (2007) *Biosens. Bioelectron.*, **23**, 695.

5 Cai, W.Y., Feng, L.D., Liu, S.H., and Zhu, J.J. (2008) *Adv. Funct. Mater.*, **18**, 3127.

6 Du, D., Chen, S.Z., Song, D.D., Li, H.B., and Chen, X. (2008) *Biosens. Bioelectron.*, **24**, 475.

**7** Huang, Y.X., Zhang, W.J., Xiao, H., and Li, G.X. (2005) *Biosens. Bioelectron.*, **21**, 817.

**8** Liu, Q., Lu, X.B., Li, J., Yao, X., and Li, J.H. (2007) *Biosens. Bioelectron.*, **22**, 3203.

**9** Xu, Y.X., Liang, J.G., Hu, C.G., Wang, F., Hu, S.S., and He, Z.K. (2007) *J. Biol. Inorg. Chem.*, **12**, 421.

**10** Wang, Z., Xu, Q., Wang, H.Q., Yin, Z.H., Yu, J.H., and Zhao, Y.D. (2009) *Anal. Sci.*, **25**, 773.

**11** Wang, Z., Xu, Q., Wang, J.H., Yang, Q., Yu, J.H., and Zhao, Y.D. (2009) *Microchim. Acta*, **165**, 387.

**12** Qian, J.M., Suo, A.L., Yao, Y., and Jin, Z.H. (2004) *Clin. Biochem.*, **37**, 155.

**13** Garjonyte, R. and Malinauskas, A. (2000) *Biosens. Bioelectron.*, **15**, 445.

**14** Wang, Q.L., Lu, G.X., and Yang, B.J. (2004) *Biosens. Bioelectron.*, **19**, 1269.

**15** Liu, S.Q., Dai, Z.H., Chen, H.Y., and Ju, H.X. (2004) *Biosens. Bioelectron.*, **19**, 963.

**16** Katz, E., Willner, I., and Wang, J. (2004) *Electroanalysis*, **16**, 19.

**17** Wang, J., Liu, G.D., Polsky, R., and Merkoci, A. (2002) *Electrochem. Commun.*, **4**, 722.

**18** Wang, J., Liu, G.D., and Merkoci, A. (2003) *J. Am. Chem. Soc.*, **125**, 3214.

**19** Wu, H., Liu, G.D., Wang, J., and Lin, Y.H. (2007) *Electrochem. Commun.*, **9**, 1573.

**20** Wang, J., Liu, G.D., Jan, M.R., and Zhu, Q.Y. (2003) *Electrochem. Commun.*, **5**, 1000.

**21** Marin, S., and Merkoci, A. (2009) *Nanotechnology*, **20**, 055101.

**22** Xiang, Y., Zhang, Y.Y., Chang, Y., Chai, Y.Q., Wang, J., and Yuan, R. (2010) *Anal. Chem.*, **82**, 1138.

**23** Liu, G.D., Lee, T.M.H., and Wang, J.S. (2005) *J. Am. Chem. Soc.*, **127**, 38.

**24** Liu, G., Lin, Y.Y., Wang, J., Wu, H., Wai, C.M., and Lin, Y. (2007) *Anal. Chem.*, **79**, 7644.

**25** Hansen, J.A., Wang, J., Kawde, A.N., Xiang, Y., Gothelf, K.V., and Collins, G. (2006) *J. Am. Chem. Soc.*, **128**, 2228.

# 11
# Functionalized Graphene for Biosensing Applications

*Minghui Yang, Chunyan Wang, Qin Wei, Bin Du, He Li, and Zhiyong Qian*

## 11.1
## Introduction

Graphene, the basal plane of graphite, is composed of a flat monolayer of carbon atoms tightly packed into a two-dimensional honeycomb lattice [1]. It is the first example of the strictly two-dimensional and one-atom-thick sheet, which has been attracting much attention owing to its unusual electronic properties and effects that arise from its truly atomic thickness [2–4]. Graphene is the basic building block for graphitic materials of all other dimensionalities. It can be wrapped up into zero-dimensional fullerenes, rolled into one-dimensional nanotubes, or stacked into three-dimensional graphite. It is flexible yet harder than diamond and conducts electricity faster at room temperature than anything else. It is suggested to be a very important material not only for fundamental research, but also for device applications [5–7]. In addition to the possibility of low-power, high-density, and high-speed switches, graphene-based devices may also be applied to other areas as atom-thick membranes for sensing pressure, as components in nanoelectromechanical systems, or in chemical sensing because of their high surface area.

Different kinds of carbon nanomaterials have been widely used for the fabrication of sensors and biosensors, such as carbon nanoparticles, carbon nanotubes, and carbon nanofibers, because of their large specific surface area, high conductivity, and good chemical stability [8–10]. However, the use of graphene for biosensor applications is still at an early stage. Here, we focus on biosensors based on functionalized graphene. At the same time, we discuss the chemical methods for the production of graphenes and the functionalization of graphene.

## 11.2
## Preparation of Grapheme

The development of various methods for producing graphene has stimulated a vast amount of research in recent years. Graphene has been made mainly by four different methods: (i) chemical vapor deposition (CVD) and epitaxial growth, such

*Biosensor Nanomaterials*. Edited by Songjun Li, Jagdish Singh, and Ipsita A. Banerjee

ISBN: 978-3-527-32841-3

as the decomposition of ethylene on a nickel surface [11]; (ii) micromechanical exfoliation of graphite [12]; (iii) epitaxial growth on electrically insulating surfaces such as SiC [13]; and(iv) creation of colloidal suspensions.

In this chapter, the preparation of graphene from colloidal suspensions made from graphite, graphite oxide, and graphite intercalation compounds is discussed. This approach is scalable, affording the possibility of high-quantity production, and enables easy chemical functionalization of the produced graphene. These advantages mean that the colloidal suspension method for producing graphene could find wide potential applications [14].

Nowadays, the most widely used method to prepare graphite oxide is Hummer's method [15]. In this method, the graphite oxide is prepared by oxidation of graphite in the presence of strong acids and oxidants [16]. The level of the oxidation can be varied on the basis of the method, reaction conditions, and precursor graphite used. Reduction of the graphene oxide by chemical methods (using reductants such as hydrazine, hydroquinone, and $NaBH_4$), thermal expansion methods, and UV-assisted methods has employed to produce electrically conducting graphene.

The reduction of aqueous graphite oxide suspension by hydrazine at the pH of the suspension results in agglomerated graphene-based nanosheets and, when dried, a black powder that is electrically conductive [17]. Elemental analysis (atomic C/O ratio around 10) of the reduced graphene oxides measured by combustion revealed the existence of a significant amount of oxygen, indicating that reduced graphene oxide is not the same as pristine graphene (Figure 11.1).

In another report, a graphene-based suspension was produced in three reaction steps: (i) "prereduction" of graphene oxide by $NaBH_4$, (ii) sulfonation by the aryl diazonium salt of sulfanilic acid, and (iii) "postreduction" of aqueous sulfonated graphene (2 mg ml$^{-1}$, pH 3–10) with hydrazine. The sulfonated graphene sheets (GSs) of step (ii) could be dispersed in water (2 mg ml$^{-1}$, pH 3–10) and after the postreduction step the chemically modified GSs could be dispersed in mixed solvents of water with certain organic solvents. It was suggested that covalent functionalization in the chemically modified GSs by sulfonyl groups was occurring [18].

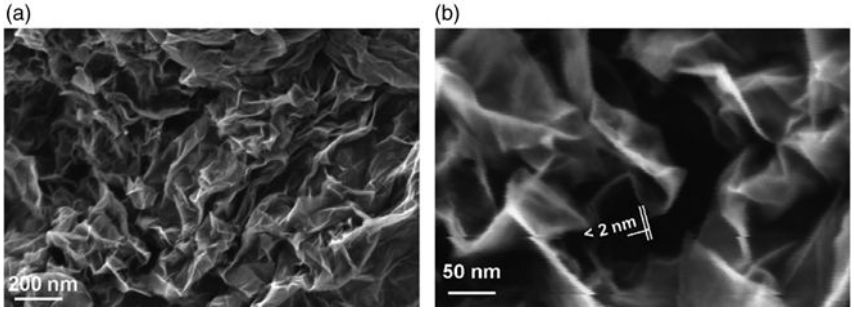


**Figure 11.1** (a) Scanning electron microscope image of aggregated RGSs. (b) A platelet having an upper bound thickness at a fold of around 2 nm. (Reprinted with permission from [17], © 2007 Elsevier.)

Through chemical reduction with dimethylhydrazine or hydrazine with either polymer or surfactant, homogeneous colloidal suspensions of electrically conducting graphene have been synthesized [19, 20]. The reduction of an aqueous suspension containing graphite oxide and poly(sodium 4-styrenesulfonate) resulted in an aqueous black suspension of reduced GSs (RGSs) coated in the polymer. A suspension of reduced graphite oxide sheets was produced by reducing isocyanate-functionalized graphite oxide in the presence of polystyrene. Sodium dodecylbenzenesulfonate (SDBS)-wrapped graphene oxide was reduced by hydrazine and followed by chemical modification with the aryl diazonium salt; the resulting SDBS-wrapped graphene could be dispersible in *N,N*-dimethylformamide, *N,N′*-dimethylacetamide, and *N*-methyl-2-pyrrolidone at concentrations up to $1\,mg\,ml^{-1}$.

Williams *et al.* reported a novel method to produce graphene based on UV-assisted photocatalytic reduction of graphite oxide [21]. In their study, they prepared a mixture of graphite oxide and $TiO_2$ in ethanol, and subjected it to steady-state UV irradiation. The suspension of graphite oxide in ethanol underwent reduction as it accepts electrons from UV-irradiated $TiO_2$ suspensions. After reduction, the absorption of the graphene oxide was changed with the color of the suspension, changing from light brown to dark brown to black. Without $TiO_2$ in the suspension, no significant changes could be observed during UV irradiation. This photocatalytic methodology supplies a novel strategy to synthesize photoactive graphene–semiconductor composites (Figure 11.2).

Thermal treatment of graphite oxide is another route that has been used to obtain reduced platelets. Rapid heating up to 1050 °C exfoliates as well as reduces graphite oxide, yielding a black powder [22]. The platelets have a similar oxygen content to that of hydrazine-reduced graphene oxide. The thermally reduced GSs could be dispersed in several organic solvents ($0.1\,mg\,ml^{-1}$), and their colloidal suspension was used to fabricate a set of composites of reduced graphenes and polymers.

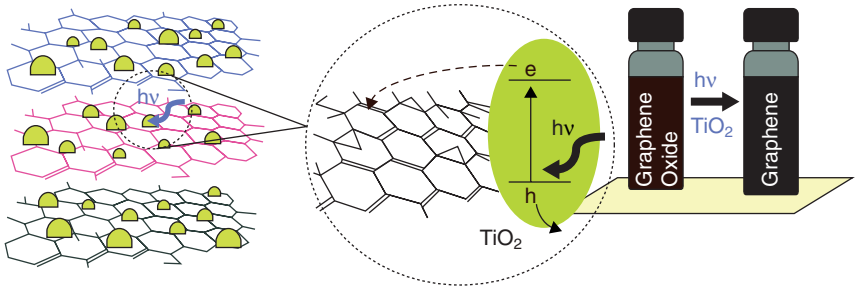


**Figure 11.2** Graphene oxide suspended in ethanol undergoes reduction as it accepts electrons from UV-irradiated $TiO_2$ suspensions. The reduction is accompanied by changes of the color of the suspension from brown to black. (Reprinted with permission from [21], © 2008 American Chemical Society.)

## 11.3
## Functionalized Graphene with Metal Nanoparticles

The modification of graphene with noble metal nanoparticles is of particular interest as the immobilized metal nanoparticles always show enhanced electrocatalytic activity. Muszynsky *et al.* reported a method to decorate GSs with gold nanoparticles (Au-NPs) [23]. In their study, the Au-NPs were synthesized using chemical reduction of $AuCl_4^-$ with $NaBH_4$ in graphene solution (Figure 11.3). The adsorption spectra of the Au-NPs changes with the changing of the graphene solution. At a low graphene concentration, the Au-NPs show rather broad adsorption, which is because the nanoparticles remain suspended, but in the aggregated state. With increasing graphene concentration, a sharp adsorption spectra was observed, indicating the Au-NPs become dispersed as individual particles.

In another study, Seger *et al.* studied the deposition of platinum nanoparticles (Pt-NPs) on graphene by reduction of $H_2PtCl_6$ in graphite oxide solution [24]. The graphene serves as a support material for the dispersion of Pt-NPs, which provides new ways to develop advanced electrocatalyst materials for fuel cells. The experimental results demonstrated the ability of GSs to support nanoparticles, which opens new ways to develop electrocatalysts for fuel cells.

Yoo *et al.* also investigated Pt-NPs supported on graphene and explored the composite material as an electrocatalyst for fuel cells [25]. The platinum catalysts supported on graphene were prepared from a mixture of platinum precursor $[Pt(NO_2)_2 \cdot (NH_3)_2]$ and the graphene powder. The powder was dispersed in ethanol, dried in air at 40 °C for 1 h, and then subjected to heat treatment in an $Ar/H_2$ (4 : 1 v/v) stream at 400 °C for 2 h in a furnace. For methanol oxidation reaction, the current density of platinum/graphene was much higher than that of platinum/

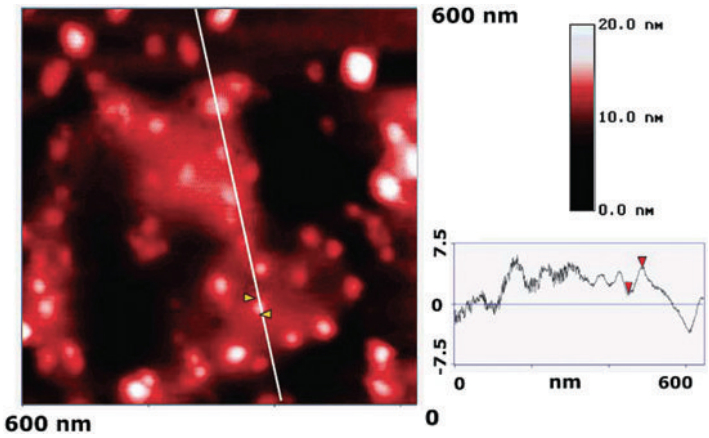


**Figure 11.3** Atomic force microscope image of Au-NPs anchored on graphene-ODA (octadecylamine). The cross-section analysis shows the height of graphene and peaks arising from Au-NPs. (Reprinted with permission from [23], © 2008 American Chemical Society.)

carbon black. Thus, graphene remarkably improved the electrocatalytic activity of the platinum catalyst, almost approaching that of platinum-ruthenium/carbon black.

## 11.4 Glucose Biosensors Based on Graphene

One of the major applications of graphene in the biosensing field is the fabrication of glucose biosensors. Due to the excellent electrical conductivity, high surface area, and good electrocatalytic activity of graphene, different metal nanoparticles were combined with graphene for the fabrication of glucose biosensors.

Zhou *et al.* reported greatly enhanced electrochemical reactivity of $H_2O_2$ at the chemically reduced graphite oxide (CR-GO)-modified glassy carbon (GC) electrode [26]. In their report, the oxidation/reduction currents on CR-GO/GC, graphite/GC, and GC electrodes started at 0.20/0.10, 0.80/−0.35, and 0.70/−0.25 V, respectively, indicating the superior electrocatalytic activity of GR-GO toward $H_2O_2$. They speculate that the superior electrocatalytic is most likely attributed to the high density of edge-plane-like defective sites on CR-GO, which may provide many active sites for electron transfer to biological species. The greatly enhanced electrochemical reactivity of $H_2O_2$ at the CR-GO/GC electrode makes CR-GO attractive for oxidase-based amperometric biosensors, which has been illustrated in connection with the fabrication of glucose biosensors. For both glucose oxidase (GOx)/graphite/GC and GOx/GC electrodes, there is no obviously current response to the glucose additions, but the CR-GO-based GOx biosensor offers substantially larger signals, reflecting the better electrocatalytic activity of the GOx/CR-GO/GC electrode (Figure 11.4). The linear range for glucose detection at the GOx/CR-GO/GC electrode (0.01–10 mM) is wider than that at other carbon materials-based electrodes, such as the PDDA (poly(diallyldimethylammonium chloride)/GOx/PDDA/CNT (carbon nanotube)-modified electrode (0.015–6 mM) [27], the GOx/carbon nanofiber-modified electrode (0.01–0.35 mM) [28], and the GOx/highly oriented pyrolytic graphite-modified electrode (0.10–1.50 mM) [29]. The detection limit for glucose at the GOx/CR-GO/GC electrode (2.00 μM at −0.20 V (versus Ag/AgCl)) is also lower than that of some reported carbon materials-based biosensors, such as the GOx/CNT paste electrode (60 μM at −0.100 V (versus Ag/AgCl)) [30], the GOx/CNT nanoelectrode (80 μM at −0.20 V (versus Ag/AgCl)) [31], the PDDA/GOx/PDDA/CNT-modified electrode (7 μM at −100 mV (versus Ag/AgCl)) [27], the GOx-carbon nanofiber-modified electrode (2.5 μM at −0.30 V (versus saturated calomel electrode)) [28], the GOx/mesocellular carbon foam/Nafion-modified electrode (70 μM at 600 mV (versus Ag/AgCl)) [32], the GOx/exfoliated graphite nanoplatelet/Nafion-modified electrode (10 μM at 0.7 V (versus Ag/AgCl)) [33], and the Nafion/GOx/highly ordered mesoporous carbon-modified electrode (156.52 μM at 0.35 V (versus Ag/AgCl)) [34].

In another report, Shan *et al.* reported a novel glucose biosensor based on immobilization of GOx in thin films of chitosan containing nanocomposites of

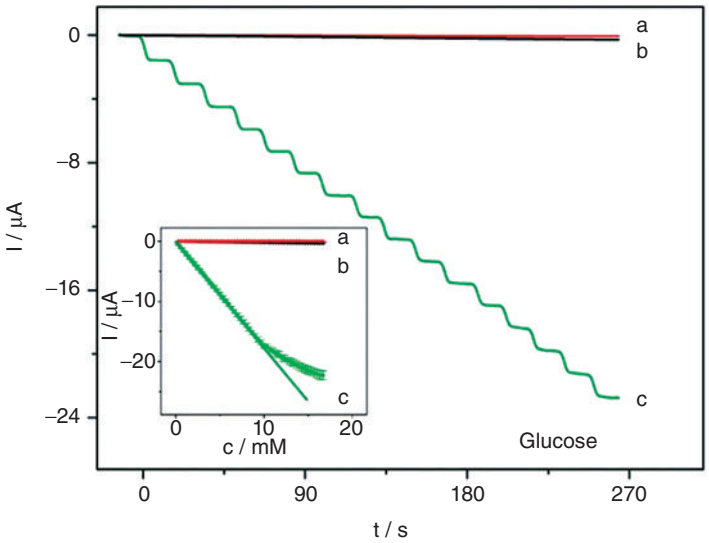


**Figure 11.4** Current–time curves for GOx/graphite/GC (a), GOx/GC (b), and GOx/CR-GO/GC (c) electrodes at –0.20 V with successive addition of 1 mM glucose. Inset: calibration curves for glucose at GOx/graphite/GC (a), GOx/GC (b), and GOx/CR-GO/GC (c) electrodes. (Reprinted with permission from [26], © 2009 American Chemical Society.)

graphene and Au-NPs at a gold electrode [35]. The resulting graphene/Au-NP/chitosan composite film exhibited good electrocatalytical activity toward $H_2O_2$. The biosensor displayed a wide linear response to $H_2O_2$ (0.2–4.2 mM, $R = 0.998$) at –0.2 V, high sensitivity of 99.5 μA $mM^{-1} cm^{-2}$, and good reproducibility. The synergistic effect of graphene and Au-NPs plays an important role for achieving good electrocatalytical activity. The graphene/Au-NP/GOx/chitosan composite-modified electrode exhibited good amperometric response to glucose. At –0.2 V, the linear range is from 2–10 mM ($R = 0.999$); at 0.5 V, the linear range is from 2 to 14 mM ($R = 0.999$). In addition, the biosensor has good reproducibility (Figure 11.5). The glucose biosensor was used for preliminarily studies of glucose concentration in human blood. Increasing the glucose concentrations from 2.5 to 7.5mM, the cathodic peak currents of the biosensor decrease linearly. The graphene/Au-NP/GOx/chitosan composite film shows prominent electrochemical response to glucose, which gives it wide potential applications for the electrochemical detection of glucose.

GOx/Pt/FGS (functional graphene sheet)/chitosan bionanocomposite film for glucose sensing was studied by Wu *et al.* [36]. Based on the electrocatalytic synergy effect of FGS and Pt-NPs, the sensitivity of the bionanocomposite film toward $H_2O_2$ was increased greatly. With the immobilization of GOx, a sensitive biosensor with a detection limit of 0.6 μM glucose was obtained. The biosensor also shows good reproducibility and good stability. In addition, the interfering signals from

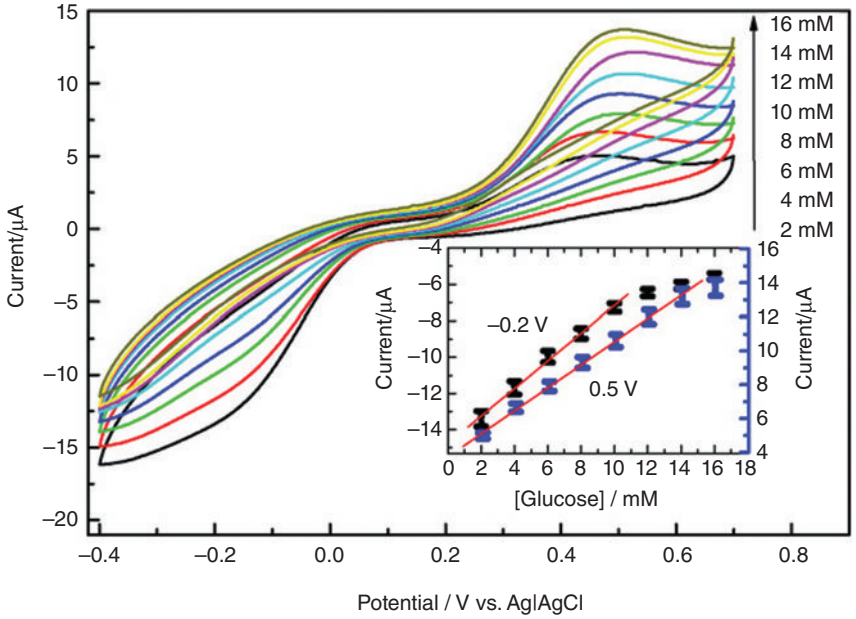


**Figure 11.5** Cyclic voltammetric measurements at graphene/Au-NP/chitosan-modified electrode in $O_2^-$ saturated phosphate buffer containing various concentrations of glucose: 2, 4, 6, 8, 10, 12, 14, and 16 mM (from down to up) Inset: calibration curves corresponding to amperometric responses at –0.2 and 0.5 V. Scan rate: 0.05 V $s^{-1}$. Error bars = standard deviation. (Reprinted with permission from [35], © 2009 Elsevier.)

ascorbic acid and uric acid were negligible compared to the response to glucose. Graphene as a sensor material has potential wide applications due to the good electrical conductivity and large surface area of graphene.

In the above-mentioned glucose biosensors, the detection of glucose was achieved through the detection of the enzyme substrate, $H_2O_2$. Apart from this type of glucose sensor, direct electrochemistry of GOx and biosensing for glucose based on graphene have also been widely researched. Shan *et al.* reported a polyvinylpyrrolidone-protected graphene/PFIL (polyethylenimine-functionalized ionic liquid)/GOx electrochemical biosensor, which achieved the direct electron transfer of GOx, maintained its bioactivity, and showed potential application for the fabrication of novel glucose biosensors [37]. In their report, GOx was immobilized onto PFIL because of the good film stability and high ionic conductivity of PFIL. The graphene/GOx/PFIL-modified electrode displays a pair of well-defined redox peaks, which is characteristic of the reversible electron transfer process of the redox active center (flavin adenine dinucleotide (FAD)) in the GOx. In a control, using graphite instead of graphene, the direct electrochemistry of GOx was not achieved. It is well known that the active redox center of GOx, FAD, is deeply embedded in a protective protein shell, which makes direct electron

communication with electrodes extremely difficult. The graphene has extraordinary electron transport properties and high specific surface area, so we speculate that graphene can promote the electron transfer of the film, and facilitate the direct electron transfer process between the GOx and electrode substrate.

In another report, Kang *et al.* studied the direct electrochemistry behavior of GOx/graphene/chitosan nanocomposites [38]. The immobilized enzyme keeps its bioactivity, and shows good stability, activity, and a fast heterogeneous electron transfer rate (rate constant ($k_s$) = 2.83 $s^{-1}$). Much higher enzyme has been loaded onto the nanocomposite than on the bare glass carbon surface. The performance of this GOx/graphene/chitosan nanocomposite film for the detection of glucose was investigated. The fabricated biosensor has a wider linearity range from 0.08 to 12 mM glucose with a detection limit of 0.02 mM. The authors drawn a conclusion that the excellent performance of the biosensor is ascribed to the large surface-to-volume ratio and high conductivity of graphene, and good biocompatibility of chitosan, which enhanced the enzyme immobilization and promoted direct electron transfer between redox sites of enzymes and the electrode surface [38].

## 11.5 Immunosensors Based on Graphene

There are still only a few reports of using graphene for the fabrication of immunosensors. In one study, Zhong *et al.* reported nanogold-enwrapped graphene nanocomposites (NGGNs) as trace labels for sensitivity enhancement of electrochemical immunosensors for the detection of carcinoembryonic antigen (CEA) [39]. Au-NPs were electrochemically deposited on the Prussian blue-modified GC electrode for further adsorption of the specific analyte-capturing molecule, anti-CEA antibody. The signal of the immunosensor was from horseradish peroxidase (HRP)-conjugated anti-CEA as secondary antibodies immobilized onto the NGGN surface (HRP/anti-CEA/NGGN) (Figure 11.6). The signal enhancement based on HRP/anti-CEA/NGGN shows high sensitivity, and exhibits a dynamic linear range of 0.05–350 ng $ml^{-1}$ with a low detection limit of 0.01 ng $ml^{-1}$ CEA (at 3 s). The application of the immunosensor for the detection of CEA in serum samples produced acceptable agreement with the reference values.

In our group, we reported an ultrasensitive electrochemical immunosensor for the detection of prostate-specific antigen (PSA) based on graphene [40]. Graphene was used to immobilize mediator thionine (TH), enzyme HRP and secondary anti-PSA antibody ($Ab_2$), and the resulting nanostructure (GS/TH/HRP/$Ab_2$) was used as the label for the immunosensor. With primary anti-PSA antibody ($Ab_1$) also immobilized onto the graphene, the immunosensor displayed a wide range of linear response (0.002–10 ng $ml^{-1}$), low detection limit (1 pg $ml^{-1}$), and good reproducibility, selectivity and stability (Figure 11.7). The good performance of the immunosensor is attributed to the graphene's high surface-to-volume ratio, which allows the immobilization of a high-level of $Ab_1$, $Ab_2$, TH, and HRP, and its good electrical conductivity, which can improve the electron transfer among TH, HRP,

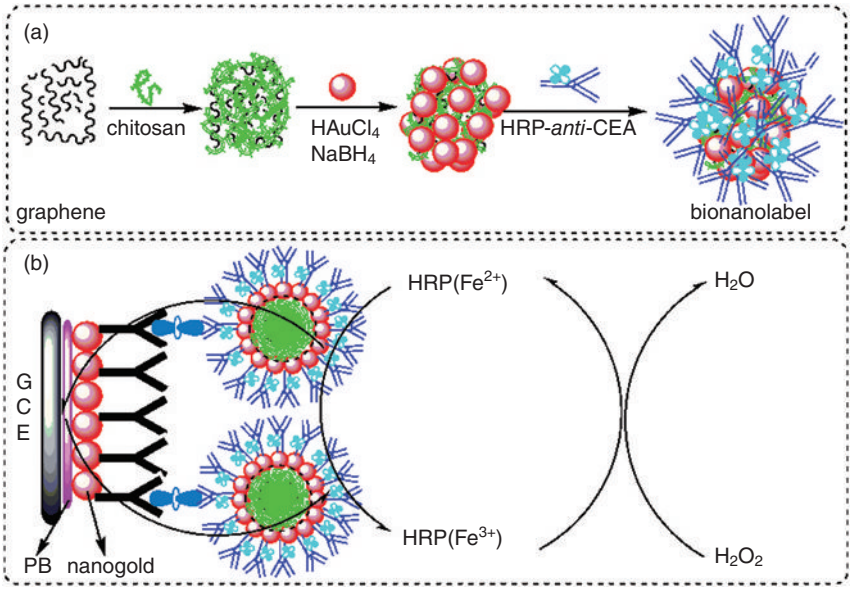


**Figure 11.6** (a) Fabrication process of the HRP/anti-CEA/NGGN bionanolabel. (b) Measurement protocol. (Reprinted with permission from [39], © 2010 Elsevier.)

$H_2O_2$, and electrode. Graphene-based labels may provide many potential applications for the detection of different cancer biomarkers.

## 11.6 Other Electrochemical Biosensors Based on Graphene

Kang *et al.* presented an electrochemical sensor based on the electrocatalytic activity of functionalized graphene for the sensitive detection of paracetamol [41]. The experimental results showed that an excellent electrocatalytic activity to paracetamol had been obtained by the graphene-modified electrode. Compared with a bare electrode, the use of graphene decreased the overpotential of paracetamol significantly. Such good electrocatalytic behavior of graphene results from its subtle electronic characteristics and strong adsorptive capability. An excellent performance for paracetamol detection was obtained. The fabricated electrochemical sensor had a detection limit of $3.2\times10^{-8}$M and a reliable reproducibility of 5.2% (relative standard deviation).

In another report, Tan *et al.* explored the feasibility of dispersing GS using β-cyclodextrin (β-CD) and then using the β-CD/GS nanocomposite in detecting the bioactive molecule dopamine [42]. When used in electrochemical detection of dopamine, the β-CD/GS-modified carbon electrode showed a low detection limit (5.0 nM), broad linear range ($9.0 \times 10^{-3}$ to 12.7 μM), along with good selectivity.

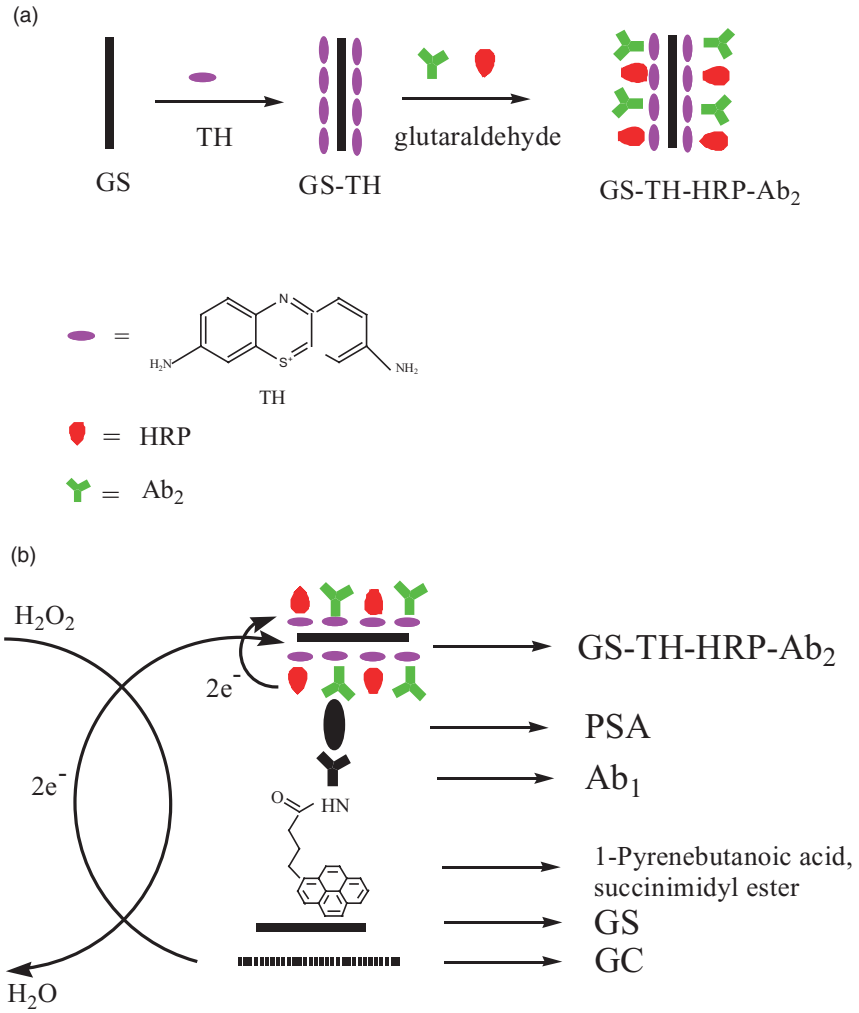


**Figure 11.7** Schematic representation of the preparation of the GS/TH/HRP/$Ab_2$ nanostructure (a) and immunosensor (b). (Reprinted with permission from [40], © 2010 Elsevier.)

The electrochemical reaction of dopamine on the β-CD/GS showed a mass diffusion-controlled process, which was different from the adsorption-controlled process on the unmodified GS.

In order to detect ascorbic acid and dopamine simultaneously, Li *et al.* prepared a water-soluble and electroactive Pt-NP/PFIL/GS nanocomposite [43]. The immobilization of Pt-NPs on graphene was investigated by scanning electron microscopy and transmission electron microscopy, which revealed Pt-NPs were densely dispersed on the transparent thin PFIL-functionalized GSs. The obtained Pt/PFIL/GS nanocomposite-modified electrode could detect ascorbic acid and dopamine simultaneously by cyclic voltammetry. The difference between the two peak poten-

tials of ascorbic acid and dopamine oxidation was over 200 mV, which can be used to easily distinguish ascorbic acid from dopamine. This electrochemical sensor could detect increasing concentrations of ascorbic acid in the presence of dopamine and increasing concentrations of dopamine in the presence of ascorbic acid by differential pulse voltammetry. For real sample analysis, in human urine samples, three independent oxidation peaks appeared in urine samples containing ascorbic acid and dopamine, indicating the potential of the Pt/PFIL/GS nanocomposite in the routine clinical analysis of ascorbic acid and dopamine.

Wang *et al.* described the electrochemical properties of RGSs for the electrocatalytic oxidation of hydrazine in alkaline media [44]. RGSs were been synthesized in high yield by a soft chemistry route involving graphite oxidation, ultrasonic exfoliation, and chemical reduction. The RGSs exhibited excellent electrocatalytic activity towards the hydrazine oxidation (Figure 11.8). The overall reaction of hydrazine oxidation catalyzed by RGSs in alkaline media can be formulated as follows:

$$N_2H_4 + 4H_2O \rightarrow N_2 + 4H_3O^+ + 4e^-$$

For the first time, low-potential nicotinamide adenine dinucleotide (NADH) detection and biosensing for ethanol were achieved at an ionic liquid-functionalized

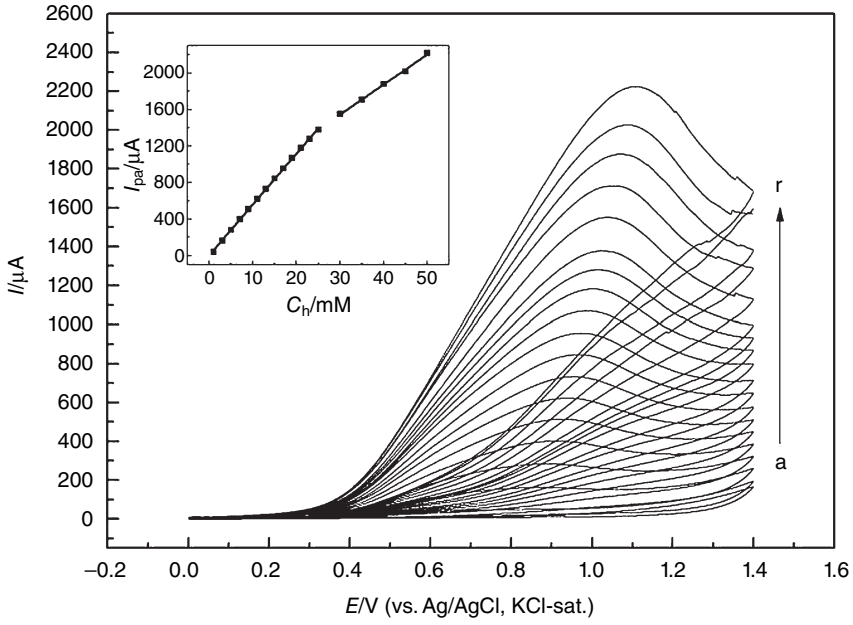


**Figure 11.8** Cyclic voltammograms at the RGS/GC electrode in 0.1 M KOH solution containing increasing concentrations of hydrazine from (a) 1, (b) 3, (c) 5, (d) 7, (e) 9, (f) 11, (g) 13, (h) 15, (i) 17, (j) 19, (k) 21, (l) 23, (m) 25, (n) 30, (o) 35, (p) 40, (q) 45 to (r) 50 mM. Scan rate: 0.1 V $s^{-1}$. Also shown as inset is the plot of $I_{pa}$ versus concentration of hydrazine. (Reprinted with permission from [44], © 2010 Elsevier.)

graphene-modified electrode by Shan *et al.* [45]. The overvoltage of the NADH oxidation was substantially decrease at the ionic liquid-functionalized graphene/chitosan-modified electrode (440 mV), with oxidation starting at around 0 V (versus. Ag/AgCl). The NADH amperometric response at such a modified electrode is more stable (95.4 and 90% of the initial activity remaining after 10 and 30 min at 1 mM NADH solution) than that at a bare electrode (68 and 46%). The linear range of the ionic liquid-functionalized graphene/chitosan-modified electrode was from 0.25 to 2 mM with high sensitivity of 37.43 $\mu A\,mM^{-1}cm^{-2}$. Novel and promising dehydrogenase-based amperometric biosensors can be fabricated due to the high sensitivity and wide linear range of ionic liquid-functionalized graphene for NADH detection. The alcohol biosensor exhibited a fast and sensitive amperometric response to ethanol (low detection limit: 5 μM) for the alcohol dehydrogenase model. Moreover, the proposed biosensor has been used to determine ethanol in real samples with satisfactory results.

Graphene has been widely used for the immobilization of redox proteins to achieve direct electron transfer between proteins and electrode. Using a chemical route to reduce graphene oxide, and dispersed fully in water to form a stable black aqueous solution, Wu *et al.* prepared chitosan-dispersed graphene nanoflakes for immobilization onto a GC electrode, which was used to adsorb cytochrome *c* onto the electrode surface to achieve direct electron transfer of cytochrome *c* [46]. The adsorbed cytochrome *c* on the electrode surface retains its bioactivity and shows an enzyme-like activity for the reduction of nitric oxide (Figure 11.9).

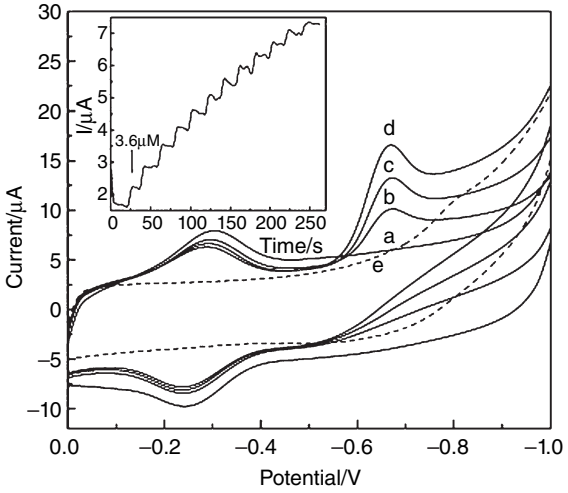


**Figure 11.9** Cyclic voltammograms of cytochrome *c*/CS-GR/GC electrode in 0.1 M phosphate-buffered saline at pH 7.0 containing (a) 0, (b) 0.1, (c) 0.2, (d) 0.3 and (e) 0.3 mM nitric oxide at the CS-GR/GC electrode. (CS-GR = chitosan-dispersed graphene nanoflake). Scan rate: 100 $mV\,s^{-1}$. Inset: recorded current–time curves with successive addition of 3.6 μM nitric oxide at a potential of –0.67 V. (Reprinted with permission from [46], © 2010 Elsevier.)

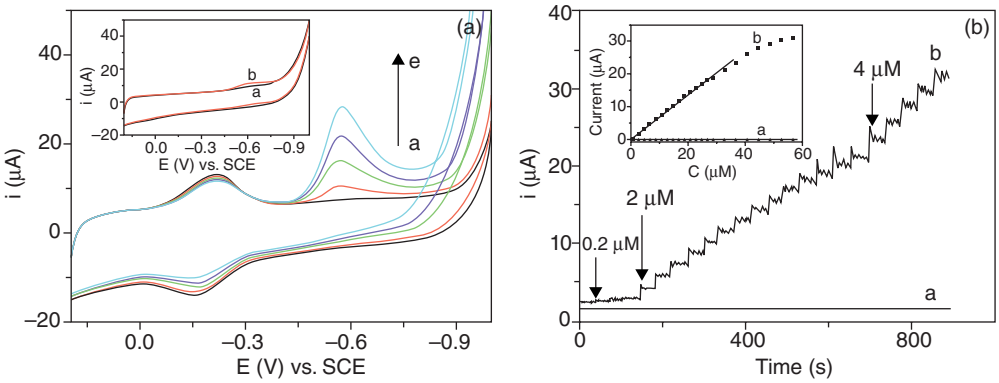


**Figure 11.10** (A) Cyclic voltammograms of hemoglobin/RTIL/PDDA-G-modified GC electrode in 0.20 M NaAc–HAc buffer at pH 2.0 containing: (a) 0, (b) 2, (c) 6, (d) 10, and (e) 16 μM $NaNO_2$. Inset: cyclic voltammograms of (a) PDDA-G/GC electrode and (b) RTIL/PDDA-G/GC electrode in 0.20 M NaAc–HAc buffer at pH 2.0 containing 16 μM $NaNO_2$. (B) Typical amperometric current–time response curves of the hemoglobin/RTIL/graphite (a) and hemoglobin/RTIL/PDDA-G (b) biosensor upon successive addition of $NaNO_2$ into 0.20 M NaAc–HAc buffer solution at pH 2.0. Applied potential: –0.58 V. Inset: linear relation between the amperometric response and $NO_2^-$ concentration. (Reprinted with permission from [47], © 2010 Elsevier.)

In another work, functionalized graphene nanosheets with PDDA were synthesized and used to combine with room temperature ionic liquid (RTIL) [47]. The resulting RTIL/PDDA-G composite displayed an enhanced capability for the immobilization of hemoglobin and the direct electrochemistry of hemoglobin was realized. Moreover, the RTIL/PDDA-G-based biosensor displayed excellent electrocatalytic activity for the detection of nitrate with a wide linear range from 0.2 to 32.6 μM and a low detection limit of 0.04 μM (Figure 11.10).

## 11.7 Conclusions

Although there are still only limited reports of using graphene for the fabrication of biosensors, we should keep in mind is that it has been less than 5 years since graphene was first reported. The most immediate application for graphene is probably its use in composite materials, which are more conductive, biocompatible, with a higher surface area and catalytic activity. These properties are key for the immobilization of biomolecules and the preparation of highly sensitive biosensors. In this respect, considering the wide applications of CNTs in the biosensing field and the clear parallels of graphene with CNTs, growing interest will be focused on the exploration of graphene as a biosensor building material.

## References


1 Geim, A.K. and Novoselov, K.S. (2007) *Nat. Mater.*, **6**, 183–191.
2 Wang, X.R., Li, X.L., Zhang, L., Yoon, Y.K., Weber, P.K., Wang, H.L., Guo, J., and Dai, H.J. (2009) *Science*, **324**, 768–771.
3 Wang, F., Zhang, Y.B., Tian, C.S., Girit, C., Zettl, A., Crommie, M., and Shen, Y.R. (2008) *Science*, **320**, 206–209.
4 Westervelt, R.M. (2008) *Science*, **320**, 324–325.
5 Stoller, M.D., Park, S.J., Zhu, Y.W., An, J., and Ruoff, R.S. (2008) *Nano Lett.*, **8**, 3498–3502.
6 Fowler, J.D., Allen, M.J., Tung, V.C., Yang, Y., Kaner, R.B., and Weiller, B.H. (2009) *ACS Nano*, **3**, 301–306.
7 Robinson, J.T., Perkins, F.K., Snow, E.S., Wei, Z.Q., and Sheehan, P.E. (2008) *Nano Lett.*, **8**, 3137–3140.
8 Yang, M.H., Jiang, J.H., Yang, Y.H., Chen, X.H., Shen, G.L., and Yu, R.Q. (2006) *Biosens. Bioelectron.*, **21**, 1791–1797.
9 Ho, J.A., Lin, Y.C., Wang, L.S., Hwang, K.C., and Chou, P.T. (2009) *Anal. Chem.*, **81**, 1340–1346.
10 Hao, C., Ding, L., Zhang, X.J., and Ju, H.X. (2007) *Anal. Chem.*, **79**, 4442–4447.
11 Eizenberg, M. and Blakely, J.M. (1970) *Surf. Sci.*, **82**, 228–236.
12 Novoselov, K.S., Geim, A.K., Morozov, S.V., Jiang, D., Zhang, Y., Dubonos, S.V., Grigorieva, I.V., and Firsov, A.A. (2004) *Science*, **306**, 666–669.
13 Berger, C., Song, Z.M., Li, X.B., Wu, X.S., Brown, N., Naud, C., *et al.* (2006) *Science*, **312**, 1191–1196.
14 Park, S.J. and Ruoff, R.S. (2009) *Nat. Nanotechnol.*, **4**, 217–224.
15 Hummers, W.S. and Offeman, R.E. (1958) *J. Am. Chem. Soc.*, **80**, 1339.
16 Liu, Z., Robinson, J.T., Sun, X.M., and Dai, H.J. (2008) *J. Am. Chem. Soc.*, **130**, 10876–10877.
17 Stankovich, S., Dikin, D.A., Piner, R.D., Kohlhaas, K.A., Kleinhammes, A., Jia, Y.Y., Wu, Y., Nguyen, S.T., and Ruoff, R.S. (2007) *Carbon*, **45**, 1558–1565.
18 Si, Y. and Samulski, E.T. (2008) *Nano Lett.*, **8**, 1679–1682.
19 Stankovich, S., Dikin, D.A., Dommett, G.H.B., Kohlaas, K.M., Zimney, E.J., Stach, E.A., Piner, R.D., Nguyen, S.T., and Ruoff, R.S. (2006) *Nature*, **442**, 282–286.
20 Stankovich, S., Piner, R.D., Chen, X., Wu, N., Nguyen, S.T., and Ruoff, R.S. (2006) *J. Mater. Chem.*, **16**, 155–158.
21 Williams, G., Seger, B., and Kamat, P.V. (2008) *ACS Nano*, **2**, 1487–1491.
22 McAllister, M.J., Li, J.L., Adamson, D.H., Schniepp, H.C., Abdala, A.A., Liu, J., Herrera-Alonso, M., David, L.M., Roberto, C., Robert, K.P., and Ilhan, A.A. (2007) *Chem. Mater.*, **19**, 4396–4404.
23 Muszynski, R., Seger, B., and Kamat, P.V. (2008) *J. Phys. Chem. C*, **112**, 5263–5266.
24 Seger, B. and Kamat, P.V. (2009) *J. Phys. Chem. C*, **113**, 7990–7995.
25 Yoo, E.J., Okata, T., Akita, T., Kohyama, M., Nakamura, J., and Honma, I. (2009) *Nano Lett.*, **9**, 2255–2259.
26 Zhou, M., Zhai, Y.M., and Dong, S.J. (2009) *Anal. Chem.*, **81**, 5603–5613.
27 Liu, G. and Lin, Y. (2006) *Electrochem. Commun.*, **8**, 251–256.
28 Wu, L., Zhang, X., and Ju, H. (2007) *Biosens. Bioelectron.*, **23**, 479–484.
29 Wang, G., Thai, N.M., and Yau, S.T. (2007) *Biosens. Bioelectron.*, **22**, 2158–2164.
30 Rubianes, M.D. and Rivas, G.A. (2003) *Electrochem. Commun.*, **5**, 689–694.
31 Lin, Y., Lu, F., Tu, Y., and Ren, Z. (2004) *Nano Lett.*, **4**, 191–195.
32 Lee, D., Lee, J., Kim, J., Na, H.B., Kim, B., Shin, C.H., and Kwak, J.H. (2005) *Adv. Mater.*, **17**, 2828–2833.
33 Lu, J., Drzal, L.T., Worden, R.M., and Lee, I. (2007) *Chem. Mater.*, **19**, 6240–6246.
34 Qian, L. and Yang, X. (2006) *Talanta*, **68**, 721–727.
35 Shan, C.S., Yang, H.F., Han, D.X., Zhang, Q.X., Ivaska, A., and Niu, L. (2010) *Biosens. Bioelectron.*, **25**, 1070–1074.
36 Wu, H., Wang, J., Kang, X., Wang, C.M., Wang, D., Liu, J., Aksay, I.A., and Lin, Y. (2009) *Talanta*, **80**, 403–406.

**37** Shan, C.S., Yang, H.F., Song, J.F., Han, D.X., Ivaska, A., and Niu, L. (2009) *Anal. Chem.*, **81**, 2378–2382.
**38** Kang, X.H., Wang, J., H. Wu, Aksay I.A., Liu, J., and Lin, Y.H. (2009) *Biosens. Bioelectron.*, **25**, 901–905.
**39** Zhong, Z.Y., Wu, W., Wang, D., Wang, D., Shan, J.L., Qing, Y., and Zhang, Z.M. (2010) *Biosens. Bioelectron.*, **25**, 2379–2383.
**40** Yang, M.H., Javadi, A., Li, H., and Gong, S.Q. (2010) *Biosens. Bioelectron.*, 26, 560–565.
**41** Kang, X.H., Wang, J., Wu, H., Liu, J., Aksay, I.A., and Lin, Y.H. (2010) *Talanta*, **81**, 754–759.
**42** Tan, L., Zhou, K.J., Zhang, Y.H., and Wang, H.X. (2010) *Electrochem. Commun.*, **12**, 557–560.
**43** Li, F.H., Chai, J., Yang, H.F., Han, D.X., and Niu, L. (2010) *Talanta*, **81**, 1063–1068.
**44** Wang, Y., Wan, Y., and Zhang, D. (2010) *Electrochem. Commun.*, **12**, 187–190.
**45** Shan, C.S., Yang, H.F., Han, D.X., Zhang, Q.X., Ivaska, A., and Niu, L. (2010) *Biosens. Bioelectron.*, **25**, 1504–1508.
**46** Wu, J.F., Xu, M.Q., and Zhao, G.C. (2010) *Electrochem. Commun.*, **12**, 175–177.
**47** Liu, K.P., Zhang, J.J., Yang, G.H., Wang, C.M., and Zhu, J.J. (2010) *Electrochem. Commun.*, **12**, 402–405.

# 12
# Current Frontiers in Electrochemical Biosensors Using Chitosan Nanocomposites

*Shivani B. Mishra, Ajay K. Mishra, and Ashutosh Tiwari*

## 12.1
## Introduction

Biosensors are sensors based on biological materials that are capable of recognizing a specific chemical moiety and signaling its presence, activity, or concentration through a chemical change. This chemical change is then captured by a transducer as a "chemical signal" and converted to a "quantifiable signal" in the form of color or intensity. Figure 12.1 shows a sketch of a typical biosensor. The other common names of biosensors include immunosensors, optrodes, chemical canneries, resonant mirrors, glucometers, biochips, biocomputers, and so on.

Research and development in the field of biosensors is growing to combat the challenges involved in the quick detection of an analyte to the finest levels. The main features involved are linearity, sensitivity, selectivity, and response time. The present scenario of commercial biosensors is limited to the glucose biosensor, which is convenient and user friendly, and diabetic patients can easily monitor their sugar levels and control. However, there are also sensors available to detect pesticides and pollutants in air and water. The market success of biosensors is still scarce as researchers across the world are struggling to find ultimate solutions to launch a biosensor that is multipurpose (i.e., able to detect more than one element), low-cost, implantable and long-lasting. To meet this challenge, scientists have focused their attention towards polymer-, composite- and nanocomposite-based biosensors.

In 1956, Professor Leland C. Clark Jr. introduced the world to the concept of biosensors in his publication on oxygen electrodes [1]. Later, in 1962, in his lecture at New York Academy of Science, he dreamt of some other electrochemical sensors that would have enzyme-based transducers. He published his dream in 1962 where he coined the term "enzyme electrodes" [2]. Based on his idea, in 1975, the Yellow Springs Instrument Company launched a glucose biosensor into the market, which proved to be a huge commercial success. This sensor was based on amperometric detection of $H_2O_2$. During the 1960s, when the concept of biosensors was still in the preliminary stage, Guilbault and Montalvo [3] discussed fabricating a urea sensor based on immobilization on urease enzyme on an

*Biosensor Nanomaterials*. Edited by Songjun Li, Jagdish Singh, and Ipsita A. Banerjee

ISBN: 978-3-527-32841-3

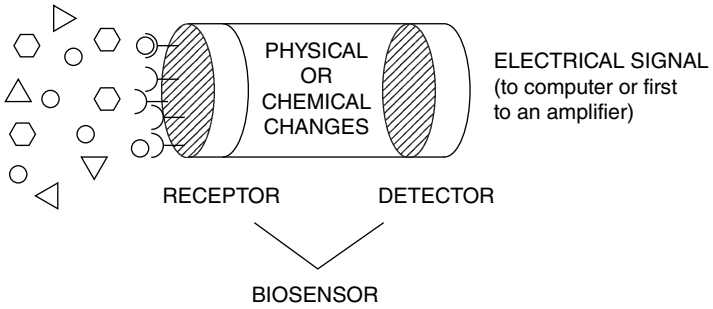


**Figure 12.1** Sketch of a typical biosensor.

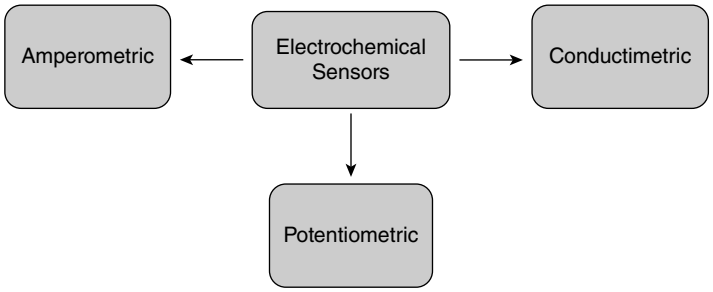


**Figure 12.2** Classification of electrochemical sensors.

ammonium-selective liquid membrane. This chapter primarily focuses on electrochemical biosensors using chitosan nanocomposites. Electrochemical biosensors are based on the principle that many chemical reactions produce or consume, which in turn causes some change in the electrical properties of the solution that can be sensed out and used as measuring parameters. Based on this, electrochemical sensors are classified (Figure 12.2) into amperometric, conductimetric, and potentiometric sensors.

In the case of amperometric sensors, the measured parameter is current and these are able to detect electroactive species present in biological test samples. For conductimetric sensors, the electrical conductance/resistance of the solution is the measured parameter, whereas for potentiometric sensors, the oxidation/reduction potential of an electrochemical reaction is the measured parameter.

## 12.2 Chitosan

Chitosan is a linear polysaccharide composed of randomly distributed β1–4-linked D-glucosamine (deacetylated unit) and *N*-acetyl-D-glucosamine (acetylated unit).

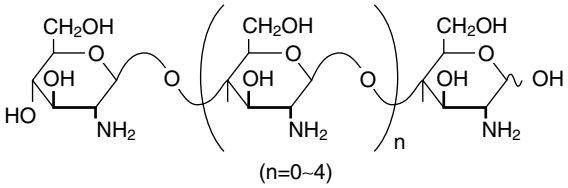


**Figure 12.3** Chemical structure of chitosan.

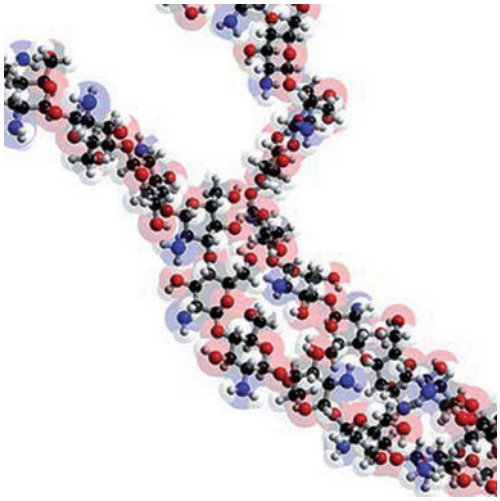

**Figure 12.4** Three-dimensional structure of chitosan.

Figures 12.3 and 12.4 show the chemical structure of chitosan and its three-dimensional model. It has a number of commercial and possible biomedical uses. Chitosan is produced commercially by deacetylation of chitin, which is the structural element in the exoskeleton of crustaceans (crabs, shrimp, etc.). Chitosan's properties allow it to rapidly clot blood, and it has recently gained approval in the US for use in bandages and other hemostatic agents. Chitosan purified from shrimp shells is used in a granular hemostatic product, Celox, made by Medtrade Biopolymers (UK) [4].

In agriculture, chitosan is used as a plant growth enhancer and as a substance that boosts the ability of plants to defend against fungal infections. It is approved for use outdoors and indoors on many plants grown commercially and by consumers. The active ingredient is found in the shells of crustaceans, such as lobsters, crabs, and shrimp, and in certain other organisms. Chitosan is considered as an eco-friendly biopolymer when used according to label directions, due to its low potential for toxicity and its abundance in the natural environment. There are many applications of chitosan. It can also be used in water processing engineering

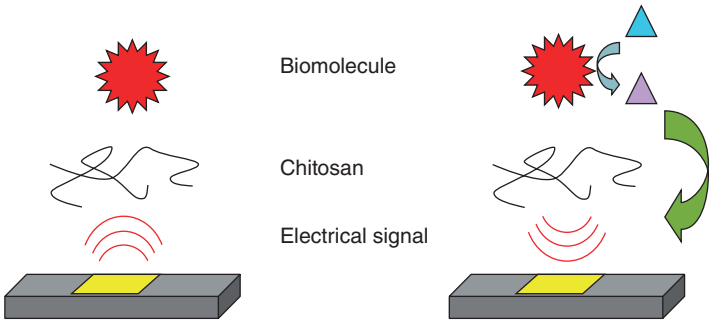


**Figure 12.5** Schematic presentation of a chitosan-based biosensor.

as a part of a filtration process. Chitosan binds the fine sediment particles that are subsequently removed with the sediment during sand filtration. In addition, it also removes phosphorus, heavy minerals, and oils from the water. Chitosan is an important additive in the filtration process. Sand filtration apparently can remove up to 50% of the turbidity alone, while chitosan with sand filtration removes up to 99% turbidity [4, 5]. Some other benefits of chitosan include self-healing coatings and hemostatic agents in bandages, and it has been sold as tablets in health stores since it is a "fat attractor" that is capable of attracting fats from the digestive system. Other applications of chitosan include its use in membranes, drug delivery systems, hydrogels, and food packaging [6–8].

Due to the above-mentioned benefits of chitosan, it is one of the most popular biopolymers used in the fabrication of nanocomposites for biosensors. Chitosan-based biosensors in general can be easily understood by the schematic presentation shown in Figure 12.5.

## 12.3 Chitosan Nanocomposite-Based Electrochemical Biosensors

This section deals with various types of chitosan nanocomposite-based biosensors – amperometric, potentiometric, conductimetric, and some other miscellaneous biosensors.

### 12.3.1 Chitosan Nanocomposite-Based Amperometric Biosensors

In some recent studies, chitosan nanocomposite-based biosensors were investigated for various types of detections. Qiu *et al.* developed a novel amperometric biosensor for glucose by entrapping glucose oxidase (GOx) in a chitosan composite doped with ferrocene monocarboxylic acid-aminated silica nanoparticles conjugate (FMC–ASNPs) and multiwall carbon nanotubes (MWNTs). They observed that the

entrapped FMC–ASNPs conjugate performed excellent redox electrochemistry and the presence of MWNTs improved the conductivity of the composite film. This biosensor was able to detect glucose with a detection limit of 10 mM in the linear range of 0.04–6.5 mM under optimal conditions [9].

In another study, an amperometric biosensor for $H_2O_2$ was developed using a "sandwich configuration," which was combo composite of ferrocene–chitosan/HRP (horseradish peroxidase)/chitosan–glyoxal applied onto a glassy carbon (GC) electrode. The biosensor surface was cross-linked with glyoxal to avoid the loss of immobilized enzyme, whereas ferrocene served as mediator on the GC electrode surface. The biosensor responded in less than 10 s to $H_2O_2$, with a linear range of $3.5 \times 10^{-5}$ to $1.1 \times 10^{-3}$ M and a detection limit of $8.0 \times 10^{-6}$ M based on a signal-to-noise ratio of 3 [10]. A new type of amperometric phenol biosensor fabricated using chitosan/layered double hydroxides organic–inorganic composite film possessed combined advantages of organic biopolymers, chitosan, and inorganic layered double hydroxides. A linear response to catechol over a concentration range of $3.6 \times 10^{-9}$ to $4 \times 10^{-5}$ M with a sensitivity of $296 \pm 4$ mA $M^{-1}$ $cm^{-2}$ and a detection limit of 0.36 nM based on a signal-to-noise ratio of 3 was reported [11]. Zou *et al*. discovered a novel route for fabricating biosensors. In their work, platinum nanoparticles (Pt-NPs) were electrodeposited on a MWNT matrix followed by immobilization of oxidase onto platinum/MWNT electrode surfaces using chitosan–$SiO_2$ gel. The resulting biosensor exhibited wide linear range from 1μ mole to 23 mM with a high sensitivity of 58.9 μA $mM^{-1}$ $cm^{-2}$. The authors reported that the exceptional results were probably due to the synergistic action of platinum and MWNTs, and the good biocompatibility of chitosan–$SiO_2$ sol–gel. The hybrid nanocomposites thus provided a new electrochemical platform for designing a variety of bioelectrochemical devices with high sensitivity and good stability [12].

Novel tyrosinase biosensors based on $Fe_3O_4$ nanoparticle–chitosan nanocomposites were developed for the detection of catechol. The large surface area of $Fe_3O_4$ nanoparticles and the porous morphology of chitosan provided the surface for high loading of enzyme. The prepared biosensor was used to determine phenolic compounds by amperometric detection of the biocatalytically liberated quinone at –0.2 V (versus saturated calomel electrode). The biosensor detected the phenolic compound with a linear range of $8.3 \times 10^{-8}$ to $7.0 \times 10^{-5}$ mol $L^{-1}$ and a detection limit of $2.5 \times 10^{-8}$ mol $L^{-1}$ [13]. In another investigation, researchers were able to modify platinum electrodes by noncovalent ionotropic gelation of a chitosan matrix with the enzyme L-glutamate oxidase. The chitosan matrix was able to retain 57% of the enzyme and the sensor was therefore able to detect $1.0 \times 10^{-7}$ monosodium glutamate MSG even after 11 h, which indicated efficient operational stability. Between 80 and 90% of the original activity of the polymer–enzyme composite was sustained even after 16 weeks [14]. A core of organosilica with a shell of chitosan cross-linked nanospheres with a diameter 70–100 nm was synthesized and the composite film exhibited a favorable microenvironment for retaining the biological activity of enzymes. HRP was then immobilized onto the composite and the biosensor was then applied to detect $H_2O_2$ [15]. In an another study, a Prussian blue/chitosan hybrid film along with GOx was electrodeposited

directly on a gold electrode. The smaller Michaelis–Menten constant indicates the chitosan is an excellent immobilizing matrix and activity holder for enzyme. The Prussian blue/chitosan hybrid film showed potential application in the detection of real blood samples [16].

In an another investigation, an electrochemical sensing platform was developed based on compounding the ionic liquid 1-butyl-3-methylimidazolium tetrafluoroborate and MWNTs with a polymeric matrix (chitosan). The composite was able to disperse in aqueous solution, providing a synergistic augmentation of the voltammetric and amperometric behaviors of electrochemical oxidation of nicotinamide adenine dinucleotide (NADH). The modified electrode showed an efficient performance as indicated by a low detection limit (0.06 M), and good regeneration and antifouling properties for determination of NADH [17]. A new nanocomposite was developed combining Prussian blue nanoparticles and MWNTs in chitosan. The Prussian blue and MWNTs had a synergistic electrocatalytic effect toward the reduction of $H_2O_2$. A chitosan/MWNT/Prussian blue nanocomposite-modified GC electrode was able to amplify the reduction current of $H_2O_2$ by around 35 times. The chitosan/MWNTs/Prussian blue nanocomposite-modified GC electrode was able to reduce $H_2O_2$ at a much lower applied potential, resisting the responses of interferents such as ascorbic acid, uric acid, and acetaminophen to detect glucose at a concentration 2.5 μM within 5 s [18].

### 12.3.2
### Chitosan Nanocomposite-Based Potentiometric Biosensors

In another investigation, a GOx/graphene/chitosan nanocomposite was fabricated, and it was found that GOx retained its bioactivity and a showed a rate constant of 2.83 $s^{-1}$ for the heterogeneous electron transfer reaction. The GOx/graphene/chitosan nanocomposite film exhibited a wider linearity range from 0.08 to 12 mM glucose with a detection limit of 0.02 mM and higher sensitivity (37.93 μA $mM^{-1}\,cm^{-2}$). The extraordinary performance of the biosensor was reported as probably being due to the large surface-to-volume ratio and high conductivity of graphene, and good biocompatibility of chitosan [19].

By changing the composition of the starting chitosan solution, various modified electrodes were prepared and electrochemically characterized. The permeability properties of the chitosan surface films for cationic $[Ru(NH_3)_6^{3+}]$ and anionic $[Fe(CN)_6^{4-}]$ species at different pH was investigated. It was observed that the electrochemical response was strongly pH-dependent for both ionic species and by changing the concentration of chitosan solution, a charge-based molecular recognition of ionic species was made possible [20]. In a different study, peroxidase isozyme (POX1B) entrapment within chitosan cross-linked with glyoxal resulted in good immobilization and activity levels, and good enzyme stability at high temperature and during storage. The composites were applied to modify the electrode to monitor peroxide detection. It was concluded that an excellent sensitivity with a detection limit of 100 nM of $H_2O_2$ was produced. It was reported that such a POX1B-based biosensor could be used to control fraud in real samples such as milk [21].

In another attempt, a highly stable biological film was deposited onto GC electrodes via step-by-step self-assembly of chitosan, laponite, and hemoglobin (Hb). The formal potential of the Hb–heme–Fe(III)/Fe(II) couple was observed to vary linearly with the increase of pH over the range of 3.0–8.0 mV, indicating an electron transfer that was accompanied by single-proton transfer in the electrochemical reaction. The linear dependence on the $H_2O_2$ concentration ranged widely from $6.2 \times 10^{-6}$ to $2.55 \times 10^{-3}$ M. Electrocatalytic response showed a detection limit of $6.2 \times 10^{-6}$ M [22].

A DNA biosensor was fabricated by applying nanocomposites of vanadium pentoxide nanobelts (nano-$V_2O_5$), MWNTs, and chitosan followed by immobilization of the single-stranded DNA probe onto a carbon ionic liquid electrode. The carbon ionic liquid electrode was prepared by using *N*-hexylpyridinium hexafluorophosphate ($HPPF_6$) as the binder with the graphite powder. The biosensor showed good stability and discrimination ability to one- and three-base mismatched single-stranded DNA sequences. The biosensor was observed to have sensitive detection of specific gene sequences [23]. A glucose/air biofuel cell and a phenolic biosensor were developed based on the synthesized acid-resistant laccase/glutarite-modified chitosan/MWNT nanocomposite film. The use of macromolecular glutarite-modified chitosan to immobilize enzyme was reported to be more suitable to construct the biofuel cell and the biosensor as compared with the direct glutarite cross-linking immobilization of laccase. This two-step cross-linking was capable of retaining high activity of the immobilized biomolecules [24]. In an another investigation, ferrocene was functionalized by polysiloxane and chitosan. The prepared composite showed electrochemical properties in solution and in immobilized states, exhibiting a reversible redox wave at $E^\circ$ = +360 mV versus Ag/AgCl, which is 110 mV more negative than that of the ferrocene-functionalized polysiloxane film [25]. Also, the composite film showed a very facile electron transport behavior with an apparent diffusion coefficient of $3.5 \times 10^{-6}$ cm$^2$ s$^{-1}$.

Two different enzymes, urease (Ur) and glutamate dehydrogenase (GLDH), were coimmobilized onto superparamegnatic iron oxide ($Fe_3O_4$) nanoparticle–chitosan-based nanobiocomposite. The film of this nanobiocomposite was deposited onto indium/tin oxide (ITO)-coated glass plates via physical adsorption for urea detection. The incorporation of $Fe_3O_4$ nanoparticles resulted in increased active surface area for immobilization of enzymes (Ur and GLDH), improving the electron transfer and increasing the shelf-life of the nanobiocomposite electrode. The Ur–GLDH/chitosan–$Fe_3O_4$/ITO bioelectrode was found to be sensitive in the 5–100 mg dl$^{-1}$ urea concentration range as shown by differential pulse voltammetry studies and was reported to detect as low as 0.5 mg dl$^{-1}$ [26]. In a similar study, fumed silica nanoparticles (nano-$SiO_2$) and chitosan-based nanobiocomposite film were used to coimmobilize rabbit immunoglobulin antibodies and bovine serum albumin (BSA) for ochratoxin-A detection. Electrochemical studies suggested that presence of nano-$SiO_2$ led to enhanced electrochemical behavior of chitosan, resulting in increased electron transport between the medium and the electrode. BSA/rabbit IgG/CH–nano-$SiO_2$/ITO immunoelectrodes had better sensing

characteristics in terms of linearity (0.5–6 ng $dl^{-1}$), detection limit (0.3 ng $dl^{-1}$), response time (25 s), and sensitivity (18 μA ng $/dL^{-1}\,cm^{-2}$) with a correlation coefficient as 0.98 [27].

### 12.3.3 Chitosan Nanocomposite-Based Conductimetric Biosensors

In some recent attempts, a novel nanocomposite gel was prepared by neutralizing a nanocomposite solution of chitosan-encapsulated gold nanoparticles formed by reducing *in situ* tetrachloroauric acid in chitosan. The bioinspired gel was developed for immobilization and electrochemical studies of cells, and monitoring adhesion, proliferation, and apoptosis of cells on electrodes. An impedance cell sensor was constructed using K562 leukemia cells as a model. The living cells immobilized on GC electrode exhibited an irreversible voltammetric response and increased the electron transfer resistance with a good correlation to the logarithmic value of concentration ranging from $1.34 \times 10^4$ to $1.34 \times 10^8$ cells $ml^{-1}$. It was concluded that the nanocomposite gel based on biopolymers and nanoparticles possessed potential applications for biosensing, and provided a new avenue for electrochemical investigation of cell adhesion, proliferation, and apoptosis [28]. A chitosan–tin oxide ($SnO_2$) nanobiocomposite film was deposited onto an ITO glass plate to immobilize cholesterol oxidase (ChOx) for cholesterol detection. This ChOx/chitosan–$SnO_2$/ITO cholesterol sensor retains 95% of enzyme activity after 4–6 weeks at 48 °C with a response time of 5 s, sensitivity of 34.7 μA $m\,mg^{-1}\,dl^{-1}\,cm^2$, and detection limit of 5 mg $dl^{-1}$ [29].

Chitosan-*graft*-polyaniline (PANI) was electrochemically prepared to investigate the immobilization of creatine amidinohydrolase (CAH). The effect of pH, temperature, and time on the CAH enzyme activity within the matrix was studied. The Michaelis–Menten constant and apparent activity for the CAH enzyme were calculated to be 0.51 mM and 83.59 mg $cm^{-2}$, which was attributed to the fact that the chitosan-*graft*-PANI matrix had a high affinity to immobilize CAH enzyme [30]. MWNTs, Pt-NPs, and a sol–gel of chitosan–silica organic–inorganic hybrid composite was used to develop a glucose biosensor. Pt-NP/chitosan solution was synthesized by reducing $PtCl_6^{2-}$ by sodium borohydride. The amino groups of chitosan helped to form a stable Pt-NP gel. A MWNT/Pt-NP/chitosan solution was prepared separately by dispersing MWNT functionalized with carboxylic groups in Pt-NP/chitosan solution. Using the sol–gel process, methyltrimethoxysilane (MTOS) was mixed with MWNT/Pt-NP/chitosan solution to form the chitosan/silica hybrid. This was followed by the immobilization of GOx into the sol–gel forming the GOx/MWNT/Pt-NP/chitosan/MTOS/GC electrode-based glucose biosensor. The biosensor was investigated by electrochemical impedance spectroscopy and cyclic voltammetry. The results show that in phosphate buffer solutions (phosphate-buffered saline, pH 6.8), glucose was detected at a low applied potential of 0.1 V, with a wide linear range of $1.2 \times 10^{-6}$ to $6.0 \times 10^{-3}$ M, low detection limit of $3.0 \times 10^{-7}$ M, high sensitivity of 2.08 μA $mM^{-1}$, and fast response time (within 5 s) [31, 32].

## 12.4 Conclusions and Future Aspects

As already mentioned, chitosan and its nanocomposites have been widely studied regarding the application of biosensors. Different types of electrochemical sensors have been fabricated that are able to sense biomolecules such as glucose, $H_2O_2$, enzymes such as tyrosinase, DNA, and urea and uric acid. Being a biocompatible and nontoxic matrix, chitosan is an easy and natural choice for nanocomposite preparations to be used for sensing applications. Various nanoparticles such as platinum, gold, tin oxide, graphene, and MWNTs were used as reinforcements for developing chitosan-based nanocomposites. Researchers have made their recommendation to search for the factors that can target an improvement in linearity, sensitivity, selectivity, and response time.

## References


**1** Clark, L.C., Jr. (1956) *Trans. Am. Soc. Artif. Intern. Organs.*, **2**, 41–48.
**2** Clark, L.C., Jr. (1962) *Ann. NY Acad. Sci.*, **102**, 29–45.
**3** Guilbault, G.G. and Montalvo, J. (1969) *J. Am. Chem. Soc.*, 2164–2569.
**4** Goosen, M.F. (1996) *Applications of Chitin and Chitosan*, CRC Press, Boca Raton, FL, pp. 132–139.
**5** Shahidi, F. and Synoweicki, J. (1991) *J. Agric. Food Chem.*, **39**, 1527–1532.
**6** Zhong, Z., Xing, R., Liu, S., Wang, L., Cai, S., and Li, P. (2008) *Carbohydr. Res.*, **343**, 566–570.
**7** Qu, X., Wirsen, A., and Albertsson, A.C. (2000) *Polymer*, **41**, 4589–4598.
**8** Huang, R., Chen, G., Sun, M., Hu, Y., and Gao, C. (2006) *J. Membr. Sci.*, **286**, 237–244.
**9** Qiu, J.-D., Guo, J., Liang, R.-P., and Xiong, M. (2007) *Electroanalysis*, **19**, 2335–2341.
**10** Wang, H.-S., Pan, Q.-X., and Wang, G.-X. (2005) *Sensors*, **5**, 266–276.
**11** Han, E., Shan, D., Xue, H., and Cosnier, S. (2007) *Biomacromolecules*, **8**, 971–975.
**12** Zoua, Y., Xiang, C., Suna, L.-X., and Xua, F. (2008) *Biosens. Bioelectron.*, **23**, 1010–1016.
**13** Wanga, S., Tana, Y., Zhaoa, D., and Liu, G. (2008) *Biosens. Bioelectron.*, **23**, 1781–1787.
**14** Zhang, M., Mullens, C., and Gorski, W. (2006) *Electrochim. Acta*, **51**, 4528–4532.
**15** Chen, S., Yuan, R., Chai, Y., Yin, B., Li, W., and Min, L. (2009) *Electrochim. Acta*, **54**, 3039–3046.
**16** Wanga, X., Gua, H., Yin, F., and Tua, Y. (2009) *Biosens. Bioelectron.*, **24**, 1527–1530.
**17** Wang, Q., Tang, H., Xie, Q., Tan, L., Zhang, Y., Li, B., and Yao, S. (2007) *Electrochim. Acta*, **52**, 6630–6637.
**18** Zhai, X., Wei, W., Zeng, J., Liu, X., and Gong, S. (2006) *Anal. Lett.*, **39**, 913–926.
**19** Kanga, X., Wanga, J., Wua, H., Aksayc, I.A., Liua, J., and Lina, Y. (2009) *Biosens. Bioelectron.*, **25**, 901–905.
**20** Martínez-Huitle, C.A., Jara, C.C., Cerro-Lopez, M., and Quiroz, M.A. (2009) *Can. J. Anal. Sci. Spectrosc.*, **54**, 53–62.
**21** Ichi, S.E., Limam, F., and Marzouki, M.N. (2009) *Mater. Sci. Eng. C*, **29**, 1662–1667.
**22** Shan, D., Han, E., Xue, H., and Cosnier, S. (2007) *Biomacromolecules*, **8**, 3041–3046.
**23** Suna, W., Qina, P., Gaob, H., Li, G., and Jiao, K. (2010) *Biosens. Bioelectron.*, **25**, 1264–1270.
**24** Tan, Y., Deng, W., Ge, B., Xie, Q., Huang, J., and Yao, S. (2009) *Biosens. Bioelectron.*, **24**, 2225–2231.

**25** Nagarale, R.K., Lee, J.M., and Shin, W. (2009) *Electrochim. Acta*, **54**, 6508–6514.
**26** Kaushik, A., Solanki, P.R., Ansari, A.A., Sumana, G., Ahmad, S., and Malhotra, B.D. (2009) *Sens. Actuators B*, **138**, 572–580.
**27** Kaushik, A., Solanki, P.R., Sood, K.N., Ahmad, S., and Malhotra, B.D. (2009) *Electrochem. Commun.*, **11**, 1919–1923.
**28** Ding, L., Hao, C., Xue, Y., and Ju, H. (2007) *Biomacromolecules*, **8**, 1341–1346.
**29** Ansari, A.A., Kaushik, A., Solanki, P.R., and Malhotra, B.D. (2009) *Electroanalysis*, **21**, 965–972.
**30** Tiwari, A., and Shukla, S.K. (2009) *eXPRESS Polym. Lett.*, **3**, 553–559.
**31** Kanga, X., Mai, Z., Zou, X., Cai, P., and Moa, J. (2008) *Talanta*, **74**, 879–886.
**32** Sugunan, A., Thanachayanont, C., Dutta, J., and Hilborn, J.G. (2005) *Sci. Technol. Adv. Mater.*, **6**, 335–340.

# 13
# Nanomaterials as Promising DNA Biosensors

*Premlata Kumari*

## 13.1
## Introduction

DNA, the main component of chromosomes in cells, is of great importance for both inheritance and good health [1, 2]. All of the genetic information is determined precisely by the base sequences in DNA. Any disorder in these base sequences can result in a distortion in inheritance or occurrence of disease [3–8]. The detection of specific DNA sequences is of significance in a wide range of areas, such as biomedical engineering, clinical diagnosis, food development, and environmental protection [9–12]. Rapid detection of genes plays a significant role in the diagnosis of disease well before any symptoms appear. In environmental and food areas, it can also be used to detect genetically modified organism or pathogenic bacteria. Using DNA biosensors and gene chips, the specific sequence information can be obtained in a faster, simpler, and cheaper manner as compared to conventional hybridization (www.motorola.com/Lifesciences and www.dnachip.toshiba.co.jp/eng/). Thus, developments in such devices helps DNA diagnosis. DNA biosensors can be made by immobilizing single-stranded DNA probes on different electrodes using electroactive indicators to measure the hybridization between DNA probes and their complementary DNA strands [13–15]. Nucleic acid-based DNA biosensors are rapid, simple, and economic for testing genetic infectious disease. They can be synthesized readily and regenerated for multiple uses. See Figure 13.1.

By modifying sensors with different functional materials, the response from DNA biosensors can be increased. Nanostructured materials of different chemical composition have attracted great attention over the past few years, as they obey neither absolute quantum chemistry nor the laws of classical physics and thereby have markedly different properties. Two major phenomena are responsible for these differences. The first is the high dispersity of nanocrystalline systems [17]. As the size of a crystal reduces, the number of atoms at the surface of the crystal increases as compared to the number of atoms in the crystal itself. The second is usually called "size quantization" arises because the size of nanomaterials is comparable to the de Broglie wavelength of their charge carriers [18]. The valence and

*Biosensor Nanomaterials*. Edited by Songjun Li, Jagdish Singh, and Ipsita A. Banerjee

ISBN: 978-3-527-32841-3

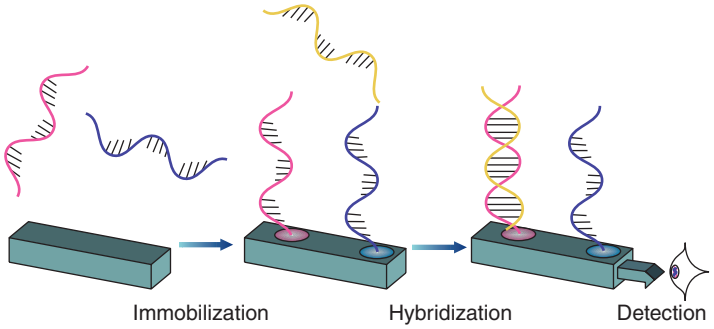


**Figure 13.1** Principle of a DNA biosensor: (i) immobilization of single-stranded ODN probes onto a substrate, (ii) hybridization, and (iii) detection. (Reprinted with permission from [16], © 2008 RSC.)

conduction bands split into discrete, quantized, electronic levels, due to the spatial confinement of the charge carriers. The properties (electrical, optical, chemical, mechanical, magnetic, etc.) of nanomaterials can be selectively controlled by engineering the size, morphology, and composition of particles associating with the two unique phenomena. These new substances will have enhanced or entirely different properties from their parent materials. The nanomaterials used in DNA biosensors including nanoparticles (such as gold nanoparticles (Au-NPs), silver nanoparticles (Ag-NPs), and CdS nanoparticles) and nanotubes (such as carbon nanotubes (CNTs), etc.). There are two main purposes of using nanomaterials in DNA biosensors: (i) as substrates for DNA attachment and (ii) as signal amplifiers for hybridization. In this chapter, we summarize the main applications of various nanomaterials, nanotubes, and quantum dots (QDs) that are associated with signal amplification.

## 13.2
## Nanomaterials as Signal Amplifiers for Hybridization

Signal amplification may be very useful if small-molecule ligands of biomedical importance do not significantly perturb the biosensor interface. Signal amplification by labeling the analyte with nanomaterials has been reported for DNA biosensors.

### 13.2.1
### Nanoparticles

The reported nanoparticles used as signal amplifiers in the literature include Au-NPs, Ag-NPs, and CdS nanoparticles. These nanoparticles are summarized for their use in DNA biosensors as follows.

#### 13.2.1.1 Gold Nanoparticles

Au-NPs have been used as signal amplifiers in electrochemical DNA biosensors. Wang *et al.* [19] demonstrated that Au-NPs could simply amplify electrochemical impedance and capacitance signals in the fluorescein/antifluorescein system. A rise in capacitance of about 400 nF $cm^{-2}$ resulted due to immobilization of fluorescein onto gold through formation of a self-assembled monolayer introducing, goat antifluorescein conjugated with 10-nm Au-NPs, whereas no change could be observed for goat antifluorescein without the Au-NP conjugate. This change in the electrochemical impedance signal of binding to goat antifluorescein conjugated with Au-NPs could be attributed to the much higher electrochemical activity of gold surfaces, relative to the underlying organic layer. It permitted construction of high-sensitivity electrochemical impedance biosensors at a single low frequency, where the signal was sensitive to the interfacial charge transfer resistance $R_{ct}$.

According to Xu *et al.* [20], Li and Hu [21] developed an electrochemical determination method for analyzing sequence-specific DNA using ferrocene-capped Au-NP/streptavidin conjugates. Thiolated DNA probes were covalently immobilized on a gold electrode with hexanethiol forming a mixed self-assembled monolayer and hybridized with target DNA containing a complementary sequence. Duplex DNA formed on the gold surface. Functional Au-NPs were then introduced via the strong interaction effect between biotin and streptavidin. The electrochemical signal of the ferrocene covering on the Au-NPs was obviously enhanced in cyclic voltammetry and differential pulse voltammetry. Optical properties of Au-NPs were also used for an optical DNA biosensor. Yao *et al.* [22] used oligonucleotide (ODN)-capped Au-NPs in a sandwich assay of ODNs or polynucleotides by flow injection surface plasmon resonance (SPR). In order to decimate nonspecific adsorption of ODN-capped Au-NPs on the SPR sensor surface, a carboxylated dextran film was immobilized. The tandem use of signal amplification via the adlayer of the ODN-capped Au-NPs and the differential signal detection by the bicell detector on the SPR resulted in a remarkable DNA detection level. Optical signal amplification by Au-NPs was also reported by Kalogianni *et al.* [23] and Martins *et al.* [24]

Au-NPs were also reported to be used as signal amplifiers for quartz crystal microbalance biosensors [25–29]. Au-NPs were attached to the quartz crystal gold electrodes via different methods to increase the mass on the electrode surface, amplifying the hybridization signal.

#### 13.2.1.2 Silver Nanoparticles

Since Ag-NPs exhibit better electrochemical activity than Au-NPs, they can be exploited as ODN labels in electrochemical detection assays. Cai *et al.* [30] reported an electrochemical DNA hybridization detection assay using Ag-NPs as the ODN labeling tag. In the assay, silver metal atoms anchored on the hybrids were released by oxidative metal dissolution with the hybridization of the target DNA with the Ag-NP–ODN DNA probe. The result indicated that the electrochemical redox reaction of silver was carried out at a low potential, under 0.4 V, and it gave a well-defined sharp voltammetric peak. The oxidative peak of silver colloid was

approximately 100 times larger than that for gold colloid of the same size and amount. Silver metal could be easily oxidized to the soluble ionic $Ag^+$ with concentrated $HNO_3$ and then released from the hybrids, but complete dissolution of a gold tag required more severe conditions (1 M HBr containing 0.1 mM $Br_2$) and the electrode might be damaged in this medium. Xu *et al.* [20], Fu *et al.* [31], and K'Owino *et al.* [32] similarly characterized electrochemically Ag-NPs used in DNA biosensors.

#### 13.2.1.3 **Cadmium Sulfide Nanoparticles**

CdS nanomaterial is a semiconductor material with attractive electrochemical properties. Several researchers reported the use of CdS as ODN-labeling tags for detection of DNA hybridization. Xu *et al.* [33] used CdS nanoparticles that bind covalently with amine group-modified target single-stranded DNA to enhance the electrochemical impedance spectroscopy (EIS) signal. The use of CdS nanoparticles significantly increased the DNA hybridization detection sensitivity because of the negative charges, space resistance, and semiconductor characteristics of CdS. Peng *et al.* [34] also used CdS nanoparticles to enhance the EIS signal. They reported an ODN sensor based on the electropolymerization of polypyrrole. The resulting trapped ODN(s) were then probed by the addition of complimentary sequence ODN. A significant improvement in sensor sensitivity was observed with the incorporation of CdS nanoparticles in the probe,

### 13.2.2 **Quantum Dots**

Fluorescence resonance energy transfer (FRET) is a distance-dependent interaction between the electronic excited states of two dye molecules in which excitation is transferred from a donor molecule to an acceptor molecule without emission of a photon. The efficiency of FRET is dependent on the inverse sixth power of the intermolecular separation, making it useful over distances comparable to the dimensions of biological macromolecules. QD emission is broad, and the excitation wavelength is both narrow and independent (i.e., different fluorescence wavelengths can be achieved by just varying the size of QDs and all colors of QDs can be excited by single source). These characteristics make QDs applicable as fluorophores for biological labeling in place of traditional dye labels and are tremendously useful for DNA detection with high sensitivity.

A novel DNA biosensor is based on QDs that are linked to specific DNA probes to capture target DNA [35]. The target DNA strand binds to a fluorescent dye (fluorophore)-labeled reporter strand, thus forming a FRET donor–acceptor assembly. QDs also function so as to concentrate the signal by confining several targets in the nanoscale domain. An unbound DNA strand produces no fluorescence, but the binding of even small amounts of target DNA (50 copies or less) may produce a very strong FRET signal. Several FRET-based DNA probes (molecular beacons and TaqMan probes) whose fluorescence signals change as a result of hybridization or enzymatic reactions have been developed for separation-free (unhybridized

DNA strand) detection of target DNA [36–39]. DNA nanosensors usually consist of two target specific DNA probes – the reporter and capture probes. The reporter probe is labeled with fluorophore, whereas the capture probe is labeled with biotin as well as with streptavidin conjugated with QDs. The QDs function as the target concentrator as well as the FRET energy donor. Target DNA in solution gets sandwiched by both the reporter and capture probes. Various sandwiched hybrids are then captured by a single QD through biotin–streptavidin binding and concentrate in the nanoscale domain [40]. The QD donor and fluorophore acceptor are in close proximity , causing fluorescence from the acceptor by means of FRET on illumination of the donor. The sensation acceptor emission suggests the presence of target DNA. The unhybridized probe is not involved in FRET and therefore does not need to be removed.

### 13.2.3
### Carbon Nanotube-Based Electrochemical DNA Sensors

CNTs have become the focus of intense research in recent decades because of their exclusive properties and promising applications in many fields. CNTs display fascinating electronic and optical properties that are distinct from other carbonaceous materials and nanoparticles because of their unique one-dimensional nanostructures. CNTs are widely used in the electronic and optoelectronic, biomedical, pharmaceutical, energy, catalytic, analytical, and material fields. The special nanostructural properties give CNTs some overwhelming advantages in fabricating electrochemical sensors: the large specific area producing high sensitivity; the tubular nanostructure and the chemical stability allowing the fabrication of ultrasensitive sensors consisting of only one nanotube; the good biocompatibility that is suitable for constructing electrochemical biosensors, especially for facilitating the electron transfer of redox proteins and enzymes; the modifiable ends and side walls providing a chance for fabricating multifunctioned electrochemical sensors via the construction of functional nanostructures; the possibility of achieving miniaturization; and the possibility of constructing ultrasensitive nanoarrays [41].

After the study of Britto *et al.* [42] regarding the electrochemistry of CNTs, numerous works have dealt with the construction of electrochemical sensors by CNTs and their applications. CNTs can effectively improve the redox currents of inorganic molecules, organic compounds, biomacromolecules, or even biological cells and reduce the redox overpotentials. Electron transfer and the direct electrochemistry of redox proteins at CNT-based electrochemical sensors were also widely observed. Owing to their well-defined structure, chemical stability, and electrocatalytic activity toward many substances, CNTs are also extensively used as carrier platforms for constructing various electrochemical sensors. The promising applications of CNTs have been reviewed by several authors [43–47].

Electrochemical DNA biosensors are currently receiving considerable attention because of their high sensitivity, portability, economy, and rapid response. Such devices rely on the conversion of the nucleic acid recognition processes into a

useful electrical signal. Similar to other electrochemical sensors, DNA electrochemical sensors benefit greatly from the use of CNTs based on the enhanced oxidation of the oxidizable bases, the improved responses of the indicators, or the excellent properties of CNTs as the carrier platforms.

A great enhancement of the oxidation signal is observed by surface confinement of multiwalled CNTs (MWNTs) that facilitate the adsorptive accumulation of guanine [48]. This indicates the advantage of CNT-coated glassy carbon (GC) electrodes over the common unmodified GC, carbon paste, and pencil graphite electrodes.

The dramatic amplification of the guanine signal has been combined with a label-free electrical detection of DNA hybridization. A similar enhancement of the guanine DNA response was observed with MWNT paste electrodes [49] and at a single-walled CNT (SWNT)-coated GC electrodes [50]. An array of vertically aligned MWNTs, embedded in $SiO_2$, has been shown useful for ultrasensitive detection of DNA hybridization [51]. DNA targets of $10^{-13}$ M or subattomolar have been measured by combining the CNT nanoelectrode array with tris(2,2′-(bipyridyl) ruthenium(II) ($Ru(bpy)_3^{2+}$)-mediated guanine oxidation. Such a CNT array was also applied for label-free detection of DNA polymerase chain reaction (PCR) amplicons and offered the detection of less than 1000 target amplicons [52]. A lower nanotube density offered higher sensitivity. Improved sensitivity of electrical DNA hybridization has been reported also in connection with the use of daunomycin redox intercalator [53]. A modified GC MWNT-COOH was used for this task along with a 5′-amino group-functionalized ODN probe and pulse voltammetric transduction. The coupling of various CNT amplification processes was used in highly sensitive bioelectronic protocols for detecting proteins and DNA [54]. In these procedures the CNTs played a dual amplification role in both the recognition and transduction events, namely as carriers for numerous enzyme tags and for accumulating the α-naphthol product of the enzymatic reaction. Coverage of around 9600 enzyme molecules per CNT (i.e., binding event) was estimated. Such a CNT-derived double-step amplification pathway (of both the recognition and transduction events) allows the detection of DNA and proteins down to 1.3 and 160 zmol, respectively, in 25- to 50-ml samples and indicates great promise for PCR-free DNA analysis. Cai *et al.* [55] described an indicator-free AC impedance measurement of DNA hybridization based on a DNA probe-doped polypyrrole film over a MWNT layer. The hybridization event led to a decrease of impedance values, reflecting the reduction of the electrode resistance. A 5-fold sensitivity enhancement was observed compared to analogous measurements without CNTs.

## 13.3 Conclusions

Nanomaterials such as different nanoparticles, QDs, CNTs, and their composites have been successfully applied to DNA biosensors to improve their sensitivity.

Advancements concerning Au-NP-, Ag-NP-, and CdS nanoparticle-assisted signal amplification have been compiled. Au-NPs and Ag-NPs were found to be effective signal amplifiers, and CdS to be an excellent fluorescent signal enhancer in DNA hybridization detection. QDs were found to be significant for multiplexed DNA detection with high sensitivity. CNTs were also discussed as a effective signal enhancer for DNA detection at low concentration.

The DNA biosensor for hybridization detection is useful to detect specific sequences of ODNs with high selectivity; this procedure requires an amplification step such as PCR in order to be readily applicable to real samples. Problems in clinical chemistry, such as blood genotyping for specific sequencing of environmental concern, or in food technology can be solved using nanomaterial-based biosensors.

## References


**1** McCarty, M. (2003) *Nature*, **421**, 406.
**2** Bostick, M., Kim, J.K., Esteve, P.O., Clark, A., Pradhan, S., and Jacobsen, S.E. (2007) *Science*, **317**, 1760–1764.
**3** Kuwayama, H., Yanagida, T., and Ueda, M. (2008) *J. Biotechnol.*, **133**, 418–423.
**4** Ainsworth, C. (2006) *Nature*, **7094**, 673.
**5** Guo, G. and Tong, T.Y. (2005) *Behav. Genet.*, **35**, 803.
**6** Alt, A., Lammens, K., Chiocchini, C., Lammens, A., Pieck, J.C., Kuch, D., Hopfner, K.P., and Carell, T. (2007) *Science*, **318**, 967–970.
**7** Borentain, P., Gerolami, V., Ananian, P., Garcia, S., Noundou, A., Botta-Fridlund, D., Le Treut, Y.P., Berge-Lefranc, J.L., and Gerolami, R. (2007) *Eur. J. Cancer*, **43**, 2479–2486.
**8** Ferrando, A., Lecis, R., Domingo-Roura, X., and Ponsa, M. (2008) *Conserv. Genet.*, **9**, 129–139.
**9** Douglas, C. and Ehlting, J. (2005) *Transgenic Res.*, **14**, 551–561.
**10** Wu, J. and Prausnitz, J. (2002) *J. Colloid Interface Sci.*, **252**, 326–330.
**11** Wang, S. and Cheng, Q. (2005) *Methods Mol. Biol.*, **316**, 49–65.
**12** Kumar, N., Dorfman, A., and Hahm, J. (2006) *Nanotechnology*, **17**, 2875–2881.
**13** Erdem, A., Kesman, K., Mesie, B., Akarea, U.S., and Osoz, M. (2000) *Anal. Chim. Acta*, **423**, 139–149.
**14** Campbell, C.N., Gal, D., Cristler, N., Banditrat, C., and Heller, A. (2002) *Anal. Chem.*, **74**, 158–162.
**15** Millan, K.M. and Mikkelsen, S.R. (1993) *Anal. Chem.*, **65**, 2317–2324.
**16** Serge, C. and Pascal, M. (2008) *Analyst*, **133**, 984–991.
**17** Weller, H. (1993) *Adv. Mater.*, **5**, 88–95.
**18** Henglein, A. (1987) *Prog. Colloid Polym. Sci.*, **73**, 1–3.
**19** Wang, J.B., Profitt, J.A., Pugia, M.J., and Suni, I.I. (2006) *Anal. Chem.*, **78**, 1769–1773.
**20** Xu, K., Huang, J., Ye, Z., Ying, Y., and Li, Y. (2009) *Sensors*, **9**, 5534–5557.
**21** Li, J.H. and Hu, J.B. (2004) *Acta Chim. Sinica*, **62**, 2081–2088.
**22** Yao, X., Li, X., Toledo, F., Zurita-Lopez, C., Gutova, M., Momand, J., and Zhou, F.M. (2006) *Anal. Biochem.*, **354**, 220–228.
**23** Kalogianni, D.P., Koraki, T., Christopoulos, T.K., and Ioannou, P.C. (2006) *Biosens. Bioelectron.*, **21**, 1069–1076.
**24** Martins, R., Baptista, P., Raniero, L., Doria, G., Silva, L., Franco, R., and Fortunato, E. (2007) *Appl. Phys. Lett.*, **90**, 023903:1–023903:3.
**25** Chen, S.H., Wu, V.C.H., Chuang, Y.C., and Lin, C.S. (2008) *J. Microbiol. Methods*, **73**, 7–17.
**26** Liu, T., Tang, J., and Jiang, L. (2004) *Biochem. Biophys. Res. Commun.*, **313**, 3–7.
**27** Nicu, L., Guirardel, M., Chambosse, F., Rougerie, P., Hinh, S., Trevisiol, E., Francois, J.-M., Majoral, J.-P., Caminade,

A.-M., Eric Cattan, E., and Bergaud, C. (2005) *Sens. Actuators B*, **110**, 125–136.
**28** Pang, L.L., Li, J.S., Jiang, J.H., Shen, G.L., and Yu, R.Q. (2006) *Anal. Biochem.*, **358**, 99–103.
**29** Willner, I., Patolsky, F., Weizmann, Y., and Willner, B. (2002) *Talanta*, **56**, 847–856.
**30** Cai, H., Xu, Y., Zhu, N.N., He, P.G., and Fang, Y.Z. (2002) *Analyst*, **127**, 803–808.
**31** Fu, Y.Z., Yuan, R., Xu, L., Chai, Y.Q., Liu, Y., Tang, D.P., and Zhang, Y. (2005) *J. Biochem. Biophys. Methods*, **62**, 163–174.
**32** K'Owino, I.O., Mwilu, S.K., and Sadik, O.A. (2007) *Anal. Biochem.*, **369**, 8–17.
**33** Xu, Y., Cai, H., He, P.G., and Fang, Y.Z. (2004) *Electroanalysis*, **16**, 150–155.
**34** Peng, H., Soeller, C., Cannell, M.B., Bowmaker, G.A., and Cooney, R.P. (2006) *Biosens. Bioelectron.*, **21**, 1727–1736.
**35** Kumar, S., and Kumar, A. (2008) *Sens. Transducers J.*, **92**, 122–133.
**36** Cady, N.C., Strickland, A.D., and Batt, C.A. (2007) *Mol. Cell. Probes*, **21**, 116–124.
**37** Han, G.X., Su, J.Z., and Nie, S. (2001) *Nat. Biotechnol.*, **19**, 631–635.
**38** Liu, X., Farmerie, W., Schuster, S., and Tan, W. (2000) *Anal. Biochem.*, **283**, 56–63.
**39** Hansen, W.J., Kawde, A.N., Xiang, Y., Gothelf, V., and Collins, G. (2006) *J. Am. Chem. Soc.*, **128**, 2228–2229.
**40** Zhang, C.-Y., Yeh, H.-C., Kuroki, M.T., and Wang, T.-H. (2005) *Nat. Mater.*, **4**, 826–830.
**41** Britto, P.J., Santhanam, K.S.V., and Ajayan, P.M. (1996) *Bioelectrochem. Bioenerg.*, **41**, 121–125.
**42** Zhao, Q., Gan, Z., and Zhuang, Q. (2002) *Electroanalysis*, **14**, 1609–1613.
**43** Li, N., Wang, J., and Li, M. (2003) *Rev. Anal. Chem.*, **22**, 19–33.
**44** Li, J., Koehne, J.E., Cassell, A.M., Chen, H., Ng, H.T., Ye, Q., Fan, W., Han, J., and Meyyappan, M. (2005) *Electroanalysis*, **17**, 15–27.
**45** Hu, C. and Hu, S. (2009) *J. Sensors*, **2009**, 187615.
**46** Wang, J. (2005) *Electroanalysis*, **17**, 7–14.
**47** Gooding, J.J. (2005) *Electrochim. Acta*, **50**, 3049–3060.
**48** Wang, J., Kawde, A., and Mustafa, M. (2003) *Analyst*, **128**, 912–916.
**49** Pedano, M. and Rivas, G.A. (2004) *Electrochem. Commun.*, **6**, 10–16.
**50** Wang, J., Li, M., Shi, Z., Li, N., and Gu, Z. (2004) *Electroanalysis*, **16**, 140–144.
**51** Li, J., Ng, H.T., Cassell, A., Fan, W., Chen, H., Ye, Q., Koehne, J., and Meyyappan, M. (2003) *Nano Lett.*, **3**, 597–602.
**52** Lin, Y., Lu, F., Tu, Y., and Ren, Z. (2004) *Nano Lett.*, **4**, 191–195.
**53** Cai, H., Cao, X., Jiang, Y., He, P., and Fang, Y. (2003) *Anal. Bioanal. Chem.*, **375**, 287–293.
**54** Wang, J., Liu, G., and Jan, M. (2004) *J. Am. Chem. Soc.*, **126**, 3010–3011.
**55** Cai, H., Xu, Y., He, P., and Fang, Y.Z. (2003) *Electroanalysis*, **15**, 1864–1870.

# 14
# Nanocomposites and their Biosensor Applications

*Ajay K. Mishra, Shivani B. Mishra, and Ashutosh Tiwari*

## 14.1
## Introduction

Detection of disease at the finest level following the discovery of devices popularly known as "biosensors" has become a blessing to biomedical science. Researchers across the world are still working on device sensors for various biomolecules that should be potent enough to detect their occurrence at levels of parts per billion in body fluids. To fabricate an electrochemical biosensor, the prime requirement is an efficient electron transfer through a mediator as the direct electron transfer between an enzyme and electrode is not efficient. This may be due to the active sites that are deeply embedded inside the enzyme and thus it becomes difficult to control the orientation of the enzyme on the surface. The mediator that participates in the electron transfer can either be put in solution or be covalently attached to a polymer matrix or sol–gel matrix [1, 2]. This apparently increases the sensitivity of the electrochemical biosensors for these biomolecules. The sol–gel matrix is able to immobilize enzymes and mediators to create an efficient system so that the communication between enzyme and mediator is enhance significantly. A good matrix should have channels and pores so that the substrates can easily enter the matrix and interact with the enzyme. To maximize the activity of the entrapped enzyme, it becomes necessary to fine-tune the physical and chemical properties of the matrix. The silica matrix is one of the popularly fabricated matrices using the sol–gel methodology where tetraethylorthosilicate acts as a precursor material [2–4]. A biosensor is basically composed of a recognition agent – a biological entity such as an enzyme, antibody, bacteria, or tissue. Such biological entities are not present in chemical sensors. Classical semiconductors, catalytic materials, solid electrolytes, metals, and insulators serve as platforms to generate sensor devices. However, it is interesting to note that organic polymers matrices usually do conduct electricity, but this is a requirement as a major component in various sensor devices among other materials. Thus, to serve the purpose of being an important component of sensors, organic polymer matrices are either an intrinsically conducting polymer coating an election surface or encapsulating material on an electrode surface. On the other

*Biosensor Nanomaterials*. Edited by Songjun Li, Jagdish Singh, and Ipsita A. Banerjee

ISBN: 978-3-527-32841-3

hand, a nonconducting polymer can be used for immobilization of specific receptor agents on a sensor device.

The phase (gaseous or liquid) of a species influences the electrical properties of the sensor devices. These changes in electrical properties help in detecting the chemical species and hence create the state of the art for solid-state sensors. Based on this principle, chemical sensors such as field-effect transistors (FETs) have been developed. However, due to various shortcomings with respect to reproducibility, stability, sensitivity, and selectivity, these FETs do not have any market value. Catalytically active moieties like thin films of tin oxide can be fabricated efficiently to semiconducting metal oxide sensors. To increase their semiconducting properties, catalysts are sometimes are added into these metal oxides [3].

The organic polymer chitosan–a linear polysaccharide–has excellent membrane-forming ability, good biocompatibility, high permeability towards water, adhesion capability, nontoxicity, and high mechanical strength, making it a most promising material for hosting enzymes and thus for use in biosensing applications. To upgrade the electrochemically behavior of chitosan, ferrocene was covalently bound, and applied to glucose sensing, $H_2O_2$ sensing [5, 6], and the electrocatalytic decomposition of $H_2O_2$ [7].

## 14.2 Nanocomposites

Nanocomposites are solid materials composed of two or more phases where one of the phases is usually in nanoscale dimensions [8]. The structure, chemical, and physical properties and dimensions of these different phases therefore result in composite materials with altogether unique and fascinating mechanical, electrical, thermal, optical, electrochemical, and catalytic properties properties. Different nanosize composites materials serve different applications, such as: below 5 nm for catalytic activity, below 20 nm for making a hard magnetic material soft, below 50 nm for refractive index changes, and below 100 nm for achieving superparamagnetism, mechanical strengthening, or restricting matrix dislocation movement.

Nanocomposites are not a new concept for Mother Nature, who developed these materials since the advent of life. Scientists across the world are now getting an interest in exploring these fascinating materials occurring in the structure of abalone shells and bones. Ancient examples of the use nanoparticles have recently been investigated in Maya blue prints that have shown the origin of the depth of color and the resistance to acids and biocorrosion [8]. In recent times, since the mid-1950s, nanoscale organoclays have been used to control the flow of polymer solutions (e.g., as paint viscosifiers) or the constitution of gels (e.g., as a thickening substance in cosmetics, keeping the preparations in homogeneous form). This was then followed in the 1970s by polymer/clay composites; however, the term “nanocomposites” was still to be coined.

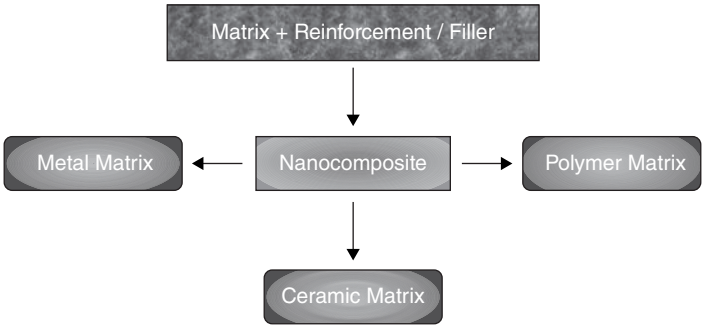


**Figure 14.1** Classification of nanocomposites popular for biomedical applications.

In nanocomposites, the reinforcing or the filler phase has an exceptionally high surface-to-volume ratio or exceptionally high aspect ratio. The reinforcing material is made up of particles (e.g., minerals, metal oxides), sheets (e.g., exfoliated clay stacks, organoclays), or fibers (e.g., carbon nanotubes (CNT)s or electrospun fibers). The interface between the matrix and reinforcement phases is a significantly better conventional composite material that influences the matrix material properties, such as those related to local chemistry, degree of thermoset cure, polymer chain mobility, polymer chain conformation, degree of polymer chain ordering, or crystallinity occurring in the vicinity of the reinforcement [9]. In addition, an advantage lies in the fact that a relatively small quantity of nanoscale-phase filler or reinforcement can have a significant effect on the macroscale properties of the composite. For example, adding CNTs as a reinforcement can readily improve the electrical and thermal conductivity of composite materials. The other types of nanofillers can improve some other properties, such as optical, dielectric, heat resistance, stiffness, strength, and resistance to wear and damage. In general, the nano reinforcement in any of the dimension is dispersed into either the polymer, ceramic, or metal matrix during processing, thus resulting in a typical class of nanocomposites as shown in Figure 14.1.

### 14.2.1 Ceramic Matrix Nanocomposites

"Ceramic" is the term given to a chemical compound from the group of oxides, nitrides, borides, silicides, and so on, that serves as a matrix to form ceramic matrix nanocomposites. Ceramic matrices (Figure 14.2) are of two types: oxides (alumina, silica and aluminosilicates), which are more mature and environmentally stable, and nonoxides (silicon carbide, boron nitride, etc.) for superior structural properties and hardness.

The reinforcement phase is usually ceramic fibers or whiskers to achieve the goal of toughness in an otherwise brittle ceramic. Similarly, the reinforcement can be either a discontinuous form that includes whiskers, platelets, and particulates

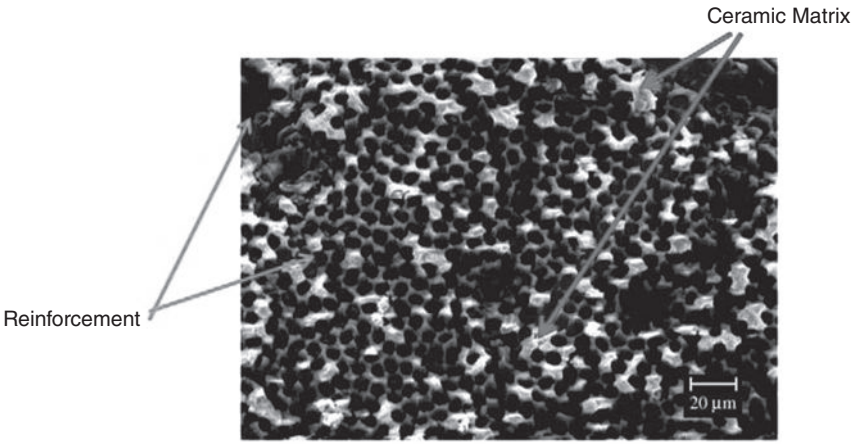


**Figure 14.2** Scanning electron micrograph of a ceramic matrix nanocomposite.

made up of silicon nitride, aluminum nitride, or silicon carbide, or a continuous form of a filament made of alumina, glass, mullite, and so on [10, 11].

### 14.2.2
### Metal Matrix Nanocomposites

In this type of nanocomposite, the nanoscale filler in the form of particles, whiskers, or sheets is distributed in a metal matrix. This type of system provides an opportunity for various unlimited combinations of metals, ceramics, and nonmetals. Metal matrix composites (Figure 14.3) are in demand in the automobile industry.

For metal matrix composites, the choice of reinforcement depends on the profile required for any particular application. Moreover, the matrix can be an alloy – a mixture of two metals – similar to that of a polymer blend as in case of polymer nanocomposites [12].

### 14.2.3
### Polymer Matrix Nanocomposites

Nanocomposites where a polymer serves as the matrix are known as polymer nanocomposites (Figure 14.4) with nanoscale filler materials in a variety of forms (particles, sheets, tubes, fibers, whiskers, etc.).

Addition of nanofillers to a polymer matrix therefore improves the performance of the polymer by simply capitalizing on the nature and properties of the nanoscale filler to yield a high-performance composite [13]. The improved properties of high-performance nanocomposites are primarily due to the high aspect ratio and/or the high surface area of the fillers [14].

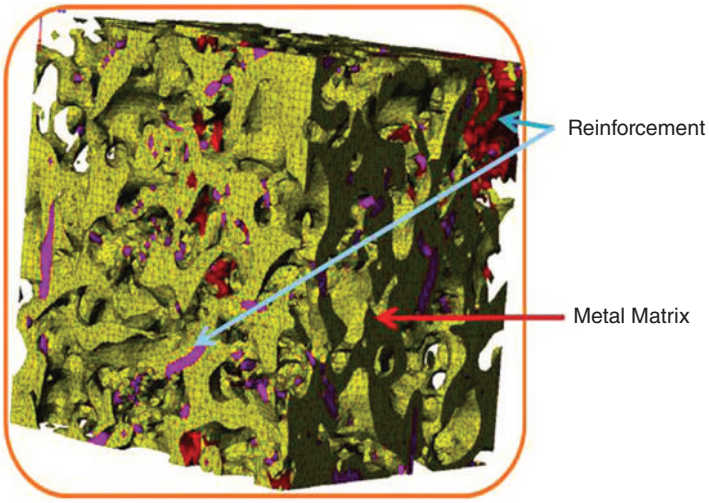


**Figure 14.3** Three-dimensional structure of a metal matrix nanocomposite.

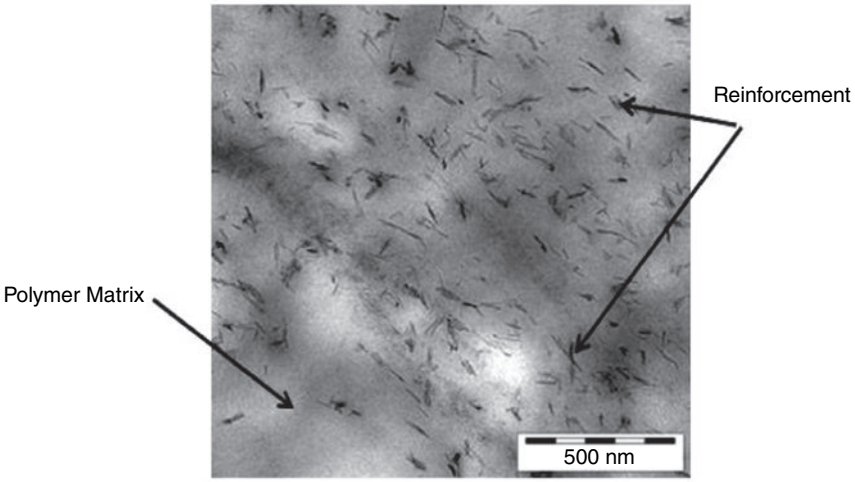


**Figure 14.4** Scanning electron image of a polymer nanocomposite.

## 14.3 Biosensors

Any tool that can detect the presence of a specific biochemical analyte and convert the biological response into an electrical signal is termed a biosensor. In simple terms a biosensor is a detecting device that can see and measure the presence of

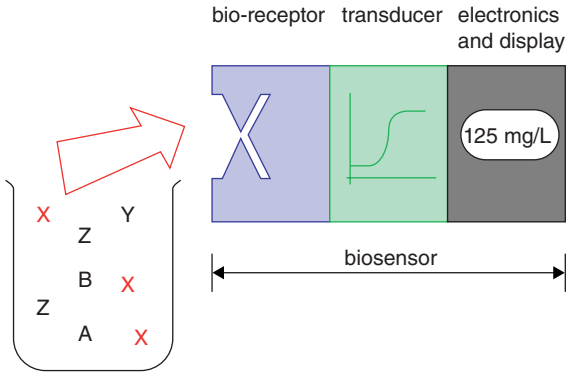


**Figure 14.5** Schematic diagram showing the main components of a biosensor.

a disease-causing agent (chemical/biochemical/analytes). This is an integrated device (Figure 14.5), composed of a biological recognition element, and) a transducer that helps in detecting the biological reaction and converts it into a signal. It is important that the sensor should be self-contained so that the desired response can be obtained without adding reagents to the sample matrix. The device is fundamentally made up of three basic parts. The first part is the bioreceptor (i.e., biorecognizing molecules such as enzymes, tissues, microorganisms, organelles, cell receptors, enzymes, antibodies, nucleic acids, etc.). This is then attached to the second important part known as the transducer (or the detector element) that works in a physicochemical way (i.e. optical, piezoelectric, electrochemical, etc.) to transform the signal resulting from the interaction of the analyte with the biological element into another signal that can be more easily measured and quantified. The final part is the made up of the detector or associated electronics or signal processors that are primarily responsible for the display of the results in a user-friendly way [15].

The biocatalyst immobilized in the vicinity of the transducer converts the substrate to product. This reaction is determined by the transducer, which converts it to an electrical signal. The output from the transducer is amplified, processed, and displayed by the detector. A common example of a commercial biosensor is the blood glucose biosensor (Figure 14.6) – a single drop of blood on the receptor is able to give information about the amount glucose levels in it.

However, for a chemist, the whole output is basically a sequence of steps in which glucose from the blood drop first oxidizes glucose and uses two electrons to reduce the flavine adenine dinucleotide (FAD) – a component of the enzyme – to $FADH_2$ as shown in Figure 14.7. This, in turn, is oxidized by the electrode (accepting two electrons from the electrode) in a number of steps. The resulting current is a measure of the concentration of glucose. In this case, the electrode is the transducer and the enzyme is the biologically active component.

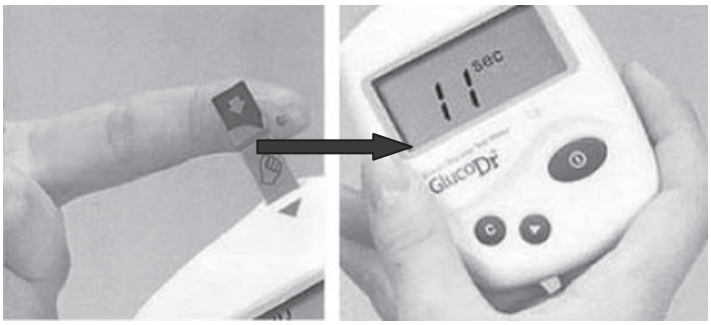


**Figure 14.6** Glucose sensor for a lay man.

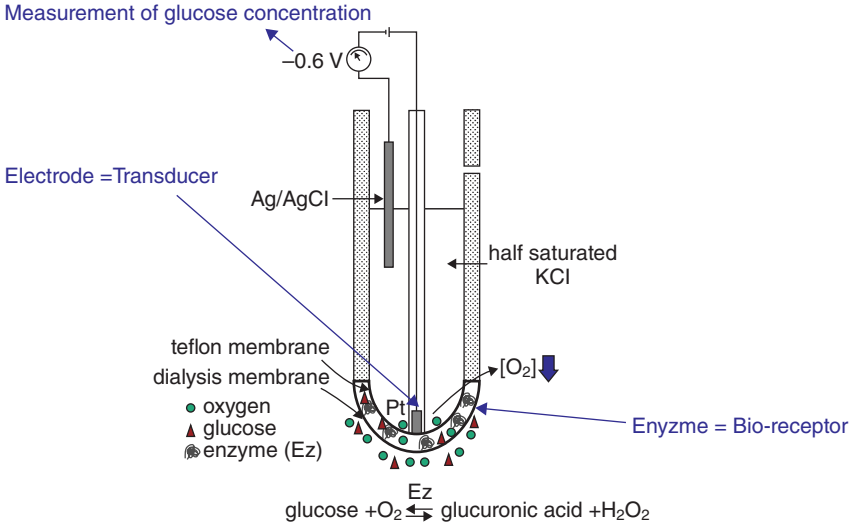


**Figure 14.7** Glucose sensor for a chemist.

## 14.4
## Types of Biosensors

Based on the principle of detection, biosensors can be classified as shown in Figure 14.8. There are basically four different types of biosensors – electrochemical, resonant, ion-sensitive, and thermal detection. The electrochemical biosensor can further be categorized as potentiometric, conductimetric and amperometric. In this section we will briefly overview the basic principles involved in the biosensor.

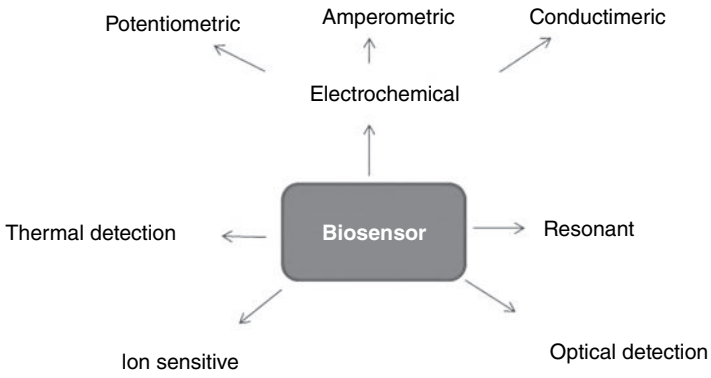


**Figure 14.8** Classification of biosensors.

### 14.4.1 Electrochemical

The basic principle behind electrochemical sensors is that many chemical reactions produce or consume ions or electrons, which that in turn cause some change in the electrical properties of the solution that can be sensed out and used as measuring parameter.

#### 14.4.1.1 **Potentiometric**

| | |
|---|---|
| *Measured parameter* | Oxidation or reduction potential of an electrochemical reaction. |
| *Principle* | The ramp voltage at which biochemical reactions takes place in a solution due to the presence of a specific biomolecule allows the current to flow through the solution and is therefore measured as the oxidation or reduction potential. |

#### 14.4.1.2 **Conductimetric**

| | |
|---|---|
| *Measured parameter* | Electrical conductance/resistance of the solution. |
| *Principle* | Changes in the conductivity or the resistivity of solutions occur due to ions or electrons that are discharged into the solution as a result of biochemical reactions. In this case these change in conductivity or resistivity are measured. |

#### 14.4.1.3 Amperometric

*Measured parameter* Current.

*Principle* The presence of enzymes catalyzes biochemical reactions producing electroactive biomolecules responsible for the flow of current, which is the measured parameter here, through an otherwise electro-passive solution.

### 14.4.2 Thermal Detection

*Measured parameter* Temperature.

*Principle* These biosensors are popularly known as enzyme thermistors, as the heat reactions of the enzymes are measured as a function of the temperature change versus analyte concentration. This heat reaction occurs due to enzyme–analyte interactions.

### 14.4.3 Ion-Sensitive

*Measured parameter* Surface electric potential.

*Principle* The electrode here is covered with polymers that act as a membrane allowing the specific analyte ion to pass through it and thus these analyte ions change the surface electrical potential of the electrode as well as change the pH of the solution. Hence, the measured surface electrical potential. This type of biosensor is known as an ion-sensitive FET.

### 14.4.4 Optical Detection

*Measured parameter* Light.

*Principle* The principle of this type of biosensor lies in the production of a diffraction signal from an electrode exposed to a laser beam. The protein containing the antibodies is the bioreceptor, which is attached to the silicon wafer acting as electrodes. The bioreceptor is thus made photo-inactive by applying a photomask and is then exposed to UV light. In order to sense the antigens present in the analyte, the electrode covered by the bioreceptor is dipped into the analyte. This thus allows the binding of antigens from the analyte to the antibodies present in the bioreceptor producing the diffraction grating. When illuminated with a laser, the diffraction signal occurs, which is the measured parameter.

### 14.4.5 Resonant

*Measured parameter* Frequency.

*Principle* The basic principle lies in the changes in the mass of the membrane, which thereby influences the resonant frequency of the transducer. This change in the mass of the membrane occurs due to attachment of analyte to the membrane.

## 14.5 Biosensors Applications

There are many potential applications of biosensors of various types. These include detection of medical health-related targets such as sugar, uric acid, folic acid, biotin, vitamin $B_{12}$, and pantothenic acid. Environmental applications include, for example, the detection of pesticides and river water contaminants, remote sensing of airborne bacteria (e.g., in counter-bioterrorism activities), detection of pathogens, and determining levels of toxic substances before and after bioremediation. Other applications include detecting toxic metabolites such as mycotoxins and food analysis [20, 21].

## 14.6 Nanocomposites for Biosensor Applications

From the above overview of the types of nanocomposites and sensors so far developed, it is now easy to predict that the transducer is the main component that has been used to apply various nanocomposites or nanonmaterials for better functioning. Research worldwide shows that only polymer nanocomposites actually play a huge role in improving the efficiency of the transducer and, finally, upgrading the quality of the biosensor.

Recently, efforts have been made in developing gold nanoparticles (Au-NPs) for their application in the field of biosensors, due to their good biological compatibility, excellent conducting capability, and high surface-to-volume ratio. Also, these have the ability to provide stable immobilization of biomolecules, retaining their bioactivity. In addition, Au-NPs allow direct electron transfer between redox proteins and bulk electrode materials. Some latest works have mostly concentrated on the application of Au-NPs in biosensors using various enzymes including glucose oxidase (GOx) [22], DNA [23], and NADH [24].

Chitosan, a natural polymer with a biodegradable and biocompatible nature, together with favorable chelating and film-forming ability, has been widely used to stabilize Au-NPs to form chitosan/Au-NP nanocomposites. However, few reports have been directly published on the application of chitosan/Au-NP nano-

composites [25]. Polyaniline (PANI)/silver chloride nanocomposites were prepared in the presence of polyvinyl pyrrolidone and applied to glassy carbon electrodes. The biosensor was investigated for dopamine detection [26]. Using ultrasonic irradiation techniques, Au-NPs were embedded in carboxyl-terminated fourth-generation poly(amidoamine) dendrimers to form hybrid nanocomposites that were used to develop glucose biosensors [27]. In a different study, researchers have developed PANI/mesoporous silica nanocomposites using chemical polymerization; the biosensor formed was investigated for uric acid detection [28]. Layer-by-layer assembly techniques were applied to develop glucose biosensors using dendrimer-encapsulated platinum nanoparticles (Pt-NPs) [29]. Biotin-incorporated polylactic acid nanofibers were prepared using the electrospinning method, which were able to capture biotinylated DNA probes [30].

Magnetic polymer nanocomposites were developed by one-pot synthesis of iron oxide/gold/polyhexanedithiol nanocomposites that contained GOx for use as amperometric glucose biosensors [31]. Immobilization of GOx was carried out on electrospun poly(vinyl alcohol) fibrous membranes, which were then deposited over the gold electrode to be used for glucose detection. This was found to be convenient way of fabricating an efficient glucose biosensor [32]. A nanocomposite was developed from titania nanotubes and poly(amidoamine) dendrimers incorporated with Pt-NPs that was applied onto GC electrodes [33]. In an another study, carcinoma antigens were detected by an immunosensor made of a composite of gold colloidal nanoparticles and Prussian blue nanoparticles protected by chitosan and poly(diallyldimethylammonium chloride) [34].

The discovery of CNTs has generated enormous interest in exploring and exploiting their unique properties for various applications [35], among which is a promising application for their use in biosensors and nanoscale electronic devices [36]. In a recent attempt, a cytochrome/poly(amidoamine)/chitosan/CNT nanocomposite was prepared and applied to a carbon glass electrode acting as a nitrite biosensor. This composite was found to be a perfect platform for electron transfer between the electrode and cytochrome *c* [37]. In another approach, multiwalled CNTs (MWNTs) based on a nanocomposite were developed using titania-incorporated polyanisidine and carbon black; the biosensor formed was investigated for impedance characteristics [38]. A glucose biosensor was fabricated by making use of nanocomposites formed by incorporating PANI-grafted CNTs into a silica/Nafion matrix. A linear response in the range of 1–10 mM for glucose within 6 s was reported [39].

In another study, the composite of poly(terthiophene carboxylic acid) and MWNTs was applied to a gold electrode for lactate detection in human serum and commercial milk [40]. Carbon nanofibers were used for making nanocomposites with a water-soluble porphyrin derivative for ethanol sensing. These nanocomposites are viewed as biomimicking the catalytic behavior of the enzymes present in nature [41]. MWNT and PANI were made use of to form a nanocomposite to be applied onto an indium/tin oxide-coated glass plate to detect cholesterol [42]. CNTs were modified by DNA, which was then attached to a sensor for label-free influenza virus detection [43].

Nickel and nickel oxide nanoparticles were deposited on CNTs and the resulting nanocomposite was deposited to a plane pyrolytic graphite electrode to be used as a sensor for hydrazine and diethylaminoethanethiol [44]. In another attempt, an ammonia gas sensor was fabricated using a nanocomposite composed of single-walled nanotubes and polypyrrole. The thin film of the nanocomposite was developed using chemical polymerization and spin-coating techniques [45]. A CNT//chitosan/platinum/cholesterol oxidase nanobiocomposite-modified electrode was investigated as a cholesterol sensor. It was reported that this sensor retained 60% of its initial activity even after 1 week [46]. A biosensor capable of detecting acetylcholinesterase was developed by one-step synthesis of a CNT and Au-NP composite. No congregation of Au-NPs onto the surface of CNTs was reported, which thus provides a hydrophilic surface [47]. Ferrocene was chosen as an electron mediator to be incorporated into CNTs and formed a nanocomposite that was applied to support GOx with the help of chitosan. This nanobiocomposite forming a reagent-less amperometric biosensor was investigated to detect glucose [48]. 1-Vinyl-3-ethylimidazolium tetrafluoroborate, which is an ionic liquid, along with Pt-NPs and CNTs, were fabricated into a nanocomposite used for sensor applications. This composite helped in the oxidation of $H_2O_2$ [49]. In a unique attempt, the nanobiocomposite of CNT/dendrimer-encapsulated Pt-NPs was used as a dopant for a polypyrrole thin film. The film showed electrocatalytic oxidation of glutamate to be efficiently detected in an analyte [50]. Some other researchers worked on developing uniform bionanomultilayer CNTs and horseradish peroxidase to detect $H_2O_2$. The authors reported uniform assembly process and homogeneity in developing this bionanomultilayer [51].

## 14.7 Conclusions

The efficiency of a biosensor largely depends upon the transducer that can sense the analyte to the finest level of existence. Hence, it becomes a important area of investigation to develop transducers that can meet the basic commercial requirements. To meet the challenge, based on the application of the biosensor, transducers are suitably modified with the help of nanomaterials or nanocomposites. Although nanocomposites are of various types, such as ceramic matrix, metal matrix and polymer matrix, it is only the polymer matrix-based nanocomposites that have been under serious investigation.

## References


**1** Wang, J. and Collinson, M.M. (1998) *J. Electroanal. Chem.*, **455**, 127–137.

**2** Kandimalla, V.B., Tripathi, V.S., and Ju, H. (2006) *Biomaterials*, **27**, 1167–1174.

**3** Brennan, J.D. (2005) *Nat. Mater.*, **4**, 189–190.

**4** Luo, T.J.M., Soong, R., Lan, E., Dunn, B., and Montemagno, C. (2005) *Nat. Mater.*, **4**, 220–224.

**5** Shchipunov, Y.A. and Karpenko, T.Y. (2004) *Langmuir*, **20**, 3882–3887.
**6** Yang, W., Zhou, H., and Sun, C. (2007) *Macromol. Rapid Commun.*, **28**, 265–270.
**7** Wu, S., Chen, Y., Zeng, F., Gong, S., and Tong, Z. (2006) *Macromolecules*, **39**, 6796–6799.
**8** Ajayan, P.M., Schadler, L.S., and Braun, P.V. (2003) *Nanocomposite Science and Technology*, Wiley-VCH Verlag GmbH, Weinheim.
**9** Jose-Yacaman, M., Rendon, L., Arenas, J., and Serra, M.C. (1996) *Science*, **273**, 223–225.
**10** Claussen, N., Rühle, M., and Heuer, A.H. (1984) *Science and Technology of Zirconia II*, American Ceramic Society, Westerville, OH.
**11** Birkholz, M., Albers, U., and Jung, T. (2004) *Surf. Coat. Technol.*, **179**, 279–285.
**12** Kainer, K.U. (2006) *Metal Matrix Composites: Custom-Made Materials for Automotive and Aerospace Engineering*, Wiley-VCH Verlag GmbH, Weinheim.
**13** Manias, E. (2007) *Nat. Mater.*, **6**, 9–11.
**14** Usuki, A., Kawasumi, M., Kojima, Y., Okada, A., Kurauchi, T., and Kamigaito, O. (1993) *J. Mater. Res.*, **8**, 1174–1178.
**15** Cavalcanti, A., Shirinzadeh, B., Zhang, M., and Kretly, L.C. (2008) *Sensors*, **8**, 2932–2958.
**16** Gupta, R. and Chaudhury, N.K. (2007) *Biosens. Bioelectron.*, **22**, 2387–2399.
**17** Liao, K.C., Hogen-Esch, T., Richmond, F.J., Marcu, L., Clifton, W., and Loeb, G.E. (2008) *Biosens. Bioelectron.*, **23**, 1458–1465.
**18** Andreescu, S. and Luck, L.A. (2008) *Anal. Biochem.*, **375**, 282–290.
**19** He, L., Musick, M.D., Nicewarner, S.R., Salinas, F.G., Benkovic, S.J., Natan, M.J., and Keating, C.D. (2000) *J. Am. Chem. Soc*, **122**, 9071–9077.
**20** Raj, C.R. and Jena, B.K. (2005) *Chem. Commun.*, 2005–2007.
**21** Li, W., Yuan, R., Chai, Y., Zhou, L., Chen, S., and Li, N. (2008) *J. Biochem. Biophys. Methods*, **70**, 830–837.
**22** Yan, W., Feng, X., Chen, X., Li, X., and Zhu, J.-J. (2008) *Bioelectrochemistry*, **72**, 21–27.
**23** Wei, Y., Li, Y., Zhang, N., Shi, G., and Jin, L. (2010) *Ultrason. Sonochem.*, **17**, 17–20.
**24** Weng, S., Lin, Z., Zhang, Y., Chen, L., and Zhou, J. (2009) *React. Funct. Polym.*, **69**, 130–136.
**25** Yao, K., Zhu, Y., Yang, X., and Li, C. (2008) *Mater. Sci. Eng. C*, **28**, 1236–1241.
**26** Li, D., Frey, M.W., and Baeumner, A.J. (2006) *J. Membr. Sci.*, **279**, 354–363.
**27** Zou, C., Fu, Y., Xie, Q., and Yao, S. (2010) *Biosens. Bioelectron.*, **25**, 1277–1282.
**28** Ren, G., Xu, X., Liu, Q., Cheng, J., Yuan, X., Wu, L., and Wan, Y. (2006) *React. Funct. Polym.*, **66**, 559–1564.
**29** Han, X., Zhu, Y., Yang, X., and Li, C. (2010) *J. Alloys Comp.*, **500**, 247–251.
**30** Chen, S., Yuan, R., Chai, Y., Xu, Y., Min, L., and Li, N. (2008) *Sens. Actuators B*, **135**, 236–244.
**31** Iijima, S. (1991) *Nature*, **354**, 56–58.
**32** Zhao, Q., Gan, Z., and Zhuang, Q. (2002) *Electroanalysis*, **14**, 1609–1613.
**33** Chenb, Q., Aia, S., Zhub, X., Yina, H., Maa, Q., and Qiua, Y. (2009) *Biosens. Bioelectron.*, **24**, 2991–2996.
**34** Carrara, S., Bavastrello, V., Ricci, D., Stura, E., and Nicolini, C. (2005) *Sens. Actuators B*, **109**, 221–226.
**35** Gopalan, A.I., Lee, K.P., Ragupathy, D., Lee, S.H., and Lee, J.W. (2009) *Biomaterials*, **30**, 5999–6005.
**36** Rahman, M.M., Shiddiky, M.J.A., Rahman, M.A., and Shim, Y.-B. (2009) *Anal. Biochem.*, **384**, 159–165.
**37** Wua, L., Lei, J., Zhang, X., and Jua, H. (2008) *Biosens. Bioelectron.*, **24**, 644–649.
**38** Dhand, C., Arya, S.K., Dattab, M., and Malhotra, B.D. (2008) *Anal. Biochem.*, **383**, 194–199.
**39** Tama, P.D., Hieu, N.V., N.D. Chien, Le A.-T., and Tuan, M.A. (2009) *J. Immunol. Methods*, **350**, 118–124.
**40** Adekunle, A.S. and Ozoemena, K.I. (2010) *J. Electroanal. Chem.*, **645**, 41–49.
**41** Hieua, N.V., Dunga, N.Q., Tamb, P.D., Trung, T., and Chien, N.D. (2009) *Sens. Actuators B*, **140**, 500–507.
**42** Tsai, Y.-C., Chen, S.-Y., and Lee, C.-A. (2008) *Sens. Actuators B*, **135**, 96–101.
**43** Dua, D., Wanga, M., Caib, J., Qina, Y., and Zhang, A. (2010) *Sens. Actuators B*, **143**, 524–529.
**44** Qiu, J.-D., Zhou, W.-M., Guo, J., Wang, R., and Liang, R.-P. (2009) *Anal. Biochem.*, **385**, 264–269.

**45** Chu, X., Wu, B., Xiao, C., Zhang, X., and Chen, J. (2010) *Electrochim. Acta*, **55**, 2848–2852.
**46** Tang, L., Zhu, Y., Yang, X., and Li, C. (2007) *Anal. Chim. Acta*, **597**, 145–150.
**47** Liu, L., Zhang, F., Xi, F., Chen, Z., and Lin, X. (2008) *J. Electroanal. Chem.*, **623**, 135–141.

# Index



*Biosensor Nanomaterials*. Edited by Songjun Li, Jagdish Singh, and Ipsita A. Banerjee

ISBN: 978-3-527-32841-3

## *q*